Applications of functionnal diphosphines quinonoid zwietterions to coordination chemistry and surface functionalization

Alessio Ghisolfi

▶ **To cite this version:**

Alessio Ghisolfi. Applications of functionnal diphosphines quinonoid zwietterions to coordination chemistry and surface functionalization. Other. Université de Strasbourg, 2014. English. NNT : 2014STRAF016 . tel-01674164

HAL Id: tel-01674164
https://theses.hal.science/tel-01674164v1

Submitted on 2 Jan 2018

HAL is a multi-disciplinary open access archive for the deposit and dissemination of scientific research documents, whether they are published or not. The documents may come from teaching and research institutions in France or abroad, or from public or private research centers.

L'archive ouverte pluridisciplinaire **HAL**, est destinée au dépôt et à la diffusion de documents scientifiques de niveau recherche, publiés ou non, émanant des établissements d'enseignement et de recherche français ou étrangers, des laboratoires publics ou privés.

UNIVERSITÉ DE STRASBOURG

ÉCOLE DOCTORALE DES SCIENCES CHIMIQUES

Institut de Chimie, UMR 7177 CNRS

THÈSE présentée par :

Alessio GHISOLFI

soutenue le : **20 juin 2014**

pour obtenir le grade de : **Docteur de l'université de Strasbourg**

Discipline/ Spécialité : Chimie

Applications de ligands diphosphines fonctionnelles et de zwitterions quinonoïdes à la chimie de coordination et à la fonctionalisation de surfaces

THÈSE dirigée par :

M. BRAUNSTEIN Pierre	Directeur de recherche CNRS, Université de Strasbourg

RAPPORTEURS :

M. ELSEVIER Cornelis, J.	Professeur, Université de Amsterdam
M. PETTINARI Claudio	Professeur, Université de Camerino

MEMBRES DU JURY :

M. ELSEVIER Cornelis, J.	Professeur, Université de Amsterdam
M. WEISS Jean	Directeur de recherche CNRS, Université de Strasbourg
M. PETTINARI Claudio	Professeur, Université de Camerino
M. BRAUNSTEIN Pierre	Directeur de recherche CNRS, Université de Strasbourg

Remerciements

Ce travail a été effectué au Laboratoire de Chimie de Coordination (Institut de Chimie, UMR 7177 CNRS) de l'Université de Strasbourg sous la direction du Dr. Pierre Braunstein, Directeur de recherche CNRS. Je tiens tout d'abord à lui exprimer toute ma reconnaissance pour la confiance qu'il m'a accordée, le soutien qu'il m'a témoigné et sa grande disponibilité.

Je souhaite remercier les membres du mon jury, plus précisément le Pr. Cornelis J. Elsevier, le Pr. Claudio Pettinari, et le Dr. Jean Weiss, de l'honneur qu'ils me font d'avoir accepté de juger ma thèse.

Je remercie également le Ministère de la Recherche et l'Université Franco-Allemande (DFH/UFA – International Research Training Group 532-GRK532) pour leur soutien financier.

Je voudrais remercier particulièrement le Dr. Christophe Fliedel, le Dr. Kirill Monakhov et le Dr. Roberto Pattacini pour tout leur soutien humain et professionnel, et pour l'amitié qu'ils m'ont témoignée.

Je remercie tous les étudiants de passage au laboratoire : Emmanuel, Francesca, Audrey, Serena et Mary, avec qui j'ai pris un plaisir énorme à travailler ainsi que toutes les personnes qui m'ont aidé dans mon travail : Marc Mermillon-Fournier, pour toutes les fois qu'il m'a sauvé la vie (même en dehors du labo); Mélanie Boucher et les services communs de l'Université de Strasbourg, RMN, spectrométrie de masse, analyse élémentaire et cristallographie ; les mecs du magasin ; Soumia Hnini et Sandrine Garcin pour tous les aspects administratifs liés à la thèse et à la survie d'un italien en France.

Je remercie très chaleureusement tous les membres du laboratoire pour leur accueil et leur soutien pendant ce temps passé ensemble: Sophie, Thomas, Paulin, Lucie, Jacky, Valentine, Pierre, Marcel, Andreas, Fan, Pengfei, Alexandre et tout particulièrement Wiki-Max-Martin, pour son amitié et tout ce que l'on a partagé ensemble.

Je remercie aussi Silvia, parce que même si nos chemins se sont divisés, elle restera toujours pour moi une personne spéciale.

Si je suis arrivé jusqu'ici, c'est grâce à vous.

Alessio GHISOLFI

Applications de ligands diphosphines fonctionnelles et de zwitterions quinonoïdes à la chimie de coordination et à la fonctionalisation de surfaces

Résumé

Le but de ce travail de thèse était de développer de nouvelles familles de ligands polyfonctionnels pour étudier, dans un premier temps, leur chimie de coordination vis-à-vis de métaux de transition et, dans un second temps, en fonction des espèces formées, leurs propriétés physiques (magnétiques par exemple) et/ou catalytiques. L'évaluation de leur potentiel pour la formation de nouveaux matériaux ou la fonctionnalisation de supports métalliques faisait également partie intégrante des objectifs de cette thèse. De ce fait, chaque ligand a été fonctionnalisé avec des groupements adaptés à l'ancrage sur surfaces, comme des fonctions zwitterioniques ou des thio-éthers.

Mots clés: Phosphines fonctionnelles, Zwitterions, Ligands quinonoïdes, Amino-alcools, Organométalliques, Oligomérisation catalytique de l'éthylène, Aimants moléculaires.

Résumé en anglais

The aim of this thesis was to develop new families of polyfunctional ligands to study their coordination chemistry towards transition metals and, depending on the products formed, to investigate their physical (e.g. magnetic) and / or catalytic properties. The evaluation of their potential for the formation of new materials as well as for the functionalization of metal surfaces was also part of the objective of this thesis. Therefore, each ligand has been functionalized with groups suitable for the anchoring on metallic surfaces, such as zwitterionic or thioethers moieties.

Keywords: Functional phosphines, Zwitterions, Quinonoid ligands, Amino-alcohols, Organometallic, Catalytic ethylene oligomerization, Single molecule magnets (smm).

INTRODUCTION GENERALE

Le but de ce travail de thèse était de développer de nouvelles familles de ligands polyfonctionnels pour étudier, dans un premier temps, leur chimie de coordination vis-à-vis de métaux de transition et, dans un second temps, en fonction des espèces formées, leurs propriétés physiques (magnétiques par exemple) et/ou catalytiques. L'évaluation de leur potentiel pour la formation de nouveaux matériaux ou la fonctionnalisation de supports métalliques faisait également partie intégrante des objectifs de cette thèse.

Ce travail a permis de développer des ligands caractérisés par diverses associations de sites donneurs en vu de la synthèse de complexes de coordination fonctionnalisés, de manière également à rendre possible une interaction avec des surfaces ou des supports solides. L'option qui nous paraissait la plus viable était d'associer des sites donneurs classiques de la chimie de coordination comme, par exemple, des phosphines ou des amino-alcools à des groupements adaptés à l'ancrage sur surface, comme par exemple des thiols, des thio-éthers ou des fonctions zwitterioniques, Selon le type de groupe fonctionnel choisi, on peut diviser ce travail en trois parties différentes :

1) Diphosphines fonctionnelles
2) Zwitterions et ligands quinonoïdes
3) Amino-alcools

Phosphines Fonctionnelles

Les ligands phosphorés sont probablement à ce jour les ligands qui ont été les plus étudiés en chimie organométallique. Associés aux métaux de transition, leurs complexes ont montré des applications nombreuses et variées dans différents domaines de la chimie et en particulier en catalyse homogène. Dans ce contexte, nous avons basé notre travail sur l'étude de la réactivité des deux ligands hybrides (porteurs de fonctions potentiellement coordinantes de nature chimique très différente), les bis(diphenylphosphino)amines **L1** et **L2** (Figure 1) fonctionnalisées par un groupement thio-éther, connu pour sa capacité à interagir avec des surfaces

métalliques (Au, Ag, Cu). La différence entre ces deux ligands repose sur la nature de l'espaceur entre le groupe donneur diphosphine et la fonction d'ancrage thio-éther. Dans le cas de **L1**, nous avons choisi une chaîne alkyle, flexible et éventuellement capable de permettre une coordination du soufre au centre métallique lié aux atomes de phosphore. En revanche, en ce qui concerne **L2**, nous avons opté pour un espaceur phényle, plus rigide et ayant une influence électronique différente sur la partie diphosphine du ligand.

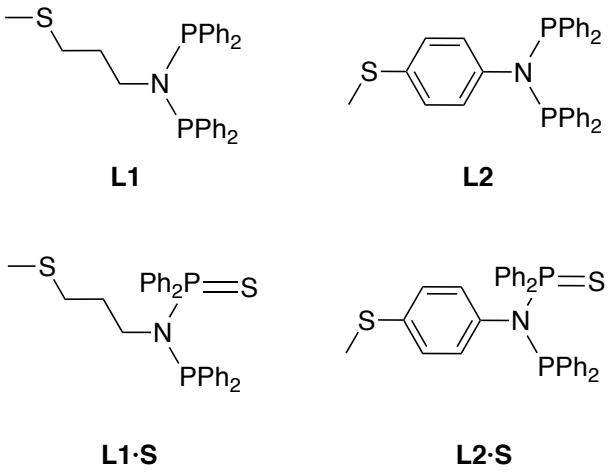

Figure 1. Représentation des ligands **L1** et **L2**.

L'étude de la chimie de **L1** et **L2** nous a conduits à la découverte de nombreux complexes d'argent et de nickel, particulièrement intéressants tant du point de vue structural que de celui des applications en catalyse homogène. Ces résultats nous ont encouragés à développer la chimie de leur dérivés respectifs **L1·S** et **L2·S** (Figure 1), qui possèdent des atomes de phosphore dans deux degrés d'oxydation différents. Cette étude s'est révélée tout aussi fructueuse, en particulier pour la synthèse de complexes non symétriques du nickel(II), actifs comme pré-catalyseurs en oligomérisation de l'éthylène.

Zwitterions et ligands quinonoïdes

Les molécules organiques possédant une structure quinonoïde constituent une classe importante de composés et possèdent des propriétés chimiques

remarquables (par exemple en catalyse, photochimie, électrochimie) et physiques (par exemple pour la fonctionnalisation de surfaces). En particulier, des benzoquinonemonoimines découvertes au laboratoire il y a une dizaine d'années appartiennent à cette famille et ont un fort potentiel comme ligands en chimie de coordination et en chimie organométallique. L'intérêt intrinsèque de ces molécules a conduit notre laboratoire à réaliser d'importantes études sur des dérivés du zwitterion « parent » représenté dans la Figure 2. La structure électronique remarquable de ces molécules à 12 électrons π, et donc potentiellement anti-aromatiques, leur confère des propriétés intrinsèquement intéressantes avec des retombées dans les domaines de la physique des surfaces, en particulier du fait de leur fort moment dipolaire (10 D) et de la possibilité de leur adjoindre diverses fonctionalités, et de la chimie de coordination en tant que ligands O_2,N_2 bis-chélatants pouvant faire pont entre deux centres métalliques. En fonctionalisant le zwitterion « parent » par deux noyaux pyridiniques connectées à la fonction azotée par un espaceur CH_2CH_2, nous avons réussi à préparer un nouveau zwitterion de type quinonoïde, pouvant jouer le rôle de ligand potentiellement hexadentate O_2,N_2,N_{Py},N_{Py} (**H_2L**) et ainsi pu étudier sa réactivité en chimie de coordination.

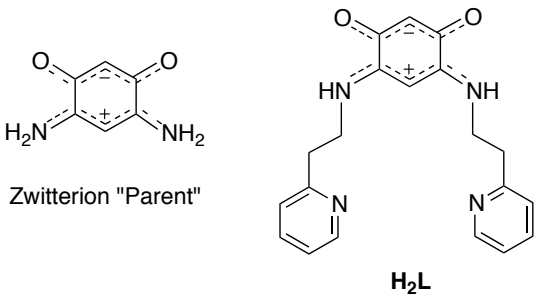

Figure 2. Représentation du zwitterion « Parent » et du ligand **H_2L**

Amino-alcools

Dans un cadre d'études consacrées à l'origine au développement de nouveaux pré-catalyseurs à base de nickel(II) pour oligomérisation de l'éthylène en phase homogène, notre laboratoire a mené, ces dernières années, de fructueuses études sur la structure, la synthèse et le comportement magnétique de plusieurs

complexes à géométrie cubane et pseudo-cubane. Ces molécules sont été synthétisées par réaction entre des ligands chélatants de type pyridyl-alcool/-ate et des précurseurs de Ni(II). En particulier, ces ligands, appartenant à la famille des amino-alcools, peuvent être obtenus par condensation entre une cétone et une picoline deprotonée. Ils constituent des « synthons » qui, grâce à leur capacité chélatante N,O et à celle de l'atome d'oxygène de faire pont entre plusieurs centres métalliques, favorisent la formation de complexes polynucléaires. Dans le cadre de ce travail et en vu de son étude en chimie de coordination, nous avons préparé un nouveau ligand appartenant à cette famille, qui est fonctionnalisé par un groupe thio-éther (HL(S)), bien adapté au dépôt des complexes métalliques correspondants sur des surfaces métalliques (Cu, Ag, Au) (Figure 3). A partir de ce ligand, nous avons réussi à isoler et caractériser deux nouveaux complexes polynucléaires de nickel(II) et de cobalt(II), dont la structure et les propriétés en catalyse homogène et en magnétisme moléculaire méritaient d'être approfondies. Nous verrons que l'un de ces complexes se comporte comme « Single Molecule Magnet » (SMM). Du fait de la présence d'une fonction thioéther, ces molécules constituent un intéressant point de départ pour l'étude ultérieure des propriétés magnétiques de clusters de coordination déposés sur surface.

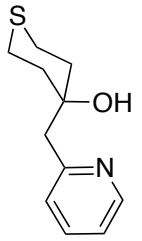

HL(S)

Figure 3. Représentation du ligand **HL(S)**.

Cette thèse est structurée en chapitres indépendants, qui sont présentés sous la forme de publications scientifiques. Chaque chapitre est donc caractérisé par sa propre numération des pages, une introduction, une discussion, une conclusion et sa propre bibliographie. Une annexe contenant des informations complémentaires sera donnée, le cas échéant, à la fin de chaque chapitre. Une

exception est celle du chapitre 1, qui a été rédigé sous la forme d'une revue bibliographique et qui servira d'introduction générale aux chapitres 2, 3 et 4 pour la section dédiée aux ligands phosphorés. Pour chaque chapitre correspondant à un travail multi-auteurs sera précisée ma contribution propre à sa réalisation.

CHAPITRE 1

Functional short-bite ligands: synthesis, coordination chemistry and applications of *N*-functionalized bis(diphenylphosphino)amine (DPPA)-type ligands.

Christophe Fliedel,[†,*] *Alessio Ghisolfi*[‡] *and Pierre Braunstein*[‡,*]

† REQUIMTE, Departamento de Quimica, Faculdade de Ciências e Tecnologia, Universidade Nova de Lisboa, Caparica, 2829-516, Portugal

‡ Laboratoire de Chimie de Coordination, Institut de Chimie (UMR 7177 CNRS), Université de Strasbourg, 4 rue Blaise Pascal, CS 90032, 67081 Strasbourg, France

KEYWORDS. Diphosphine Short-bite Ligands, P,P-chelates and bridges, Metal Complexes, Catalysis, Materials.

CONTENTS.

1. Introduction

Short-bite ligands such as bis(diphenylphosphino)amine (DPPA) or bis(diphenylphosphino)methane (DPPM) and the *N*-substituted derivatives of DPPA continue to attract much attention owing to the diversity of their coordination modes (monodentate, bridging, chelating) which results in a rich coordination chemistry for the neutral ligands, *e.g.* $Ph_2PNHPPh_2$, as well as their deprotonated forms, *e.g.* $(Ph_2PNPPh_2)^-$ (Chart 1).[1] In the latter case, coordination of the nitrogen atom to a metal center becomes an additional possibility to that offered by the phosphorus donors. Furthermore, it is possible to introduce an additional donor group by functionalization of the nitrogen atom of the DPPA, and the resulting *N*-functionalized DPPA-type ligands may form polynuclear assemblies, or the additional donor can act as a labile ligand to stabilize reactive species, *via* intra- or intermolecular interactions, e.g. during a catalytic cycle.[2] Finally, if a suitably *N*-functionalized tail is used, new possibilities arise to anchor organometallic species into sold matrices or on metallic surfaces.

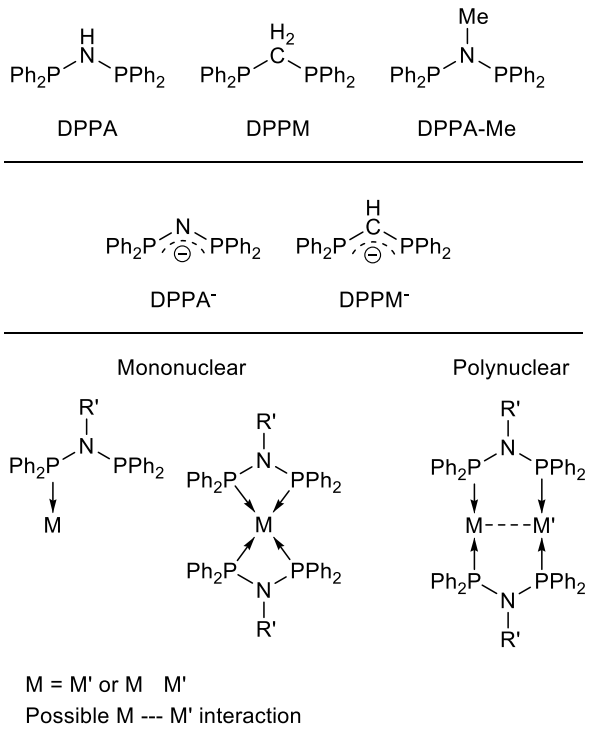

Chart 1. DPPA, DPPM and an example of *N*-functionalized DPPA-type ligand DPPA-Me (Top), the deprotonated forms of DPPA and DPPM (Middle), and the possible coordination modes of such ligands, resulting in mono- or polynuclear complexes (Bottom).

Although other methods were reported (see below), most of these *N*-functionalized DPPA-type ligands were accessible from the corresponding amine, by a classical aminolysis reaction and were obtained in good yield (Scheme 1).

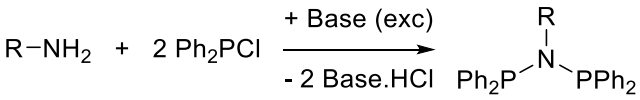

Scheme 1. General aminolysis reaction for the formation of *N*-functionalized DPPA-type ligands.

This review focuses on *N*-functionalized DPPA-type ligands, in which the *N*-substituent contains at least one typical donor-and therefore excludes pure *N*-alkyl or *N*-aryl substituents. We also discard from this survey the PNP ligand in which the substituents on the P are not phenyl rings. We will summarize the various ways to access such *N*-functionalized DPPA-type ligands, their use for the formation of mono- or polynuclear complexes or clusters and the reactivity of the latter. The applications in catalysis or material sciences of the metal complexes containing such modified DPPA-type ligands will also be mentioned, but not detailed. This review will also highlight that the ligands themselves can exhibit original reactivity, leading to P migration which open the way to various ligands architectures.

Note to the Thesis referees:

Owing to lack of time, this chapter does not represent the final form of the review, however it contains the sections most related to the work done during my PhD. To complete this review, different parts will be added:

8. Poly-bis(diarylphosphino)amine derivatives
9. *N*-functionalized bis(dialkyl/dibenzylphosphino)amine derivatives
10. *N*-Metal functionalization

An extensive and comprehensive discussion about the applications of such compounds, in particular in homogeneous catalysis and oligomerization of ethylene, is also in preparation and will be of interest for the readers.

11. Applications
    - 11.1. Homogeneous catalysis
    - 11.2. Material sciences
    - 11.3. Heterogeneous catalysis
12. Conclusion and Perspectives

2. Nitrogen-based

A large variety of nitrogen-containing chemical functions have been used to develop original *N*-functionalized DPPA-type ligands. Although no N•••Metal interactions involving these donor functions could be evidenced so far in their metal complexes, the behavior of the latter in catalytic applications was found to be affected by the nature of the *N*-functionality. Furthermore, the presence of specific *N*-hydrazide or *N*-pyridyl groups in these DPPA-type ligands induced original reactivity.

2.1. Amino group

A series of bis(diphenylphosphino)amine-type ligands bearing as *N*-substituent an amino group have been recently reported, and the authors took advantage of the wide range of amine substituents available and their possible combinations in $NR^1R^2R^3$, with $R^1 \neq R^2 \neq R^3$, to develop poly-DPPA ligands or to fine-tune the steric and/or electronic properties of the resulting *N*-functionalized DPPA-type ligands in order to examine the influence of the *N*-functional group on the activity and/or selectivity of the resulting metal complexes in some catalytic reactions.

Kim *et al.*[3] pointed out the effects of pendant amine donor functions in the design of chromium-based complexes for catalysis purposes. Typically, tertiary amines are used, separated from the DPPA moiety by a spacer (Scheme 2). During the formation of the pre-catalyst, the dangling amine is not involved in the complexation of the metal center, but once the catalytic process is started, the additional binding site on the nitrogen may interact with the active species. In particular, it can behave as a hemilabile stabilizing agent, or it can modify the transition states in the catalytic process. Therefore, such functionalization converts the simple DPPA from a

bidentate to a potentially hemilabile, tridentate, mixed-donors ligand. For this purpose, the nature of the spacer, its length and flexibility, represent critical aspects. In particular Kim *et al*. reported that, if compared with the conventional PNP ligand **1,** the length of the spacer in molecules **2-6** strongly influences the selectivity of the catalytic ethylene tetramerization reaction. The Cr complexes were generated *in situ* without being isolated for characterization. The ^{31}P NMR chemical shifts of these free ligands were found in the typical range for *N*-alkyl functionalized DPPA-derivatives, between 61.9 and 63.7 ppm, and are detailed in Table 1. The catalytic performances of the corresponding metal complexes are discussed in Section 11.1.

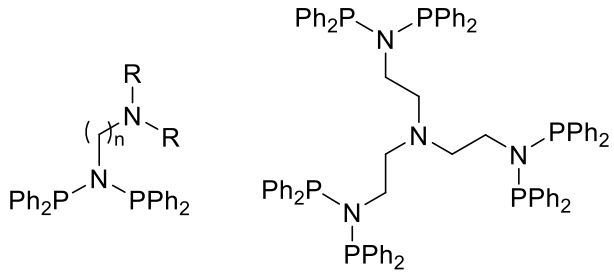

7

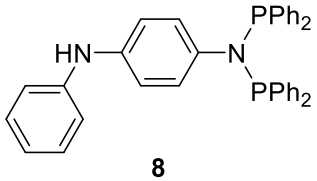

8

Scheme 2. DPPA-type ligands *N*-functionalized with an amino group.

In 2008, Baysal *et al*.[4] and Jiang *et al*.[5] developed at the same time, but following different reaction conditions, a new hexadentate phosphinoamine ligand (**7**) *via* aminolysis reaction of the commercially available tris(2-aminoethyl)amine (Scheme 2). Baysal *et al*. investigated the coordination chemistry of ligand **7** towards group 10 metals and they were able to prepare two trinuclear complexes of Pd(II) (**9**) and Pt(II) (**10**) by reaction of ligand **7** with 3 equiv. of the

corresponding [MCl_2(COD)] precursor (Scheme 3). The ^{31}P NMR spectrum of complex **9** exhibited a singlet signal at 30.7 ppm, while **10** displayed a singlet at 16.9 ppm flanked by satellites ($^1J_{P,Pt}$ = 3400 Hz) due to coupling of the phosphorus atoms with the Pt center (Table 1). These NMR data were in agreement with the proposed structures, which could unfortunately not be confirmed by single crystal X-ray diffraction studies. The authors studied these compounds in the Heck and Suzuki cross coupling reactions (see Section 11.1).

Jiang *et al*. focused their interest on the *in situ* development of a new (pre)catalyst for the Cr-based ethylene tetramerization (see Section 11.1). Despite these two very different approaches, both groups came to the same conclusion that the connection of multiple DPPA moieties based on a tertiary aminoethyl linker, constitutes an efficient, versatile and inexpensive route to prepare functional complexes for different aims.

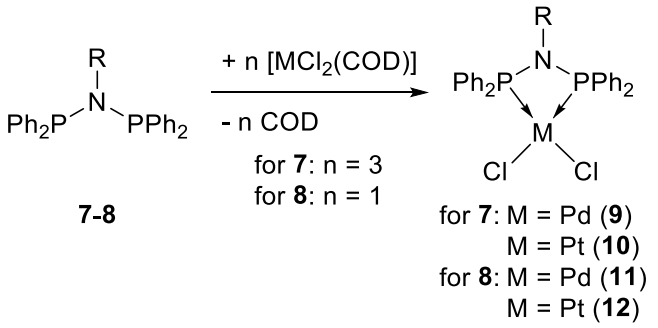

Scheme 3. Synthesis of Pd(II) (**9** and **11**) and Pt(II) (**10** and **12**) complexes from ligands **7**-**8**.

Table 1. ^{31}P NMR data of the free ligands **1**-**8** and metal complexes **9**-**12**.[a]

	M	L	δ (mult.)	Ref.
1			63.7 (s)[b]	[3]
2			61.9 (s)[b]	[3]
3			63.2 (s)[b]	[3]

4			63.0 (s)[b]	[3]
5			62.9 (s)[b]	[3]
6			62.5 (s)[b]	[3]
7			62.0 (s)[b]	[4]
8			69.3 (s)[b]	
9	Pd	**7**	30.7 (s)[c]	[4]
10	Pt	**7**	16.9 (s)[c,d]	[4]
11	Pd	**8**	35.9 (s)[b]	[6]
12	Pt	**8**	21.2 (s)[b,d]	[6]

[a] Chemical shifts given in ppm, Multiplicity: s = singlet, [b] in $CDCl_3$, [c] in d_6-DMSO, [d] two satellites are observed $^1J_{P,Pt}$ = 3400 (**10**) and 3336 Hz (**12**).

In 2011, Biricik *et al*.[6] described the synthesis of ligand **8** with a bulky *N*-substituent, starting from 4-aminodiphenylamine. This ligand, which presents a ^{31}P NMR singlet signal at 69.3 ppm, was then reacted with 1 equiv. of [MCl_2(COD)] (M = Pd, Pt) to produce the corresponding complexes **11** and **12**, respectively (Scheme 3). The characteristic ^{31}P NMR data recorded (Table 1) included for complex **11** a singlet at 35.9 ppm, and for **12**, a singlet at 21.2 ppm flanked with satellites ($^1J_{P,Pt}$ = 3336 Hz). Both Pd(II) and Pt(II) complexes were evaluated in the Suzuki and Heck cross-coupling reactions and the results will be discussed in the Section 11.1. This study concluded that complexes **11** and **12** are air-stable, show a good reactivity and do not require an induction period in catalysis.

2.2. Hydrazine group.

As reported by Faught in 1975[7] (**13**) and more recently by Kornev *et al*.[8] (**14**-**16**), the standard aminolysis reaction applied to hydrazine-type precursors, of general formula (RR'N-

NH_2), leads to a series of *N*-functionalized DPPA-type ligands called diphosphinohydrazides, which display a direct N-N single bond (Scheme 4). While ligand **13** exhibits a singlet resonance in its ^{31}P NMR spectrum at 48.3 ppm, which is high-filed shifted compared to *N*-alkyl functionalized DPPA-type ligands, the PNP fragment of compounds **14**-**17** resonates at lower field, between 70.5 and 77.8 ppm (Table 2). However, their structural parameters remain very close and similar to those of ligand **17** (see below and Table 2). Deprotonation with $LiN(SiMe_3)_2$ of the derivatives **14**-**16**, containing one N-H substituent, gave rise to a rearrangement and the migratory insertion of a PPh_2 group into the N-N bond with formation of the diphosphazenide products **14**$^-$-**16**$^-$ (Scheme 4). Formally, this rearrangement is associated to a redox process, where a three-coordinate P(III) atom becomes a four-coordinate P(V) one, while one N atom reduces its coordination number from 3 to 2. The authors assumed that this process is influenced by the nature of the substituent on the nitrogen (NHR) atom, and a strong local negative charge on the *N*HR atom causes an elongation of the N-N bond and its subsequent cleavage, which makes possible the insertion of the Ph_2P group (through several postulated intermediates).[8a-c]

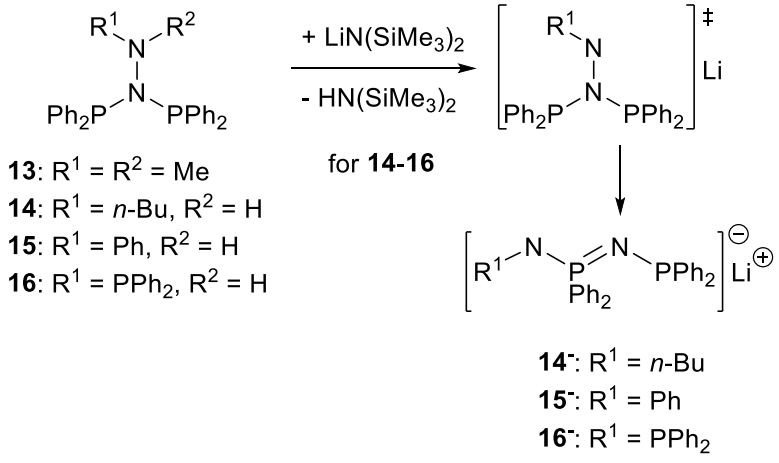

Scheme 4. Faught's (**13**) and Kornev's (**14-16**) diphosphinohydrazides, and rearrangement after deprotonation leading to the diphosphazenide group in (**14**$^-$**-16**$^-$).

Furthermore, the use of the 8-quinolylhydrazine-based DPPA derivative (**17**) allowed Kornev and co-workers to produce selectively three types of migration products, by selective formation of new P-C (**A**), P-N (**B**) or P-P (**C**) bonds, as a function of the reaction conditions (Scheme 5).[8b] The rearranged products **17a** and **17b** (transformation A) were obtained by heating ligand **17** in toluene (or pyridine) at 130 °C for 1 h under vacuum, or by reaction with $LiN(SiMe_3)_2$ at room temperature, respectively. Reaction of ligand **17** with half an equivalent of ZnI_2 led to transformation B and the formation of the dinuclear complex **17c**, along with 1 equiv **17**·HI. Finally, as observed for other DPPA-type ligands attached in ortho position of a pyridine ring (see Section 2.4), protonation of ligand **17** led to transformation C. All the PPh_2 migration reactions are represented in Scheme 5. The resulting supporting ligands (**17a**-**d**) are no longer of the DPPA-type and involve a P(V) donor, for this reason they are not detailed in this review.[8b,8d,9] However, the authors could synthesize a coordination compound (**17e**) of the modified DPPA-type ligand **17**, by deprotonation of the latter, and further reaction with the ZnI_2 precursor (Scheme 5, D). *A contrario* to the "classical" coordination compounds of *N*-functionalized DPPA-type ligands, in **17e** the metal center was bis-chelated by the two donors of the *N*-tail and none of the P atoms was involved in metal coordination. Selected bond lengths, angles and spectroscopic data of the DPPA-type ligands **13**-**17** and complex **17e** (except the products resulting from PPh_2 migration) are listed in Table 2.

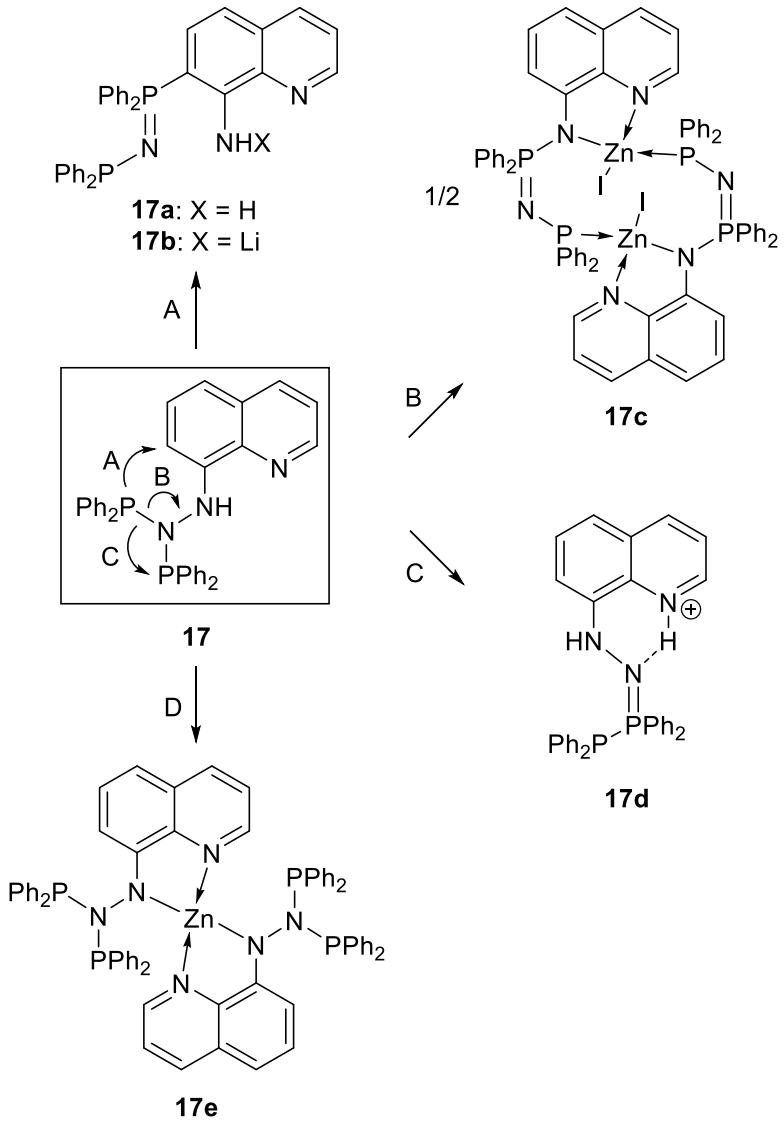

Scheme 5. Different PPh_2 migration reactions observed in **17**. Conditions for transformations: A: Toluene or pyridine, 130 °C, 1 h, vacuum pressure (**17a**), or $LiN(SiMe_3)_2$, toluene/Et_2O, room temp (**17b**); B: 0.5 equiv ZnI_2, THF, room temp, along with formation of 1 equiv **17**·HI; C: H^+; D: 1 equiv *n*BuLi, followed by addition of 0.5 equiv ZnI_2, THF, room temp, 3 h.

Table 2. ^{31}P NMR data and characteristic structural parameters of the free ligands **13**-**17**.[a]

	δ (mult.)	P-N	N-N	PNP	Ref.
13	48.3 (s)[b]	1.715	1.449(4)	126.3(5)	[3,7]
14	71.0 (s)[c]	1.720	1.445(1)	120.4(1)	[8d]
15	70.5 (s)[b]				[9]
16	77.8 (d)[d]	1.720	1.437(3)	124.8(1)	[8a]
	47.1 (t)				
17	70.7 (s)[b]	1.729	1.418(1)	124.5(6)	[8b]
17e	71.1 (br)[e]	1.722	1.436 (aver.)	124.1 (aver.)	[8b]

[a] Chemical shifts, P-N (aver.) and N-N bond lengths and PNP angle given in ppm, Å and deg, respectively, [b] in $CDCl_3$, [c] in d_8-toluene, [d] in C_6D_6 the signal at 77.8 ppm is attributed to the PNP fragment and this at 47.1 ppm to the PNH one ($J_{P,P}$ = 9 Hz), [e] in d_8-THF.

2.3. Nitro group

In 2006, Dyson *et al*. reported the synthesis of the group 10 metal complexes **20**-**23**, supported by a *meta*- or *para*-cyanoaryl-functionalized DPPA-type ligand, resulting from the rearrangement of the corresponding iminodiphosphine precursors **18** and **19**, by reaction with $[MCl_2(COD)]$ (M = Pd, Pt), as depicted in Scheme 6.[10] In the solid-state, the metal center of all the resulting complexes presents a square-planar coordination geometry, with the DPPA-type ligand acting as a chelate. Typical ^{31}P NMR resonances were observed for the $PdCl_2$ (36.1 (**20**) and 37.8 (**21**) ppm) and $PtCl_2$ (22.4 (**22**) and 27.7 (**23**) ppm) complexes of these *N*-aryl-substituted DPPA ligands. ^{31}P NMR data and selected bond lengths and angles are listed in Table 3. This reaction represents a new approach to the synthesis of chelating and bis-chelating transition metal complexes, since not all bis(diarylphosphino)amines can be obtained using the standard aminolysis reaction and/or are stable in this form.

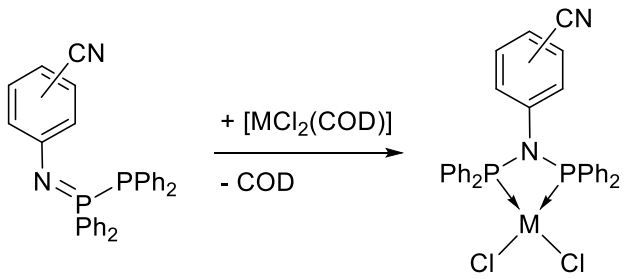

18: 4-CN
19: 3-CN

4-CN: M = Pd (**20**)
M = Pt (**21**)
3-CN: M = Pd (**22**)
M = Pt (**23**)

Scheme 6. Synthesis of complexes **20**-**23**, starting from the corresponding iminodiphosphine precursors (**18**-**19**).

Table 5. ^{31}P NMR data and characteristic structural parameters (P-M bond lengths and PMP bite angle) of complexes **20**-**23**.[a]

	δ (mult.)	$^1J_{P,Pt}$	P-M	PNP	PMP	Ref.
20	36.1 (s)[b]		2.221	100.1(2)	72.62(4)	[10]
21	22.4 (s)[c]	3343	2.201	98.7(7)	73.38(1)	[10]
22	37.8 (s)[b]		2.219	100.2(2)	72.29(5)	[10]
23	23.7 (s)[c]	3350	2.212	99.9(1)	72.77(3)	[10]

[a] Chemical shifts, $^1J_{P,Pt}$, P-M (aver.) bond lengths and PNP and PMP bond angles are given in ppm, Hz, Å and deg., respectively, [b] in CD_2Cl_2, [c] in $CDCl_3$.

2.4. *N*-heterocycle pendant tail

In 2003 Dyson *et al*. reported the synthesis of ligand **24**, obtained *via* the classical aminolysis reaction of 2,6-diaminopyridine (Scheme 7).[11] This is a potentially pentadentate ligand based on the association of two DPPA-type units linked through a pyridine linker in its 2 and 6 positions. Owing to the presence of numerous donor groups, such ligands allow the

synthesis of polynuclear metal complexes and macrocyclic ring systems (see also Section 8 for poly-DPPA derivatives). Consistently, Dyson and co-workers reacted **24** with 2 equiv. of $[Mo(CO)_4(NBD)]$ and 4 equiv. [AuCl(THT)] to form the dinuclear and tetranuclear neutral complexes **25** and **26**, respectively (Scheme 7).[11-12] The solid-state molecular structures of both metal complexes were determined by XRD and revealed that in complex **25** both metal centers adopt an octahedral coordination geometry, while in **26** the four gold atoms display a linear coordination geometry. Probably induced by the high van der Waals radius of the Mo(0) center, the PNP angles in complex **25** (103.6(2) and 103.4(2)°) is in the upper range of the values found in *N*-functionalized DPPA-supported metal chelate complexes and the P-M bond lengths are quite long (aver. 2.483 Å, Table 6). In further studies, Dyson *et al*. reported that the protonation of DPPA-type moieties attached to pyridine in *ortho*-position, as in ligand **24**, affords quantitatively the corresponding iminobiphosphine species.[13] Monitoring by ^{31}P NMR spectroscopy of the reaction of ligand **24** with 1 equiv. HBF_4 showed the disappearance of the initial signal at 59.0 ppm and the concomitant appearance of two doublets centered at 17.2 and -20 ppm, with a $^1J_{P,P}$ value of 227 Hz, indicative of the iminobiphosphine structure of **27** (Scheme 7). Deprotonation of the iminobiphosphinium salt regenerated the starting DPPA-type structure quantitatively. ^{31}P NMR data and main structural parameters of the latter compounds are detailed in Table 6.

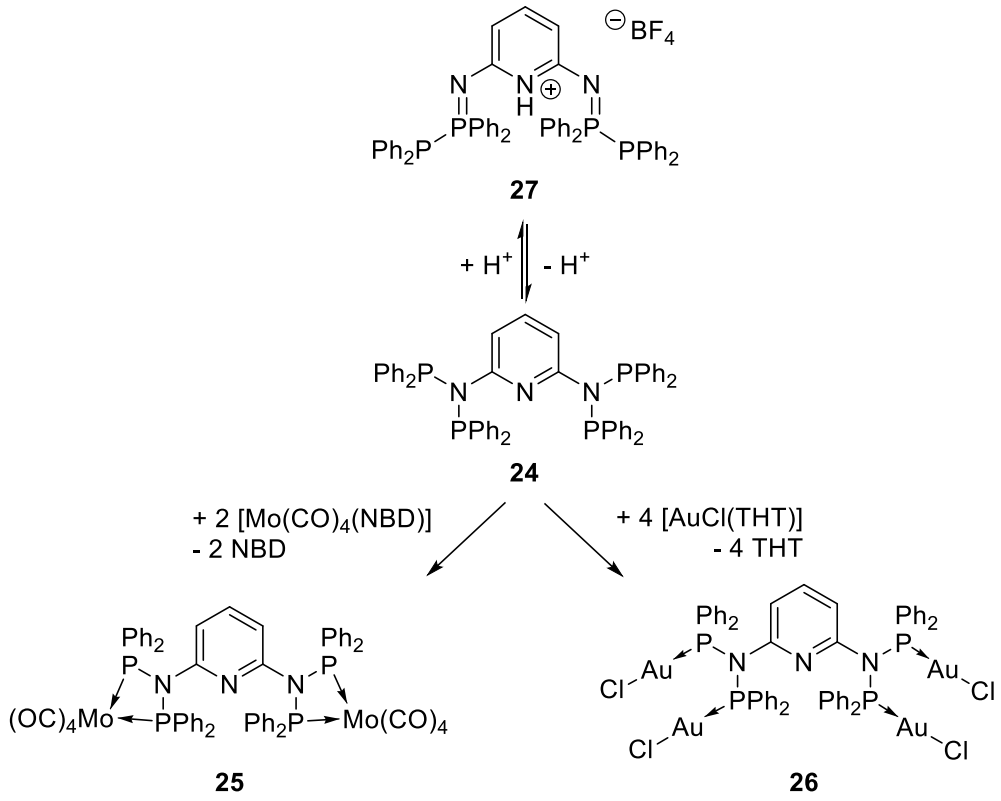

Scheme 7. Reactivity of ligand **24** towards metal precursors (**25-26**) and protic conditions (**27**).

Scopelliti *et al*. reported the synthesis of a DPPA-type ligand functionalized on the nitrogen atom by a 2-picolyl group (**28**) and a study of its coordination chemistry towards Pd(II) and Pt(II) (Scheme 8).[14] Ligand **28** was prepared by classical aminolysis of 2-picolylamine with 2 equiv. of Ph_2PCl in presence of a base and its ^{31}P NMR spectrum displays a single resonance at 62.6 ppm. This ligand readily reacted with $[MCl_2(COD)]$ (M = Pd, Pt) to lead the corresponding *P*,*P*-complexes **29** and **30**, respectively (Scheme 8). The ^{31}P NMR spectra of both complexes exhibited typical singlet resonances at 34.2 (**29**) and 20.2 ppm ($^1J_{P,Pt}$ = 3308 Hz) (**30**), and their typical square-planar coordination geometry could be confirmed by XRD studies. Even the P-N and P-M bond lengths and PMP bite-angle are in the typical range of group 10 dihalide

complexes of DPPA-type ligands (Table 6). Both complexes were found to be active catalysts in C-C cross coupling reactions (see Section 11.1).

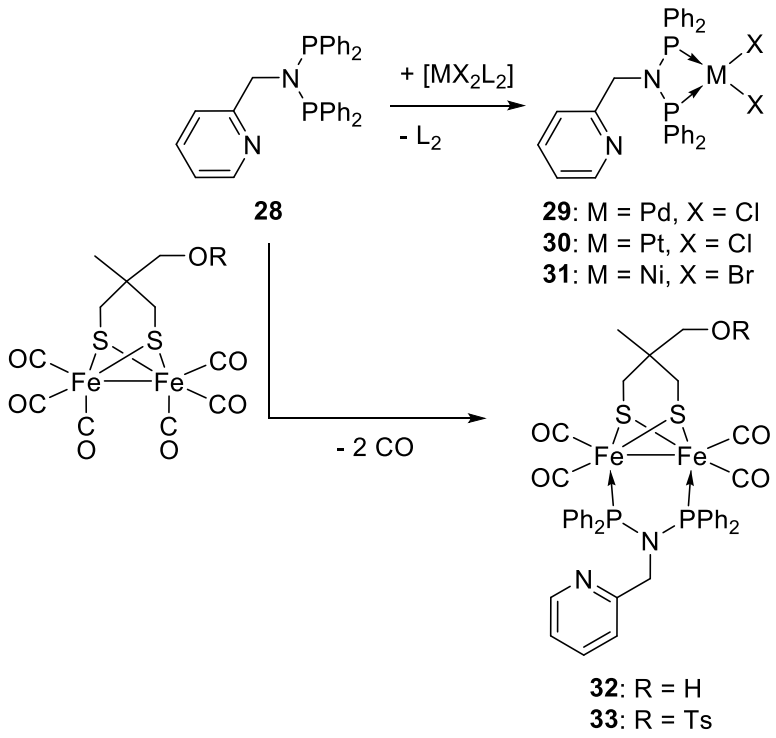

Scheme 8. Synthesis of dihalide group 10 complexes **29-31** and diiron complexes **32-33** supported by the DPPA-type derivative **28**. Note: L_2 = COD for Pd and Pt, and DME for Ni.

The reaction of ligand **28** with the Ni(II) precursor [$NiBr_2$(DME)] allowed Wu *et al*. to synthesize and isolate the corresponding complex **31** (Scheme 8).[15] Complex **31** presents a square-planar coordination geometry around the Ni(II) center, with the PNP ligand acting as a chelate, the coordination sphere of the metal being completed by two bromine atoms. The structural parameters of **31** are similar to those in its Pd(II) and Pt(II) analogues and are detailed in Table 6. Complex **31** was found to be diamagnetic, due to retention of its square-planar geometry in solution, and this allowed recording its ^{31}P NMR spectrum, which displays a single

peak at 52.3 ppm (Table 6). Complex **31** was used as precatalyst in ethylene oligomerization and its performances will be discussed in section 11.1. To evaluate the effect of the *N*-substituent in this catalytic process, the authors also attempted to isolate an analog of **31** with a longer spacer between the aromatic ring and the PNP moiety, *i.e.* a CH_2CH_2 group instead of CH_2. Unfortunately, this ligand could not be isolated, due to its rapid oxidation during purification by column chromatography in air.

In 2009, Liu *et al*. described the use of ligand **28** to model the diiron sub-unit center of the H-cluster of the enzyme [Fe-Fe]-hydrogenase. In Nature, this active site is formed by two low oxidation state iron atoms, bridged by three dithiolate ligands and coordinated with three carbonyl and two cyanide ligands, with an additional water molecule or an hydroxide. As described in Scheme 8, the authors used ligand **28** to displace two CO ligands in the model, and at the same time, to introduce an internal base (pyridyl substituent), whose presence is known to produce dynamic interactions, *e.g*. H transfer from internal base to the diiron center.[16] Liu *et al*. were thus able to isolate and characterize two Fe-Fe complexes **32** and **33** and describe their protonating and electrochemical mechanism by using IR spectroscopy, cyclic voltammetry and digital simulating techniques. The ^{31}P NMR spectra of **32** and **33** were found to be very similar and exhibited a single resonance at 121.9 and 120.0 ppm, respectively, due to their electronic and structural similarity. The solid-state molecular structure of complex **33** was confirmed by XRD studies and the P-M bond lengths were found in the range of the other structurally characterized metal complexes of ligand **28**, while the PNP angle was found larger (119.4(2)°) due to the fact that in this case, the PNP ligand acts as a bridge (Fe-Fe 2.481(11) Å) instead of a chelate (Table 6).

In bioinorganic chemistry, metal complexes able to form complementary hydrogen bonds represent an ever-increasing important class of compounds in the development of biochemically active molecules. With the aim to produce original compounds with antiviral or anticancer activity, Woollins *et al*. described the synthesis of the new functionalized DPPA-type ligand **34**, which resulted from the aminolysis of a functionalized adenine derivative (Figure 1).[17] The authors reported compound **34** as a byproduct of the targeted compound; however its ^{31}P NMR data were provided and the PNP fragment resonates as a singlet at *ca*. 64 ppm (Table 6). The coordination chemistry of **34** was not investigated.

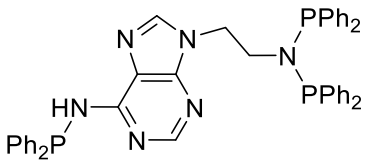

34

Figure 1. Adenine-based DPPA-type ligand **34**.

Table 6. ^{31}P NMR data and characteristic structural parameters of the free ligands **24**, **28** and **34** and metal complexes **25**-**26** and **29-33**.[a]

	δ (mult.)[b]	P-N	P-M	PNP	PMP	Ref.
24	59.0 (s)					[9]
25	95.0 (s)	1.726	2.483	103.5[c]	66.0[c]	[9]
26	84.0 (s)					[10]
28	62.6 (s)					[14]
29	34.2 (s)	1.705	2.228	100.2(1)	71.85(2)	[14]

30	20.2 (s)	1.717	2.208	99.4(4)	71.49(4)	[14]
31	52.3 (s)	1.692	2.122	97.7(2)	73.80(5)	[15]
32	121.9 (s)					[16]
33	120.0 (s)	1.727	2.202	119.4(2)		[16]
34	64 (s)[d]					[15]
	27 (s)[e]					

[a] Chemical shifts, P-N (aver.) and P-M (aver.) bond lengths and PNP and PMP angles given in ppm, Å and deg, respectively, [b] in $CDCl_3$, [c] average, [d] corresponds to the PNP fragment, [e] corresponds to the PNH fragment, the authors do not provide high precision values.

2.5. Other *N*-containing functional groups

Recently, Roesky *et al*. described the synthesis of the *N*-functionalized DPPA-type ligand **35**, the diazenyl analog of the amino derivative **8** (Scheme 9).[18] Ligand **35** exhibits a singlet resonance in its ^{31}P NMR spectrum at 69.0 ppm (in $CDCl_3$), which is consistent with the value found for **8** (69.3 ppm in $CDCl_3$, Table 1). Reaction of **35** with 2 equiv. of the gold(I) precursor [AuCl(THT)] afforded the corresponding dinuclear complex **36** (Scheme 9). The latter exhibits a singlet resonance at 88.3 ppm in its ^{31}P NMR spectrum ($CDCl_3$). In the solid-state, complex **36** crystallizes in the monoclinic space group $P2_1/n$, while the azo function adopts an *E* configuration. The gold(I) centers were found in a typically linear coordination geometry with P-N and P-Au bond lengths in the usual ranges (aver. 1.704 and 2.235 Å, respectively), while the PNP angle is quite large (123.4(4)°), due to the bridging mode adopted by the ligand, which support an aurophilic interaction (Au•••Au 3.0095(7) Å).[19,20]

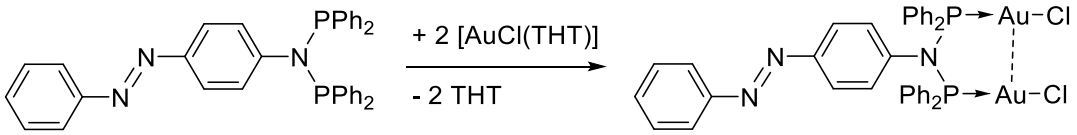

35 **36**

Scheme 9. DPPA-type ligand **35** functionalized with a diazenyl function and its dinuclear Au(I) complex **36**.

Another example of DPPA-type ligand integrating a *N*-morpholinyl group (**82**), *i.e.* a N- and O- donor function, was reported and it is discussed in Section 3.1.

3. Oxygen-based donor

3.1. Ether group

Furane derivatives

In 2009 Wu *et al.*[15] reported the synthesis of the *N*-furfuryl functionalized DPPA-type ligand **37** (Scheme 10). Due to the short spacer between the PNP moiety and the additional donor group, this type of functionality is not expected to be involved in the coordination sphere of the metal center coordinated to the DPPA fragment (intramolecular interaction – scorpionate-type ligand), however it may play a role during a catalytic process by stabilizing active and/or low-valent species in an intermolecular fashion. In its ^{31}P NMR spectrum, ligand **37** exhibits a single peak at 63.2 ppm (Table 7). With the aim to develop a new precatalyst for ethylene oligomerization, the authors synthesized the Ni(II) complex **38** by reaction of ligand **37** with [$NiBr_2$(DME)] in a 1:1 molar ratio (Scheme 10). Complex **38** was found to be diamagnetic in solution, allowing the recording of its ^{31}P NMR spectrum, exhibiting a singlet signal at 52.4 ppm (Table 7). The structure of complex **38** was confirmed in the solid-state by XRD analysis, revealing a Ni(II) center in square planar coordination geometry, forming a four membered chelate ring (NiP_2N) with ligand **37**. The P-N (aver. 1.694 Å), P-M (aver. 2.128 Å) bond lengths and PNP (97.83(11)°) and PMP (73.74(3)°) angles were found in line with other [NiX_2(PNP)]

complexes (Table 7 *vs*. *e.g*. Table 6). As for the *N*-pycolyl derivatives (see above) the short spacer between the PNP fragment and the additional donor did not lead to coordination of the latter, either in solution or in the solid-state, although intermolecular coordination could have been conceivable. The catalytic performances of complex **38**, in ethylene oligomerization with MAO or $EtAlCl_2$ as co-catalyst, are discussed in Section 11.1.

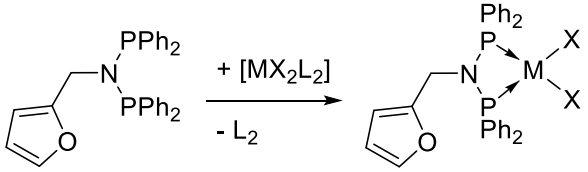

37

38: M = Ni, X = Br
39: M = Pd, X = Cl
40: M = Pt, X = Cl
41: M = Pt, X = Me

Scheme 10. *N*-furfuryl-functionalized DPPA-type ligand **37** and its group 10 metal complexes **38-41**. Note: L_2 = COD for Pd and Pt, and DME for Ni.

More recently, Aydemir *et al*. reported the synthesis of a variety of other group 10 metal complexes supported by the DPPA-type ligand **37**. Simple reaction of an equimolar amount of the latter with $[MX_2L_2]$ (M = Pd, Pt; X = Cl, Me, L_2 = COD, DME) precursors led to the formation of the corresponding complexes $[MX_2(\mathbf{37})]$ (**39**: M = Pd, X = Cl; **40**: M = Pt, X = Cl; **41**: M = Pt, X = Me;) (Scheme 10).[21] The dichloride complexes exhibited typical (see *e.g*. Table 6) singlet resonances in their ^{31}P NMR spectra at 33.2 ppm for **39** and at 19.3 ppm for **40**, along with a $^1J_{P,Pt}$ = 3301 Hz. It is noteworthy that the nature of the X ligands in $[MX_2(PNP)]$-type complexes strongly affects their ^{31}P NMR spectra, as illustrated with complex **41**, which is an analog of **40** with X = Me instead of Cl, for which the PNP fragment resonates as a singlet signal at 50.6 ppm with a $^1J_{P,Pt}$ value of 1546 Hz (Table 7). The expected square planar coordination

geometry around the metal center, as well as the chelating coordination mode of the DPPA-type ligand, could be confirmed in the solid-state by XRD on complexes **39** and **40**. The P-N (aver. 1.695 Å (**39**) and 1.698 Å (**40**)) and P-M (aver. 2.221 Å (**39**) and 2.203 Å (**40**)) bond lengths and PNP (100.5(3)° (**39**) and 100.3(3)° (**40**)) and PMP (72.3(1)° (**39**) and 72.8(1)° (**40**)) angles were found in the range of analogous group 10 metal complexes (Table 7 *vs*. Table 6). Complexes **39**-**41** have been evaluated as catalysts in Suzuky cross-coupling reactions and the results will be discussed in Section 11.1.

Aydemir and Baysal *et al*. also reported the synthesis of Rh(I) and (III) and Ru(II) metal complexes of the functionalized DPPA-type ligand **37** (Scheme 11). While the reaction of ligand **37** with the $[Rh(COD)_2]BF_4$ cationic precursor, in a 2:1 ligand/metal ratio, led to the mono-cationic Rh(I) bis-chelate complex **42**,[22] the mono-chelate half-sandwich Rh(III) (**43**) and Ru(II) (**44**) complexes were obtained by reacting ligand **37** with $[RhCl(\mu\text{-}Cl)Cp^*]_2$ and [RuCl(Cp*)(COD)] in 1:1 ligand/metal ratio, respectively (Scheme 11).[23]

The Rh complexes **42** and **43** exhibited both typical ^{31}P NMR doublet resonances, due to Rh-P coupling, centered at 69.0 and 70.5 ppm, respectively, with each a $^1J_{P,Rh}$ coupling constant of 120 Hz. In contrast, the Ru(II) complex **44** exhibited a singlet signal at 92.0 ppm for the equivalent P-atoms of the N-functionalized ligand **37** (Table 7). All these Rh and Ru complexes were evaluated in catalytic transfer hydrogenation of ketones and the results will be discussed in Section 11.1.

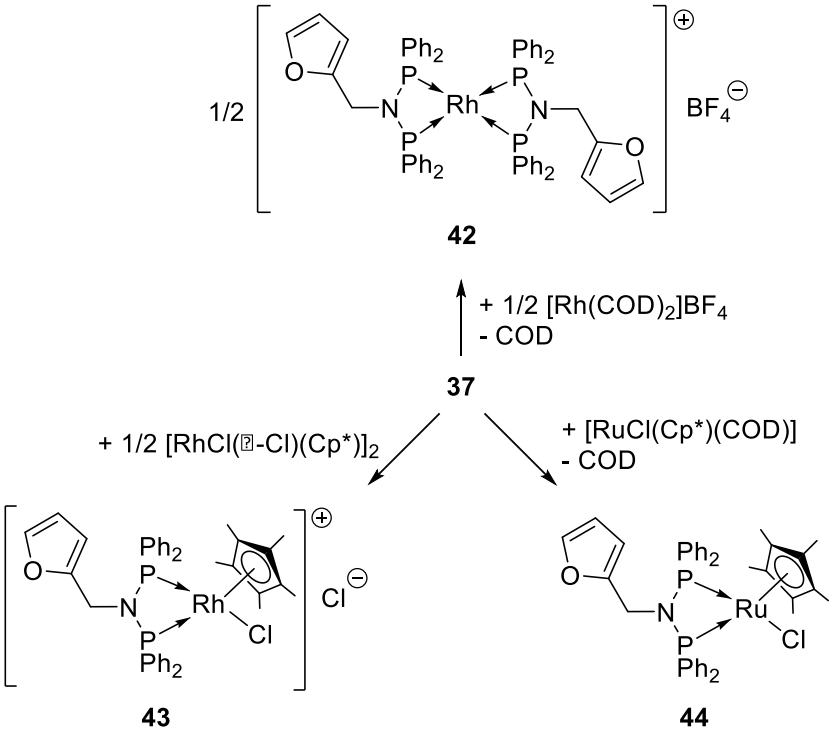

Scheme 11. Synthesis of Rh(I) and (III) and Ru(II) complexes of ligand **37**.

Table 7. ^{31}P NMR data and characteristic structural parameters of the free ligand **37**, and metal complexes **38**-**44**.[a]

	δ (mult.)	$^1J_{P,M}$	P-N	P-M	PNP	PMP	Ref.
37	63.2 (s)[b]						[15]
38	52.4 (s)[b]		1.694	2.128	97.83(1)	73.74(3)	[15]
39	33.2 (s)[c]		1.695	2.221	100.5(3)	72.3(1)	[21]
40	19.3 (s)[c]	3301	1.698	2.203	100.3(3)	72.8(1)	[21]
41	50.6 (s)[c]	1546					[21]
42	69.0 (d)[b]	120					[22]
43	70.5 (d)[b]	120					[23]

44	92.0 (s)[b]	[23]

[a] Chemical shifts, $^{1}J_{P,M}$, P-N (aver.) and P-M (aver.) bond lengths and PNP and PMP angles given in ppm, Hz, Å and deg, respectively, [b] in $CDCl_3$, [c] d_6-DMSO.

Alkyl and aryl mono-ether moieties

Lin *et al*. reported the novel *N*-aryl-ether DPPA-type ligand [$Ph_2PN(p\text{-}C_6H_4OMe)Ph_2$] (**45**), prepared by the classical aminolysis reaction of *p*-methoxyaniline (Scheme 12).[24] Ligand **45** exhibits in its ^{31}P NMR spectrum a singlet resonance at 70.0 ppm. Reaction of the latter with $NiCl_2$ afforded the distorted square-planar (XRD evidence) complex **46** in moderate yield, which presents a characteristic ^{31}P NMR singlet at 47.6 ppm (Scheme 12 and Table 8). Combined with MAO as co-catalyst, this complex showed a high activity in catalytic vinyl polymerization of norbornene (see Section 11.1).

Smith *et al*. described the formation of the Pd(II) analog complex **47** of **46** by reaction of ligand **45** with the [$PdCl_2$(COD)] precursor (Scheme 12). In solution, complex **47** displayed a singlet at 70.1 ppm in its ^{31}P NMR spectrum, while in the solid-state, its expected distorted square-planar geometry was confirmed by XRD studies, forming a nearly planar four-membered (PdP_2N)-ring (Table 8).[25] The low field chemical shift recorded was assumed to be due to the electron-withdrawing inductive effect of the aryl-ether ring. Complex **47** was found to be an active catalyst in the hydroformylation of 1-octene (see Section 11.1).

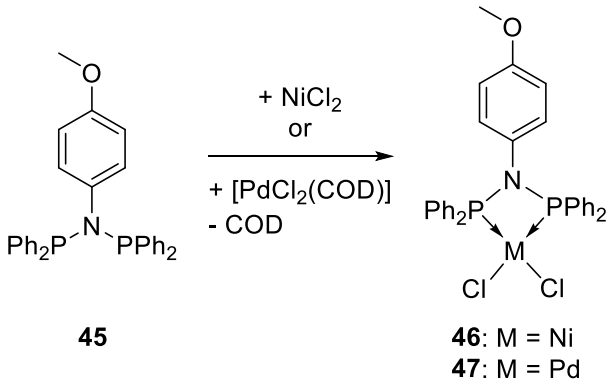

Scheme 12. Synthesis of group 10 metal complexes **46** and **47** of ligand **45**.

Bercaw *et al*. reported a study on the tail-influence of various R-OMe functionalized DPPA-type ligands in the chromium-catalyzed tri- and tetramerization of ethylene (**48**-**51**, Scheme 13).[26] These ligands were obtained by the classical aminolysis route and exhibited ^{31}P NMR singlet resonances in the region 63.1-65.5 ppm (Table 8). The electron-withdrawing effect of the substituents and of their position can be illustrated by the difference in chemical shift between ligands **50** (65.5 ppm) and **45** (70.0 ppm, described above), which are formally *ortho*- and *para*-substituted isomers. Reactions between ligands **48**-**51** and $[CrCl_3(THF)_3]$ led to the formation of the chloro-bridged dinuclear Cr(III) complexes **52**-**55**, on the basis of the solid-state molecular structure of **52**, which was established by XRD studies. The metal center was found in a octahedral coordination geometry, with the PNP ligand acting as a chelate and occupying one apical and one equatorial sites, resulting in a strong distortion away from a regular octahedron (Cl_{apical}-Cr-P_{apical} < 180° and Table 8). In the presence of MAO as co-catalyst, the (PNP)Cr(III) complexes **52**-**55** were found to be efficient catalysts for the selective tri- and tetramerization of ethylene (see Section 11.1).

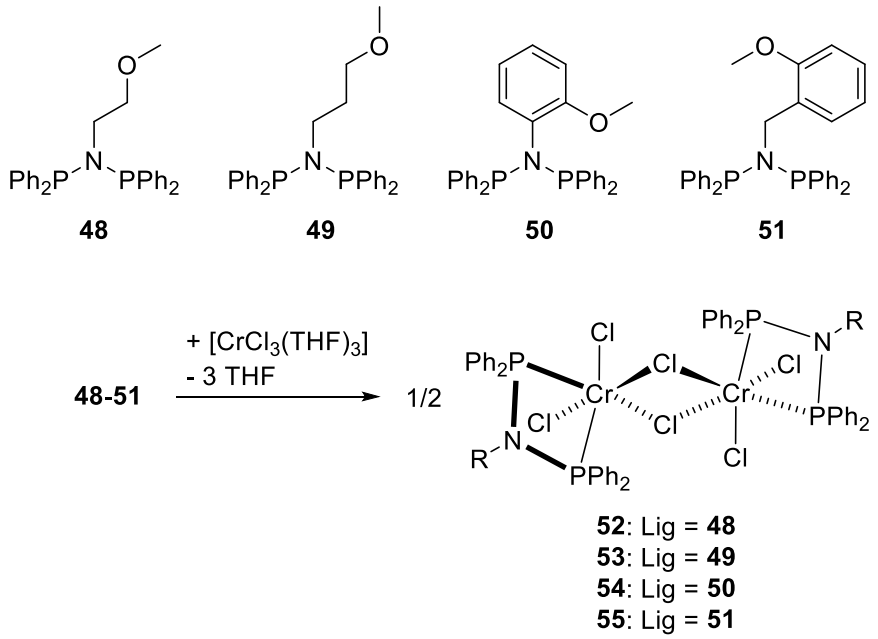

Scheme 13. *N*-ether-functionalized DPPA-type ligands (**48**-**51**) and synthesis of their corresponding Cr(III) complexes **52**-**55**.

Slawin *et al*. extensively studied the coordination chemistry of the *N*-functionalized DPPA-type ligand **50**, towards Mo(0), Ru(II), divalent group 10 and monovalent group 11 (d^{10}) metal centers (Scheme 14).[27] Equimolar reactions between ligand **50** and [MX_2(COD)] precursor complexes (M = Pd, Pt; X = Cl, Me) afforded the corresponding [MX_2(**50**)] complexes **56**-**58** (Scheme 14). While the Pd(II) complex **56** exhibited a singlet resonance in its ^{31}P NMR spectrum at 37.9 ppm, both Pt(II) complexes **57** and **58** displayed a single peak flanked with satellites, due to P-^{195}Pt coupling, at 22.6 ($^1J_{P,Pt}$ = 3343 Hz) and 52.0 ppm ($^1J_{P,Pt}$ = 1607 Hz), respectively (Table 8). The solid state molecular structure of complex **56** was determined by XRD analysis and confirmed the expected distorted square-planar geometry around the Pd(II) center, due to the bite-angle imposed by the DPPA-type chelating ligand (Table 8).

Reaction of ligand **50** with 1 equiv of $[Mo(CO)_4(NBD)]$ resulted in the displacement of the labile NBD ligand and the formation of the octahedral Mo(0) complex **59**, in which the ligand acts as a chelate, occupying two equatorial coordination sites, while four CO ligands complete the coordination sphere of the metal. The ^{31}P NMR spectrum of complex **59** contains a single signal at 92.4 ppm. The neutral Ru(II) bis-chelate complex **60** was obtained from $[Ru(p\text{-Cym})(\mu\text{-Cl})Cl]_2$ (89% yield) or $[RuCl_2(DMSO)_4]$ (33% yield), in a 2:1 ligand/metal molar ratio. Complex **60** has been characterized in the solid state by single crystal XRD analysis and presents an octahedral Ru(II) center bis-chelated by two mutually *trans* PNP ligands **50**, and two axial chlorines complete the metal coordination sphere. The reaction between ligand **50** (2 equiv) and $[Cu(NCMe)_4]PF_6$ also afforded the mono-cationic bis-chelate complex (**61**) in which the Cu(I) center is in a tetrahedral coordination environment, as deduced from XRD studies. The ^{31}P NMR spectrum of **61** exhibited a broad signal ($\omega_{1/2}$ = 110 Hz) centered at 89.1 ppm. Another d^{10} metal complex of ligand **50** was obtained by reaction of the latter with 2 equiv of the Au(I) precursor [AuCl(THT)]. The proposed dinuclear structure of complex **62**, with two AuCl units bridged by one ligand **50**, was supported by the classical downfield shift of its ^{31}P NMR singlet signal at 84.9 ppm, and the observation of the Au-Cl stretching band at 326 cm^{-1} in its FTIR spectrum.

Scheme 14 summarizes the coordination study realized by Slawin *et al.*, while relevant ^{31}P NMR data and structural parameters are reported in Table 8.

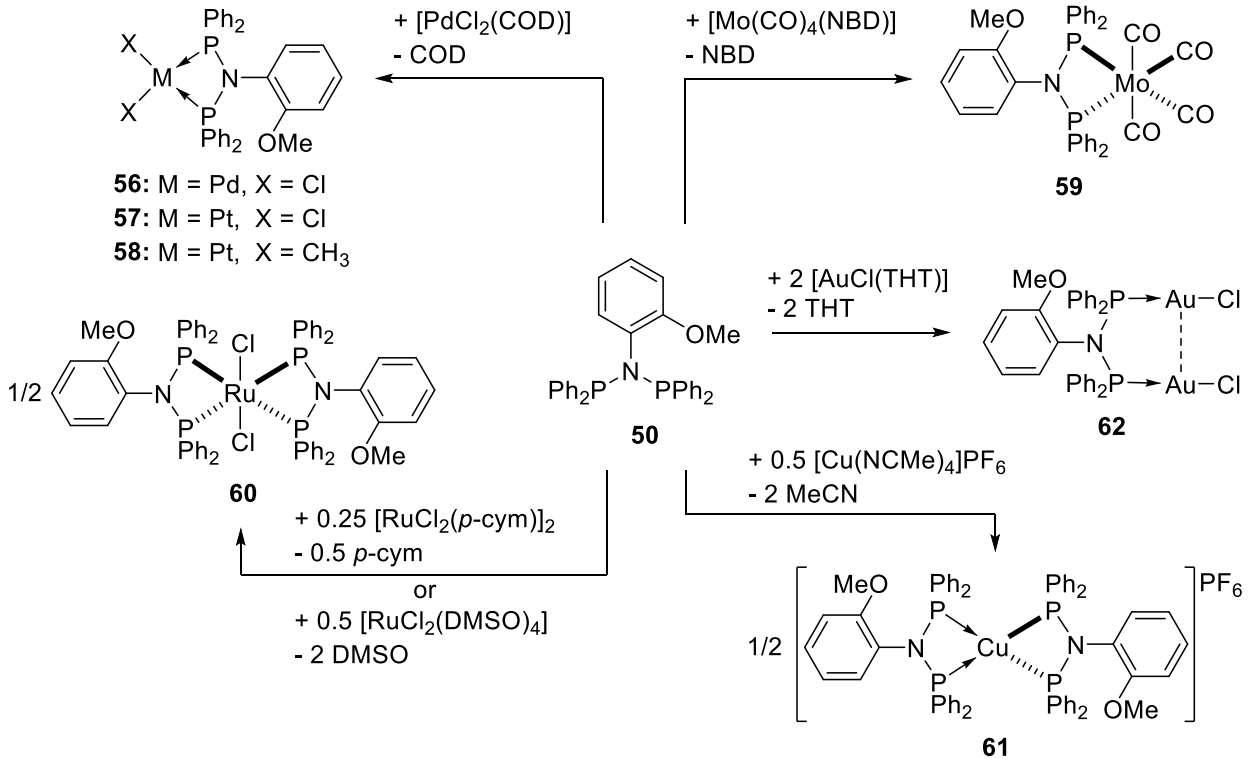

Scheme 14. Study of the coordination chemistry of the *N*-(*ortho*-methoxy)phenyl-functionalized ligand **50** towards various metal centers.

Table 8. ^{31}P NMR data and characteristic structural parameters of the free ligands **45**, and **48**-**51** and metal complexes **46**-**47**, **52** and **56**-**62**.[a]

	δ (mult.)	$^1J_{P,M}$	P-N	P-M	PNP	PMP	Ref.
45	70.0 (s)[b]						[24]
46	47.6 (s)[b]		1.712	2.118	96.3(2)	73.99(5)	[24]
47	71.1 (s)[b]						[25]
48	64.6 (s)[b]						[26]
49	63.1 (s)[b]						[26]
50	65.5 (s)[b]						[26]

51	59.9 (s)[b]						[26]
52			1.705	2.456	105.0(8)		[26]
56	37.9 (s)[b]		1.707	2.214	99.3(2)	71.99(5)	[27]
57	22.6 (s)[b]	3343					[27]
58	52.0 (s)[b]	1607					[27]
59	92.4 (s)[b]		1.729	2.499	103.4(3)	65.78(2)	[27]
60	77.7 (s)[c]		1.734	2.290	101.2(4)	69.84(9)	[27]
61	89.1 (br)[d]		1.718	2.314	106.8(2)	73.19(4)	[27]
					107.1(2)	73.06(4)	
62	84.9 (s)[b]						[27]

[a] Chemical shifts, $^{1}J_{P,M}$, P-N (aver.) and P-M (aver.) bond lengths and PNP and PMP angles given in ppm, Hz, Å and deg, respectively, [b] in $CDCl_3$, [c] $CDCl_3$/MeOH, [d] in $CDCl_3$ for the PNP moiety, and PF_6^- anion at δ = - 144 ppm.

Aryl bis-ether moieties

Biricik *et al*. studied the coordination chemistry, towards d^8 and d^{10} metal centers, of a series of new *N*-aryl-(*bis*-ether)-functionalized DPPA-type ligands of general formula $(Ph_2P)_2N\text{-}C_6H_3\text{-}R$ (R = 3,5-OMe (**63**), 2,5-OMe (**64**), 2,4-OMe (**65**), 3,4-OMe (**66**)) prepared *via* the classical aminolysis reaction of the respective, commercially available, dimethoxyanilines (Scheme 15).[28] The important difference in chemical shifts observed in their ^{31}P NMR spectra (68.6 (**63**), 64.7 (**64**), 66.1 (**65**) and 71.1 (**66**) ppm) illustrates the influence of the substituents position in such *N*-functionalized DPPA-type ligands (Table 9). Equimolar reaction between ligands **63**-**66** and the $[MCl_2(COD)]$ (M = Pt, Pd) precursors afforded the corresponding platinum and palladium dichloride complexes **67**-**70** and **71**-**74**, respectively (Scheme 15). The ^{31}P NMR spectra of the Pt(II) complexes **67**-**70** exhibited each a singlet resonance between 20.0 and 25.3 ppm, flanked by the typical $^{1}J_{P,Pt}$ satellites (3229-3414 Hz) and those of the Pd(II) complexes **71**-**74** displayed a

single peak in the range 34.1-38.2 ppm (Table 9). The expected distorted square-planar coordination geometry around the d^8 metal centers, along with the chelating coordination mode of the PNP ligands were established by XRD studies. Relevant structural parameters are reported in Table 9. The [$PdCl_2$(PNP)] complexes **71**-**74** were evaluated in Heck and Suzuki coupling reactions of aryl bromides with styrene and phenylboronic acid, respectively (see Section 11.1).

Bis-chelated mono-cationic Cu(I) complexes **75**-**78** were synthesized by reaction of [$Cu(NCMe)_4$]PF_6 with ligands **63**-**66** in 1:2 ratio, respectively. Similar ^{31}P NMR spectra were recorded for these four complexes, with a typical singlet resonance in the range 87.6-89.0 ppm (Table 9) and a septet at *ca*. -144 ppm for the counter anion PF_6^-. These data are in agreement with the tetrahedral coordination geometry depicted in Scheme 15 also observed with complex **61** (see above).

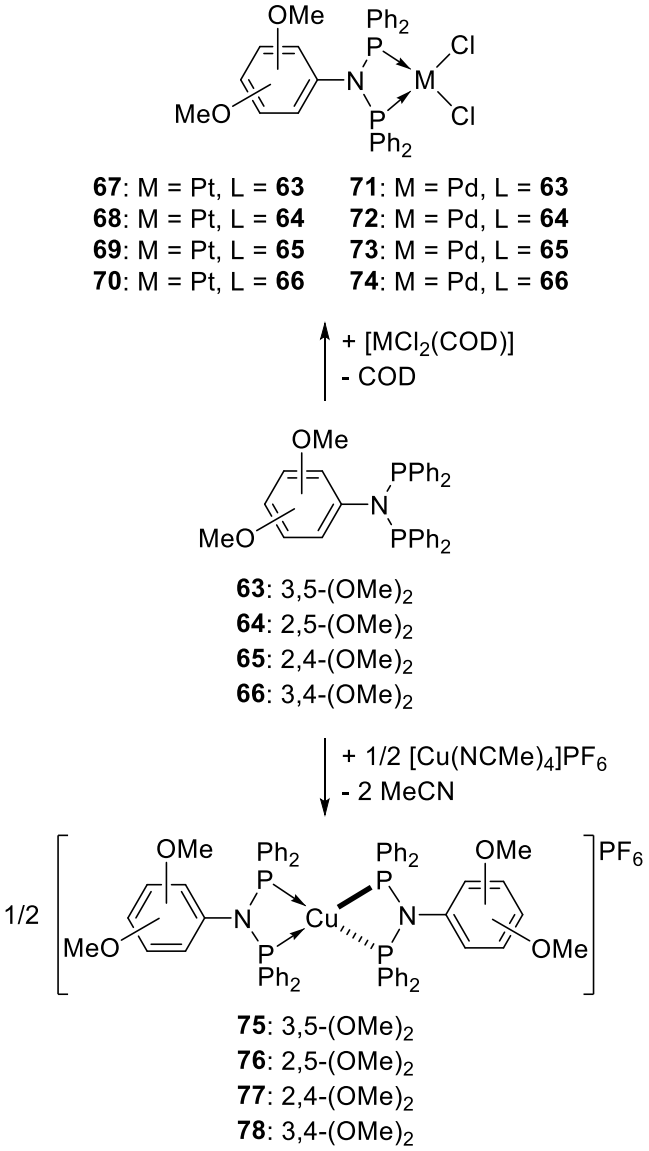

Scheme 15. Synthesis of d^8 (**67**-**74**) and d^{10} (**75**-**78**) metal complexes of ligands **63**-**66**.

Table 9. ^{31}P NMR data and characteristic structural parameters of the free ligands **63**-**66** and Pt(II), Pd(II) and Cu(I) metal complexes **67**-**70**, **71**-**74** and **75**-**78**, respectively.[a]

	δ (mult.)	$^1J_{P,M}$	P-N	P-M	PNP	PMP	Ref.
63	68.6 (s)[b]						[28]

64	64.7 (s)[b]						[28]
65	66.1 (s)[b]						[28]
66	78.1 (s)[b]						[28]
67	20.0 (s)[b]	3414	1.707	2.202	99.6(1)	72.59(3)	[28]
68	22.9 (s)[b]	3344					[28]
69	22.5 (s)[b]	3229	1.717	2.201	98.7(3)	72.54(8)	[28]
70	25.3 (s)[b]	3325					[28]
71	34.1 (s)[b]		1.712	2.221	99.4(2)	71.9(5)	[28]
72	38.2 (s)[b]						[28]
73	37.9 (s)[b]		1.719	2.215	98.8(3)	72.20(6)	[28]
74	34.9 (s)[b]						[28]
75	87.6 (s)[c]						[28]
76	88.8 (s)[c]						[28]
77	89.0 (s)[c]						[28]
78	87.6 (s)[c]						[28]

[a] Chemical shifts, $^{1}J_{P,M}$, P-N (aver.) and P-M (aver.) bond lengths and PNP and PMP angles given in ppm, Hz, Å and deg, respectively, [b] in $CDCl_3$, [c] in $CDCl_3$ for the PNP moiety, and PF_6^- anion at δ = - 144 ppm.

Other N-functional groups containing a R-O-R' moiety

Kayan *et al*. reported the synthesis of the new *N*-methoxyaryl-functionalized bis-DPPA-type ligand **79**, and its corresponding dinuclear Pd(II) and Pt(II) complexes **80** and **81**, respectively. These were obtained by ligand substitution reaction between 1 equiv of the tetraphosphine ligand **79** and 2 equiv of the corresponding $[MCl_2(COD)]$ (M = Pd, Pt) precursor (Scheme 16).[29] The four equivalent P atoms of ligand **79** resonate as a singlet peak at 68.8 ppm in ^{31}P NMR spectrum. The high symmetry of the ligand is maintained in both dinuclear Pd_2 and Pt_2 complexes, which exhibit singlet resonances at 41.4 ppm for **80** and at 19.5 ppm, flanked by

satellites ($^1J_{P,Pt}$ = 3110 Hz), for the Pt complex **81** (Table 10). Both complexes were evaluated as catalysts in the Suzuki cross-coupling reaction of aryl bromides and phenylboronic acid, but only the Pd derivative **80** showed a good activity (see Section 11.1).

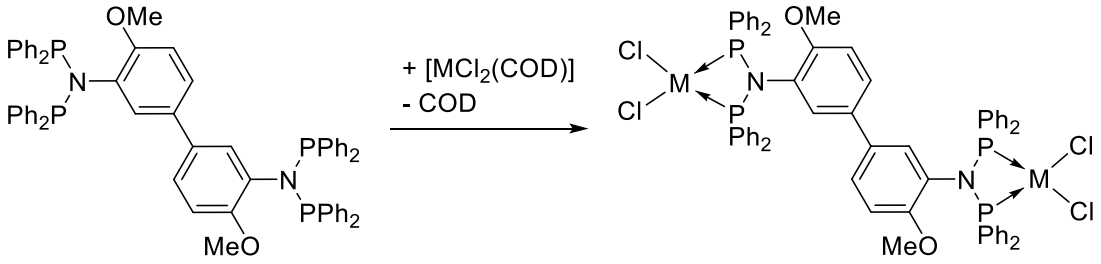

79

80: M = Pd
81: M = Pt

Scheme 16. Ligand **79** and its Pd(II) (**80**) and Pt(II) (**81**) complexes.

Blann *et al*. studied the influence of the ligand-structure, *i.e*. the nature of the *N*-pendant group, on the selectivity of the Cr(III)-catalyzed ethylene tetramerization, and among the ligands used, one of them presented as *N*-substituent a morpholinyl derivative (**82**, Figure 2).[30] The latter DPPA-type ligand exhibited in ^{31}P NMR a singlet signal at 62.6 ppm (Table 10). Metallation of ligand **82**, by addition of 0.33 equiv of [Cr(acac)$_3$], was performed *in situ*, and the mixture was then combined with MAO and used in catalytic ethylene oligomerization (see Section 11.1).

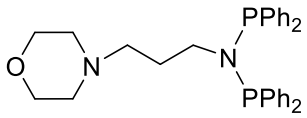

82

Figure 2. Ligand **82**, bearing as *N*-functional group a morpholinyl derivative.

Table 10. ^{31}P NMR data of the free ligands **79** and **82** and the metal complexes **80**-**81**.[a]

	δ (mult.)	$^{1}J_{P,M}$	Ref.
79	68.8 (s)		[29]
80	41.4 (s)		[29]
81	19.5 (s)	3110	[29]
82	62.6 (s)		[30]

[a] Chemical shifts and $^{1}J_{P,Pt}$ given in ppm and Hz, respectively, and spectra recorded in $CDCl_3$.

3.2. Ester group

Aryl ester moieties

Roesky *et al*. reported the synthesis of 5-[*N*,*N*-bis(diphenylphosphanyl)amino] isophthalate (**83**), a DPPA-type ligand functionalized on the N atom by a bis-ester-aryl group, resulting from the aminolysis reaction of dimethyl 5-aminoisophthalate (Scheme 17).[31] Its ^{31}P NMR spectrum exhibited a singlet signal at 69.1 ppm. Ligand **83** was also characterized in the solid-state by XRD analysis and selected bond distances and angles are listed in Table 11. Depending of the metal precursor and the stoichiometry used, two types of Au(I) complexes could be obtained. Reaction between ligand **83** and 2 equiv of [AuCl(THT)] afforded the neutral dinuclear complex **84**, and this resulted, in its ^{31}P NMR spectrum, to a low-field shift of the P resonance to 87.8 (s) ppm for **84** (*vs*. free ligand **83**, Table 11). The equimolar reaction between ligand **83** and the cationic Au(I) precursor $[Au(THT)_2]ClO_4$ resulted in the formation of the dicationic complex **85**, which displayed a similar low-field shift of the ^{31}P NMR resonance of the PNP moiety to 97.9 ppm (*vs*. free ligand **83**, Table 11). Both dinuclear Au(I) complexes were characterized in the solid-state by XRD studies and revealed a typical linear coordination

geometry for the gold(I) centers, *i.e*. P-Au-Cl in **84** and P-Au-P in **85**, with ligand **83** acting as bridging ligand and supporting Au•••Au aurophilic interactions (Au-Au 3.0593(7) and 2.798(2) Å in **84** and **85**, respectively).[19,20] Selected NMR data and structural parameters of compounds **83**-**85** are reported in Table 11.

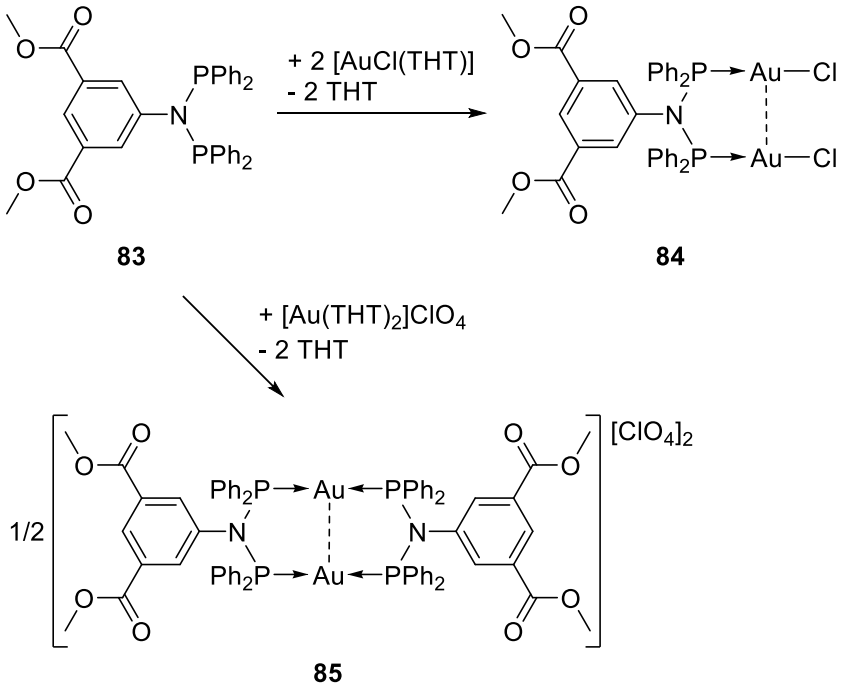

83 **84** **85**

Scheme 17. Synthesis of Au(I) complexes **84** and **85** from ligand **83**.

Smith *et al*. reported the synthesis of two other DPPA-type ligands of general formula $Ph_2P(R)PPh_2$ [R = C_6H_4(3-CO_2Me) **86**, C_6H_4(4-CO_2Me) **87**] (Scheme 18), which carry on their nitrogen atom a mono-ester-aryl function.[32] The latter diphosphine ligands exhibited a single ^{31}P NMR resonance at 69.0 (**86**) and 68.5 (**87**) ppm, very close to that of the bis-ester derivative **83** described by Roesky *et al*. (see above and Table 11).[31] The authors intensively studied the coordination chemistry of ligands **86** and **87**, along with that of ligand **83**, towards the group 10 metal centers of $[MX_2(COD)]$ (M = Pt, Pd, X = Cl, Br, I) (Scheme 18). The difference of ligand

substitution and/or of the halogen nature in the PtX_2 (X = Cl, Br, I) complexes (**88**-**92**) did only slightly affect the chemical shift of the equivalent P atoms of the ligands (17.4-22.5 ppm) and the P-Pt coupling constants (3066 < $^1J_{Pt,P}$ < 3339 Hz) in their ^{31}P NMR spectra, however the overall trend of the magnitude of the Pt-P magnetic coupling in complexes **88**, **91**, **92** is consistent with the observation of increasing *trans* influence of the halide on going from Cl > Br > I (Table 11). The $PdCl_2$ complex **93**, analogous to **88**, could be obtained by replacing the platinum(II) precursor by [$PdCl_2$(COD)], and its ^{31}P NMR spectrum exhibited a typical single resonance at 36.1 ppm. Complexes **89** and **92** could be characterized in the solid-state by XRD analysis and confirmed the expected distorted square-planar coordination geometry around the Pt(II) metal center, with the PNP ligand acting as a chelate.

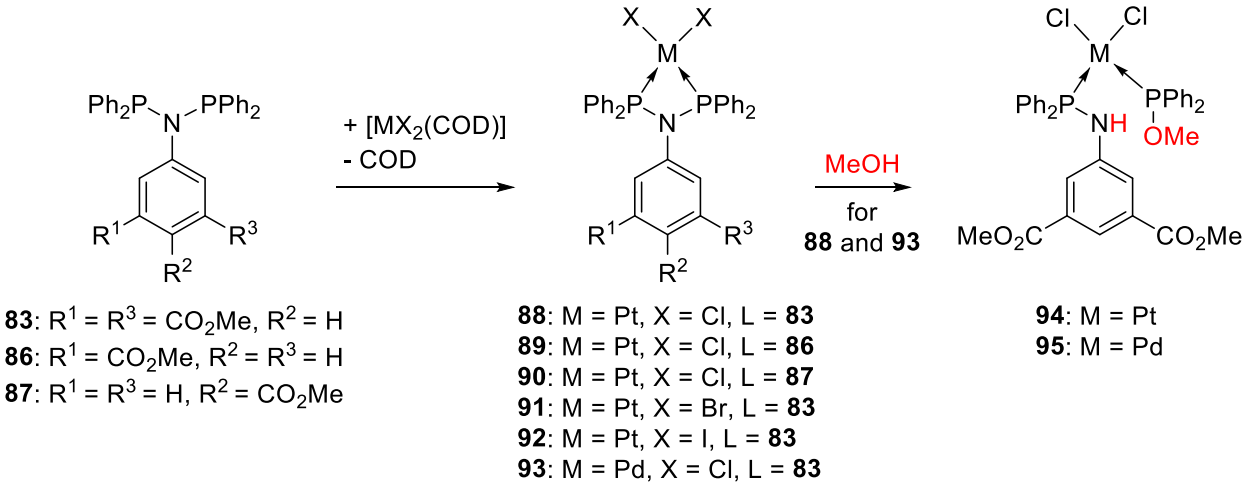

83: $R^1 = R^3 = CO_2Me$, $R^2 = H$
86: $R^1 = CO_2Me$, $R^2 = R^3 = H$
87: $R^1 = R^3 = H$, $R^2 = CO_2Me$

88: M = Pt, X = Cl, L = **83**
89: M = Pt, X = Cl, L = **86**
90: M = Pt, X = Cl, L = **87**
91: M = Pt, X = Br, L = **83**
92: M = Pt, X = I, L = **83**
93: M = Pd, X = Cl, L = **83**

94: M = Pt
95: M = Pd

Scheme 18. Synthesis of the Pt(II) and Pd(II) complexes **88**-**93** of the ester-functionalized ligands **83**, and **86**-**87**, and reactivity towards MeOH.

The authors could observe that complexes **88** and **93** react with MeOH at room temperature, leading to clean and selective cleavage of one P-N bond, to afford complexes **94** and **95**,

respectively (Scheme 18).[32] The NMR and structural data of the resulting mono-phosphine-supported Pt(II) and Pd(II) complexes will not be further discussed here.

Table 11. ^{31}P NMR data and characteristic structural parameters of the free ligands **83** and **86**-**87** and the Au(I) (**84**-**85**), Pt(II) (**88**-**92**) and Pd(II) (**93**) complexes.[a]

	δ (mult.)	$^1J_{P,M}$	P-N	P-M	PNP	PMP	Ref.
83	69.1 (s)		1.730		115.6(7)		[31]
84	87.8 (s)		1.711	2.227	118.6(5)		[31]
85	97.9 (s)		1.675	2.234	130.1(1)		[31]
86	69.0 (s)						[32]
87	68.5 (s)						[32]
88	22.5 (s)	3339					[32]
89	21.4 (s)	3334	1.711	2.200	99.1(5)	72.68(1)	[32]
90	21.3 (s)	3330					[32]
91	21.3 (s)	3260					[32]
92	17.4 (s)	3066	1.712	2.210	100.15(2)	72.89(4)	[32]
93	36.1 (s)						[32]

[a] Chemical shifts, $^1J_{P,M}$, P-N (aver.) and P-M (aver.) bond lengths and PNP and PMP angles given in ppm, Hz, Å and deg, respectively, and spectra recorded in $CDCl_3$.

Alkyl ester moieties

Beck *et al*. investigated the coordination chemistry of the optically active bis(diphenylphosphino)-α-(*S*)-aminoacid methylester derivatives **96-99**,[33] of general formula $(Ph_2P)_2NCH(R)CO_2Me$ (R = H **96**, Me (*S*) **97**, Bn (*S*) **98**, *i*-Pr (*S*) **99**) towards piano-stool derivatives $[(\eta^5\text{-}C_5H_5)MCl(CO)_3]$ (M = Mo, W) and examined the reactivity of the resulting

complexes (Scheme 19).[34] Initial reactions between these chiral ligands and the metal precursors led to the cationic Mo(II) (**100**-**103**) and W(II) (**104**-**105**) complexes of general formula: [(η^5-C_5H_5)M(CO)$_2$(**L**)]Cl (L = **96**-**99**) by displacement of one carbonyl and one chlorine ligands. The Mo complexes **100** and **102** and the W complexes **104**-**105** could be characterized in solution by ^{31}P NMR spectroscopy, and for all of them a sharp singlet signal was observed. Their chemical shift much depends on the nature of the metal center, since the molybdenum derivatives resonate at 95.2 (**100**) and 101.8 (**102**) ppm and the tungsten complexes at 63.0 (**104**) and 65.9 (**105**) ppm (Table 12). An anion metathesis reaction was performed with the tungsten derivatives **104**-**105**, by reaction with KPF_6, and led to the corresponding salts **106**-**107** (Scheme 19).

Providing energy ($h\nu$ or ΔT) to complexes **100-105** allowed the elimination of 1 more equiv of CO and the re-insertion of the chloride counter-ion into the coordination sphere of metal center, leading to the neutral complexes **108**-**113** (Scheme 19). This complete series of neutral complexes displayed two diastereomers R_MS_C and S_MS_C, which could easily be distinguished by ^{1}H and ^{31}P NMR. The detailed list of the ^{31}P NMR data is provided in Table 19. Noteworthy, the tungsten PF_6 derivatives **106**-**107**, do not exhibit further reactivity even after exposure to higher temperature or light.

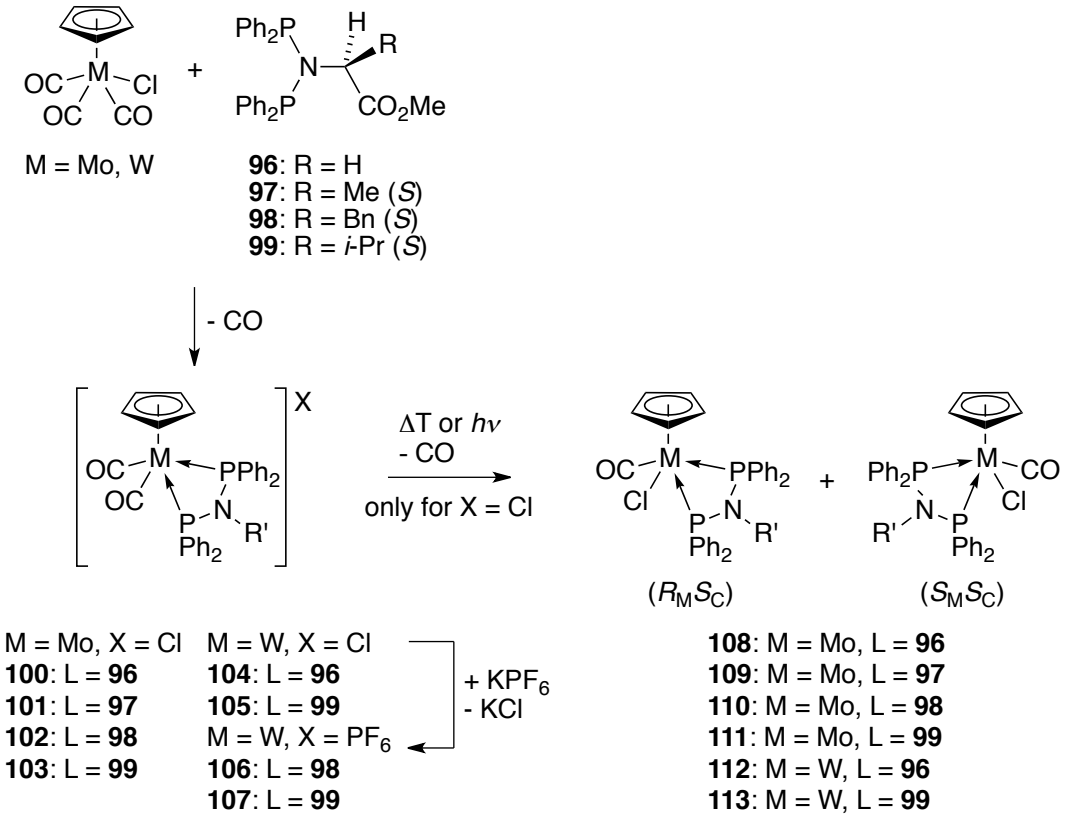

Scheme 19. Synthesis of piano-stool Mo(II) (**100**-**103** and **108**-**111**) and W(II) (**104**-**107** and **112**-**113**) complexes of the chiral ligands **96**-**99**.

Table 12. ^{31}P NMR data of the free ligands **96**-**99**, the cationic Mo (**100**-**103**), W (**104**-**107**) and neutral Mo (**108**-**111**), W (**112**-**113**) complexes.[a]

	δ (mult.)	$^2J_{P,P}$	Ref.
96	66.1 (s)[b]		[33]
97	55.5 (s)[b]		[33]
98	56.5 (s)[b]		[33]
99	56.9 (s)[b]		[33]
100	95.2 (s)[c]		[34]

102	101.8 (s)[b]		[34]
104	63.0 (s)[c]		[34]
105	65.9 (s)[b]		[34]
108	103.3 (d)[c]	118	[34]
	128.2 (d)[c]		
109	101.6 (d)[c]	114	[34]
($R_{Mo}S_c$)	124.7 (d)[c]		
109	102.0 (d)[c]	116	[34]
($S_{Mo}S_c$)	123.9 (d)[c]		
110	106.6 (d)[b]	118	[34]
($R_{Mo}S_c$)	130.7 (d)[b]		
110	107.0 (d)[b]	118	[34]
($S_{Mo}S_c$)	128.8 (d)[b]		
111	104.8 (d)[c]	118	[34]
($R_{Mo}S_c$)	128.2 (d)[c]		
111	105.9 (d)[c]	124	[34]
($S_{Mo}S_c$)	122.9 (d)[c]		
112	73.7 (d)[c]	77	[34]
	92.7 (d)[c]		

[a] Chemical shifts and $^2J_{P,P}$ given in ppm and Hz, respectively, [b] in CH_2Cl_2, [c] in 80% $CDCl_3$ / 20% C_6D_6.

3.3. Other *O*-containing functional groups

Ellermann *et al*. reported an elegant route toward the synthesis of metal carbonyl complexes supported by *N*-functionalized DPPA-type ligands, by direct reaction of preformed metallated and lithiated [$M(CO_4)(Ph_2P)_2NLi$] (M = Cr **114**, Mo **115**, W **116**) derivatives with benzoyl chloride (Scheme 20).[35] The resulting complexes [$M(CO_4)(Ph_2P)_2NC(O)Ph$] (M = Cr

117, Mo **118**, W **119**) were characterized by ^{31}P NMR spectroscopy, and displayed singlet resonances at 119.5 (in CD_2Cl_2), 93.4 ppm (in 80% CH_2Cl_2/20% d_6-acetone), for the Cr(0) and the Mo(0) derivatives, respectively, while the W(0) complex exhibited a singlet at 70.7 ppm (in 80% CH_2Cl_2/20% d_6-acetone) flanked by two satellites ($^1J_{W,P}$ = 222 Hz). The authors assumed that this DPPA functionalization required preliminary metallation.

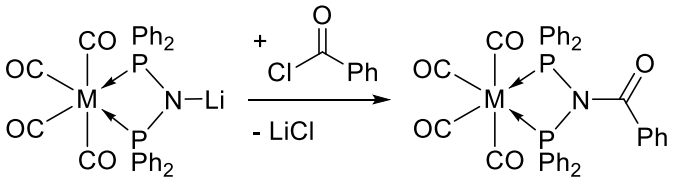

114: M = Cr
115: M = Mo
116: M = W

117: M = Cr
118: M = Mo
119: M = W

Scheme 20. Post-metallation functionalization of DPPA with benzoyl chloride, to form complexes **117-119**.

4. Phosphorus-based donors

4.1. Phosphino groups

In their study of the post-metallation functionalization of lithiated DPPA derivatives of the type $[M(CO_4)(Ph_2P)_2NLi]$ (M = Cr, **114**; Mo, **115**; W, **116**), Ellermann *et al*. reported the formation of *N*-phosphino-functionalized DPPA-type ligands, by reaction of complexes **114**-**116** with an equimolar amount of $ClPPh_2$. The corresponding complexes $[M(CO_4)(Ph_2P)_2NPPh_2]$ (M = Cr, **120**; Mo, **121**; W, **122**) were isolated (Scheme 21).[35] Complexes **121** and **122** were characterized by ^{31}P NMR. The Mo(0) species **121** presented an A_2X spin system, resulting in one doublet signal centered at 102.9 ppm for the two equivalent P atoms coordinated to the metal

center (PNP chelate moiety), coupled ($^2J_{P,P}$ of 22 Hz) to the free phosphorus donor which appeared as a triplet resonance at 76.0 ppm (Table 13). The W(0) complex **122** was found to be a strongly coupled A_2B system, but its signal pattern was not well-resolved, and therefore only a partial description was possible: the A-group of signals was centered at 77.1 ppm while the B-group was centered at 75.7 ppm. The authors could also deduce a $^2J_{P,P}$ coupling constant of 22 Hz, which is in accordance with that measured in **121**, and a $^1J_{W,P}$ of 194 Hz (Table 13).

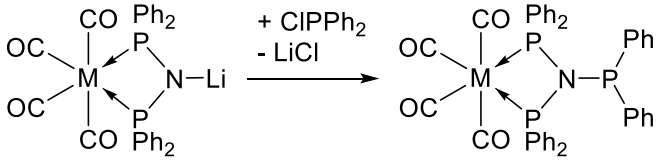

114: M = Cr
115: M = Mo
116: M = W

120: M = Cr
121: M = Mo
122: M = W

Scheme 21. Post-metallation functionalization of DPPA with diphenylchlorophosphine, to form complexes **120-122**.

Bhaduri and Lahiri *et al*. reported the synthesis of ligand **123**, which presents a PNP moiety functionalized on the N atom with a dangling $–CH_2CH_2PPh_2$ group (Scheme 22).[36] The ^{31}P NMR spectrum of this *N*-alkylphosphine-functionalized DPPA derivative presented two singlet signals: one at 60.6 ppm for the two equivalents P atoms (P^1 and P^2) of the PNP moiety and one at -21.8 ppm, attributed to the terminal PPh_2 group (P^3) (Table 13). The solid-state molecular structure of ligand **123** was determined by XRD analysis, and characteristic bond lengths and angles are reported in Table 13. An equimolar reaction of the triphosphine ligand **123** with the $[PdCl_2(COD)]$ precursor afforded the $[PdCl_2(P,P)]$ complex **124**, in which the metal center is chelated by one PPh_2 moiety of the PNP (P^1Ph_2) fragment and the P^3Ph_2 substituent (Scheme 22).

In its ^{31}P NMR spectrum, complex **124** exhibited three inequivalent phophane signals with different multiplicities ($J_{P,P}$ coupling not provided) at 74.1 (dd, P^1), 56.2 (d, P^2) and 19.0 (s, P^3) ppm (Table 13). Single crystals suitable for XRD analysis were grown from a 1:1 MeCN/hexane mixture of **124** over a period of two weeks, and their study revealed the structure of the dinuclear palladium(II) complex **125**, in which an additional [$PdCl_2$(NCMe)] was found coordinated to the remaining P^2Ph_2 group of ligand **123** (Scheme 22). This transformation was assumed to be the consequence of the slow crystallization process in a coordinating solvent (MeCN). Both the Pd(II) centers in the dinuclear complex **125** displayed a typical distorted square-planar coordination geometry, with classical bond lengths and angles (Table 13). The mono-palladium complex **124** was found active in oxidative hydroxylation of arylboronic acids to phenols and the oxidative coupling of arylboronic acids (see Section 11.1).

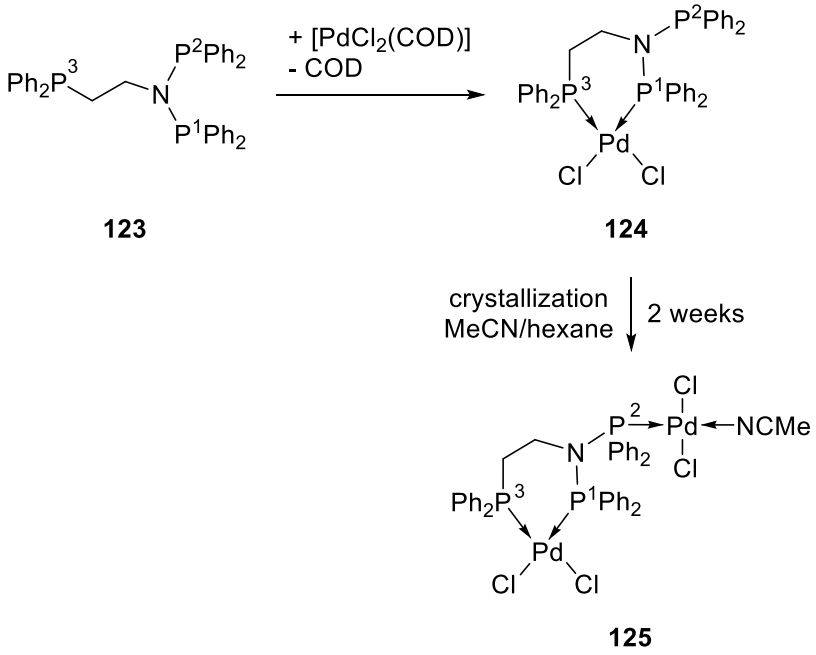

123 **124** **125**

Scheme 22. *N*-alkylphosphino-functionalized DPPA-type ligand **123** and its mono- and dipalladium(II) complexes **124** and **125**, respectively.

4.2. Other *P*-containing functions

Aladzheva *et al*. reported an easy access to the 1,2-azaphophanolanes species (**126**-**129**), by the one-pot reaction between the corresponding 3-halopropylamine hydrohalides and 2 equiv of $ClPPh_2$ in the presence of an excess NEt_3, used as HCl scavenger (Scheme 23).[37] Although these ligands do not present an additional *P*-donor function, they constitute a class of *N*-functionalized DPPA-type ligands, involving a P atom (P_{R4}^+ moiety). The iodide **128** and the perchlorate **129** derivatives could be isolated in good yield (> 80%) and the authors provided their complete FTIR, ^1H and ^{31}P NMR spectroscopic characterization. In particular, the ^{31}P NMR spectrum of **128** exhibited two doublets centered at 44.7 and 64.2 ppm, coupled with a $^2J_{P,P}$ of 67 Hz, while **129** displayed a similar pattern with two doublet resonances centered at 44.8 and 64.1 ppm and a $^2J_{P,P}$ of 67 Hz. Compound **129** could also be characterized in the solid state by single crystal XRD analysis, which revealed notably different P-N bond lengths, N-PPh_2 1.736(3) *vs*. N-$P^+Ph_2CH_2$ 1.636(4) Å, although the P-N-P angle of 123.5(2)° is in the usual range (*vs*. 124.9(5)° for **123**, Table 13).

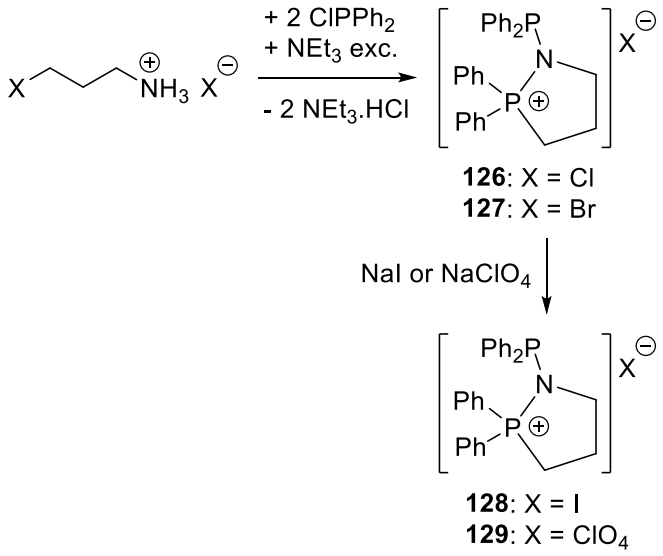

Scheme 23. Synthesis of modified DPPA-type ligands **126**-**129**.

Table 13. ^{31}P NMR data and characteristic structural parameters of the free ligands **123** and **128**-**129** and the metal complexes **121**-**122** and **124**-**125**.[a]

	δ (mult.)	$^2J_{P,P}$	$^1J_{P,M}$	P-N	P-M	PNP	PMP	Ref.
121	102.9 (d)[b]	22						[35]
	76.0 (t)[b]							
122	77.1 (br)[b]	22	194					[35]
	75.7 (br)[b]							
123	60.6 (s)[c,d]			1.717		124.9(5)		[36]
	-21.8 (s)[c,e]							
124	74.1 (dd)[f]							[36]
	56.2 (d)[f]							
	19.0 (s)[f]							
125				1.719	2.256	124.4(3)	92.15(2)	[36]

128	44.7 (d)[c]	67			[37]
	64.2 (d)[c]				
129	44.8 (d)[c]	67	1.736(3)[g]	123.5(2)	[37]
	64.1 (d)[c]		1.636(4)[h]		

[a] Chemical shifts, $^2J_{P,P}$, $^1J_{P,M}$, P-N (aver.) and P-M (aver.) bond lengths and PNP and PMP angles given in ppm, Hz, Å and deg, respectively, [b] in CD_2Cl_2, [c] in $CDCl_3$, [d] for the equivalent P^1 and P^2, [e] for P^3, [f] d_6-DMSO see attribution in the text, [g] N-PPh_2 fragment, [h] N-$P^+Ph_2CH_2$ fragment.

5. Sulfur-based donor

Thiophene derivatives

Wu *et al*. reported the synthesis of two DPPA-type ligands functionalized with *N*-methyl-2-thiophene (**130**) and *N*-ethyl-2-thiophene (**131**) pendant groups (Scheme 24).[15] Both amino-phosphine ligands exhibited a singlet resonance in their ^{31}P NMR spectra at 62.7 and at 63.2 ppm, respectively (Table 14). Reaction of the latter PNP ligands **130**-**131** with [$NiBr_2$(DME)], in a 1:1 molar ratio, afforded the neutral, diamagnetic and square-planar complexes **132**-**133**, respectively, as deduced from their ^{31}P NMR (52.4 (s) and 48.8 (s) ppm, respectively) data and single-crystal XRD analysis (Scheme 24 and Table 14). All main structural parameters were found to be in the range of other [NiX_2(PNP)] complexes. Both nickel(II) complexes are active catalysts in ethylene oligomerization, after prior activation with Et_2AlCl as co-catalyst (see Section 11.1).

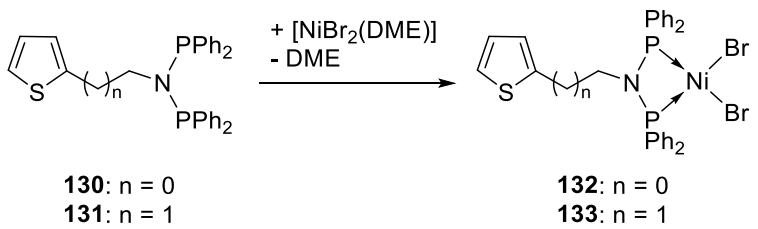

130: n = 0
131: n = 1

132: n = 0
133: n = 1

Scheme 24. *N*-thiophene-functionalized DPPA-type ligands **130**-**131** and their $NiBr_2$ complexes **132**-**133**.

In the early 2010's, Aydemir *at al*. intensively studied the coordination chemistry of ligand **130** towards ruthenium and rhodium precursors with the aim to produce new catalytic species for the transfer hydrogenation of aromatic ketones (see Section 11.1).[22-23,38] Reaction of the *N*-thiophene-functionalized DPPA-type ligand **130** with $[RuCl(\mu\text{-}Cl)(\eta^6\text{-}p\text{-}Cym)]_2$ in a 4:1 ligand/metal ratio afforded the neutral complex **134**, in which the Ru(II) center was found in an octahedral coordination geometry, bis-chelated by two PNP ligands **130** in *trans* position, and occupying the basal positions, while two chlorine ligands complete the coordination sphere of the metal in the apical positions (XRD proof, Scheme 25 and Table 14). The ^{31}P NMR spectrum of complex **134** exhibited a singlet resonance at 78.0 ppm for the four equivalent P atoms. The crystallization process of a solution of **134** also afforded few crystals of its *cis* isomer **134'** suitable for XRD studies, and selected bond distances and angles are reported in Table 14. Reaction of ligand **130** with an equimolar amount of $[RuCl(\mu\text{-}Cl)(\eta^6\text{-}p\text{-}Cym)]_2$ led to the mono-cationic chelate complex **135**, which exhibits a characteristic singlet resonance at 88.2 ppm in its ^{31}P NMR spectrum. The PNP ligand **130** has displaced one chlorine atom from the coordination sphere of the metal center, to allow the latter to adopt its preferred coordination geometry (Scheme 25).

When the cationic $[Rh(COD)_2]BF_4$ precursor was reacted with 2 equiv of ligand **130**, the mono-cationic tetrahedral complex **136**, displaying a typical doublet centered at 68.9 ppm with a $^1J_{Rh,P}$ of 119.9 Hz in its ^{31}P NMR spectrum, was generated (Scheme 25, Table 14).

Baysal *et al*. also synthesized the half-sandwich cationic Rh(III) (**137**) and neutral Ru(II) (**138**) complexes of the chelating ligand **130**, by reaction of the latter with 0.5 equiv $[Rh(Cp^*)(\mu\text{-}Cl)Cl]_2$ or 1 equiv [RuCl(Cp*)(COD)], respectively. Both complexes **137** and **138** were characterized in solution by ^{31}P NMR spectroscopy, and exhibited, respectively, a doublet

resonance centered at 71.4 ppm with a $^{1}J_{Rh,P}$ of 119.9 Hz, and a singlet signal at 92.6 ppm (Scheme 25, Table 14).

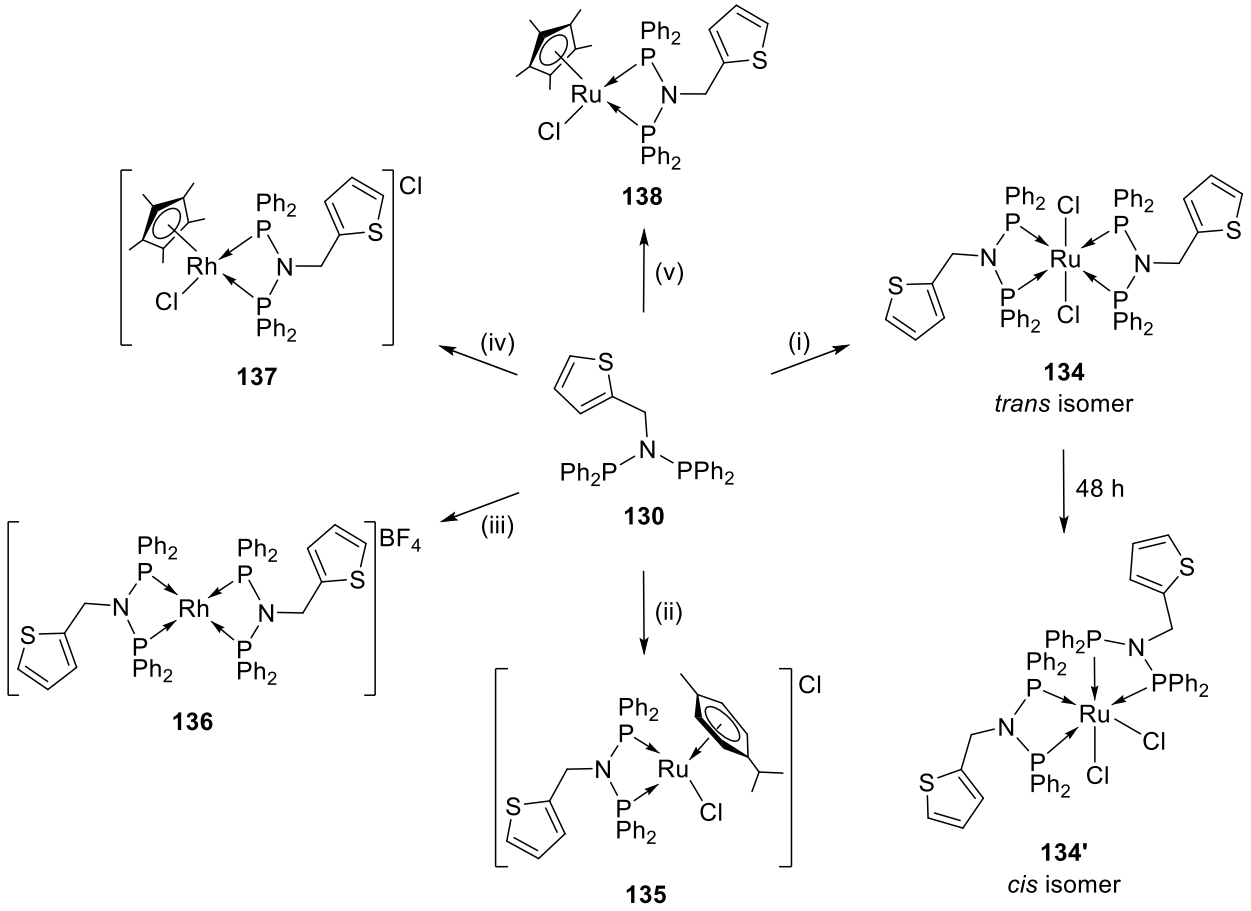

Scheme 25. Ruthenium and rhodium complexes of the *N*-thiophene-functionalized DPPA-type ligands **130**. Reagents: (i) 0.25 equiv $[RuCl(\mu\text{-}Cl)(\eta^6\text{-}p\text{-}Cym)]_2$, (ii) 0.5 equiv $[RuCl(\mu\text{-}Cl)(\eta^6\text{-}p\text{-}Cym)]_2$, (iii) 0.5 equiv $[Rh(COD)_2]BF_4$, (iv) 0.5 equiv $[Rh(Cp^*)(\mu\text{-}Cl)Cl]_2$, (v) 1 equiv [RuCl(Cp*)(COD)].

Table 14. ^{31}P NMR data and characteristic structural parameters of the free ligands **130**-**131** and the metal complexes **132**-**138**.[a]

	δ (mult.)	$^1J_{P,Rh}$	P-N	P-M	PNP	PMP	Ref.
130	62.7 (s)		1.669				[15]
131	63.2 (s)						[15]
132	52.4 (s)		1.685	2.126	98.0(2)	73.47(6)	[15]
133	48.8 (s)		1.701	2.122	96.4(1)	73.39(3)	[15]
134	78.0 (s)		1.718	2.338	101.5(3)	69.39(6)	[38]
134'			1.726	2.309	100.4	70.65	[38]
135	88.2 (s)						[38]
136	68.9 (d)	120					[22]
137	71.4 (d)	120					[23]
138	92.6 (d)						[23]

[a] Chemical shifts, $^1J_{P,Rh}$, P-N (aver.) and P-M (aver.) bond lengths and PNP and PMP angles given in ppm, Hz, Å and °, respectively, and spectra recorded $CDCl_3$. (Sigma) value not given if average value.

Alkyl and aryl thioether moieties

Smith *et al*. described the synthesis of the novel octadentate 1,2,4,5-$\{(Ph_2P)_2NCH_2CH_2SCH_2\}_4C_6H_2$ (**137**) ligand, which consists in four independent DPPA units connected to a phenyl ring by four thioether-based spacer ($CH_2CH_2SCH_2$) (Scheme 26).[39] Its ^{31}P NMR spectrum exhibited a singlet resonance at 101.3 ppm and confirmed the equivalence of the eight P atoms. The authors synthesized the tetranuclear Mo(0) complex **138**, by reacting the octopodal ligand **137** with 4 equiv [$Mo(CO)_4$(NBD)]. The four equivalent [$Mo(CO)_4$(PNP)] fragments resonate as a sharp singlet at 95.0 ppm in its ^{31}P NMR spectrum (Table 15).

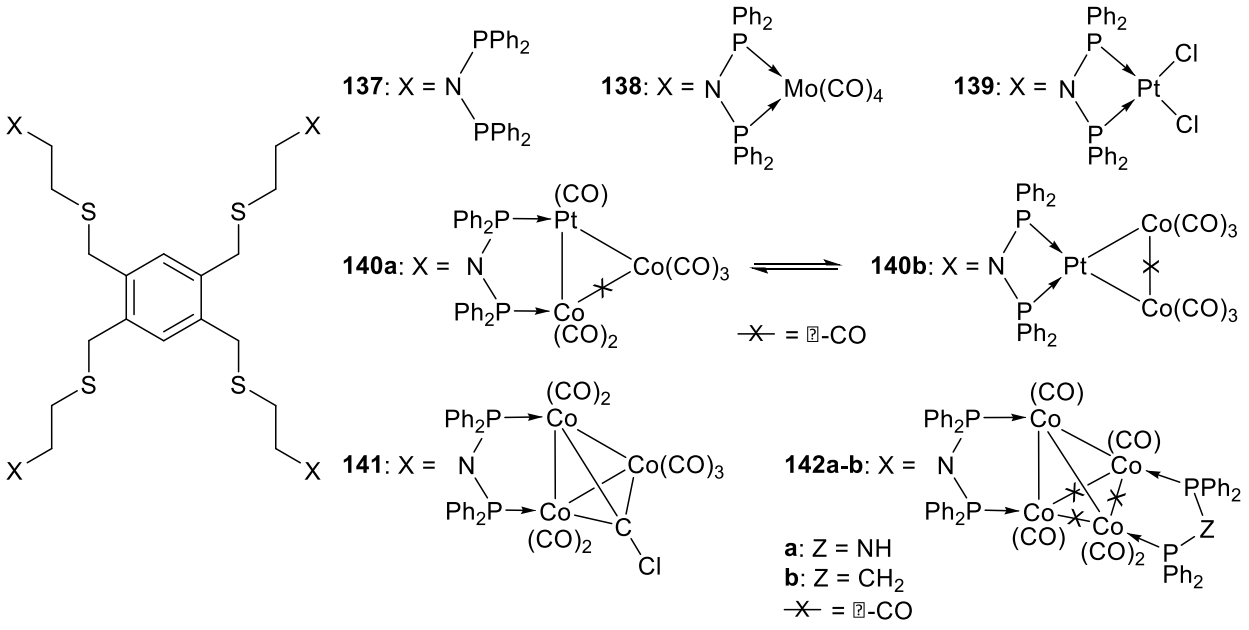

Scheme 26. Octopodal *N*-thioether-functionalized DPPA-type ligand **137** and its mono- (**138**-**139**) and polynuclear metal complexes (**140**-**142**).

Braunstein *et al*. further studied the coordination chemistry of ligand **137**, with the objective of stabilizing mixed Co/Pt molecular clusters.[40] The authors first synthesized the tetranuclear Pt(II) complex **139**, by reaction of the tetra-DPPA-type ligand **137** with 4 equiv of $[PtCl_2(COD)]$ (Scheme 26). The ^{31}P NMR spectrum of the former complex exhibited a singlet resonance at 17.3 ppm, flanked with $^{1}J_{Pt,P}$ = 3298 Hz satellites, while as expected its ^{195}Pt NMR spectrum displayed a triplet resonance at -4028 ppm ($^{1}J_{P,Pt}$ = 3298 Hz, Table 15). Complex **139** was then further reacted with 8 equiv $Na[Co(CO)_4]$, to afford the polynuclear mixed Pt/Co complex **140**. Multinuclear (^{31}P, ^{195}Pt) NMR spectroscopic analyses performed on the latter were consistent with the presence of two isomers (**140a**-**b**), in which four PNP moieties stabilize four Co_2Pt heterotrinuclear clusters in a bridging (**140a**) or chelating (**140b**) mode (Scheme 26). The ^{31}P

NMR spectrum of a solution of complex **140** exhibited a broad signal at 100.0 ppm for the Co-bound *P* atom and a doublet centered at 71.0 ppm ($^2J_{P,P}$ = 23 Hz), flanked by ^{195}Pt satellites ($^1J_{P,Pt}$ = 3629 Hz) and a singlet with ^{195}Pt satellites at 56.0 ppm ($^1J_{P,Pt}$ = 3010 Hz), corresponding to the Pt-bound *P* atom in the bridged (**140a**) and chelate (**140b**) forms, respectively. Accordingly, the ^{195}Pt NMR spectrum presented a broad doublet at -4129 ppm ($^1J_{P,Pt}$ = 3629 Hz) and a triplet at -4330 ppm ($^1J_{P,Pt}$ = 3010 Hz) for isomers **140a** and **140b**, respectively (Table 15).

As an alternative route to building stepwise the **137**-supported clusters, Braunstein *et al*. reacted the $[Co_3(\mu_3\text{-CCl})(CO)_9]$ precursor with ligand **137**, in a 4:1 ratio, respectively, which afforded the desired "cluster of clusters" **141**. The latter presented, in its ^{31}P NMR spectrum a singlet signal at 109 ppm, for the eight equivalent P atoms (Table 15). The solid-state structure of **141** was established by XRD analysis, and each PNP fragment bridges one edge of each Co_3 triangle, which is capped by one μ_3-CCl group (selected bond distances and angles listed in Table 15).

While the reaction of ligand **137** with $[Co_4(CO)_{12}]$ afforded a mostly insoluble material, which could correspond to a polymeric species, a higher selectivity in the displacement of CO ligands was achieved with the precursor $[Co_4(CO)_{10}(\mu\text{-DPPZ})]$ (Z = A or M). Therefore, the authors could produce selectively the tetra-(Co_4) "cluster of clusters" **142a**-**b**, in which each DPPA fragments of ligand **137** bridges one edge (one basal Co and the apical Co) of each $[Co_4(CO)_8]$ tetrahedron (XRD proof for **142a**, Table 15). The quadrupolar nature of the Co center was responsible of a broadening of the NMR signals, which prevented their complete assignment.

Mastrorilli and Braunstein *et al*. reported the synthesis of two *N*-thioether-functionalized DPPA-type ligands **143** and **144**, which presented both the same typical ^{31}P NMR resonance, as singlet signal, at 62.9 ppm (Scheme 27, Table 15).[41] Since the corresponding amines were not

commercially available, these precursors have been synthesized by derivatization of 2-aminoethanethiol with the relevant alkyl halide, followed by classical aminolysis.

The product of the equimolar reaction between ligands **143** and **144** with [$PtCl_2$(COD)] was found to be dependent of the velocity of the addition of the ligand to the metal precursor. Rapid addition of a solution of ligand **143** to a solution of [$PtCl_2$(COD)] only afforded the di-cationic and bis-chelated [Pt(**143**)$_2$]Cl_2 (**145**) species, along with 1 equiv of unreacted metal precursor (Scheme 27). Complex **145** was characterized in solution by multinuclear NMR analysis: its ^{31}P NMR spectrum displayed a characteristic singlet signal at 29.7 ppm flanked with Pt-P satellites ($^1J_{Pt,P}$ = 2373 Hz), while the ^{195}Pt NMR spectrum confirmed bis-chelated nature of the complex with the presence of a quintet at -4383 ppm with a $^1J_{P,Pt}$ of 2373 Hz (Table 15). The absence of absorption bands corresponding to Pt-Cl stretching vibrations in the FTIR spectrum of **145** confirmed its ionic nature. In solution in dichloromethane, complex **145** slowly isomerizes into the bridged dinuclear complex **146** (Scheme 27). ^{31}P NMR spectra of the aged solution showed the progressive disappearance of the signals relative to **145** with a concomitant growing of an AA'XX' spin system ascribable to **146**, where A (65.6 ppm) corresponds to the P atom of the bridging ligands and X (42.4 ppm) to that of the chelating ligands. The observation of a triplet of triplets signal centered at -4682 ppm with $^1J_{P(A),Pt}$ of 2698 Hz and $^1J_{P(X),Pt}$ of 1908 Hz in the ^{195}Pt NMR spectrum of **146** was also in agreement with the proposed structure (Table 15).

However, when a solution of ligand **143** or **144** was added dropwise, over a period of at least 2 h, to an equimolar amount of [$PtCl_2$(COD)], the desired [$PtCl_2$(PNP)] complexes **147** and **148** were isolated, respectively (Scheme 27). Multinuclear NMR spectroscopy of the latter complexes were fully consistent with the proposed structure, especially the singlet resonances at 17.8 (**147**) and 17.7 (**148**) ppm, in their ^{31}P NMR spectra, and the triplet signals centered at -4037

(**147**) and -4038 (**148**) ppm, in their ^{195}Pt NMR spectra, in each case surrounded by $^{1}J_{Pt,P}$ of 3304 (**147**) and 3308 (**148**) Hz (Table 15). Complex **147** was also characterized in the solid-state single crystal XRD analysis and exhibited the typical distorted square-planar coordination geometry around the metal center, with ligand **143** acting as a chelate, and the bond distances and angles were found in the typical range (Table 15).

According to the calculations performed by the authors, complex **147** presented a P.C.C.% (percentage pyramidal character) of 17.7%, which indicates an higher ring strain in the latter compared to *e.g.* [$PtCl_2$(DPPA-Me)] (9.2%) and [Pt(DPPA-Me_2)]$^{2+}$ (14.6%). This data suggests that the thermodynamically stable complex **146** (presenting ligand **143** in both chelating and bridging modes) results from the compromise between the strong tendency of ligand **143** to act as a chelate, demonstrated by the inevitable formation of **145** (rapid addition) and **147** (slow addition), and the high ring strain imposed by the chelation.

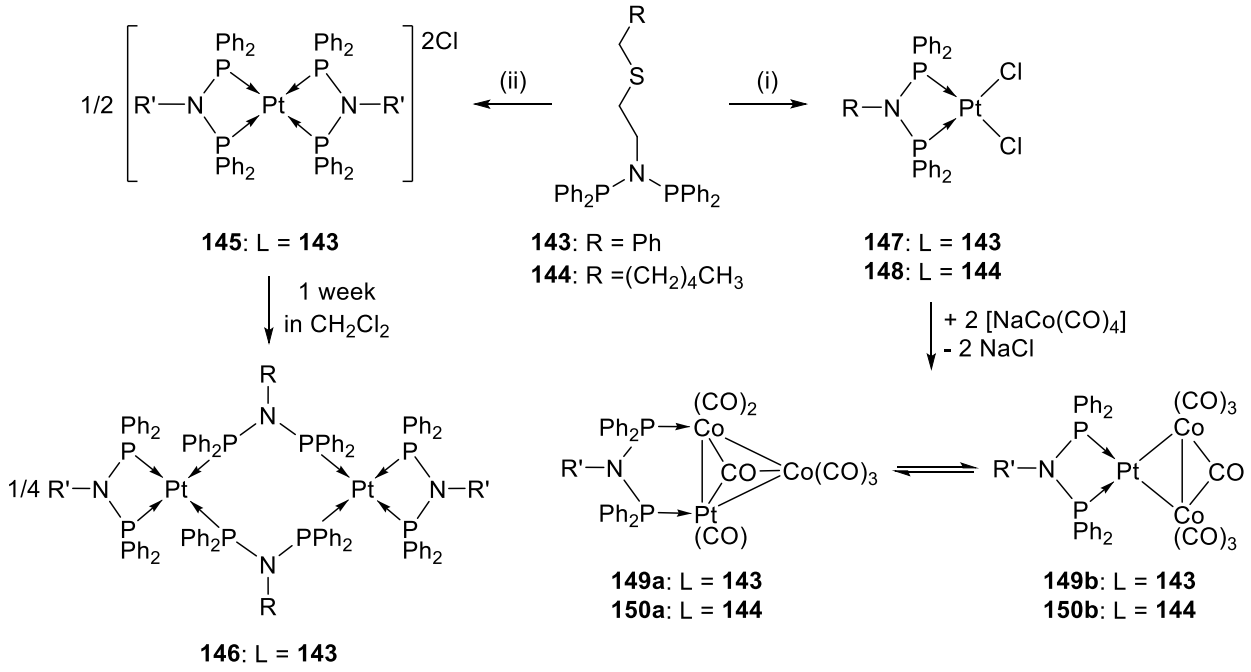

Scheme 27. Reactivity of the *N*-tioether-functionalized DPPA-type ligands **143**-**144** towards [$PtCl_2$(COD)] (**145**-**148**), and PNP-supported mixed Pt/Co molecular clusters (**149**-**150**). Conditions: (i) 1 equiv [$PtCl_2$(COD)] added dropwise over 2 h, (ii) 1 equiv [$PtCl_2$(COD)] added by parts.

Reaction of the $PtCl_2$ complexes **147**-**148** with 2 equiv of [$NaCo(CO)_4$] led to the formation of the heterobimetallic Co_2Pt clusters **149**-**150**, respectively (Scheme 27). Both clusters present a dynamic behavior in solution, due to an equilibrium between a bridging (**149a**-**150a**) and a chelating (**149b**-**150b**) coordination fashion of the ligands. The ^{31}P NMR spectra of the **a**-type isomers presented a broad signals at 99.5 (**149a**) and 98.4 (**150a**) ppm, corresponding to the Co-bound P atom, and a higher field doublet resonance at 70.3 ($^2J_{P,P}$ of 26 Hz, **149a**) and 69.5 ($^2J_{P,P}$ = 28 Hz, **150a**) ppm, flanked with satellites corresponding to the Pt-bounded P atom $^1J_{Pt,P}$ of 3604 (**149a**) and 3604 (**150a**) Hz. In contrast, the **b**-type isomers presented only one singlet resonance at 55.2 (**149b**) and 54.3 (**150b**) ppm, with satellites characterized by $^1J_{Pt,P}$ of 3019 (**149b**) and 3015 (**150b**) Hz (Table 15). In their ^{195}Pt NMR spectra, the isomers **149a**-**b** exhibited a doublet of doublets resonance at -4120 ppm ($^1J_{P,Pt}$ = 3589 Hz, $^{2+3}J_{P,Pt}$ = 78 Hz) and a triplet signal at -4325 ($^1J_{P,Pt}$ = 3006 Hz), respectively. Similar patterns were observed for the couple **150a**-**b**, which displayed a double of doublets resonance at -4136 ppm ($^1J_{P,Pt}$ = 3604 Hz, $^{2+3}J_{P,Pt}$ = 80 Hz) for the isomer **a** and a triplet signal at -4333 ($^1J_{P,Pt}$ = 3015 Hz) for isomer **b**. The ratio of the **a**- and **b**-type isomers was found to depend on the temperature and the nature of the solvent. Attempts to crystallize a solution of complex **149** led to suitable crystals for XRD analysis, which revealed the structure of the chelate isomer **149b**. Characteristic P-N, P-Pt bond lengths and PNP and PMP angles were found very close from those in the monometallic complex **147** (Table 15).

Weng and Hor *et al*. described the synthesis of the *N*-3(methylthio)propyl substituted, DPPA-type ligand **151**, along with other *N*-functionalized aminodiphosphines (see Section 9), and synthesized its corresponding Cr(III) complexes (**152**-**154**, Scheme 28).[42] For their studies in selective Cr-catalyzed ethylene teramerization, the authors do not used the isolated Cr complexes, but reacted together [$Cr(acac)_3$] with 2 equiv of the PNP ligand and 440 equiv MAO (see Section 11.1). The *N*-thioether-functionalized ligand **151** was prepared by the classical aminolysis reaction of the corresponding amine and exhibited a characteristic ^{31}P NMR single resonance at 63.5 ppm. Its solid-state molecular structure could be determined by XRD analysis and revealed P-N bond lengths and a PNP angle in the range of the few other DPPA-type ligands structurally characterized (Table 15). Equimolar reaction between ligand **151** and the [$CrCl_3(THF)_3$] precursor led to the displacement of the labile THF ligands and the assumed formation of the neutral dinuclear complex **152**, in which two [$CrCl_2$(**151**)] moieties are connected through two bridging chlorines. The authors assumed that the formation of a halogen-bridged complex with stronger donors such as 4Cl and 2P, was preferred over the coordination of the weak thioether donor, leading to the formation higher nuclearity, or polymeric complexes. Furthermore, the dinuclear complex **152** could readily be converted into the nitrile adducts **153**-**154** (by cleavage of the μ-Cl bridges), by dissolution of the former in the coordinating MeCN and EtCN solvents, respectively. The solid-state molecular structures of complexes **153** and **154** were found to be very similar, with Cr(III) metal centers in a distorted octahedral coordination geometry, the PNP ligand acting as a chelate and occupying two equatorial coordination sites. The two other equatorial sites were occupied by two chlorine atoms, while the nitrile ligand and the last Cl were found on the apical sites. Selected bond lengths and angles are reported in Table 15.

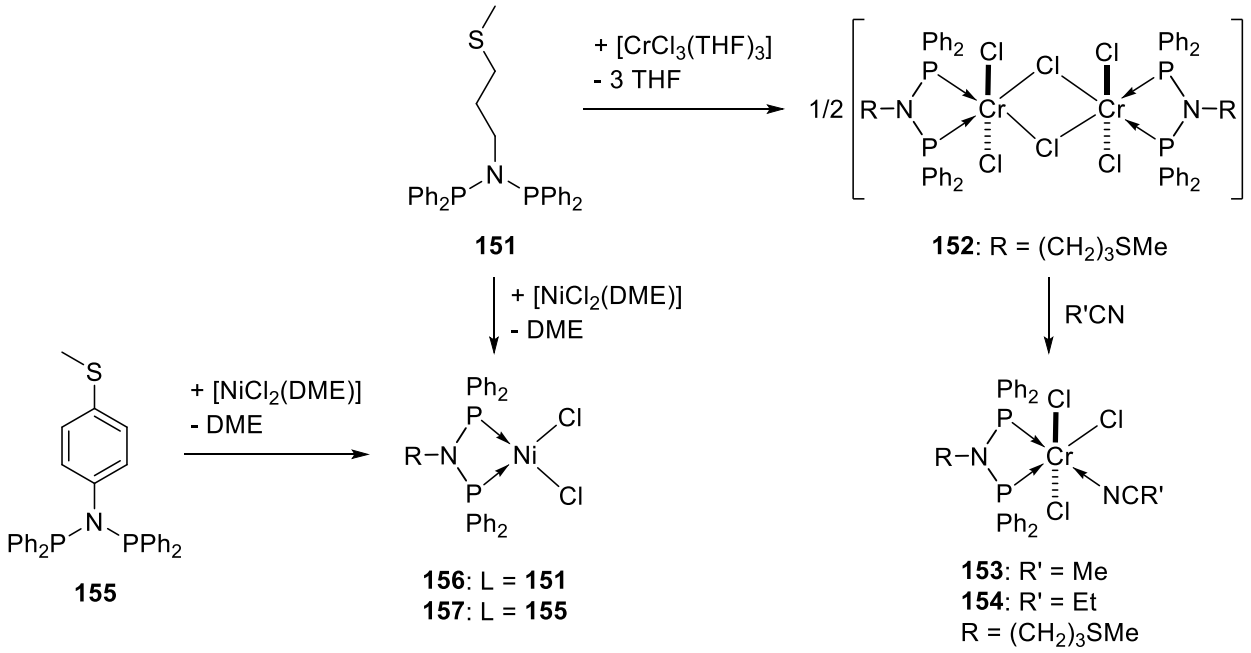

Scheme 28. Synthesis of Ni(II) (**156**-**157**) and Cr(III) (**152**-**154**) complexes of the *N*-thioether functionalized DPPA-type ligand **151** and **155**.

Also targeting potential (pre)catalysts for the selective oligomerization of ethylene, Fliedel and Brauntein *et al*. reported the synthesis of the Ni(II) complexes **156**-**157** of the *N*-alkylthioether-functionalized DPPA-type ligand **151**, developed by Hor *et al*. (see above), and the *N*-arylthioether derivative **155**, respectively (Scheme 28).[43,44] The latter ligand was characterized in solution by a characteristic ^{31}P NMR resonance at 69.36 ppm, and in the solid-state. Its crystal structure presented some original features (*vs*. other structurally characterized *N*-functionalized DPPA-type ligands), especially the orientation of the P lone pairs and Ph rings. Both nickel dichloride complexes were obtained by reaction between the [$NiCl_2$(DME)] precursor and the corresponding PNP ligand, in a 1:1 molar ratio. As deduced from XRD analysis, the

[$NiCl_2$(PNP)] complexes **156**-**157** presented in the solid-state the usual distorted square-planar coordination geometry (selected bond lengths and angles reported in Table 15), leading to diamagnetic species in solution, which displayed in their ^{31}P NMR spectra singlet resonances at 42.9 (**156**) and 45.4 (**157**) ppm. These complexes were found to be, after activation with EADC, active catalysts for the selective oligomerization of ethylene (see Section 11.1).

Motivated by the synthesis of polynuclear complexes that display d^{10}-d^{10} interactions,[20,45] Braunstein *et al*. studied the coordination chemistry of ligands **151** and **155** towards Ag(I) ions, a versatile metal center.[46,47] Equimolar reaction of the latter ligands with $AgBF_4$ afforded the corresponding dicationic, dinuclear complexes **158**-**159** (Scheme 29). Both complexes exhibited in their ^{31}P NMR spectra a similar pattern, *i.e*. two triplets resonances (82.1 and 86.6 ppm for **158**, and 86.3 and 89.8 ppm for **159**) flanking a central broad signal (84.3 ppm for **158**, and 88.0 ppm for **159**). The complexity of this spectrum could originate from an AMM' spin system (A = ^{31}P, M = ^{107}Ag, M' = ^{109}Ag) with the expected mixture of isotopomers in the proportions 26.9 : 49.9 : 23.2 corresponding to $(^{107}Ag)_2$, $2x(^{107}Ag)(^{109}Ag)$ and $(^{109}Ag)_2$, respectively, which is consistent with the presence in solution of dinuclear dinuclear entities. However the broadness of the ^{31}P and ^{1}H NMR signals may suggests a dynamic behavior in solution, involving an equilibrium between species in which the ligand(s) switches from a bridging to a chelating coordination mode with concomitant coordination of the additional thioether donor in the *N*-substituent.[46] Reaction between ligand **159** and $AgBF_4$ in CH_2Cl_2 afforded a mixture of products, and results triggered a series of experiment which are detailed below and Scheme 30.

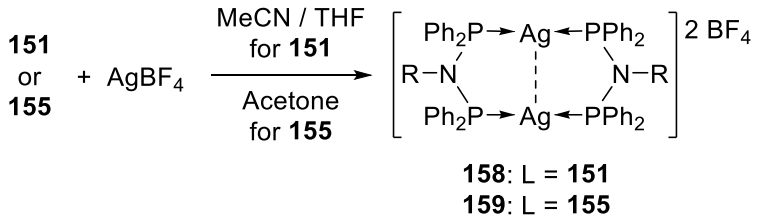

Scheme 29. Equimolar reaction of $AgBF_4$ with the *N*-thioether functionalized DPPA-type ligand **151** and **155**.

Complex **158** crystallizes only in presence of MeCN a coordinating solvent, and a linear coordination polymer is formed in the solid-state (Figure 3A), in which the repeat unit is composed by two dinuclear centrosymmetric $[Ag_2(\mathbf{151})_2(NCMe)_2]$ subunits: "Block A" and "Block B". Each A block is linked to two adjacent B blocks through the thioether functions of its **151** supporting ligands, while in the B blocks, the thioether functions of the ligands remain uncoordinated. It results two different coordination geometries around the Ag metal centers, ignoring the Ag•••Ag interactions, the Ag(I) ions of the block A are in a strongly distorted trigonal planar geometry (N-Ag-P angles of 114.42(9) and 106.73(9)° and P-Ag-P angle of 138.80(3)°) composed of two phosphine donors from two different μ^2-bridging **151** ligands, and one acetonitrile molecule. In contrast, the Ag(I) centers in block B were found in a distorted trigonal pyramidal coordination geometry composed again by two P donors, and one MeCN molecule, and completed by one $S_{thioether}$ donor of an adjacent A subunit (angles: N-Ag-P 14.09(9) and 106.81(9)°, P-Ag-P 138.80(3)° and N-Ag-S 85.18(9)°). In each block (A and B), Ag•••Ag argentophilic interactions were supported by the μ^2-bridging **151** ligands (2.9776(5) and 3.1184(6) Å for blocks A and B, respectively), and the resulting positive charges were balanced by two BF_4^- anions, which do not present any interaction with the metal centers.[46]

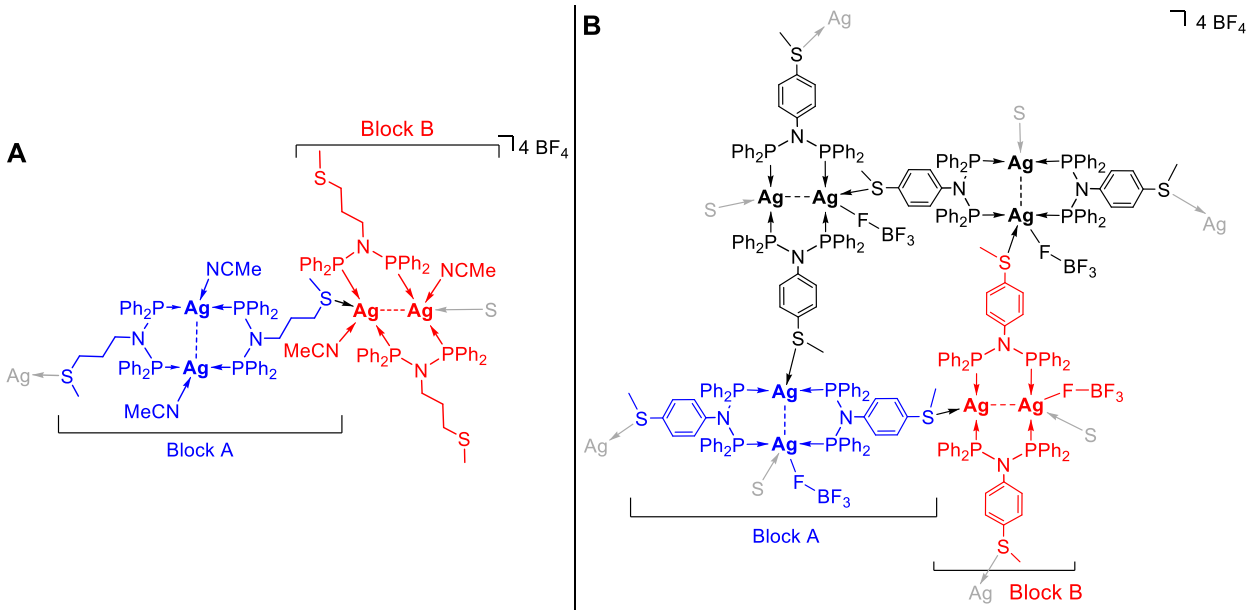

Figure 3. 1D and 2D coordination polymers formed by complexes **158** (A) and **159** (B) in the solid state, respectively.

Complex **159** crystallized as a 2D coordination polymer (XRD proof, Figure 3B), which presented a linear array of blocks A and B, similar to that described for **158**, however in this case the coordinating MeCN solvent was replaced in block A by the dangling aromatic thioether tail of an adjacent block B units, resulting in the formation of second dimension of the structure. Another structural difference with the complex **158** is that in each subunits which compose the solid-state structure of **159**, one BF_4 counter-ion was found in interaction, through one of its F atom, with one Ag(I) ion. Therefore, in this case were found in each A or B block, one Ag(I) center in a distorted trigonal planar geometry (P, P, S ligands) and one in distorted trigonal pyramidal environment (P, P, S, F ligands).[47]

Braunstein *et al*. observed initially that the equimolar reaction of ligand **155** with $AgBF_4$ in CH_2Cl_2 did not led pure **159** (*ca*. 90%), as observed in acetone, but the presence of an additional

species (*ca*. 10%), product of Cl^- abstraction from the solvent was produced (see below and Scheme 30).[46] The formation of the latter and the possible intermediates involved were rationalized by a series of experiments, which allowed the attribution of the different ^{31}P NMR resonances observed (Scheme 30).[47]

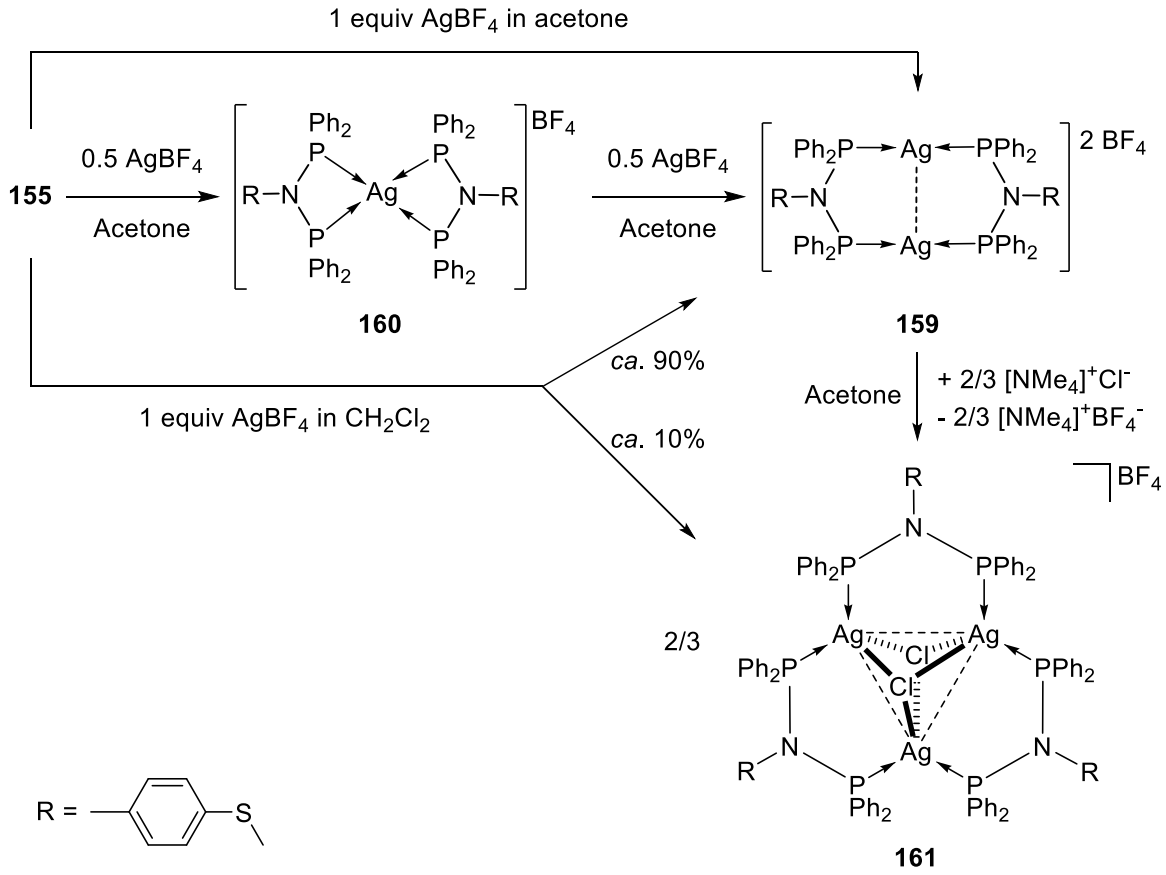

Scheme 30. Stepwise formation of the trinuclear Ag(I) complex **161**, involving the intermediate complexes **159-160**.

All the complexes described in this paragraph were characterized even in solution by multinuclear NMR spectroscopy techniques (^{31}P NMR being the most helpful) and in solid-state

by XRD studies, and selected spectroscopic data, bond distances and angles are reported in Table 15. First of all, reaction of ligand **155** with 0.5 equiv $AgBF_4$ in acetone afforded the tetrahedral bis-chelated cationic complex **160**, which displayed in its ^{31}P NMR spectrum the expected two doublets resonances centered at 98.1 ppm, resulting from the superposition of the P-Ag coupling of both the isotopomers with ^{107}Ag and ^{109}Ag ($^1J_{(107)Ag,P}$ = 222 Hz, $^1J_{(109)Ag,P}$ = 252 Hz) (Scheme 30). These couplings were found consistent with a gyromagnetic ratio $\gamma(^{109}Ag)/\gamma(^{107}Ag)$ = 1.15. Further reaction of complex **160** with 0.5 equiv $AgBF_4$ in acetone resulted in the formation of the dinuclear dicationic complex **159** (see above). Finally, by reacting this complex with 2/3 equiv NEt_4Cl in acetone allowed the quantitative formation of the trinuclear complex **161**, which was initially obtained as side-product in CH_2Cl_2. Its ^{31}P NMR spectrum exhibited two broad quadruplets centered at 77.9 and 74.8 ppm. The molecular structure of complex **161** was confirmed by single crystal XRD analysis and confirmed the formation of a nearly equilateral triangle of distorted tetrahedral Ag(I) cations of which each edge is supported by one ligand **155**, in a μ^2-bridging mode. The Ag•••Ag separations (aver. 3.088 Å) are compatible with the existence of argentophilic interactions. The coordination sphere of the Ag(I) metal centers is completed by two triply bridging chloride ligands, resulting in a trigonal bipyramidal $Ag_3(\mu_3\text{-}Cl)_2$ *core*, while one BF_4^- anion balance the resulting positive charge of the cluster (Scheme 30 and Table 15).[46-47]

Very recently, Braunstein and co-workers also reported a series of bis-chelate dicationic group 10 metal complexes of ligands **151** and **155**. While the Pd(II) derivatives (**162a**-**163a**) were used as "simple and visible" tools for the validation of anchoring of S-functionalized compounds on metal surfaces (see Section 11.2),[48] the Ni(II) species (**162b**-**163b**) were found to undergo CH_2Cl_2 activation in the presence of Zn(0) as reducing agent under smooth conditions.[47] The ^{31}P

NMR spectra of the resulting complexes (**164**-**165**) clearly show the dissymetrization of the PNP ligands and with the formation of one P(V) center and therefore they will not be detailed here. Characteristic NMR and structural data of complexes **162**-**163** are summarized in Table 15.

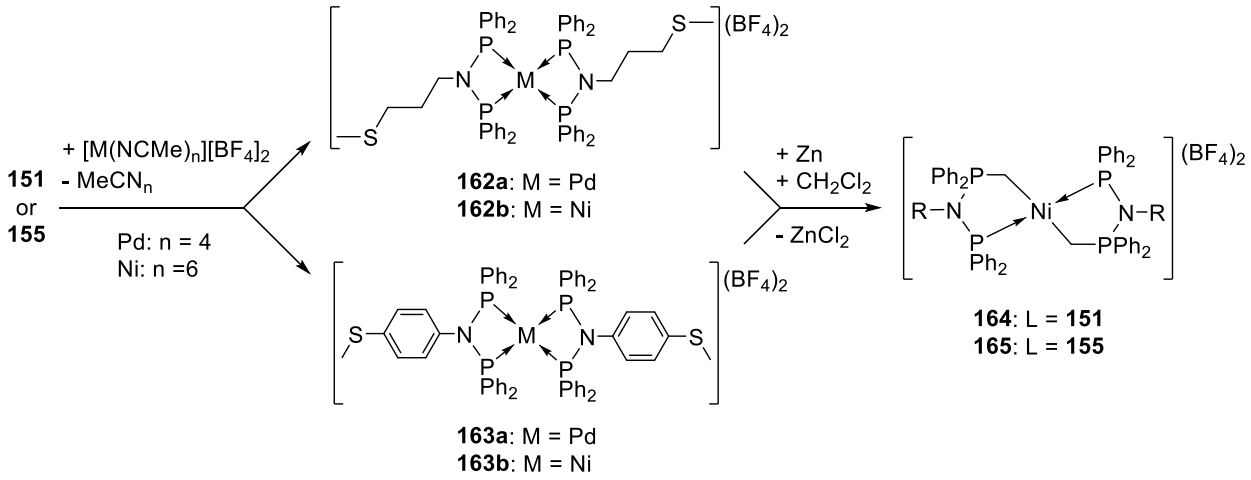

Scheme 31. Bis-chelate dicationic complexes **162-163** of ligands **151** and **155** and reactivity.

Table 15. ^{31}P NMR data and characteristic structural parameters of the free ligands **137**, **143**-**144**, **151** and **155** and the metal complexes and clusters **138**-**142**, **145**-**150**, **152**-**154** and **156**-**161**.[a]

	δ (mult.)	$^2J_{P,P}$	P-N	P-M	M-M'	PNP	PMP	Ref.
137	101.3 (s)[b]							[39]
138	95.0 (s)[b]							[39]
139	17.4 (br) [b]							[40]
140a	100.0 (br)[b]							[40]
	71.0 (d) [b]	23						
140b	56.0 (s)[b]							[40]
141	109.0 (s)[b]		1.702	2.181	2.466	117.96		[40]

142a			1.711	2.173	2.489	118.79		[40]
143	62.9 (s)[b]							[41]
144	62.9 (s)[b]							[41]
145	29.7 (s)[b]							[41]
146	65.6 (AA')[b]							[41]
	42.4 (BB')[b]							
147	17.8 (s)[b]		1.706	2.207		99.34(1)	72.06(3)	[41]
148	17.7 (s)[b]							[41]
149a	99.5 (br)[c]							[41]
	70.3 (d)[c]	26						
149b	55.2 (s)[c]		1.706	2.239	2.5511(7)	100.21(15)	71.53(3)	[41]
					Co-Co			
					2.5426(5)			
					Co-Pt			
150a	98.4 (br)[c]							[41]
	69.5 (d)[c]	28						
150b	54.3 (s)[c]							[41]
151	63.5 (s)[b]		1.719			110.7(3)		[42]
153			1.692	2.480		106.7(4)	66.37(9)	[42]
154			1.699	2.485		105.7(2)	66.01(5)	[42]
155	69.4 (s)[b]		1.730			120.8(1)		[49]
156	42.9 (s)[d]		16.91	2.122		97.59(1)	73.69(3)	[43]
157	45.4 (s)[b]		1.712	2.119		96.70(2)	74.20(6)	[49]
158	86.6 (t)[e]		1.707	2.444	2.9778(3)	116.5		[46]
	84.3 (br)[e]				Block A			
	82.1 (t)[e]				3.1184(6)			
					Block B			

159	89.8 (t)[d]	1.676	2.424	2.933(3)	126.2		[47]
	88.0 (br)[d]			Block A			
	86.3 (t)[d]			and B			
160	98.1 (2 d)[d]	1.721	2.509		109.8(3)	68.51(6)	[47]
161	77.6 (br q)[e]	1.710	2.441	3.088	122.4		[46]
	74.8 (br q)[e]						
162a	48.4 (s)[b]	1.703	2.304		101.48(9)	68.80(2)	[48]
162b	60.8 (s)[d]	1.701	2.189		99.1(2)	72.4(6)	[47]
163a	55.5 (s)[b]	1.711	2.301		102.2(2)	70.77(4)	[48]
163b	69.5 (s)[d]	1.708	2.184		100.02(9)	73.62(2)	[47]

[a] Chemical shifts, $^2J_{P,P}$, P-N (aver.), P-M (aver.) and M-M' bond lengths and PNP and PMP angles given in ppm, Hz, Å and °, respectively. (Sigma) value not given if average value. [b] In $CDCl_3$. [c] In CH_2Cl_2. [d] In CD_2Cl_2. [e] In d_6-acetone.

6. Halogen Functionalization

Braunstein *et al*. reported the synthesis *via* the classical aminolysis reaction of two *N*-bromo-aryl funtionalized DPPA-type ligands, of the type $Ph_2PN(Ar)PPh_2$ (**166**, Ar = *p*-BrC_6H_4; **167**, Ar = *p*-BrC_6H_4-C_6H_4) and studied their coordination chemistry towards group 10 and 11 (single) metal precursors, and Co(0) molecular clusters (Scheme 32).[50] Ligands **166** and **167** exhibited each a characteristic ^{31}P NMR singlet resonance at 70.8 and 69.8 ppm, respectively. As depicted in Scheme 32, their reaction with $[MCl_2(COD)]$ (M = Pd, Pt) precursors, in a 1:1 molar ratio led to the formation of the corresponding awaited neutral, square-planar $[MCl_2(\mathbf{L})]$ complexes **168**-**170**. The ^{31}P NMR spectra of the Pd complexes **168** and **169** presented a single signal at 35.8 and 36.3 ppm while the spectrum of the Pt derivative **170** displayed a singlet at 23.0 ppm flanked with satellites ($^1J_{Pt,P}$ = 3337 Hz, Table 16). The solid-state structures of the Pd complexes **168**-

169 were established by XRD analysis and the characteristic bond distances and angles were found close to similar [(PNP)$PdCl_2$] complexes (Table 16). Mononuclear (**171**) and dinuclear (**172**) complexes of d^{10} ions were obtained by reaction of ligand **166** with [$Cu(NCMe)_4$]PF_6 and [AuCl(THT)], in a 1:2 and 2:1 metal/ligand ratio, respectively (Scheme 32). The resulting [$Cu(\mathbf{166})_2$]PF_6 (**171**) and [$(AuCl)_2(\mu^2$-**166**)] (**172**) complexes were characterized in solution by ^{31}P NMR, and exhibited classical singlet resonances 60.9 and 89.4 ppm, respectively, and the solid-state molecular structure of **172** was confirmed by XRD studies and was found similar to other DPPA-type supported [$(AuCl)_2(\mu^2$-*P*,*P*)] complexes (Table 16).

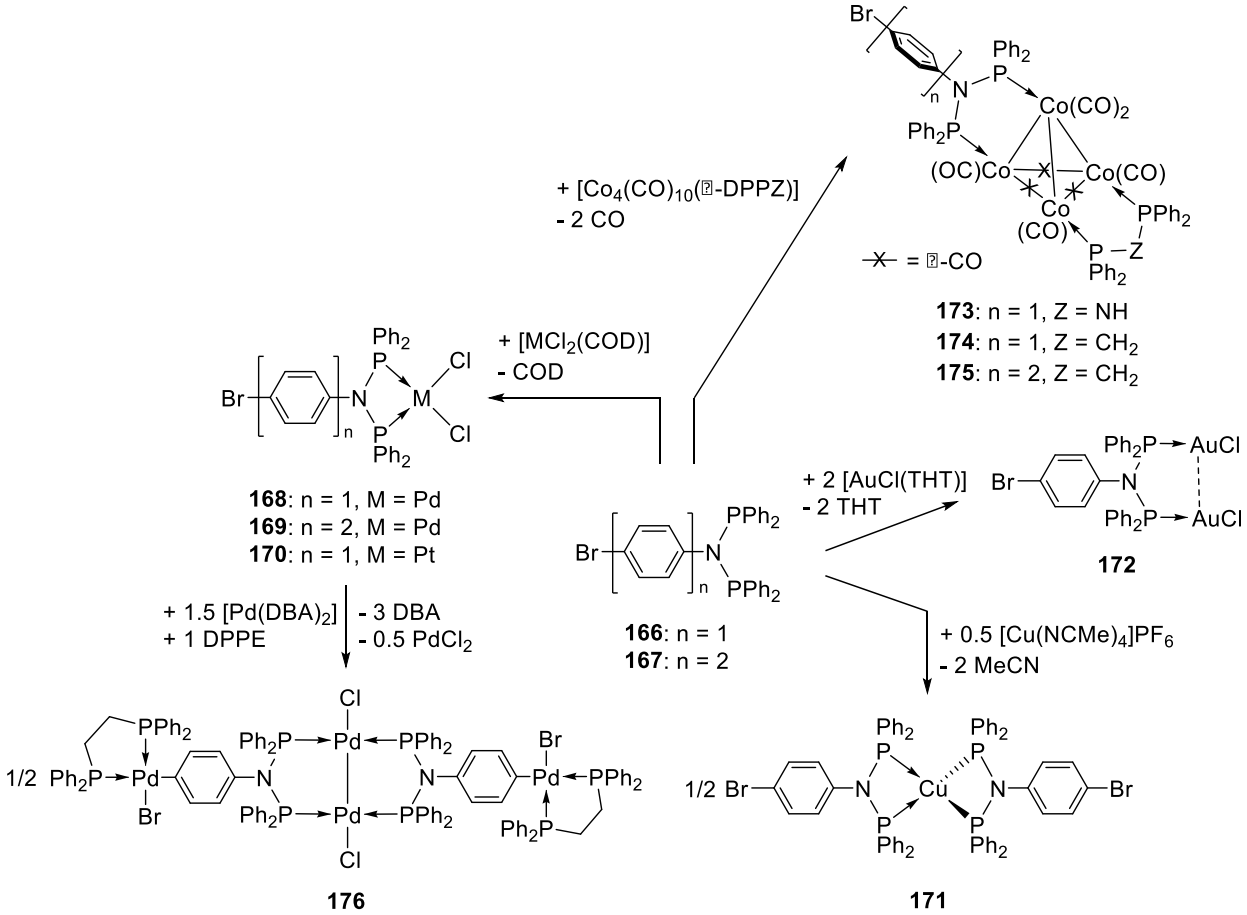

Scheme 32. Ligands **166** and **167** and their mono- (**168**-**171**), di- (**172**) and tetranuclear (**173**-**176**) metal complexes.

Since Braunstein *et al*. are strongly involved in the chemistry of molecular metal clusters (vide infra) they studied the possibility to stabilize low-valent cobalt carbonyl clusters by the new *N*-bromo-aryl funtionalized DPPA-type ligands (**166**-**167**). Reaction of the latter with 1 equiv of the Co_4 *core* tetrahedral clusters $[Co_4(CO)_{10}(\mu^2\text{-DPPZ})]$ (Z = A, M) afforded the corresponding $[Co_4(CO)_{10}(\mu^2\text{-DPPZ})(\mu^2\text{-}\mathbf{L})]$ (**173**-**175**) complexes after silica gel column chromatography (Scheme 32). These complexes exhibited characteristic, and similar, broad resonances (quadrupolar nature of Co) in their ^{31}P NMR spectra constituted of: 1) one signal for the P atom of the modified DPPA-type ligand occupying the apical position of the Co_4 tetrahedron at 116.6 ($P_{\mathbf{166}/apical}$, **173**), 112.0 ($P_{\mathbf{166}/apical}$, **174**) and 112.2 ($P_{\mathbf{167}/apical}$, **175**); 2) one signal for the P atom of the DPPA-type ligand linked to a basal position of the Co_4 tetrahedron at 97.1 ($P_{\mathbf{166}/basal}$, **173**), 97.4 ($P_{\mathbf{166}/basal}$, **174**), and 96.7 ($P_{\mathbf{167}/basal}$, **175**); and 3) signals corresponding to the DPPZ (Z = A, M) coordinated to the two other basal Co centers at 74.0 ($2P_{dppa}$, **173**), 28.8 and 25.2 ($2P_{dppm}$, **174**) and 28.5 and 24.8 ($2P_{dppm}$, **175**) ppm. The solid-state structure of both **173** and **174** were determined by XRD analysis and revealed comparable structures, even if the nature of the DPPZ (Z = A, M) ligand was found to influence slightly the CO arrangement in the latter, and the main structural parameters were found in the range of the previously reported (DPPA-type)-supported Co_4 *core* cluster **142a** (Table 16 *vs*. Table 15).

Finally, to evaluate the reactivity of the C-Br function present in the ligand tail, and its potential for eventual cross-coupling reactions, Braunstein *et al*. reacted 2 equiv of the Pd(II) complex **168** with 3 equiv of the Pd(0) complex $[Pd(DBA)_2]$ in presence of 2 equiv DPPE, as a stabilizing ligand, with the objective to mimic the oxidative insertion of Pd(0) into the carbon-bromide bond. This reaction allowed the partial characterization (unstable in solution) of the tetranuclear complex **176**, which was composed of a dinuclear Pd(I)-Pd(I) entity supported by

two μ^2-bridging ligands **166** and two (*cis*-DPPE)Pd fragments inserted into the C-Br bond of the ligand **166** (Scheme 31), which was characterized by ^{31}P NMR spectroscopy and exhibited a singlet resonance at 63.7 ppm for to the two equivalent P atoms of ligand **166** and two doublets at 67.6 and 39.0 ppm, coupled with a $^3J_{P,P}$ coupling constant of 26.0 Hz, assigned to the P of the DPPE (Table 16).

Lau *et al*. described the synthesis of a DPPA-type ligand functionalized on the nitrogen atom by *para*-trifluoromethyl-aryl substituent (**177**), obtained *via* the classical aminolysis route, and studied its coordination towards the [RuCl(Tp)(PPh_3)$_2$] precursor and the reactivity of the resulting species (Scheme 33).[51] The free ligand **177** exhibited a characteristic ^{31}P NMR singlet siganl at 68.6 ppm (Table 16). Reaction of the latter with 1 equiv of [RuCl(Tp)(PPh_3)$_2$] led to the displacement of both PPh_3 ligands and *cis* coordination of ligand **177**, to form the neutral complex **178** which displayed a single resonance at 88.8 ppm in its ^{31}P NMR spectrum. Complex **178** cleanly reacted with 1 equiv of AgOTf, as chloride abstractor to lead; 1) when the reaction was performed THF, to the neutral complex **179** in which the OTf replace the Cl ligand, or 2) in a THF/MeCN mixture to the cationic complex **180** presenting one MeCN molecule coordinated to the Ru(II) center and a non-coordinated OTf counter-ion (Scheme 33). The ^{31}P NMR chemical shift of ligand **177** in these compounds (89.9 ppm for **179** and 87.0 ppm for **180**, both as singlets) was not strongly affected by comparison with complex **178** (88.8 ppm, Table 16). The authors studied then complexes **179**-**180** in the catalytic addition of β-diketones to 1-alkynes, and complex **179**, performing the best, was tested towards various substrates and also in the anti-Markovnikov addition of secondary amines to aromatic 1-alkynes (see Section 11.1).

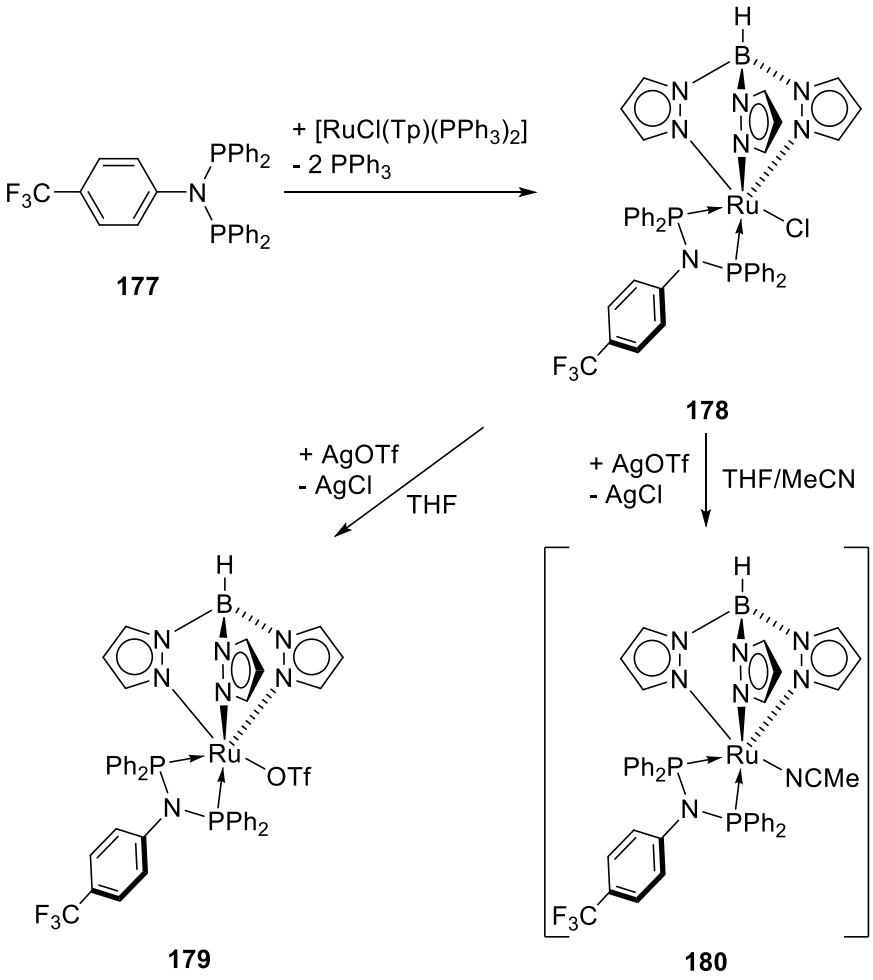

Scheme 33. Ligand **177** and its corresponding neutral (**178**-**179**) and cationic (**180**) Tp-supported Ru(II) complexes.

Tao *et al*. reported a series of *N*-(halogen)aryl-functionalized DPPA-type ligands **181**-**190** (Figure 4), which in combination the [$Cr(acac)_3$] precursor and MAO as co-catalyst afforded highly active catalytic systems for the selective tetramerization of ethylene (see Section 11.1).[52] The *N*-functionalized DPPA-type ligands were obtained *via* the classical aminolysis route in moderate to good yields, and characterized by ^{1}H NMR, MS and EA and the Cr(III) complexes were prepared *in situ* and no additional data were provided.

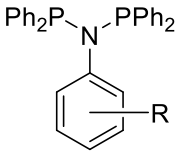

181: R = 2-F
182: R = 2-Cl
183: R = 2-Br
184: R = 2-I
185: R = 3-Cl
186: R = 3-Br
187: R = 2,3-Cl_2
188: R = 2,5-Cl_2
189: R = 3,5-Cl_2
190: R = 3,4-Cl_2

Figure 4. Mono- (**181**-**186**) and bis-halogenated (**187**-**190**) DPPA-type ligands.

Table 16. ^{31}P NMR data and characteristic structural parameters of the free ligands **166**-**167**, **177** and **181**-**190** and the metal complexes and clusters **168**-**176** and **178**-**180**.[a]

	δ (mult.)	P-N	P-M	M-M	PNP	PMP	Ref.
120	70.8 (s)[b]						[50]
121	69.8 (s)[b]						[50]
122	35.8 (s)[b]	1.716	2.203		99.0(2)	72.66(5)	[50]
123	36.3 (s)[b]	1.700	2.222		100.6(5)	72.5(1)	[50]
124	23.0 (s)[b]						[50]
125	89.4 (s)[b]	1.717	2.257	3.0402(2)	118.4(3)		[50]
126	60.9 (s)[b]						[50]
127	116.6 (br s)[b]	1.729	2.188	2.494	117.7(1)		[50]
	97.1 (br s)[b]						
128	112.0 (br s)[b]	1.729	2.186	2.507	115.2(2)		[50]
	97.4 (br s)[b]						
129	112.2 (br s)[b]						[50]

	96.7 (br s)[b]	
130	63.7 (s)[b]	[50]
131	68.6 (s)[c]	[51]
132	88.8 (s)[c]	[51]
133	89.9 (s)[c]	[51]
134	87.0 (s)[c]	[51]

[a] Chemical shifts, P-N (aver.), P-M (aver.), M-M bond lengths and PNP and PMP angles given in ppm, Å and °, respectively. (Sigma) value not given if average value. [b] In $CDCl_3$. [c] In C_6D_6.

7. Silicon-based anchoring function

The *N*-functionalization of DPPA-type ligands with $-Si(OR)_3$ or $-SiR_2(OR')$ groups was essentially investigated with the aim to anchor metal complexes (or metallic clusters) into porous supports, for the formation of potential heterogeneous catalysts. This section will only detail the ligands developed for this purpose and the isolated and characterized metal complexes, while *in-situ* generated compounds and materials preparation, characterization and use will be discussed in the Sections 11.2 and 11.3.

The design of this class of ligands consists in a DPPA moiety connected to an alkoxy- or mixed alkyl/alkoxy silyl group through a simple aliphatic flexible (**191**-**192** and **195**) or aromatic rigid (**194**) spacer, or a spacer containing an additional donor (**193**, Figure 5). Until now, only five examples of such ligands were reported, and they were obtained through aminolysis of the corresponding amines, and exhibited ^{31}P NMR singlet resonances, mostly affected by the nature of the spacer (cf. **194**), in the usual range (62.0 – 68.6 ppm, Table 17). The crystal structure of **194** was determined by XRD studies and revealed P-N bond lengths (1.732(3) and 1.720(3) Å)

and a PNP angle (113.64(18)°) comparable to the other rare examples of free *N*-functionalized DPPA-type ligand.[53]

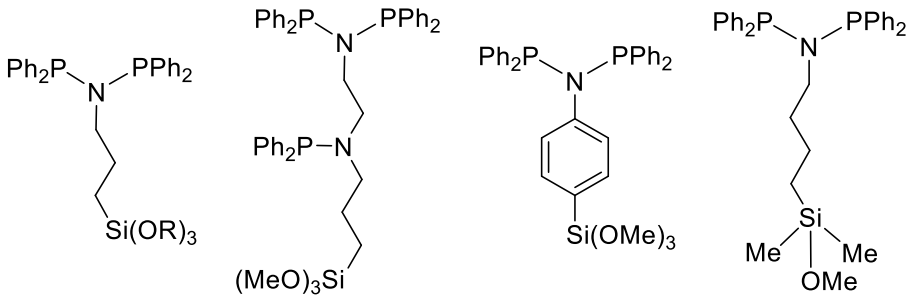

191: R = Me
192: R = Et

193 **194** **195**

Figure 5. *N*-functionalized DPPA-type ligands integrating a silicon-based group **191**-**195**.

Braunstein and Schmid *at al*. reported the synthesis of the cationic [Pd(DMBA)(PNP)]Cl complexes **196** and **197**, resulting from the reaction between **191** and **195** with half an equivalent of the dimeric [Pd(μ-Cl)(DMBA)]$_2$ precursor (Scheme 34).[54] Both Pd(II) complexes **196** and **197** exhibited in their ^{31}P NMR spectra a characteristic couple of doublet, for the non-equivalent P atoms, centered at 57.8 and 63.8 ($^2J_{P,P}$ = 57 Hz) ppm and at 53.1 and 64.0 ($^2J_{P,P}$ = 58 Hz) ppm, respectively. Simple $PdCl_2$ (**198**) and $PtCl_2$ (**199**) adducts of ligand **192** were accessible in high yields by ligand displacement reaction between the aforementioned DPPA-type ligand and the corresponding [MCl_2(COD)] (M = Pd, Pt) precursors, and the resulting complexes exhibited typical ^{31}P NMR singlet resonances at 30.8 and 16.3 ($^1J_{P,Pt}$ = 3293 Hz) ppm.[55] Furthermore, reaction between excess **195** and the Co_4 *core* cluster [$Co_4(CO)_{10}$(μ-DPPA)] resulted in the displacement of two labile CO ligands and formation of the metal cluster **200**, which exhibited a

characteristic (see Sections 5 and 6) ^{31}P NMR pattern composed of three broad signals at 72.1 (2P, P_{dppa}-Co_{basal}), 92.0 (1P, $P_{\mathbf{195}}$-Co_{basal}) and at 103.1 (1P, $P_{\mathbf{195}}$-Co_{apical}) ppm (Table 17).

Similarly, Braunstein *et al*. reported the reaction of ligand **192** with the [$Co_4(CO)_{10}$(μ-DPPM)] precursor, which resulted in the formation of the metal cluster **201**, analogous to **200**, which could be characterized in solution (^{31}P NMR: 28.1 (br) and 100.5 (br) ppm) and in the solid-state (Scheme 34 and Table 17). The bond lengths and angles involving the *N*-functionalized DPPA-type ligand were found close to other Co_4 cluster of this type structurally characterized (see Sections 5 and 6).[56] In this paper, the authors also showed that the reaction between the [$Co_4(CO)_{12}$] precursor and ligand **192** afforded the corresponding Co_4 *core* cluster (**202**) with one **192** ligand bridging one edge of the Co_4 tetrahedron (Scheme 35). Further reaction with a terminal alkyne led to the formation of the butterfly cluster **203a**. A strong shift of the ^{31}P NMR broad resonance was observed, going from **202** (92.8 br, $w_{1/2}$ 166 Hz) to **203a** (81.0 br, $w_{1/2}$ 337 Hz, Table 17). Alternatively, cluster **203b**, an isomer of **203a** exhibiting the same ^{31}P NMR spectrum, could be obtained by preliminary reaction between [$Co_4(CO)_{12}$] and PhC□CH, leading to the butterfly cluster **204** and followed by addition of **192** (Scheme 35).

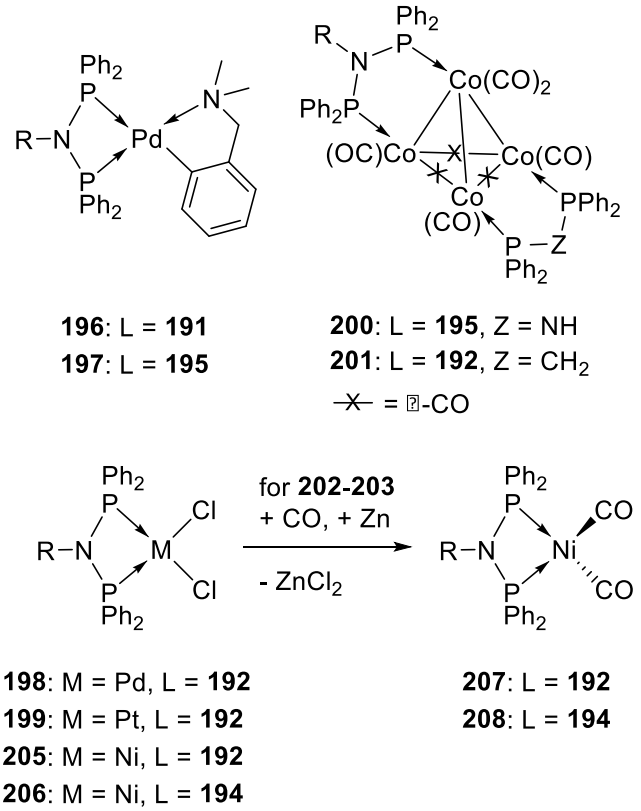

Scheme 34. Metal complexes and clusters supported by *N*-functionalized DPPA-type ligands containing alkyl or alkyl/alkoxy sylil groups and reactivity.

Blümel *et al*. reported the synthesis of the $[NiCl_2(PNP)]$ complexes **205**-**206**, resulting from the equimolar reaction of ligands **192** and **194** with $[NiCl_2Py_4]$, respectively (Scheme 34). The diamagnetic nature of the resulting Ni(II) complexes, probably due to a square-planar coordination geometry, allowed their characterization by ^{31}P CP/MAS NMR, as polycrystalline samples, due to their non-solubility in common organic solvents, and they exhibited singlet resonances at 38.3 and 40.0 ppm (Table 17). Furthermore, reaction of complexes **205**-**206** with CO(g), in the presence of metallic Zn (powder), resulted in the reduction of the Ni(II) center to Ni(0) and replacement of both chlorine ligands by two CO molecules, affording complexes **207**-

208 respectively. Alternatively, the latter could be obtained by reaction of the free ligands **192** and **194** with the Ni(0) precursor [Ni(COD)$_2$], followed by treatment with CO(g), however the first method gave better yields and do not require the use of the air-sensitive Ni(0) precursor. As result of the increased electron density to the Ni(0) centers in **207**-**208** compared to the Ni(II) in **205**-**206** a downfield shift of the P resonances to 91.0 (**207**) and 96.0 (**208**) ppm was observed in their ^{31}P NMR spectra (Table 17). The dicarbonylnickel(0) complex **207** could be characterized in the solid state by XRD analysis and revealed a distorted tetrahedral coordination geometry around the metal center, with the PNP ligand acting as a chelate, and both CO ligands completing the coordination sphere of the complex, the main structural features (P-N, P-Ni bond lengths and PNP, PNiP angles) of the complex are in the range of other group 10 metal complexes and are reported in Table 17.

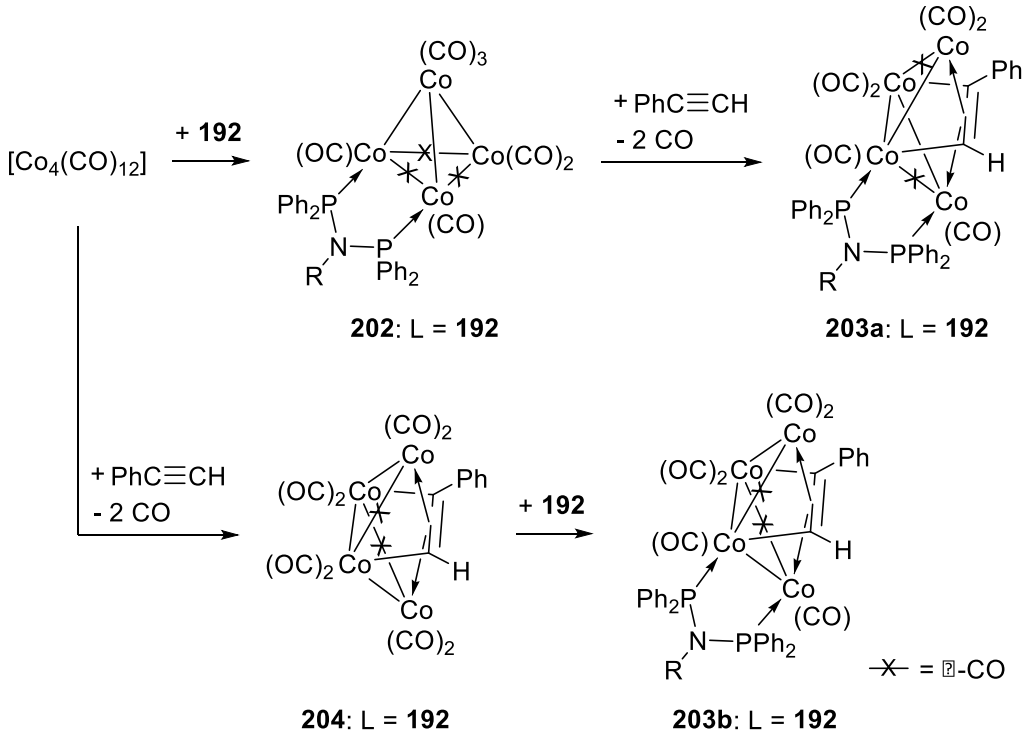

202: L = **192** **203a**: L = **192**

204: L = **192** **203b**: L = **192**

Scheme 35. Synthesis of the Co_4 cluster **202** supported by ligand **192**, and reactivity towards a terminal alkyne (**203a**-**b**).

Braunstein *et al*. also showed that DPPA-type ligands, functionalized on the nitrogen atom by a Si-containing pendant group were able to stabilize low-valent organometallic species or heterometallic clusters.[57,58] In particular, reaction between ligand **192** and a mixture of Pd(0) $[Pd_2(DBA)_3]\square CHCl_3$ and Pd(II) $[PdCl_2(NCPh)_2]$ precursors in a 2:0.5:1 molar ration, respectively, led to the dinuclear Pd(I) complex **209**, in which both PdCl units are bridged by two ligands **192** (Scheme 36).[57] Its ^{31}P NMR spectrum a singlet resonance for the four equivalent P atoms at 79.1 ppm (Table 17). The dinuclear complex **209** could be reacted with 2 equiv $Na[Co(CO)_4]$ to afford in good yield the trinuclear cluster **210**, in which one ligand **192** was found bridging the Pd-Pd edge of the triangle, and the other **192** ligand bridges one Pd-Co edge (Scheme 36). In this case, each P atom of both PNP ligand gave rise to one distinct signal, along with various P,P couplings. Therefore, the most low-field shifted P resonance at 101.6 ppm (dm, $^3J_{P1,P4}$ 194 Hz) was attributed to P4, the other resonances were found closer to each other: P1 at 76.7 ppm (ddd, $^3J_{P1,P4}$ 194 Hz, $^3J_{P1,P2}$ 149 Hz, $^3J_{P1,P3}$ 16 Hz), P3 at 71.7 ppm (m, $^3J_{P3,P2}$ 53 Hz, $^3J_{P3,P1}$ 16 Hz) and finally P2 at 64.4 ppm (ddd, $^3J_{P2,P3}$ 53 Hz, $^3J_{P2,P4}$ 21 Hz) and other coupling constants were not resolved (Table 17).

A similar Pd_2/Co *core* cluster, in which each edge of the triangle was bridged by one *N*-functionalized ligand **191** could be produced by treatment of the tris-DPPA derivative **211** with excess KH, to deprotonate the NH of the DPPA ligands, and further reaction with $I(CH_2)_3Si(OMe)_3$ (Scheme 37).[57] The latter cluster exhibited in its ^{31}P NMR spectrum only three

signals, as multiplets, at 99.1 ppm, assigned to the P atoms linked to the Co center, and at 64.8 and 58.7 ppm attributed to the four remaining P centers linked to Pd centers (Table 17).

More recently, Braunstein et *al*. reported that the reaction between ligand **192** and one equiv of the tetranuclear mixed clusters $[Co_2Pd_2(\mu_3\text{-}CO)_2(CO)_5(\mu\text{-}DPPZ)_2]$ (Z = M or A) in presence of one equiv of $[NH_4][PF_6]$ afforded the trinuclear mixed PNP ligand clusters **215** and **216**, respectively (Scheme 34).[58] The ^{31}P NMR spectrum of **215** exhibited for the modified DPPA ligand **192** one multiplet signal at 101.9 ppm attributed to the P atom linked to the Co center and one doublet of multiplets at 62.3 ppm for the Pd-bounded P atom, while the signals corresponding to the DPPM were found at 26.2 (m, P-Co) and -7.2 (m, P-Pd) ppm (Table 17). A similar pattern could be observed for the DPPA derivative cluster **216**, with multiplets at 79.5 (P-Co) and 45.4 (P-Pd) ppm for the functionalized PNP ligand (Table 17).

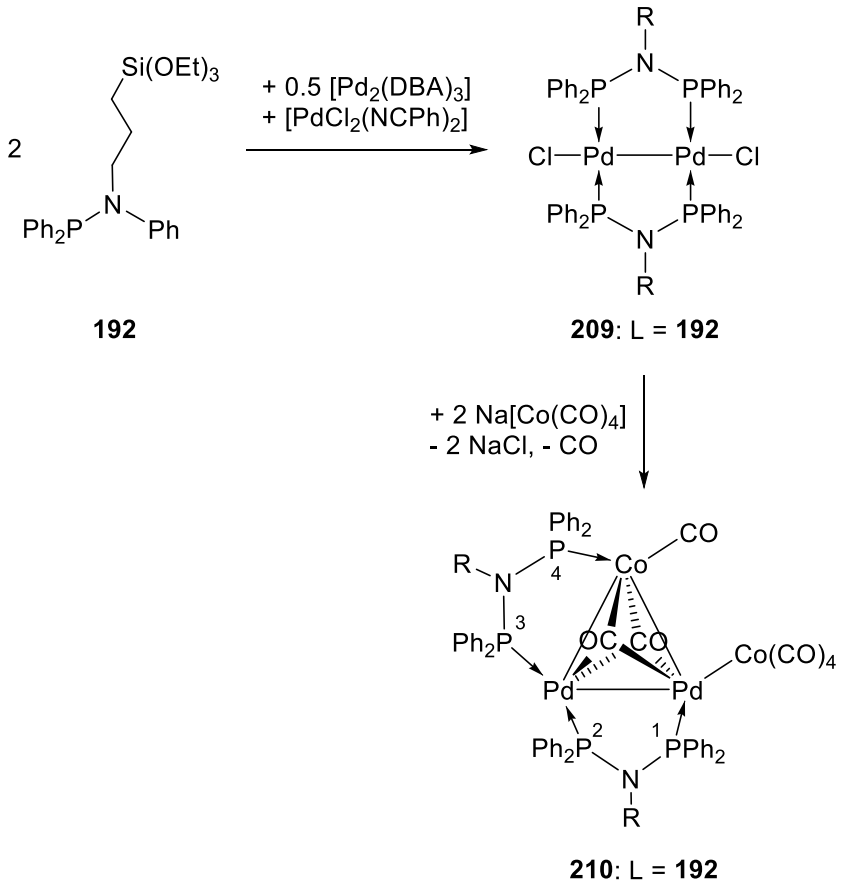

192

209: L = **192**

210: L = **192**

Scheme 36. Synthesis of dinuclear Pd(I) complex **209**, supported by μ-bridging ligands **192**, and formation of the trinuclear mixed Pd/Co cluster **210**. Définir R

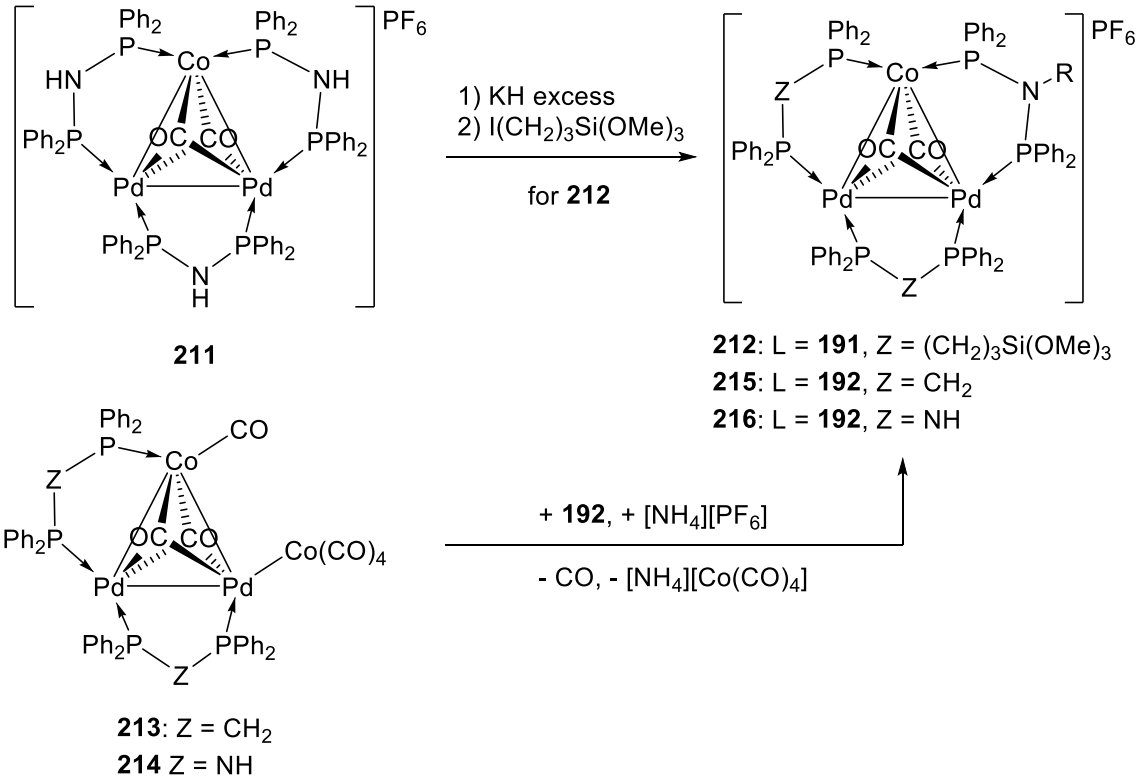

Scheme 37. Functionalization of trinuclear mixed-metal clusters with pendant $Si(OR)_3$ groups via two routes, leading to clusters **212** and **215**-**216**.

Table 17. ^{31}P NMR data (of the *N*-functionalized DPPA-type ligand) and characteristic structural parameters of the free ligands **191**-**195** and the metal complexes and clusters **196**-**216**.[a]

	δ (mult.)	P-N	P-M	PNP	PMP	Ref.
191	62.2 (s)[b]					[54]
192	63.1 (s)[c]/62.0 (s)[d]					[53]
194	68.6 (s)[c]	1.726		113.64(18)		[53]
195	62.2 (s)[b]					[54]
196	57.8 (d)[b]					[54]
	63.8 (d)[b]					

197	53.1 (d)[b]					[54]
	64.0 (d)[b]					
198	30.8 (s)[b]					[55]
199	16.3 (s)[b]					[55]
200	92.0 (br)[b]					[54]
	103.1 (br)[b]					
201	28.1 (br)[b]	1.702	2.186	114.9(2)		[56]
	100.5 (br)[b]					
202	92.8 (br, $w_{1/2}$ 166 Hz)[b]					[56]
203a/b	81.0 (br, $w_{1/2}$ 337 Hz)[b]					[56]
205	38.3 (s)[e]					[53]
206	40.0 (s)/47.8 (s)[e]					[53]
207	91.0/91.4[c+d]	1.710	2.218	102.12(15)	73.68(3)	[53]
208	96.0 (s)[c]					[53]
209	79.1 (s)[c]					[57]
210	101.6, 76.7, 71.7, 64.4[c,f]					[57]
211	99.1, 64.8, 58.7[c,f]					[57]
215	101.9 (m)[c]					[58]
	62.3 (dm)[c]					
216	79.5 (m)[c]					[58]
	45.4 (m)[c]					

[a] Chemical shifts, P-N (aver.) and P-M (aver.) bond lengths and PNP and PMP angles given in ppm, Å and °, respectively. [b] In $CDCl_3$. [c] In d_6-acetone. [d] In C_6D_6. [e] polycrystalline sample. [f] see text for details.

AUTHOR INFORMATION

Corresponding Author

*E-mail addresses: christophe.fliedel@fct.unl.pt (C. Fliedel); braunstein@unistra.fr (P. Braunstein). Fax: (+351) 212 948 550 (CF); (+33) 368 851 322 (PB)

ACKNOWLEDGMENT

We are grateful to the *Fundação para a Ciência e Tecnologia*, (FCT) (fellowship SFRH/BPD/73253/2010 to C.F.), the CNRS, the Ministère de la Recherche (Paris) and the DFH/UFA (International Research Training Group 532-GRK532, PhD grant to A.G.) for funding.

ABBREVIATIONS

Acac, Acetylacetonate; EA, Elemental analysis; EADC, Ethylaluminum dichloride; COD, 1,5-Cyclooctadiene; Cp* = 1,2,3,4,5-Pentamethylcyclopentadiene; DME, 1,2-Dimethoxyethane; DMSO, Dimethylsulfoxyde; DPPA, bis(diphenylphosphino)amine; DPPA-Me, bis(diphenylphosphino)(*N*-methyl)amine; DPPM, bis(diphenylphosphino)methane; FTIR, Fourier transform infrared spectroscopy; MAO, Methylaluminoxane; NBD, 2,5-Norbornadiene; P.C.C.%, Percentage of pyramidal character; *p*-Cym (*para*-Cymene), 1-Methyl-4-(1-methylethyl)benzene; THT, Tetrahydrothiophene; Ts, Tosyl; XRD, X-ray diffraction.

(1) (a) Hierso, J.-C.; Amardeil, R.; Bentabet, E.; Broussier, R.; Gautheron, B.; Meunier, P.; Kalck, P. *Coord. Chem. Rev.* **2003**, *236*, 143; (b) Appleby, T.; Woollins, J. D. *Coord. Chem. Rev.* **2002**, *235*, 121; (c) Bhattacharyya, P.; Woollins, J. D. *Polyhedron* **1995**, *14*, 3367.

(2) (a) Braunstein P. *J. Organomet. Chem.* **2004**, *689*, 3953; (b) Braunstein P.; Naud F. *Angew. Chem. Int. Ed.* **2001**, *40*, 680.
(3) Sa, S.; Lee, S. M.; Kim, S. Y. *J. Mol. Catal. A: Chem.* **2013**, *378*, 17.
(4) Aydemir, M.; Baysal, A.; Gümgüm, B. *J. Organomet. Chem.* **2008**, *693*, 3810.
(5) Mao, G.; Ning, Y.; Hu, W.; Li, S.; Song, X.; Niu, B.; Jiang, T. *Chin. Sci. Bull.* **2008**, *53*, 3511.
(6) Kayan, C.; Biricik, N.; Aydemir, M. *Transition Met. Chem. (London)* **2011**, *36*, 513.
(7) Faught, J. B. *Can. J. Chem.* **1976**, *54*, 738.
(8) (a) Sushev, V. V.; Belina, N. V.; Fukin, G. K.; Kurskiy, Y. A.; Kornev, A. N.; Abakumov, G. A. *Inorg. Chem.* **2008**, *47*, 2608; (b) Kornev, A. N.; Belina, N. V.; Sushev, V. V.; Panova, J. S.; Lukoyanova, O. V.; Ketkov, S. Y.; Fukin, G. K.; Lopatin, M. A.; Abakumov, G. A. *Inorg. Chem.* **2010**, *49*, 9677; (c) Panova, Y. S.; Kornev, A. N.; Sushchev, V. V.; Cherkasov, A. V.; Abakumov, G. A. *Dokl. Chem.* **2012**, *445*, 159; (d) Kornev, A. N.; Sushev, V. V.; Panova, Y. S.; Belina, N. V.; Lukoyanova, O. V.; Fukin, G. K.; Ketkov, S. Y.; Abakumov, G. A.; Lönnecke, P.; Hey-Hawkins, E. *Inorg. Chem.* **2011**, *51*, 874.
(9) Sushev, V. V.; Kornev, A. N.; Min'ko, Y. A.; Belina, N. V.; Kurskiy, Y. A.; Kuznetsova, O. V.; Fukin, G. K.; Baranov, E. V.; Cherkasov, V. K.; Abakumov, G. A. *J. Organomet. Chem.* **2006**, *691*, 879.
(10) Fei, Z.; Ang, W. H.; Zhao, D.; Scopelliti, R.; Dyson, P. J. *Inorg. Chim. Acta* **2006**, *359*, 2635.
(11) Biricik, N.; Fei, Z.; Scopelliti, R.; Dyson, P. J. *Helvetica Chimica Acta* **2003**, *86*, 3281.
(12) Biricik, N.; Fei, Z.; Scopelliti, R.; Dyson, Paul J. *European Journal of Inorganic Chemistry* **2004**, *2004*, 4232.
(13) Fei, Z.; Biricik, N.; Zhao, D.; Scopelliti, R.; Dyson, P. J. *Inorg. Chem.* **2004**, *43*, 2228.
(14) Biricik, N.; Durap, F.; Kayan, C.; Gümgüm, B.; Gürbüz, N.; Özdemir, İ.; Ang, W. H.; Fei, Z.; Scopelliti, R. *J. Organomet. Chem.* **2008**, *693*, 2693.
(15) Song, K.; Gao, H.; Liu, F.; Pan, J.; Guo, L.; Zai, S.; Wu, Q. *Eur. J. Inorg. Chem.* **2009**, *2009*, 3016.
(16) Wang, Y.; Li, Z.; Zeng, X.; Wang, X.; Zhan, C.; Liu, Y.; Zeng, X.; Luo, Q.; Liu, X. *New J. Chem.* **2009**, *33*, 1780.
(17) Zhang, Q.; Hua, G.; Bhattacharyya, P.; Slawin, A. M. Z.; Derek Woollins, J. *Dalton Trans.* **2003**, 3250.
(18) Sarcher, C.; Lebedkin, S.; Kappes, M. M.; Fuhr, O.; Roesky, P. W. *J. Organomet. Chem.* **2013**, *751*, 343.
(19) (a) Schmidbaur, H.; Schier, A. *Chem. Soc. Rev.* **2012**, *41*, 370; (b) Schmidbaur, H.; Schier, A. *Chem. Soc. Rev.* **2008**, *37*, 1931.
(20) Sculfort, S.; Braunstein, P. *Chem. Soc. Rev.* **2011**, *40*, 2741.
(21) Aydemir, M.; Baysal, A.; Sahin, E.; Gumgum, B.; Ozkar, S. *Inorg. Chim. Acta* **2011**, *378*, 10.
(22) Aydemir, M.; Meric, N.; Kayan, C.; Ok, F.; Baysal, A. *Inorg. Chim. Acta* **2013**, *398*, 1.
(23) Ok, F.; Aydemir, M.; Durap, F. *Appl. Organomet. Chem.* **2014**, *28*, 38.
(24) Sun, Z.; Zhu, F.; Wu, Q.; Lin, S.-a. *Appl. Organomet. Chem.* **2006**, *20*, 175.
(25) Kistamurthy, D.; Otto, S.; Moss, J.; Smith, G. *Transition Met. Chem. (London)* **2010**, *35*, 633.

(26) Elowe, P. R.; McCann, C.; Pringle, P. G.; Spitzmesser, S. K.; Bercaw, J. E. *Organometallics* **2006**, *25*, 5255.
(27) Gaw, K. G.; Smith, M. B.; Slawin, A. M. Z. *New J. Chem.* **2000**, *24*, 429.
(28) Biricik, N.; Kayan, C.; Gümgüm, B.; Fei, Z.; Scopelliti, R.; Dyson, P. J.; Gürbüz, N.; Özdemir, İ. *Inorg. Chim. Acta* **2010**, *363*, 1039.
(29) Kayan, C.; Biricik, N.; Aydemir, M.; Scopelliti, R. *Inorg. Chim. Acta* **2012**, *385*, 164.
(30) Blann, K.; Bollmann, A.; de Bod, H.; Dixon, J. T.; Killian, E.; Nongodlwana, P.; Maumela, M. C.; Maumela, H.; McConnell, A. E.; Morgan, D. H.; Overett, M. J.; Prétorius, M.; Kuhlmann, S.; Wasserscheid, P. *J. Catal.* **2007**, *249*, 244.
(31) Wiedemann, D.; Gamer, M. T.; Roesky, P. W. *Z. Anorg. Allg. Chem.* **2009**, *635*, 125.
(32) Gaw, K. G.; Smith, M. B.; Wright, J. B.; Slawin, A. M. Z.; Coles, S. J.; Hursthouse, M. B.; Tizzard, G. J. *J. Organomet. Chem.* **2012**, *699*, 39.
(33) Lednor, P. W.; Beck, W.; Fick, H.-G.; Zippel, H. *Chem. Ber.* **1978**, *111*, 615.
(34) Fick, H.-G.; Beck, W. *J. Organomet. Chem.* **1983**, *252*, 83.
(35) Ellermann, J.; Wend, W. *Nouveau Journal de Chimie* **1986**, *10*, 313.
(36) Chowdhury, A. D.; Mobin, S. M.; Mukherjee, S.; Bhaduri, S.; Lahiri, G. K. *Eur. J. Inorg. Chem.* **2011**, *2011*, 3232.
(37) Aladzheva, I. M.; Lobanov, D. I.; Bykhovskaya, O. g. V.; Petrovskii, P. V.; Lyssenko, K. A.; Mastryukova, T. A. *Heteroat. Chem.* **2003**, *14*, 596.
(38) (a) Aydemir, M.; Baysal, A.; Özkar, S.; Yıldırım, L. T. *Polyhedron* **2011**, *30*, 796; (b) Aydemir, M.; Baysal, A.; Özkar, S.; Yıldırım, L. T. *Inorg. Chim. Acta* **2011**, *367*, 166.
(39) Gaw, K. G.; Smith, M. B.; Steed, J. W. *J. Organomet. Chem.* **2002**, *664*, 294.
(40) Rodriguez-Zubiri, M.; Gallo, V.; Rose, J.; Welter, R.; Braunstein, P. *Chem. Commun.* **2008**, 64.
(41) Gallo, V.; Mastrorilli, P.; Nobile, C. F.; Braunstein, P.; Englert, U. *Dalton Trans.* **2006**, 2342.
(42) Weng, Z.; Teo, S.; Andy Hor, T. S. *Dalton Trans.* **2007**, 3493.
(43) Ghisolfi, A.; Fliedel, C.; Rosa, V.; Pattacini, R.; Thibon, A.; Yu. Monakhov, K.; Braunstein, P. *Chemistry – An Asian Journal* **2013**, *8*, 1795.
(44) Ghisolfi, A.; Fliedel, C.; Rosa, V.; Monakhov, K. Y.; Braunstein, P. *Organometallics* **2014**, 140506144239008.
(45) Sculfort, S.; Croizat, P.; Messaoudi, A.; Bénard, M.; Rohmer, M.-M.; Welter, R.; Braunstein, P. *Angewandte Chemie International Edition* **2009**, *48*, 9663.
(46) Rosa, V.; Fliedel, C.; Ghisolfi, A.; Pattacini, R.; Aviles, T.; Braunstein, P. *Dalton Trans.* **2013**, *42*, 12109.
(47) Ghisolfi, A.; Fliedel, C.; Rosa, V.; Braunstein, P. *Unpublished results*.
(48) Fliedel, C.; Faramarzi, V.; Rosa, V.; Doudin, B.; braunstein, P. *Chem. Eur. J* **2014**, *20*, 1263.
(49) Ghisolfi, A.; Fliedel, C.; Rosa, V.; Yu. Monakhov, K.; Braunstein, P. *Organometallics* **2014**, submitted.
(50) Fliedel, C.; Pattacini, R.; Braunstein, P. *J. Cluster Sci.* **2010**, *21*, 397.
(51) Cheung, H. W.; So, C. M.; Pun, K. H.; Zhou, Z.; Lau, C. P. *Adv. Synth. Catal.* **2011**, *353*, 411.
(52) Jiang, T.; Chen, H.; Cao, C.; Mao, G.; Ning, Y. *Chin. Sci. Bull.* **2010**, *55*, 3750.
(53) Posset, T.; Rominger, F.; Blümel, J. *Chem. Mater.* **2005**, *17*, 586.

(54) Braunstein, P.; Kormann, H.-P.; Meyer-Zaika, W.; Pugin, R.; Schmid, G. *Chemistry- A European Journal* **2000**, *6*, 4637.
(55) Bachert, I.; Bartusseck, I.; Braunstein, P.; Guillon, E.; Rosé, J.; Kickelbick, G. *J. Organomet. Chem.* **1999**, *580*, 257.
(56) Choualeb, A.; Braunstein, P.; Rosé, J.; Bouaoud, S.-E.; Welter, R. *Organometallics* **2003**, *22*, 4405.
(57) Bachert, I.; Braunstein, P.; Hasselbring, R. *New J. Chem.* **1996**, *20*, 993.
(58) Bachert, I.; Braunstein, P.; McCart, M. K.; Fabrizi de Biani, F.; Laschi, F.; Zanello, P.; Kickelbick, G.; Schubert, U. *J. Organomet. Chem.* **1999**, *573*, 47.
(59) Gümgüm, B.; Akba, O.; Durap, F.; Yıldırım, L. T.; Ülkü, D.; Özkar, S. *Polyhedron* **2006**, *25*, 3133.
(60) Akba, O.; Durap, F.; Aydemir, M.; Baysal, A.; Gümgüm, B.; Özkar, S. *J. Organomet. Chem.* **2009**, *694*, 731.
(61) (a) Jiang, T.; Chen, H.; Ning, Y.; Chen, W. *Chin. Sci. Bull.* **2006**, *51*, 521; (b) Zhang, B.; Wang, Y.; Jiang, T.; Xing, L. *Chinese J. Catal.* **2006**, *27*, 416.
(62) Jiang, T.; Tao, Y.; Gao, X.; Mao, G.; Chen, H.; Cao, C.; Ning, Y. *Chin. Sci. Bull.* **2012**, *57*, 1510.
(63) Gaw, K. G.; Smith, M. B.; Steed, J. W. *J. Organomet. Chem.* **2002**, *664*, 294.
(64) Biricik, N.; Fei, Z.; Scopelliti, R.; Dyson, P. J. *Helv. Chim. Acta* **2003**, *86*, 3281.
(65) Majoumo, F.; Lönnecke, P.; Kühl, O.; Hey-Hawkins, E. *Z. Anorg. Allg. Chem.* **2004**, *630*, 305.
(66) Naik, S.; Mague, J. T.; Balakrishna, M. S. *Inorg. Chim. Acta* **2013**, *407*, 139.

CHAPITRE 2

Ce chapitre est présenté sous forme d'une publication parue dans *Dalton Trans.*, **2013**, 42, 12109.

Les contributions respectives des auteurs sont :

A. Ghisolfi, V. Rosa, C. Fliedel, T. Aviles, P. Braunstein – *développement du projet*

A. Ghisolfi, V. Rosa – *Synthèse et caractérisation des ligands et des complexes*

A. Ghisolfi – *simulation des spectres NMR*

R. Pattacini – *étude structurale par diffraction des rayons X*

Influence of a thioether function in short-bite diphosphine ligands on the nature of their silver complexes: structure of a trinuclear complex and of a coordination polymer

Vitor Rosa,[a,b] Christophe Fliedel,[a,b] Alessio Ghisolfi,[a] Roberto Pattacini,[a] Teresa Avilés[b] and Pierre Braunstein*[a]

[a] Laboratoire de Chimie de Coordination Institut de Chimi (UMR7177 CNRS), Université de Strasbourg, 4 rue Blaise Pascal, CS 90032, 67081 Strasbourg (France).

[b]REQUIMTE, Departamento de Quimica Faculdade de Ciéncias e Tecnologia Universidade Nova de Lisboa, Caparica, 2829-516 (Portugal).

Des informations complémentaires sont disponibles en internet sur :

http://www.rsc.org/suppdata/dt/c3/c3dt50555c/c3dt50555c.pdf

Résumé du Chapitre 2

Des nouveaux complexes on été préparés par réaction du précurseur d'argent(I) $AgBF_4$ avec deux ligands phosphoré $Ph_2PN(p\text{-}ArSMe)PPh_2$ (**L1**) et $Ph_2PN(n\text{-}PrSMe)PPh_2$ (**L2**), fonctionnalisés par un groupement thio-éther connu pour sa capacité à interagir avec des surfaces métalliques, de Cu, Ag et Au. Selon leur flexibilité, ces ligands présentent un comportement adaptable à la nature du métal avec lequel ils réagissent, et aux conditions expérimentales, peuvent présenter différents modes de coordination et donner lieu à des composés à la géométrie de coordination, la nucléarité... originaux. En particulier dans le cas de **L2** on observe la formation d'un polymère de coordination composé de deux sous-unités qui sont définies par deux modes de coordination différents du ligand sur les centres métalliques. Une réaction analogue menée avec **L1** conduit à la formation d'un complexe radicalement différent, un cluster avec un noyau triangulaire Ag_3Cl_2 cationique, stabilisé par trois ligands **L1** pontants. Les deux atomes de chlore viennent du solvant de réaction (CH_2Cl_2).

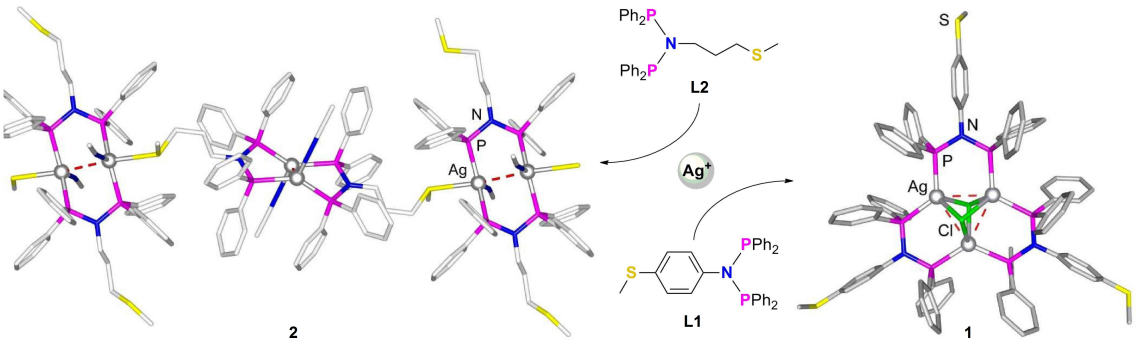

Dalton Transactions

RSC Publishing

PAPER

View Article Online
View Journal

Cite this: DOI: 10.1039/c3dt50555c

Influence of a thioether function in short-bite diphosphine ligands on the nature of their silver complexes: structure of a trinuclear complex and of a coordination polymer†‡

Vitor Rosa,[a,b] Christophe Fliedel,[a,b] Alessio Ghisolfi,[a] Roberto Pattacini,[a] Teresa Avilés[b] and Pierre Braunstein*[a]

Received 28th February 2013,
Accepted 8th April 2013

DOI: 10.1039/c3dt50555c

www.rsc.org/dalton

New cationic Ag(I) complexes were prepared by reaction of $AgBF_4$ with two thioether-functionalized bis(diphenylphosphino)amine ligands, $Ph_2PN(p\text{-}ArSMe)PPh_2$ (**L1**) and $Ph_2PN(n\text{-}PrSMe)PPh_2$ (**L2**), and compared with those obtained from the unfunctionalized ligands $Ph_2PN(Ph)PPh_2$ (**L3**) and $Ph_2PN(n\text{-}Bu)PPh_2$ (**L4**), respectively. The complex $[Ag_3(\mu_3\text{-}Cl)_2(\mu_2\text{-}\mathbf{L1}\text{-}P,P)_3](BF_4)$ (**1**·BF_4) contains a triangular array of Ag centres supported by three bridging **L1** ligands and two triply-bridging chlorides. In contrast, ligand **L2** led to the coordination polymer $[\{Ag_2(\mu_3\text{-}\mathbf{L2}\text{-}P,P,S)_2(MeCN)_2\}\{Ag_2(\mu_2\text{-}\mathbf{L2}\text{-}P,P)_2(MeCN)_2\}(BF_4)_4]_n$ (**2**) in which the tethered thioether group connects intermolecularly a Ag_2 unit to the diphosphine bridging the other Ag_2 unit. With **L3** and **L4**, two similar complexes were obtained, $[Ag_2(\mu_2\text{-}\mathbf{L3})(BF_4)_2]$ (**3**) and $[Ag_2(\mu_2\text{-}\mathbf{L4})(BF_4)_2]$ (**4**), respectively, with bridging diphosphine ligands and a BF_4 anion completing the coordination sphere of the metal. Complexes **1**·BF_4·CH_2Cl_2, **2**·THF, **3**·$3CH_2Cl_2$ and **4** have been fully characterized, including by single crystal X-ray diffraction.

Published on 08 April 2013 on http://pubs.rsc.org | doi:10.1039/C3DT50555C
Downloaded on 04/05/2013 13:38:45.

Introduction

The short-bite ligand bis(diphenylphosphino)amine ($Ph_2PNHPPh_2$, dppa) has attracted much interest owing to its versatile behaviour, as a monodentate, chelating or bridging ligand, and the relative ease with which it can be further functionalized at the N atom.[1,2] The latter aspect represents a significant advantage over the related ligand $Ph_2PCH_2PPh_2$ (dppm) whose CH protons are much less acidic. Because of the general current interest in (i) the coordination chemistry and properties of the coinage metals, and in particular their ability to develop inter- or intramolecular metallophilic interaction,[3] and (ii) the preparation of transition metal complexes and clusters that may be subsequently deposited/anchored on metal surfaces using S-based functionalities,[4] we decided to explore the reactivity of two thioether N-functionalized dppa-type ligands toward d^{10} Ag(I) cations. For a better understanding of these systems, their analogues with non-S-functionalized ligands were also synthesized. Silver(I) ions are well known for their ability to readily form complexes with phosphine ligands and adopt diversified coordination geometries in mononuclear, polynuclear and cluster complexes. In the latter two cases, argentophilic interactions often occur that may generate interesting supramolecular structures and give rise to enhanced photophysical properties (Scheme 1).[3d,5] Short-bite ligands such as dppa or dppm are known to promote the formation of dinuclear Ag(I) complexes having an

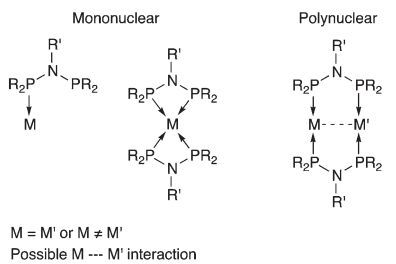

Scheme 1 Typical coordination modes of dppa-type ligands in their metal complexes.

[a]Laboratoire de Chimie de Coordination, Institut de Chimie (UMR 7177 CNRS), Université de Strasbourg, 4 rue Blaise Pascal, CS 90032, 67081 Strasbourg, France. E-mail: braunstein@unistra.fr; Fax: (+33)390 241 322
[b]REQUIMTE, Departamento de Química, Faculdade de Ciências e Tecnologia, Universidade Nova de Lisboa, Caparica, 2829-516, Portugal

†Dedicated to Professor Irina P. Beletskaya on the occasion of her birthday for her considerable contribution to chemistry.

‡Electronic supplementary information (ESI) available: Experimental details, characterisation and X-ray crystal structures of **1**·BF_4·CH_2Cl_2, **2**·THF, **3**·$3(CH_2Cl_2)$ and **4**. CCDC 925659, 925660, 925967 and 925968. For ESI and crystallographic data in CIF or other electronic format see DOI: 10.1039/c3dt50555c

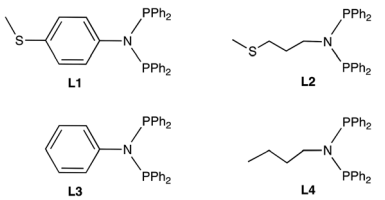

Scheme 2 Dppa-type ligands used in this work.

eight-membered cyclic structure (Scheme 1), and such features are also encountered in Cu(I) and Au(I) chemistry.[6]

Herein, we compare the bonding behaviour of the bidentate diphosphinoamine ligands, $Ph_2PN(p\text{-}ArSMe)PPh_2$ (Ar = C_6H_4) (**L1**)[7] and $Ph_2PN\{(CH_2)_3SMe\}PPh_2$ (**L2**)[1d] (Scheme 2), toward Ag(I) ions and we will show that despite their similarities, these ligands lead to two very different homopolynuclear complexes upon reaction with $AgBF_4$, the triangular cluster $[Ag_3(\mu_3\text{-}Cl)_2\{\mu_2\text{-}\mathbf{L1}PPh_2\}_3](BF_4)$ (**1**·BF_4) and the coordination polymer $[\{Ag_2(\mu_3\text{-}\mathbf{L2}\text{-}P,P,S)_2(MeCN)_2\}\{Ag_2(\mu_2\text{-}\mathbf{L2}\text{-}P,P)_2(MeCN)_2\}(BF_4)_4]_n$ (**2**), respectively.

For comparison and in order to gain a better insight into the influence of the thiomethyl functionality on the coordination properties of **L1** and **L2**, two analogous ligands, $Ph_2PN(Ph)PPh_2$ (**L3**) and $Ph_2PN(n\text{-}Bu)PPh_2$ (**L4**) (Scheme 2), were reacted with $AgBF_4$ under the same conditions as for **L1** and **L2**. To the best of our knowledge, only one other aryl-substituted dppa Ag(I) complex[8] has been structurally characterized before complexes **1**·BF_4 and **3**.

Results and discussion

Synthesis and characterization

The ligands **L1** and **L2** were reacted with $AgBF_4$ in a 1 : 1 ratio and afforded the complexes **1**·BF_4 and **2**, respectively (see the Experimental part) (Schemes 3 and 4). The determination of their structures by single crystal X-ray diffraction established the presence of a triangular Ag_3 *core* in **1**·BF_4 whereas **2** forms in the solid state a coordination polymer involving

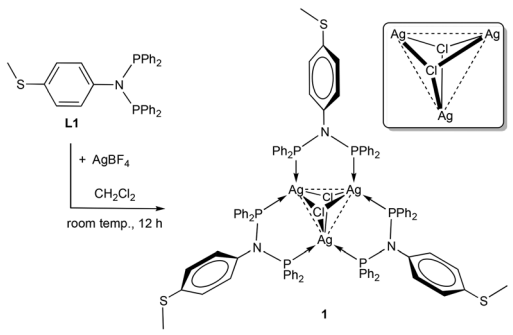

Scheme 3 Synthesis of the monocationic, trinuclear complex in **1**·BF_4. In the inset the trigonal bipyramidal $Ag_3(\mu_3\text{-}Cl)_2$ *core* is magnified (BF_4 omitted).

intermolecular interactions between the thioether groups of one dinuclear unit and an adjacent one. These structures will be detailed below.

Since these ligands present a similar P–N–P backbone, with a diphosphine unit and a thioether donor function separated by a N-bound organic spacer, one could have expected the formation of structurally similar complexes with Ag(I), *e.g.* a dinuclear unit of the type $[Ag(L^2)(L')^+]_2$ (L^2 = μ_2-*P*N(spacer-SMe)*P*; L′ = solvent) in which the bridging, short-bite diphosphine ligands would favour an argentophilic interaction (Scheme 5A), with the thioether remaining non-coordinated. A reasonable alternative was the formation of a coordination polymer of the type $[(AgL^3)^+]_n$ (L^3 = μ_3-*P*N(R*S*Me)*P*) involving the phosphorus and thioether donor functions present in the ligand with no additional coordinating solvent (Scheme 5B).

The trinuclear complex 1·BF_4. The solid-state structure of the trinuclear cation in complex **1**·BF_4·CH_2Cl_2 is based on Ag(I) centres forming a nearly equilateral triangle, of which each edge is supported by a diphosphine ligand **L1** (Fig. 1).

The Ag···Ag separations (aver. 3.088 Å) are compatible with the existence of argentophilic interactions.[3d] Selected bond distances and angles are reported in Table 1. The two triply bridging chloride ligands that complete the coordination sphere of the Ag cations must originate from the dichloromethane used as a solvent; however we do not know yet at what stage of the reaction this occurred. This results in a trigonal bipyramidal $Ag_3(\mu_3\text{-}Cl)_2$ *core*. All silver centres are in a similar, distorted tetrahedral coordination environment, with average P–Ag–P and Cl–Ag–Cl angles of 122.5° and 97.4°, respectively. Interestingly, no interaction involving the thioether donor of **L1** was observed in the solid-state. This opens up the future possibility (i) to form higher nuclearity entities by coordination of this thioether function to another metal centre (*e.g.* Rh^I, $Ru^{II\ or\ III}$ or Pd^{II}) known to react with the alkyl- or aryl-thioether function of S-NHC ligands,[9] or (ii) to deposit and anchor this complex on metal (Au) surfaces. The high symmetry of the complex revealed in the solid-state is retained in solution, as shown by the equivalence of the phosphorus nuclei in $^{31}P\{^1H\}$ NMR (see below).

Although we have previously studied the reactivity of d^{10} silver ions with homo- or hetero-bidentate ligands and the formation of polynuclear complexes exhibiting argentophilic interactions supported by mixed ligands and μ_2- and/or μ_3-halides,[9c,10] to the best of our knowledge, only five crystal structures similar to that of complex **1**·BF_4 with dppa or dppa-type ligands and with the silver ions bridged by chlorides have been reported.[11] In these structures, the chlorides also occupied the apical positions of a trigonal bipyramid formed by the Ag_3Cl_2 *core*. With dppa-type ligands, no other halogens than chlorides have been reported so far in this type of coordination geometry. However, in the case of dppm derivatives, structures with capping iodides[12,13a] or bromides are known.[13b,14] The structure of **1**·BF_4 appears to be the first reported for an *N*-aryl dppa-derivative; the other five structures mentioned presented a N–H or a *N*-alkyl group.

Published on 08 April 2013 on http://pubs.rsc.org | doi:10.1039/C3DT50555C
Downloaded on 04/05/2013 13:38:45.

 This journal is © The Royal Society of Chemistry 2013

Published on 08 April 2013 on http://pubs.rsc.org | doi:10.1039/C3DT50555C
Downloaded on 04/05/2013 13:38:45.

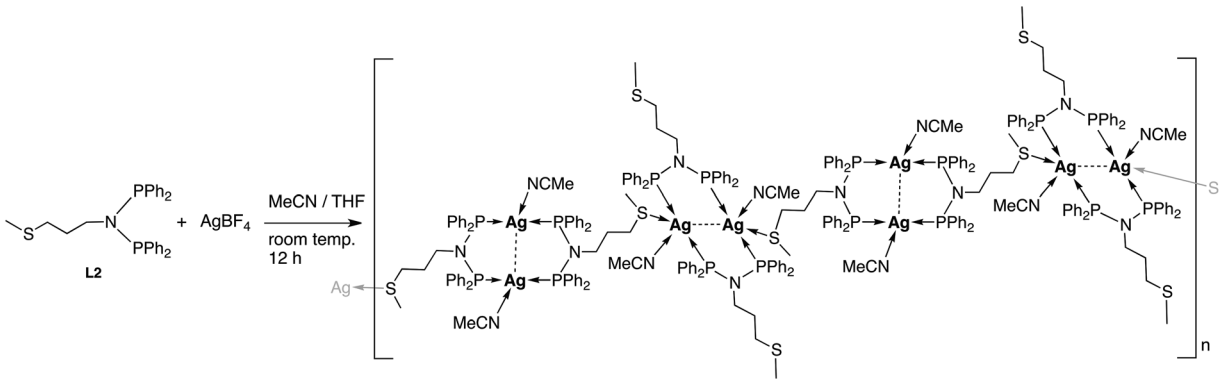

Scheme 4 Synthesis of the coordination polymer **2**. There is one BF_4 anion for each Ag cation (omitted for clarity).

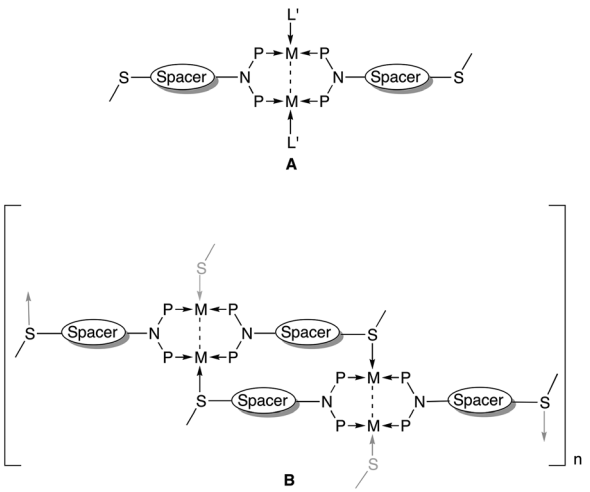

Scheme 5 A: Coordination of the functional ligand acting as a diphosphine bridge; B: possible coordination arrangement involving all the potential donor atoms of the ligand.

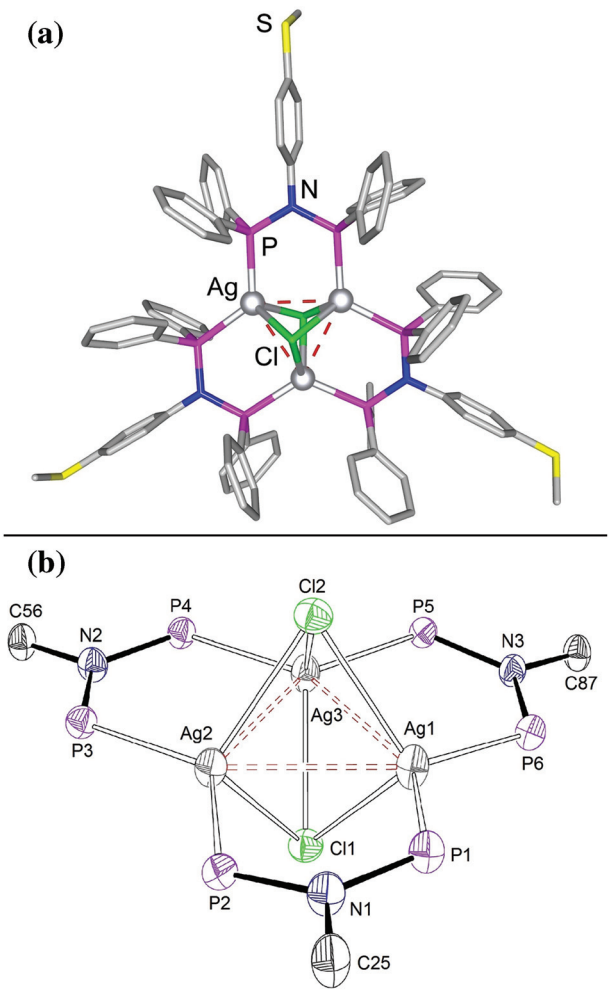

Fig. 1 (a) Molecular structure of the monocationic complex **1**. H atoms are omitted for clarity. (b) ORTEP view of the $Ag_3(\mu_3\text{-}Cl)_2(\mu_2\text{-}PNP)_3$ *core*. Ellipsoids represented at 30% probability levels.

There is a significant difference between the average Ag···Ag distances in complexes bearing dppa and substituted dppa ligands, the latter displaying shorter distances (Table 2).

The $^{31}P\{^1H\}$ NMR spectrum of the crude reaction mixture, after 1 h reaction time, contained two sets of signals (see the ESI: Fig. S1‡): (i) the signals assigned to **1**·BF_4 (see the discussion on NMR spectroscopic studies), indicating that the formation of the triangular cluster occurs rapidly, and (ii) a signal with a pattern similar to those described for **2**, **3** and **4**, typical of a Ag_2L_2 unit (L = dppa-R in a μ_2-bridging mode) (see below). One can speculate whether this compound could be a possible intermediate in the formation of **1**·BF_4. Note that mixing **L1** with a suspension of AgCl in dichloromethane did not lead to the analogous complex **1**·Cl.

The coordination polymer $[\{Ag_2(\mu_3\text{-}L2,\text{-}P,P,S)_2(MeCN)_2\}\text{-}\{Ag_2(\mu_2\text{-}L2\text{-}P,P)_2(MeCN)_2\}(BF_4)_4]_n$ (2). This complex was obtained by reaction of a THF solution of **L2** with a suspension of $AgBF_4$ in acetonitrile (Scheme 4). It could only be isolated in the presence of acetonitrile. In its absence, a colourless powder was immediately formed, which was insoluble in common organic solvents. The coordination polymer **2** is also poorly soluble in most organic solvents. Its structure was established by X-ray diffraction (Fig. 2).

This complex forms a linear coordination polymer in which the repeat unit is composed of two centrosymmetric dinuclear $Ag_2(L2)_2(NCMe)_2$ subunits A and B, the former being linked to

Published on 08 April 2013 on http://pubs.rsc.org | doi:10.1039/C3DT50555C
Downloaded on 04/05/2013 13:38:45.

Table 1 Selected bonds lengths (Å) and angles (°) in complexes **1**·BF_4·CH_2Cl_2 and **2**·THF

Complex **1**·BF_4·CH_2Cl_2		Complex **2**·THF	
Ag1–Ag2	3.1434(5)	Ag1–Ag1′	2.9776(5)
Ag1–Ag3	3.0600(4)	Ag2–Ag2′	3.1184(6)
Ag2–Ag3	3.0613(4)	Ag1–P1	2.4430(9)
Ag–P (aver.)	2.4413(11)	Ag1–P2	2.4307(9)
Ag–Cl (aver.)	2.7015(10)	Ag2–P3	2.4432(9)
		Ag2–P4	2.4606(9)
		Ag2–S1	2.9028(10)
Cl–Ag–Cl (aver.)	97.39(3)		
Ag–Cl–Ag (aver.)	69.72(2)	P1–Ag1–P2	138.8(3)
P–Ag–P′ (aver.)	122.3(4)	P3–Ag2–P4	138.5(3)
P–N–P (aver.)	122.4(2)	P–N–P (aver.)	116.5(17)

Table 2 Comparison of the average Ag···Ag distances in **1**·BF_4·CH_2Cl_2 with related complexes

CCDC ref. code	Complex	Aver. Ag···Ag (Å)
1·BF_4·CH_2Cl_2	$[Ag_3(\mu_3\text{-}Cl)_2(\mu_2\text{-}\mathbf{L2})_3]$	3.088
RETHEE[11]	$[Ag_3(\mu_3\text{-}Cl)_2(\mu_2\text{-}Ph_2PN(i\text{-}Pr)PPh_2)_3][PF_6]$	3.055
RETHII[11]	$[Ag_3(\mu_3\text{-}Cl)_2(\mu_2\text{-}dppa)_3][PF_6]$	3.228
BONQEB[15]	$[Ag_3(\mu_3\text{-}Cl)_2(\mu_2\text{-}dppa)_3][CO_2CF_3]$	3.174
BONQIF[14]	$[Ag_3(\mu_3\text{-}Cl)_2(\mu_2\text{-}dppa)_3][GaCl_4]$	3.216
BONQOL[14]	$[Ag_3(\mu_3\text{-}Cl)_2(\mu_2\text{-}dppa)_3][FeCl_4]$	3.202

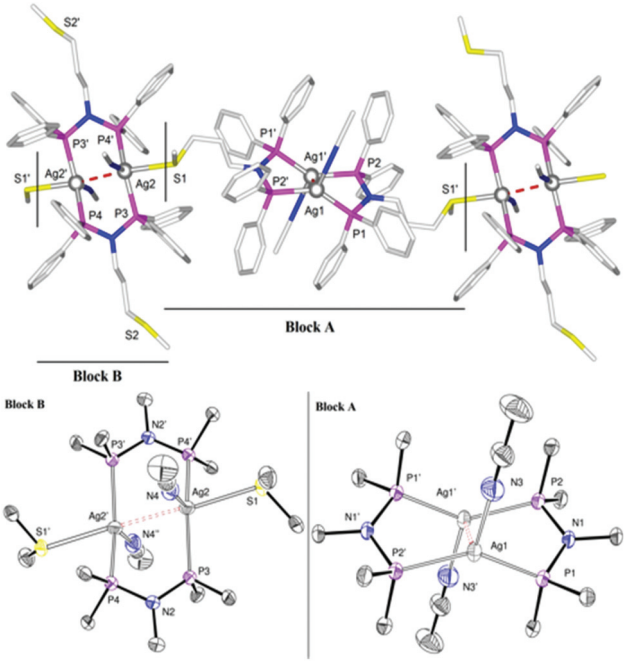

Fig. 2 General view of the molecular structure of the coordination polymer **2** in **2**·THF (top) and zoom of the bimetallic *cores* of Block A and B (bottom). BF_4^- anions and H atoms are omitted for clarity. Ellipsoids represented at 30% probability levels.

adjacent B units through the thioether functions of ligands **L2**. In B, the thioether functions of **L2** remain uncoordinated. In each subunit, a molecule of acetonitrile completes the silver coordination sphere. The silver centres adopt two different coordination geometries depending on whether they belong to Block A or Block B (Fig. 2, bottom). If one ignores the Ag···Ag interaction, Ag1 and Ag1′ (Block A) have a strongly distorted trigonal planar coordination geometry (N3–Ag1–P2 114.42(9)°, N3–Ag1–P1 106.73(9)°, P2–Ag1–P1 138.80(3)°), whereas Ag2 and Ag2′ (Block B) are four-coordinated, in a distorted trigonal pyramidal coordination environment (N4–Ag2–P3 106.81(9)°, N4–Ag2–P4 114.09(9)°, P3–Ag2–P4 138.50(3)°, N4–Ag2–S1 85.18(9)°). In Block A, Ag1 and Ag1′ are each coordinated by one phosphorus donor of two **L2** ligands (P1 and P2), acting as μ_2-bridging ligands and supporting an Ag···Ag argentophilic interaction (2.9776(5) Å). The coordination sphere of the Ag ions contains an acetonitrile molecule. The structure of Block B is very similar to that of Block A but, in addition, each silver is coordinated by the sulphur atom (S1) of the thioether function from a **L2** ligand of Block A. The Ag–S bond length is slightly longer than the average values for Ag–S (thioether) or Ag···Ag–S (thioether) systems, possibly owing to the presence of three additional donor ligands on the Ag centres (see ESI Scheme S1 and Fig. S10 and S11‡). These Ag–S bonds, which are collinear with the Ag2···Ag2′ interaction, are the reason for a longer metal–metal separation compared to Ag1···Ag1′ (3.1184(6) Å *vs.* 2.9776(5) Å).

The structural features of silver-containing coordination polymers are often found to be solvent- and anion-dependent.[15] Only four structures comparable to the central unit of the coordination polymer **2** were found in the Cambridge Structural Database (CSD), but none exhibited a similar coordination geometry for the polymeric form with dppa-type ligands. In the case of dppm-type ligands, however, we could find five structures in CSD presenting a polymeric arrangement.[16]

As can be seen from Table 3, the distance between the two silver ions is influenced by the nature of the ligand occupying

Table 3 Comparison between the Ag···Ag distances, P–Ag–P′ and P–N–P angles in **2**·THF, **3** and **4** and related complexes exhibiting a $Ag_2(\mu\text{-}dppa)_2$ fragment[6h]

CCDC code	Complex	P–Ag–P′ angle (°)	P–N–P angle (°)	Ag···Ag (Å)
Complex **2**·THF	$\{[Ag_4(\mu_2\text{-}\mathbf{L2})_4(MeCN)_4][BF_4]_4\}_n$	138.5 B-block 138.8 A-block	115.1 B-block 117.8 A-block	3.1184(6) B-block 2.9776(5) A-block
Complex **3**	$[Ag_2(\mu_2\text{-}\mathbf{L3})][(BF_4)_2]$	151.7	121.6	2.8946(7)
Complex **4**	$[Ag_2(\mu_2\text{-}\mathbf{L4})][(BF_4)_2]$	148.0	117.5	2.8848(10)
MUNJAG[6h]	$[Ag_2(\mu_2\text{-}dppa)_2(NCMe)_2][PF_6]_2$	148.5	122.1	2.961
GIYQAG[17]	$[Ag_2(\mu_2\text{-}dppa)_2(THF)_2][BF_4]_2$	146.7	116.4	2.911
HUKZOC[18]	$[Ag_2(\mu_2\text{-}dppa)_2(NCMe)_2][Mo(S_2C_4N_2)_3]_2$	156.5	125.9	2.950
RETHOO[11]	$[Ag_2(\mu_2\text{-}Ph_2PN(i\text{-}Pr)PPh_2)_2][CF_3SO_3]_2$	143.4	113.7	2.868

 This journal is © The Royal Society of Chemistry 2013

Published on 08 April 2013 on http://pubs.rsc.org | doi:10.1039/C3DT50555C
Downloaded on 04/05/2013 13:38:45.

the third coordination site (when ignoring the Ag···Ag interaction). This is illustrated by the similarity of the Ag···Ag distances in **3** and **4** (2.895(1) and 2.885(1) Å), which contain a coordinated BF_4 anion, whereas in complexes where this site is occupied by a MeCN molecule, the Ag···Ag distances range from 2.950 to 2.978 Å.

Interestingly, the number of structures of silver complexes with dppm-type ligands is substantially larger than with dppa-type ligands.

To better evaluate the effects of the thiomethyl function and have a comparison model for our NMR studies, the closely related ligands, $Ph_2PN(Ph)PPh_2$ (**L3**) and $Ph_2PN(n\text{-}Bu)PPh_2$ (**L4**) (Scheme 2), were used to prepare silver complexes and $[Ag_2(\mu_2\text{-}\mathbf{L3})(BF_4)_2]$ (**3**) and $[Ag_2(\mu_2\text{-}\mathbf{L4})(BF_4)_2]$ (**4**) were obtained under the same experimental conditions as for **1**·BF_4 and **2**, respectively (Scheme 6).

Single crystals suitable for X-ray diffraction were obtained for both complexes (Fig. 3 and 4 and Fig. S8 and S9‡). In both centrosymmetric structures, two diphosphine ligands bridge two silver ions and an F atom of each BF_4 anion occupies the fourth coordination site of the metal (when considering a metal–metal interaction), forming a Ag–Ag′–F angle of 101.9(4) and 108.6(1)° in **3** and **4**, respectively (see the ESI – Fig. S8 and S9‡). The position of the coordinated BF_4 anion is reminiscent of that of the acetonitrile ligands in **2**. It is noteworthy that reactions of ligands **L1** and **L3** with $AgBF_4$, under otherwise identical conditions, did not lead to the same type of complex although the Ag/P ratio of 1 : 2 was retained. This result indicates a significant, although indirect effect of the thiomethyl function on the reactivity of the ligand. Selected bond lengths and angles for **3**·3(CH_2Cl_2) and **4** are reported in ESI Table S3.‡

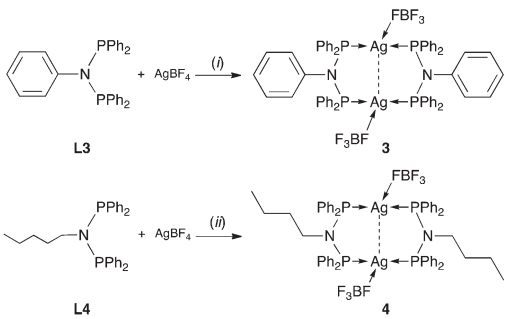

Scheme 6 Synthesis of complexes **3** and **4**. (i) CH_2Cl_2, room temperature, 12 h; (ii) MeCN/THF, room temperature, 12 h.

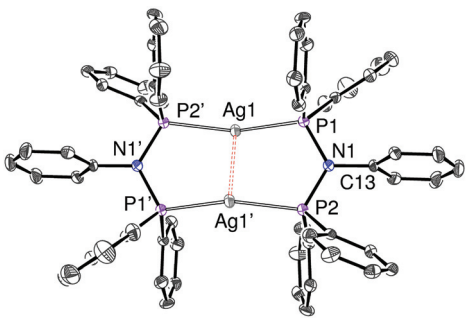

Fig. 3 View of the molecular structure of **3** in **3**·3(CH_2Cl_2). Ellipsoids represented at 30% probability levels. The BF_4^- anions and the H atoms are omitted for clarity. Each BF_4^- anion interacts with an Ag ion through one of the F atoms: Ag–F2 = 2.653(1), Ag1–Ag1′ = 2.8946(7) Å.

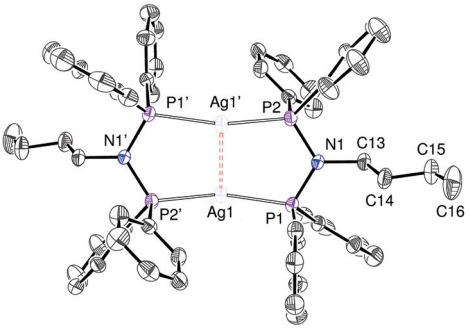

Fig. 4 View of the molecular structure of the centrosymmetric complex **4**. Ellipsoids represented at 30% probability levels. The BF_4^- anions and the H atoms are omitted for clarity. Each BF_4^- anion interacts with an Ag ion through one of the F atoms: Ag–F2 = 2.572(1), Ag1–Ag1′ = 2.8946(7) Å.

A decrease of the transoid P–Ag–P′ angles in $[Ag_2(\mu_2\text{-dppa})_2][X]_2$-type complexes resulting in an inward "pinching" is often associated with shorter Ag···Ag distances (see Table 3), as observed in complexes **3**, **4** and $[Ag_2(\mu_2\text{-}Ph_2PN(i\text{-}Pr)PPh_2)_2][CF_3SO_3]_2$. This is generally accompanied by a decrease of the P–N–P bite angle. However, with complexes of the type $[Ag_2(\mu_2\text{-dppa})_2(NCMe)_2]X_2$ such as complex **2** Block A, $[Ag_2(\mu_2\text{-dppa})_2(NCMe)_2][PF_6]_2$ and $[Ag_2(\mu_2\text{-dppa})_2(NCMe)_2][Mo(S_2C_4N_2)_3]_2$, an opposite trend is observed, a decrease of the P–Ag–P′ angles being associated with an increase of the Ag···Ag distance. Nevertheless, the P–N–P bite angle decreases as the P–Ag–P′ angle decreases. The situation in **2**·THF is rather unique, with small P–Ag–P′ angles but rather long Ag···Ag distances.

It is noteworthy that in this series of structures only the complex $[Ag_2(\mu_2\text{-dppa})_2(THF)_2][BF_4]_2$ (CCDC ref: GIYQAG) presents a mutual *syn* conformation of the three ligands coordinated to the silver ions (Scheme 7) while all the other complexes, including the ones described in this work, present an *anti* conformation.[19]

Finally, one should also consider that in the latter case, the Ag ions are not situated within the mean plane formed by the four P atoms of the short bite ligands, but slightly above and below, respectively. Table 4 provides a comparison between the Ag···Ag distances and the distance between the silver ion and the mean P1P2P1′P2′ plane in **2**·THF, **3** and **4** and other di-silver complexes containing μ-dppa-type ligands.

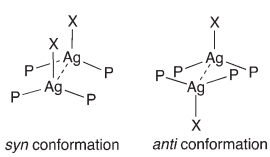

Scheme 7 Respective conformations of the ligands around the silver cations.

Table 4 Comparison between the Ag···Ag separations and the Ag-plane P1P2P′1P′2 distances in **2**·THF, **3** and **4** and other complexes containing a Ag_2(μ-dppa-type)$_2$ moiety

CCDC ref. code	Complex	Ag···Ag (Å)	Ag distance to the mean P1P2P1′P2′ plane
	2·THF	3.1184(6) B-block	0.858 B-block
		2.9776(5) A-block	0.828 A-block
MUNJAG	$[Ag_2(\mu_2\text{-dppa})_2(NCMe)_2][PF_6]_2$	2.961	0.647
HUKZOC	$[Ag_2(\mu_2\text{-dppa})_2(NCMe)_2][Mo(S_2C_4N_2)_3]_2$	2.950	0.484
	$[Ag_2(\mu_2\text{-}\mathbf{L3})][(BF_4)_2]$ (**3**)	2.8946(7)	0.567
	$[Ag_2(\mu_2\text{-}\mathbf{L4})][(BF_4)_2]$ (**4**)	2.8848(10)	0.643
RETHOO	$[Ag_2(\mu_2\text{-}Ph_2PN(i\text{-}Pr)PPh_2)_2][CF_3SO_3]_2$	2.868	0.735

Published on 08 April 2013 on http://pubs.rsc.org | doi:10.1039/C3DT50555C
Downloaded on 04/05/2013 13:38:45.

NMR spectroscopic studies

The ^{1}H-NMR spectrum of the Ag complex **1**·BF_4 revealed a highly symmetric compound. It contained a singlet for the SCH_3 protons at 2.33 ppm and two doublets at 6.11 and 6.74 ppm, integrating for 6 protons each, for the thioether-substituted phenyls, with a coupling constant $^3J_{HH}$ of 8.7 Hz (AA′BB′ spin system); the other aromatic protons were not assigned. The low solubility of **2** did not allow determination of the phosphorus–carbon coupling in ^{13}C-NMR, as could be done for the free ligand.

The ^{107,109}Ag nuclei being characterized by a spin of I = 1/2, the observation in $^{31}P\{^1H\}$ NMR of $^1J(^{107,109}Ag,^{31}P)$ couplings is expected.[20] The $^{31}P\{^1H\}$ NMR spectrum of **1**·BF_4 consists of two well resolved doublets centred at 98.15 ppm, with values of $^1J(^{109}Ag–P)$ = 254 Hz and $^1J(^{107}Ag–P)$ = 220 Hz consistent with the gyromagnetic ratio $\gamma(^{109}Ag)/\gamma(^{107}Ag)$ = 1.15 (Fig. 5). Such coupling constants are typically in the range 200–1000 Hz.[21]

The pattern of this $^{31}P\{^1H\}$ NMR spectrum is explained by the approximately three-fold molecular symmetry observed in the solid state (see X-ray diffraction results discussed above) which is retained in solution and generates two sets of three chemically and magnetically equivalent $^{107}AgP_2$ and $^{109}AgP_2$ systems, each giving rise to a doublet, with no manifestation of isotopic shift or $^{2+3}J(^{107/109}AgP)$ coupling.[22] There is an excellent fit between the experimental and simulated NMR spectra (see the ESI – Fig. S2‡).

Owing to the low solubility of **2**, its NMR spectra were recorded in acetone-d_6. All the signals due to ligand **L2** were assigned in the ^{1}H-NMR spectrum: the triplets at 7.70 and 7.60 ppm to the *meta* and *para* protons of the P-bound phenyl groups, respectively, and the broad signal at 7.49 ppm to the *ortho* protons of the phenyl groups. At higher field, whereas the resonances assigned to NCH_2 (2.82 ppm) and $CH_2CH_2CH_2$ (0.60 ppm) were broad, the signal assigned to the SCH_2 (1.68 ppm) protons was well defined and presented the expected triplet pattern. The protons of the S-bound methyl group resonate at 1.52 ppm.

Interestingly, the $^{31}P\{^1H\}$ NMR spectrum of complex **2** in acetone revealed two triplets, at 82.1 and 86.6 ppm, flanking a broad signal at 84.3 ppm (Fig. 6 and ESI, Fig. S3‡). Since acetone is a donor solvent, present in large excess, it can readily compete with weaker donors. We only observe by NMR spectroscopy a fragment of the coordination polymer **2**, in which the thioether moiety is reversibly displaced by an acetone molecule, inducing the broadening of the signals observed for the aliphatic chain.[23] The complexity of the spectrum could originate from an AMM′ spin system (A = ^{31}P, M and M′ = Ag) with the expected mixture of isotopomers in the following proportions: 26.9 : 49.9 : 23.2 corresponding to $(^{107}Ag)_2$, 2× $(^{107}Ag)(^{109}Ag)$ and $(^{109}Ag)_2$, respectively. This spectrum suggests the presence in solution of dinuclear entities (Fig. 2, Block A-type).[21,24]

This analysis implies partial or complete dissociation of the polymer in solution, which may be coupled with a solvent

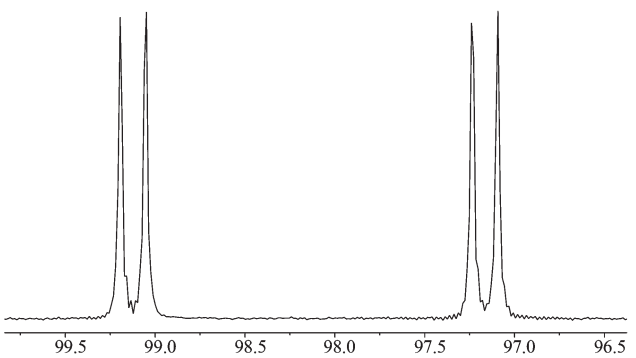

Fig. 5 $^{31}P\{^1H\}$ NMR spectrum of **1**·BF_4 in d_6-acetone.

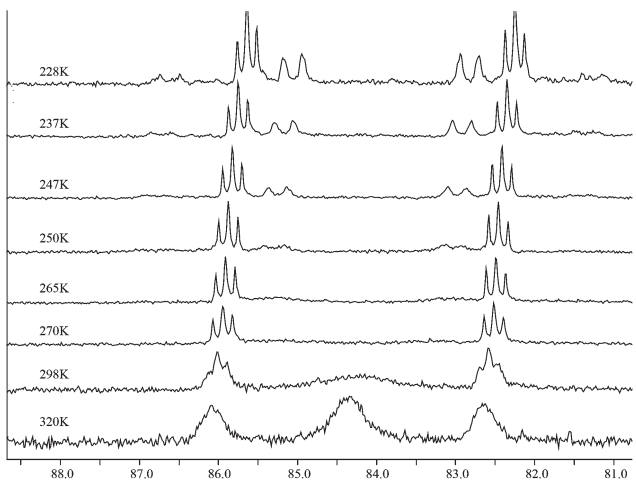

Fig. 6 Variable-temperature $^{31}P\{^1H\}$ NMR spectra of complex **2**.

 This journal is © The Royal Society of Chemistry 2013

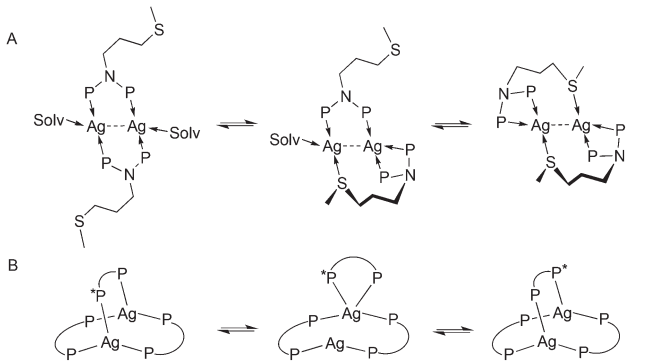

Scheme 8 A: Proposed rearrangement equilibrium for **2**. B: Dynamic rearrangement proposed in the literature for dinuclear diphosphine Ag(I) complexes.

Published on 08 April 2013 on http://pubs.rsc.org | doi:10.1039/C3DT50555C
Downloaded on 04/05/2013 13:38:45.

association/dissociation mechanism and/or the participation of the thioether donor function, leading to $Ag_2(\mu\text{-}\mathbf{L2})_2(solv)_n$ (n = 0–2) species, respectively (Scheme 8A). This dynamic behaviour could explain the broadening of the ^1H NMR signals of the aliphatic protons and of the $^{31}P\{^1H\}$ NMR signals. A series of ^1H and $^{31}P\{^1H\}$ NMR variable-temperature experiments were performed to clarify this dynamic behaviour. Upon decreasing the temperature, the $^{31}P\{^1H\}$ NMR spectra recorded for **2** showed splitting of the central broad signal in several well-defined peaks (Fig. 6). A similar evolution was observed when recording the variable-temperature $^{31}P\{^1H\}$ NMR spectrum of compound **4**. These experiments confirm the existence of a dynamic behaviour of the PNP ligands between chelating and bridging modes, as previously described in the literature for similar systems (Scheme 8B).[24b] In the case of **2**, one could expect the involvement of the sulphur atom in the process (Scheme 8A). A variable-temperature ^1H NMR experiment for compound **2** showed an upfield shift of the singlet assigned to the acetonitrile ligand and a downfield shift of the signal assigned to the *S*-methyl protons (see the ESI, Fig. S5‡). These two results suggest the occurrence of an equilibrium between the following species: (1) a structure with two **L2** (or **L4**) ligands bridging two silver ions and an acetonitrile molecule completing the coordination of each silver ion (Scheme 8A, left), and (2) a non-solvated complex in which an intramolecular rearrangement involves a κ_3-bridging/chelating coordination mode, with the intervention of the thioether function (Scheme 8A, right). This highlights the non-spectator role of the thioether function present in **L2**, both in the solid-state (polymer formation) and in solution (Ag/L 1 : 1 ratio retained contrary to the reported examples involving an additional diphosphine ligand).[24]

Mass spectrometry studies

MALDI-TOF-MS spectrometry is increasingly used for the analysis of metal complexes and nicely complements ESI techniques.[25] We first determined whether the use of a matrix was required since previous experiments with Ag(I) complexes showed that this is not always mandatory.[26] However, in the present case, this led to very complex spectra and the sample had to be ionized with high energies. This resulted in numerous fragmentation peaks (see Fig. S6 and S7‡). Some of them could be assigned to the fragmented ligands, with or without Ag, or to fragments containing several Ag cations, but no definitive information could be gained.

Two different matrices were then used in order to lower the ionization energy, Dithranol and DHB (2,5-dihydroxy benzoic acid), and they led to different outcomes. The best result for $\mathbf{1}\cdot BF_4$ was obtained using DHB as a matrix, the energy required to obtain a clean spectrum being lower than in the other cases (see Fig. S6‡), whereas for **2**, Dithranol was found to be a better matrix than DHB (see Fig. S7‡).

A comparison of the spectra obtained by ESI and MALDI-TOF-MS revealed some common peaks but the MALDI-TOF-MS method gave a different fragmentation pattern of complex $\mathbf{1}\cdot BF_4$. In no case could we find peaks corresponding to a fragment containing a chloride, and this is indicative of the relatively low binding energy of these ligands to the silver ions. The ESI method indicated two fragments at 3542.5 and 2329.3 corresponding to the cations $(3(\mathbf{L1}Ag) + 2BF_4)$ and $(2(\mathbf{L1}Ag) + BF_4)$, respectively. These fragments were not observed by MALDI-TOF-MS analysis. The fragments **L1**Ag and $(\mathbf{L1})_2Ag$ were identified by both techniques and were the major peaks. Another fragmentation peak was found by MALDI-TOF-MS analysis, but not by ESI, at 939.9 which corresponds to $(2\mathbf{L1}Ag - PPh_2)^+$ and to the loss of a PPh_2 fragment.

Both ESI and MALDI-TOF-MS methods gave for complex **2** the same fragment as the major peak (1055.12), corresponding to two ligands **L2** and one Ag cation: $[2\mathbf{L2}Ag]^+$. Even when modulating the energy or using different matrices, we could not find any evidence of higher mass peaks corresponding to an oligo- or poly-meric structure related to that determined by single crystal X-ray diffraction.

Conclusion

A comparison between the Ag(I) complexes obtained from the thioether-functionalized ligands **L1** and **L2** and from the non-functionalized ligands **L3** and **L4** revealed the influence of the thioether group on the resulting coordination complexes. This role can be indirect, as in the case of **L1** since there is no thioether–silver interaction in the corresponding complex $[Ag_3(\mu_3\text{-}Cl)_2(\mu_2\text{-}\mathbf{L1}\text{-}P,P)_3](BF_4)$ $(\mathbf{1}\cdot BF_4)$. A similar triangular cluster was not obtained with **L3** and the dinuclear complex $[Ag_2(\mu_2\text{-}\mathbf{L3})(BF_4)_2]$ (**3**) was isolated instead. The thioether function plays a direct role in the assembling of the 1D-coordination polymer $[\{Ag_2(\mu_3\text{-}\mathbf{L2}\text{-}P,P,S)_2(MeCN)_2\}\{Ag_2(\mu_2\text{-}\mathbf{L2}\text{-}P,P)_2(MeCN)_2\}(BF_4)_4]_n$ (**2**) which is constituted by alternating dinuclear units, A and B, linked by the thioether function. Interestingly, only half of the thioether functions available are engaged in bonding interactions. The other half offers the potential for further coordination or deposition on *e.g.* Au surfaces. The variable-temperature NMR studies on complex **2** in

Published on 08 April 2013 on http://pubs.rsc.org | doi:10.1039/C3DT50555C
Downloaded on 04/05/2013 13:38:45.

solution revealed the existence of a dynamic behaviour involving the flexible thioether chain of the ligand **L2**, a situation not possible with the rigid spacer present in **L1**. This work illustrates further the rich coordination chemistry of dppa-type short-bite ligands and how subtle changes in ligand design can strongly affect the structural properties of the resulting metal complexes.

Experimental part

Materials and instrumentation

All operations were carried out using standard Schlenk techniques under an inert atmosphere. Solvents were purified and dried under argon by conventional methods. CD_2Cl_2 and acetone-d_6 were dried over 4 Å molecular sieves, degassed by freeze–pump–thaw cycles and stored under argon. NMR spectra were recorded at room temperature on a Bruker AVANCE 300 spectrometer (^{1}H, 300 MHz; ^{13}C, 75.47 MHz; ^{31}P, 121.49 MHz and ^{19}F, 282.38 MHz) and referenced using the residual proton solvent (^{1}H) or solvent (^{13}C) resonance. Chemical shifts (δ) are given in ppm. Infrared spectra were recorded in the region 4000–100 cm^{-1} on a Nicolet 6700 FT-IR spectrometer (ATR mode, SMART ORBIT accessory, Diamond crystal). Elemental analyses were performed at the Analytical Services of the Laboratory of REQUIMTE-Departamento de Química, Universidade Nova de Lisboa, on a Thermo Finnigan-CE Flash-EA 1112-CHNS Instrument. Electro-spray mass spectra (ESI-MS) were recorded on a microTOF (Bruker Daltonics, Bremen, Germany) instrument using nitrogen as a drying agent and a nebulizing gas at University of Strasbourg. MALDI-TOF-MS (Matrix Assisted Laser Desorption-Ionization Time-Of-Flight-Mass Spectrometry) analyses were obtained in the REQUIMTE-MALDI-TOF-MS Service Laboratory, and have been performed in a MALDI-TOF-MS voyager DE-PRO Biospectrometry Workstation equipped with a nitrogen laser radiating at 337 nm from Applied Biosystems (Foster City, United States). MALDI mass spectra were acquired and treated with Data Explorer software version 4 series. A MALDI-TOF-MS study in dichloromethane was carried out for all the synthesized compounds. Samples were dissolved in dichloromethane (1 mg mL^{-1}), and 1 to 2 mL of the corresponding solution was spotted on a well of a MALDI-TOF-MS sample plate and allowed to dry. No matrix was added. Measurements were performed in the reflector positive or negative ion mode, with a 20 kV accelerating voltage, 80% grid voltage, 0.005% guide wire, and a delay time of 200 ns. Mass spectral analysis for each sample was based on the average of 500 laser shots. TOF-MS-EI (Time-of-Flight Mass Spectrometry Electron Impact) and TOF-MS-FD (Time-of-Flight Mass Spectrometry Field Desorption) spectra were obtained in the REQUIMTE-MS Service Laboratory using a Micromass GCT model. The ligands Ph_2PN-(*p*-ArSMe)PPh_2 (**L1**),[7] $Ph_2PN\{(CH_2)_3SMe\}PPh_2$ (**L2**),[1d] Ph_2PN-(*n*-Bu)PPh_2 (**L3**)[27] and $Ph_2PN(Ph)PPh_2$ (**L4**)[28] were synthesized according to the literature. Other chemicals were commercially available and used as received.

Crystal structure determinations

Single crystals suitable for X-ray diffraction analysis were obtained by layering a saturated CH_2Cl_2 solution of **1**·BF_4 or **3** with pentane, which afforded **1**·BF_4·CH_2Cl_2 and **3**·3CH_2Cl_2, the reaction mixture leading to **2** with Et_2O, which afforded **2**·THF, and a saturated acetone solution of **4** with *n*-pentane, respectively. Crystal data were collected at 173(2) K on a Kappa CCD diffractometer[29] (graphite monochromated Mo-Kα radiation, λ = 0.71073 Å). The structures were solved by direct methods[30] (SHELXS-97) and refined by full-matrix least-squares procedures (based on F^2, SHELXL-97) with anisotropic thermal parameters for all the non-hydrogen atoms. The hydrogen atoms were introduced into the geometrically calculated positions (SHELXS-97 procedures) and refined *riding* on the corresponding parent atoms. The BF_4 anion in **1**·CH_2Cl_2, which should balance the charge of the complex, was found severely disordered and since attempts to identify the atomic positions failed, a PLATON-SQUEEZE procedure was applied.[31] The residual electron density was assigned to one molecule of the tetrafluoroborate counter anion and one molecule of the dichloromethane solvent [220/2 = 110e per asymmetric unit; one molecule of BF_4 and one molecule of CH_2Cl_2 would give 83e]. This data treatment resulted in an improved quality of the model. A MULTISCAN absorption correction was applied.[32] The details of the structure solution and refinement **1**·BF_4·CH_2Cl_2 and **2**·THF are given in Table S1,‡ and selected bonds and angles are given in Table 1. A summary of the X-ray diffraction data, selected bond distances and angles as well as figures of the molecular structures of complexes **3** in **3**·3CH_2Cl_2 and **4** is given in the ESI (Tables S2 and S3 and Fig. S8 and S9‡).

Synthesis of complex $[Ag_3(\mu_3\text{-}Cl)_2(\mu_2\text{-}L1\text{-}P,P)_3](BF_4)$ (1·BF_4). A dichloromethane solution (15 mL) of **L1** (0.200 g, 0.40 mmol) was added to a suspension of silver tetrafluoroborate (0.077 g, 0.40 mmol) in dichloromethane (5 mL). The reaction mixture was stirred for 12 h, then filtered and layered with pentane. Pale pink crystals of **1**·BF_4 were obtained after two days. Yield: 0.13 g, 49%. Anal. Calcd for $C_{93}H_{81}Ag_3BCl_2F_4N_3P_6S_3$ (2004.01): C, 55.74; H, 4.07; N, 2.10. Found: C, 55.98; H, 3.88; N, 2.11. ^{1}H NMR (CD_2Cl_2) δ: 2.33 (9H, s, CH_3), 6.11 [6H, d, $^3J_{HH}$ = 8.7 Hz, N(C_6H_4S), $H_{ortho/N}$], 6.74 [6H, d, $^3J_{HH}$ = 8.7 Hz, N(C_6H_4S), $H_{meta/N}$], 7.32–7.60 (60H, m, H-phenyl); ^{13}C{^{1}H} NMR (CD_2Cl_2) δ: 15.5 (S-*C*H_3), 126.1, 127.5, 128.6, 129.0, 133.8, 134.3 (*C*-S), 138.5, 139.5 (*C*-N); ^{31}P{^{1}H} (CD_2Cl_2) δ: 98.15 (dd); ^{19}F{^{1}H} NMR (CD_2Cl_2) δ: 152.7 (BF_4). FTIR (solid, cm^{-1}): 3052, 2921, 2324, 1583, 1479, 1433, 1217, 1095, 1052 (s, BF_4), 1013, 993, 959, 916, 893, 746, 696; Far-IR (solid, cm^{-1}): 517, 476, 432, 408, 381, 371, 331, 311, 265, 236, 212, 187. MS (ESI): *m*/*z* = 1121.16 [2**L1**Ag]$^+$, 2329.37 [2(2**L1**Ag) + BF_4]$^+$, 3541.48 [3(2**L1**Ag) + 2BF_4]$^+$. MALDI-TOF-MS: *m*/*z* = 614.0 [**L1**Ag]$^+$, 939.95 [2**L1**Ag − PPh_2]$^+$, 1123.14 [(2**L1**Ag)]$^+$.

Synthesis of complex $[Ag_4\{\mu_3\text{-}L2,\text{-}P,P,S\}_2(\mu_2\text{-}L2\text{-}P,P)_2(MeCN)_4(BF_4)_4]_n$ (2). The coordination polymer **2** was obtained by the addition of a THF solution (15 mL) of **L2** (0.200 g, 0.42 mmol) to a suspension of silver(I) tetrafluoroborate

 This journal is © The Royal Society of Chemistry 2013

Published on 08 April 2013 on http://pubs.rsc.org | doi:10.1039/C3DT50555C
Downloaded on 04/05/2013 13:38:45.

(0.083 g, 0.42 mmol) in acetonitrile (5 mL). After the mixture was stirred for 12 h, layering of the solution with diethyl ether led to the formation of colourless crystals. Yield 0.37 g, 62%. Anal. Calcd for $C_{60}H_{64}Ag_2B_2F_8N_4P_4S_2$ (1418.55): C, 50.80; H, 4.55; N, 3.95. Found: C, 50.63; H, 4.32; N, 3.71. ^{1}H NMR (acetone-d_6) δ: 0.60 (4H, m, $CH_2CH_2SCH_3$), 1.51 (6H, s, CH_2SCH_3), 1.68 (4H, m, CH_2SCH_3), 2.08 (6H, s, CH_3CN), 2.82 (4H, m, NCH_2CH_2), 7.49 (16H, b, *ortho* H-phenyl), 7.60 (16H, t, *meta* H-phenyl), 7.71 (8H, m, *para* H-phenyl); ^{13}C{^{1}H} NMR (acetone-d_6) δ: 14.78 (CH_3), 25.58 (CH_2SCH_3), 30.18 ($CH_2CH_2SCH_3$), 67.47 (NCH_2CH_2), 129.69 (Ph), 132.20 (Ph), 132.98 (Ph); ^{31}P{^{1}H} (acetone-d_6) δ: 82.1 (t), 84.3 (m, br), 86.6 (t); ^{19}F{^{1}H} NMR (acetone-d_6) δ: 148.3 (BF_4). FTIR (solid, cm^{-1}): 3055, 2922, 2874, 2268 (m, C≡N), 2162, 1481, 1457, 1435, 1096, 1051 (s, BF_4), 1033, 996, 883, 746, 694; Far-IR (solid, cm^{-1}): 521, 495, 474, 463, 391, 216. MS (ESI): m/z = 1053.20 [**2L2Ag**]$^+$; MALDI-TOF-MS: m/z = 582.02 [**L2Ag**]$^+$, 1055.12 [**2L2Ag**]$^+$.

Synthesis of complex [Ag$_2${μ$_2$-Ph$_2$PN(Ph)PPh$_2$}(BF$_4$)$_2$] (3). Following the same procedure as described for compound **1**·BF_4 using 0.43 mmol of **L3** and $AgBF_4$, complex **3** was obtained. Yield: 0.193 g, 68%. Anal. Calcd for $C_{60}H_{50}Ag_2B_2F_8N_2P_4{\cdot}3CH_2Cl_2$ (1567.09): C, 48.29; H, 3.60; N, 1.79. Found: C, 48.15; H, 3.90; N, 1.83. ^{1}H NMR (acetone-d_6) δ: 6.16 (4H, d, H-phenyl), 6.82 (4H, t, H-phenyl), 7.07 (2H, t, H-phenyl), 7.47 (16H, m, H-phenyl), 7.51 (16H, t, H-phenyl), 7.67 (8H, t, H-phenyl); ^{13}C{^{1}H} NMR (acetone-d_6) δ: 128.3, 128.6, 129.3, 130.3, 131.4, 132.6, 133.7; ^{31}P{^{1}H} (acetone-d_6) δ: 86.5 (t), 88.2 (m, br), 89.9 (t); ^{19}F{^{1}H} NMR (acetone-d_6) δ: 151.3 (BF_4). FTIR (solid, cm^{-1}): 3059, 1587, 1571, 1482, 1438, 1319, 1280, 1268, 1195, 1173, 1161, 1067 (s, BF_4), 1023, 954, 898, 760, 744, 726, 689, 656, 616; Far-IR (solid, cm^{-1}): 544, 518, 487, 471, 431, 420, 358, 284, 226, 203, 187, 170. MS (ESI): m/z = 569.05 [**L4Ag**]$^+$.

Synthesis of complex [Ag$_2${μ$_2$-Ph$_2$PN(*n*-Bu)PPh$_2$}(BF$_4$)$_2$] (4). Following the same procedure as described for compound **2** using 0.45 mmol of **L4** and $AgBF_4$, compound **4** was obtained. Yield: 0.224 g, 78%. Anal. Calcd for $C_{56}H_{58}Ag_2B_2F_8N_2P_4{\cdot}2MeCN$ (1354.42): C, 53.20; H, 4.76; N, 4.10. Found: C, 52.35; H, 4.80; N, 3.83. ^{1}H NMR (acetone-d_6) δ: 0.29 (6H, t, CH_3), 0.60 (8H, m, $NCH_2(CH_2)_2CH_3$) 2.99 (4H, br, $NCH_2(CH_2)_2CH_3$), 7.50 (16H, b, *ortho* H-phenyl), 7.61 (16H, m, *meta* H-phenyl), 7.73 (8H, m, *para* H-phenyl); ^{13}C{^{1}H} NMR (acetone-d_6) δ: 12.32 (CH_3), 19.29 ($CH_2)_2CH_3$), 32.57, 129.64 (Ph), 132.47 (Ph), 132.82 (Ph); ^{31}P{^{1}H} (acetone-d_6) δ: 82.0 (t), 83.8 (m, br), 85.4 (t); ^{19}F{^{1}H} NMR (acetone-d_6) δ: 151.9 (BF_4). FTIR (solid, cm^{-1}): 3058, 2959, 2875, 2271 (m, C≡N), 2161, 1979, 1586, 1482, 1467, 1460, 1435, 1371, 1311, 1283, 1187, 1162, 1096, 1047 (s, BF_4), 997, 956, 872, 780, 745, 693, 669, 615; Far-IR (solid, cm^{-1}): 520, 495, 478, 474, 386, 224, 214. MS (ESI): m/z = 549.09 [**L4Ag**]$^+$.

Acknowledgements

We are grateful to the CNRS, the Ministère de la Recherche (Paris), the DFH/UFA (International Research Training Group 532-GRK532, PhD grant to C.F.), and the *Fundação para a Ciência e Tecnologia* (FCT) (project PTDC/QUI-QUI/099873/2008 and fellowships SFRH/BPD/73253/2010 (C.F.) and SFRH/BPD/44262/2008 (V.R.)) for funding. We thank the Service de Radiocristallographie, Institut de Chimie (UMR 7177 CNRS-UdS) for the X-ray diffraction studies and Mélanie Boucher for technical assistance.

References

1 See *e.g.* (*a*) K. G. Gaw, M. B. Smith, J. B. Wright, A. M. Z. Slawin, S. J. Coles, M. B. Hursthouse and G. J. Tizzard, *J. Organomet. Chem.*, 2012, **699**, 39; (*b*) C. Fliedel, R. Pattacini and P. Braunstein, *J. Cluster Sci.*, 2010, **21**, 397; (*c*) K. Song, H. Gao, F. Liu, J. Pan, L. Guo, S. Zai and Q. Wu, *Eur. J. Inorg. Chem.*, 2009, 3016; (*d*) Z. Weng, S. Teo and T. S. A. Hor, *Dalton Trans.*, 2007, 3493; (*e*) M. Said, D. L. Hughes and M. Bochmann, *Polyhedron*, 2006, **25**, 843; (*f*) P. R. Elowe, C. McCann, P. G. Pringle, S. K. Spitzmesser and J. E. Bercaw, *Organometallics*, 2006, **25**, 5255; (*g*) T. Posset, F. Rominger and J. Blümel, *Chem. Mater.*, 2005, **17**, 586; (*h*) D. S. McGuinness, P. Wasserscheid, W. Keim, C. Hu, U. Englert, J. T. Dixon and C. Grove, *Chem. Commun.*, 2003, 334; (*i*) V. V. Sushev, A. N. Kornev, Y. V. Fedotova, Y. A. Kursky, T. G. Mushtina, G. A. Abakumov, L. N. Zakharov and A. L. Rheingold, *J. Organomet. Chem.*, 2003, **676**, 89; (*j*) M. Valderrama, R. Contreras and D. Boys, *J. Organomet. Chem.*, 2003, **665**, 7; (*k*) F. Schweyer-Tihay, P. Braunstein, C. Estournès, J. L. Guille, B. Lebeau, J.-L. Paillaud, M. Richard-Plouet and J. Rosé, *Chem. Mater.*, 2003, **15**, 57; (*l*) A. Chouleb, P. Braunstein, J. Rosé, S.-E. Bouaoud and R. Welter, *Organometallics*, 2003, **22**, 4405; (*m*) A. Carter, S. A. Cohen, N. A. Cooley, A. Murphy, J. Scutt and D. F. Wass, *Chem. Commun.*, 2002, 858; (*n*) P. Braunstein, H.-P. Kormann, W. Meyer-Zaika, R. Pugin and G. Schmid, *Chem.–Eur. J.*, 2000, **6**, 4637; (*o*) I. Bachert, P. Braunstein, M. K. McCart, F. Fabrizi de Biani, F. Laschi, P. Zanello, G. Kickelbick and U. Schubert, *J. Organomet. Chem.*, 1999, **573**, 47; (*p*) I. Bachert, I. Bartusseck, P. Braunstein, E. Guillon, J. Rosé and G. Kickelbick, *J. Organomet. Chem.*, 1999, **588**, 143; (*q*) I. Bachert, P. Braunstein, E. Guillon, C. Massera, J. Rosé, A. DeCian and J. Fischer, *J. Cluster Sci.*, 1999, **10**, 445; (*r*) T. Kremer, F. Hampel, F. A. Knoch, W. Bauer, A. Schmidt, P. Gabold, M. Schütz, J. Ellermann and P. von Ragué Schleyer, *Organometallics*, 1996, **15**, 4776; (*s*) I. Bachert, P. Braunstein and R. Hasselbring, *New J. Chem.*, 1996, **20**, 993; (*t*) J. T. Mague, *J. Cluster Sci.*, 1995, **6**, 217; (*u*) P. Bhattacharyya and J. D. Woolins, *Polyhedron*, 1995, **14**, 3367; (*v*) M. S. Balakrishna, V. S. Reddy, S. S. Krishnamurthy, J. F. Nixon and J. C. T. R. Burckett St. Laurent, *Coord. Chem. Rev.*, 1994, **129**, 1.

Published on 08 April 2013 on http://pubs.rsc.org | doi:10.1039/C3DT50555C
Downloaded on 04/05/2013 13:38:45.

2 For a theoretical study of chelation *versus* bridging of dppa-type ligands, see: M. L. McKee and W. E. Hill, *J. Phys. Chem. A*, 2002, **106**, 6201.

3 See *e.g.* (*a*) H. Schmidbaur and A. Schier, *Chem. Soc. Rev.*, 2012, **41**, 370; (*b*) G. A. Bowmaker, J. V. Hanna, B. W. Skelton and A. H. White, *Dalton Trans.*, 2012, **41**, 5409; (*c*) Q.-H. Jin, R. Wang, K.-Y. Hu, Y.-L. Xiao, L.-N. Cui and C.-L. Zhang, *Inorg. Chim. Acta*, 2011, **367**, 93; (*d*) S. Sculfort and P. Braunstein, *Chem. Soc. Rev.*, 2011, **40**, 2741; (*e*) S. Sculfort, P. Croizat, A. Messaoudi, M. Bénard, M.-M. Rohmer, R. Welter and P. Braunstein, *Angew. Chem., Int. Ed.*, 2009, **48**, 9663; (*f*) P. Pyykkö, *Chem. Soc. Rev.*, 2008, **37**, 1967; (*g*) P. Pyykkö, *Inorg. Chim. Acta*, 2005, **358**, 4113; (*h*) P. Pyykkö, *Angew. Chem., Int. Ed.*, 2004, **43**, 4412; (*i*) M. A. Carvajal, J. J. Novoa and S. Alvarez, *J. Am. Chem. Soc.*, 2004, **126**, 1465; (*j*) M. A. Carvajal, S. Alvarez and J. J. Novoa, *Chem.–Eur. J.*, 2004, **10**, 2117; (*k*) P. Pyykkö, *Angew. Chem., Int. Ed.*, 2002, **41**, 3573; (*l*) P. Pyykkö, *Chem. Rev.*, 1997, **97**, 597.

4 (*a*) P. Croizat, F. Müller, H. Mantz, A. Englisch, R. Welter, S. Hüfner and P. Braunstein, *C. R. Chim.*, 2009, **12**, 1228; (*b*) M. Rodriguez-Zubiri, V. Gallo, J. Rosé, R. Welter and P. Braunstein, *Chem. Commun.*, 2008, 64; (*c*) V. Gallo, P. Mastrorilli, C. F. Nobile, P. Braunstein and U. Englert, *Dalton Trans.*, 2006, 2342; (*d*) P. Braunstein, *J. Organomet. Chem.*, 2004, **689**, 3953.

5 (*a*) G. F. Manbeck, W. W. Brennessel, R. A. Stockland Jr. and R. Eisenberg, *J. Am. Chem. Soc.*, 2010, **132**, 12307; (*b*) I. O. Koshevoy, P. V. Ostrova, A. J. Karttunen, A. S. Melnikov, M. A. Khodorkovskiy, M. Haukka, J. Jänis, S. P. Tunik and T. A. Pakkanen, *Dalton Trans.*, 2011, **39**, 9022; (*c*) M. J. Calhorda, C. Ceamanos, O. Crespo, M. C. Gimeno, A. Laguna, C. Larraz, P. D. Vaz and M. D. Villacampa, *Inorg. Chem.*, 2010, **49**, 8255; (*d*) R. Meijboom, R. J. Bowen and S. J. Berners-Price, *Coord. Chem. Rev.*, 2009, **253**, 325; (*e*) V. W.-W. Yam, W.-Y. Lo, C.-H. Lam, W. K.-M. Fung, K. M.-C. Wong, V. C.-Y. Lau and N. Zhu, *Coord. Chem. Rev.*, 2003, **245**, 39; (*f*) V. W.-W. Yam, *Acc. Chem. Res.*, 2002, **35**, 555; (*g*) C.-M. Che, M.-C. Tse, M. C. W. Chan, K.-K. Cheung, D. L. Phillips and K.-H. Leung, *J. Am. Chem. Soc.*, 2000, **122**, 2464; (*h*) V. W.-W. Yam and K. K.-W. Lo, *Chem. Soc. Rev.*, 1999, **28**, 323.

6 (*a*) B. Gil, G. A. Cooke, D. Nolan, G. M. O. Maille, S. Varughese, L. Wang and S. M. Draper, *Dalton Trans.*, 2011, **40**, 8320; (*b*) Y. Takemura, H. Takenaka, T. Nakajima and T. Tanase, *Angew. Chem., Int. Ed.*, 2009, **48**, 2157; (*c*) D. Wiedemann, M. T. Gamer and P. W. Roesky, *Z. Anorg. Allg. Chem.*, 2009, **635**, 125; (*d*) B. Nohra, E. Rodriguez-Sanz, C. Lescop and R. Réau, *Chem.–Eur. J.*, 2008, **14**, 3391; (*e*) B. Nohra, Y. Yao, C. Lescop and R. Réau, *Angew. Chem., Int. Ed.*, 2007, **46**, 8242; (*f*) J. Mo, H.-Y. Qian, X.-D. Du and W. Chen, *Acta Crystallogr., Sect. E: Struct. Rep. Online*, 2007, **63**, m2449; (*g*) A. Maspero, I. Kani, A. A. Mohamed, M. A. Omary, R. J. Staples and J. P. Fackler Jr., *Inorg. Chem.*, 2003, **42**, 5311; (*h*) H. Liu, M. J. Calhorda, M. G. B. Drew, V. Felix, J. Novosad, L. F. Veiros, F. Fabrizi de Biani and P. Zanello, *J. Chem. Soc., Dalton Trans.*, 2002, 4365; (*i*) W.-F. Fu, K.-C. Chan, K.-K. Cheung and C.-M. Che, *Chem.–Eur. J.*, 2001, **7**, 4656; (*j*) W.-F. Fu, K.-C. Chan, V. M. Miskowski and C.-M. Che, *Angew. Chem., Int. Ed.*, 1999, **38**, 2783; (*k*) J. S. Field, J. Grieve, R. J. Haines, N. May and M. M. Zulu, *Polyhedron*, 1998, **17**, 3021; (*l*) M. C. Gimeno, A. Laguna, M. Laguna, F. Sanmartin and P. G. Jones, *Organometallics*, 1993, **12**, 3984; (*m*) E. J. Fernandez, M. C. Gimeno, P. G. Jones, A. Laguna, M. Laguna and J. M. Lopez-de-Luzuriaga, *J. Chem. Soc., Dalton Trans.*, 1993, 3401; (*n*) H. Schmidbaur, T. Pollok, R. Herr, F. E. Wagner, R. Bau, J. Riede and G. Muller, *Organometallics*, 1986, **5**, 566.

7 C. Fliedel, V. Faramarzi, V. Rosa, B. Doudin and P. Braunstein, in preparation.

8 C. Ganesamoorthy, M. S. Balakrishna, J. T. Mague and H. M. Tuononen, *Inorg. Chem.*, 2008, **47**, 2764.

9 (*a*) M. Bierenstiel and E. D. Cross, *Coord. Chem. Rev.*, 2011, **255**, 574; (*b*) C. Fliedel, A. Sabbatini and P. Braunstein, *Dalton Trans.*, 2010, **39**, 8820; (*c*) C. Fliedel and P. Braunstein, *Organometallics*, 2010, **29**, 5614; (*d*) C. Fliedel, G. Schnee and P. Braunstein, *Dalton Trans.*, 2009, 2474.

10 M. Raynal, X. H. Liu, R. Pattacini, C. Vallée, H. Olivier-Bourbigou and P. Braunstein, *Dalton Trans.*, 2009, 7288.

11 H. Krishna, S. S. Krishnamurthy and M. Nethaji, *Polyhedron*, 2006, **25**, 3189.

12 W.-B. Zhou, Z.-C. Dong, J.-L. Song, H.-Y. Zeng, R. Cao, G.-C. Guo, J.-S. Huang and J. Li, *J. Cluster Sci.*, 2002, **13**, 119.

13 (*a*) U. Schubert, D. Neugebauer and A. A. M. Aly, *Z. Anorg. Allg. Chem.*, 1980, **464**, 217; (*b*) A. A. M. Aly, D. Neugebauer, O. Orama, U. Schubert and H. Schmidbaur, *Angew. Chem., Int. Ed. Engl.*, 1978, **17**, 125.

14 H. T. Shi, T. K. Duan, C. Xu and Q. F. Zhang, *Z. Naturforsch., B: Chem. Sci.*, 2009, **64**, 204.

15 (*a*) C. Desmarets, I. Azcarate, G. Gontard and H. Amouri, *Eur. J. Inorg. Chem.*, 2011, **29**, 4558; (*b*) G. S. M. Tong, S. C. F. Kui, H.-Y. Chao, N. Zhu and C.-M. Che, *Chem.–Eur. J.*, 2009, **15**, 10777; (*c*) G.-G. Luo, R.-B. Huang, J.-H. Chen, L.-R. Lin and L.-S. Zheng, *Polyhedron*, 2008, **27**, 2791; (*d*) P. Braunstein, C. Frison, N. Oberbeckmann-Winter, X. Morise, A. Messaoudi, M. Bénard, M.-M. Rohmer and R. Welter, *Angew. Chem., Int. Ed.*, 2004, **43**, 6120; (*e*) T. Q. Ly and J. D. Woollins, *Coord. Chem. Rev.*, 1998, **176**, 451.

16 (*a*) L.-L. Song, Q.-H. Jin, L.-N. Cui and C.-L. Zhang, *Inorg. Chim. Acta*, 2010, **363**, 2425; (*b*) L.-L. Song, L.-N. Cui, Q.-H. Jin and C.-L. Zhang, *Acta Crystallogr., Sect. E: Struct. Rep. Online*, 2010, **66**, m1237; (*c*) P. Teo, L. L. Koh and T. S. A. Hor, *Inorg. Chem.*, 2008, **47**, 9561; (*d*) Y.-Y. Lin, S.-W. Lai, C.-M. Che, W.-F. Fu, Z.-Y. Zhou and N. Zhu, *Inorg. Chem.*, 2005, **44**, 1511; (*e*) D. Perreault, M. Drouin, A. Michel, V. M. Miskowski, W. P. Schaefer and P. D. Harvey, *Inorg. Chem.*, 1992, **31**, 695.

17 C. S. Browning, D. H. Farrar and D. C. Frankel, *Z. Kristallogr. – New Cryst. Struct.*, 1997, **212**, 201.

 This journal is © The Royal Society of Chemistry 2013

18 H. W. Xu, Z. N. Chen and J. G. Wu, *Acta Crystallogr., Sect. E: Struct. Rep. Online*, 2002, **58**, M631.
19 D. M. Ho and R. Bau, *Inorg. Chem.*, 1983, **22**, 4073.
20 (*a*) G. H. Penner and X. Liu, *Prog. Nucl. Magn. Reson. Spectrosc.*, 2006, **49**, 151; (*b*) K. Zangger and I. M. Armitage, Silver and gold NMR, *Metal-Based Drugs*, 1999, **6**, 239.
21 (*a*) E. J. Sekabunga, M. L. Smith, T. R. Webb and W. E. Hill, *Inorg. Chem.*, 2002, **41**, 1205; (*b*) E. L. Muetterties and C. W. Alegranti, *J. Am. Chem. Soc.*, 1970, **92**, 4114.
22 T. C. Deivaraj and J. J. Vittal, *J. Chem. Soc., Dalton Trans.*, 2001, 322.
23 M. Raynal, C. S. J. Cazin, C. Vallée, H. Olivier-Bourbigou and P. Braunstein, *Chem. Commun.*, 2008, 3983.
24 (*a*) Effendy, J. V. Hanna, F. Marchetti, D. Martini, C. Pettinari, R. Pettinari, B. W. Skelton and A. H. White, *Inorg. Chim. Acta*, 2004, **357**, 1523; (*b*) P. A. W. Dean, J. J. Vittal and R. S. Srivastava, *Can. J. Chem.*, 1987, **65**, 2628.
25 (*a*) A. Mêmе, A. R. Stefankiewicz, J. Harrowfield, X.-Y. Cao, J. Huuskonen, K. Rissanen, J.-M. Lehn, H. Nierengarten and E. Leize, *Eur. J. Inorg. Chem.*, 2012, 647; (*b*) M. F. Wyatt, *J. Mass Spectrom.*, 2011, **46**, 712.
26 V. Rosa, C. I. Santos, R. Welter, G. Aullon, C. Lodeiro and T. Aviles, *Inorg. Chem.*, 2010, **49**, 8699.
27 D. F. Clemens and W. E. Perkinson, *Inorg. Chem.*, 1974, **13**, 333.
28 W. von Seidel and M. Alexiev, *Z. Anorg. Allg. Chem.*, 1978, **438**, 68.
29 Bruker-Nonius, Nonius BV, The Netherlands, 1998.
30 G. M. Sheldrick, *SHELXL-97, Program for the Refinement of Crystal Structure*, University of Göttingen, Germany, 1997.
31 A. L. Spek, *J. Appl. Crystallogr.*, 2003, **36**, 7.
32 R. H. Blessing, *Acta Crystallogr.*, 1995, **51**, 33.

Published on 08 April 2013 on http://pubs.rsc.org | doi:10.1039/C3DT50555C
Downloaded on 04/05/2013 13:38:45.

CHAPITRE 3

Ce chapitre est présenté sous forme d'une publication parue dans *Chem.* Asian J., **2013**, 8, 1795.

Les contributions respectives des auteurs sont :

A. Ghisolfi, C. Fliedel, V. Rosa, P. Braunstein – *développement du projet*

A. Ghisolfi – *Synthèse et caractérisation du ligand et des complexes, simulation des spectres NMR*

A. Thibon – *mesures UV-Vis*

K. Yu. Monakhov – *calculs théorétiques*

R. Pattacini – *étude structurale par diffraction des rayons X*

Solvent-Dependent Reversible Ligand Exchange in Nickel Complexes of a Monosulfide Bis(diphenylphosphino)(N-thioether)amine

Alessio Ghisolfi, [a] Christophe Fliedel,*[a,c] Vitor Rosa,[a,c] Roberto Pattacini,[a] Aurore Thibon, [b] Kirill Yu. Monakhov, [d] and Pierre Braunstein*[a]

[a] Laboratoire de Chimie de Coordination Institut de Chimi (UMR7177 CNRS), Université de Strasbourg, 4 rue Blaise Pascal, CS 90032, 67081 Strasbourg (France).

[b]Laboratoire de Chimie Biomimétique des Métaux de Transition, Institut de Chimie (UMR 7177 CNRS), Université de Strasbourg, 4 rue Blaise Pascal, CS 90032, 67081 Strasbourg (France).

[c]REQUIMTE, Departamento de Quimica Faculdade de Ciéncias e Tecnologia Universidade Nova de Lisboa, Caparica, 2829-516 (Portugal).

[d]Institut fir Anorganische Chemie RWTH-Aachen University, Landoltweg 1, 52074 Aachen (Germany)

Des informations complémentaires sont disponibles sur internet:

http://onlinelibrary.wiley.com/store/10.1002/asia.201300687/asset/supinfo/asia_201300687_sm_miscellaneous_information.pdf?v=1&s=ffd60e6e7ab2a582b3a21fecc9a85aefeecbd91d

Résumé du Chapitre 3

La réactivité du ligand fonctionnel $N(PPh_2)_2(CH_2)_3SMe$ **L1** ainsi que celle de son dérivé monosulfure $(Ph_2P)N\{P(S)Ph_2\}(CH_2)_3SMe$ (**L1·S**) a été étudiée vis-à-vis des ions Ni(II) dans le but de préparer des pré-catalyseurs pour l'oligomérisation de l'éthylène. Alors que **L1** forme exclusivement un complexe plan-carré diamagnétique [$NiCl_2$(**L1**)], **L1·S** donne lieu à la mise en place d'un équilibre entre un complexe mono-chélate [$NiCl_2$(**L1·S**)] diamagnétique, et une paire d'ions formée par un complexe bis-chélate dicationique [Ni(**L1·S**)$_2$]$^{2+}$ associé au dianion paramagnétique $[NiCl_4]^{2-}$. Tous ces complexes ont été entièrement caractérisés par diffraction des rayons X et grâce aux techniques spectroscopiques de résonance magnétique nucléaire (RMN), infrarouge et UV-visible ainsi que par des calculs théoriques. Sur la base de travaux antérieurs du laboratoire, nous avons pu montrer que cet équilibre dépend de la température et de la polarité du solvant.

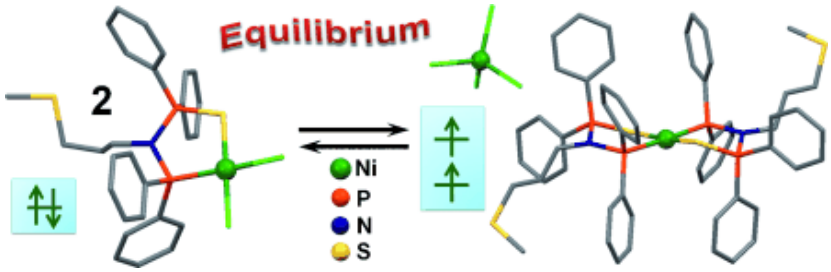

DOI: 10.1002/asia.201300687

Solvent-Dependent Reversible Ligand Exchange in Nickel Complexes of a Monosulfide Bis(diphenylphosphino)(*N*-thioether)amine

Alessio Ghisolfi,[a] Christophe Fliedel,*[a, c] Vitor Rosa,[a, c] Roberto Pattacini,[a] Aurore Thibon,[b] Kirill Yu. Monakhov,[a, d] and Pierre Braunstein*[a]

Abstract: The coordination chemistry of the DPPA-type functional phosphine bis(diphenylphosphino)(*N*-thioether)-amine $N(PPh_2)_2(CH_2)_3SMe$ (**1**) and its monosulfide derivative, $(Ph_2P)N\{P(S)Ph_2\}(CH_2)_3SMe$ (**1·S**), towards Ni^{II} precursors has been investigated. The crystal structures of $N\{P(S)Ph_2\}_2(CH_2)_3SMe$ (**1·S$_2$**), $[NiCl_2\{(Ph_2P)_2N(CH_2)_3SMe\text{-}P,P\}]$ (**2**), $[NiCl_2((Ph_2P)N\{P(S)Ph_2\}(CH_2)_3SMe\text{-}P,S)]$ (**3**), $[Ni((Ph_2P)N\{P(S)Ph_2\}(CH_2)_3SMe\text{-}P,S)_2]NiCl_4$ (**3′**), $[Ni((Ph_2P)N\{P(S)Ph_2\}(CH_2)_3SMe\text{-}P,S)_2](BF_4)_2$ (**4**), and $[Ni((Ph_2P)NH\{P(S)Ph_2\}\text{-}P,S)_2]Cl_2$ (**5**) have been determined by single-crystal X-ray diffraction. In all of the complexes with the hybrid ligand **1·S**, P,S-chelation to the Ni^{II} center is observed. Despite the stability generally associated with five-membered ring chelation, easy migration of this LL′-type P,S-chelating ligand from one metal center to another was observed, which accounts for the reversible ligand-redistribution reaction occurring in the equilibrium between the neutral, diamagnetic complex $[NiCl_2LL']$ and the paramagnetic ion-pair $[Ni(LL')_2][NiCl_4]$. Detailed investigations by multinuclear NMR, UV/Vis, and FTIR spectroscopic methods and DFT calculations are reported. Each of the formula isomers **3** and **3′** can be selectively obtained, depending on the experimental conditions.

Keywords: chelates · ligand exchange · nickel · short-bite ligands · solvent effects

Introduction

Bis(diphenylphosphino)amine (DPPA)-type ligands (Scheme 1, **A** and **B**) and their unsymmetrical mono-oxidized derivatives, which contain one P^{III} atom and one P^{V} atom (Scheme 1, **C**), continue to attract much attention owing to the diversity in their coordination modes (monodentate, bridging, chelating), which results in a rich coordination chemistry for the neutral ligands, such as $Ph_2PNHPPh_2$ and $Ph_2P(E)NHPPh_2$, as well as their deprotonated forms, that is, $(Ph_2PNPPh_2)^-$ and $(Ph_2P(E)NPPh_2)^-$ (Scheme 1, **D** and **E**, respectively).[1] In the latter two cases, coordination of the nitrogen atom to a metal center becomes an additional possibility. Furthermore, DPPA-type ligands are also attractive because of the relative ease with which various substituents can be introduced onto the nitrogen atom (Scheme 1, **B** and **C**) and suitable *N*-pendant groups can allow the formation of polymetallic complexes[2] or the anchoring of coordination compounds into mesoporous materials[3] or on metallic surfaces.[4] Metal complexes

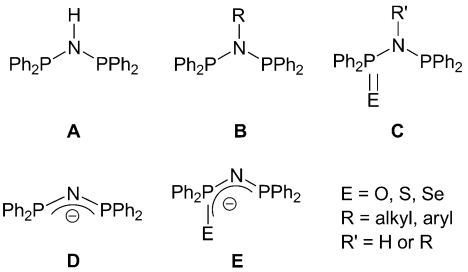

Scheme 1. Structures of the neutral DPPA ligand (**A**), an *N*-substituted DPPA-type ligand (**B**), its mono-oxidized derivative (**C**), and the deprotonated forms of the DPPA and mono-oxidized DPPA (R′ = H) ligands (**D** and **E**, respectively).

[a] A. Ghisolfi, Dr. C. Fliedel, Dr. V. Rosa, Dr. R. Pattacini, Dr. K. Yu. Monakhov, Prof. P. Braunstein
Laboratoire de Chimie de Coordination
Institut de Chimie (UMR 7177 CNRS)
Université de Strasbourg
4 rue Blaise Pascal, CS 90032, 67081 Strasbourg (France)
Fax: (+33) 368-851-322
E-mail: braunstein@unistra.fr

[b] Dr. A. Thibon
Laboratoire de Chimie Biomimétique des Métaux de Transition, Institut de Chimie (UMR 7177 CNRS)
Université de Strasbourg
4 rue Blaise Pascal, CS 90032, 67081 Strasbourg (France)

[c] Dr. C. Fliedel, Dr. V. Rosa
Current Address:
REQUIMTE, Departamento de Quimica
Faculdade de Ciências e Tecnologia
Universidade Nova de Lisboa
Caparica, 2829-516 (Portugal)
E-mail: christophe.fliedel@fct.unl.pt

[d] Dr. K. Yu. Monakhov
Current Address:
Institut für Anorganische Chemie
RWTH-Aachen University
Landoltweg 1, 52074 Aachen (Germany)

Supporting information for this article is available on the WWW under http://dx.doi.org/10.1002/asia.201300687.

© 2013 Wiley-VCH Verlag GmbH & Co. KGaA, Weinheim

of such short-bite ligands display various catalytic properties[5] and their Ni and Cr derivatives have been found to be excellent precursors for the catalytic production of polyethylene or for the selective oligomerization of ethylene.[6] The characterization of the active species that are formed in the presence of organoaluminum co-catalysts in such processes remains challenging and the few examples that have been reported revealed a non-innocent behavior of the ancillary ligand.[7] Therefore, non-ambiguous characterization of the pre-catalyst, preferably both in the solid-state and in solution, is required to understand and improve the catalyst properties. Subtle changes (e.g., solvent, temperature, pressure) can profoundly affect the structure of the complexes, as was recently observed in 1) the temperature-dependent isolation of mono- or dinuclear Ni^{II} complexes with P,N chelates;[8] 2) the pressure-induced fragmentation of a tetranuclear complex with $20e^-$ Ni centers into mononuclear complexes $[NiCl_2(P,N)]$ with $16e^-$ Ni centers (Scheme 2, left);[9] and 3) the equilibrium in solution between two formula isomers, $[Ni(P,N)_2][NiCl_4]$ and $[NiCl_2(P,N)]$, of a Ni^{II} complex that contains a DBU-derived P,N ligand (DBU = 1,8-diazabicyclo[5.4.0]undec-7-ene; Scheme 2, right).[10]

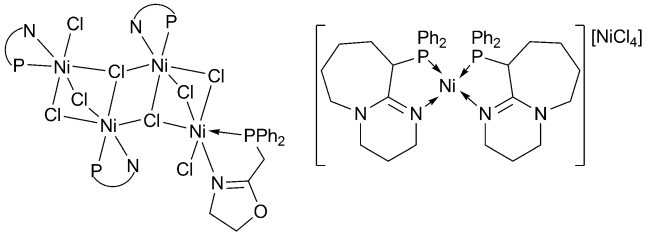

Scheme 2. Tetranuclear phosphino oxazoline Ni^{II} (left) and bis-chelated DBU-*P* $Ni^{II}/NiCl_4$ complexes (right), which show an equilibrium with their monochelated $[NiCl_2LL']$ formula isomers.[9,10]

Ligand rearrangement and/or coordination/decoordination mechanisms in coordination complexes can strongly affect their physical properties and/or reactivities and can lead to switchable catalysts.[11] This phenomenon is one of the reasons why metal complexes that contain ligands with mixed donor sets of different hard/soft properties, also called "hybrid ligands", are of long-standing interest to us. This type of ligand can exhibit a hemilabile behavior by the reversible coordination/decoordination of the weaker donor and, thus, facilitate substrate coordination, which may, in turn, result in improved catalytic activity.[12,17]

Herein, we report new nickel(II) complexes of a *N*-thioether-functionalized DPPA-type ligand, $N(PPh_2)_2(CH_2)_3SMe$ (*P*,*P*; **1**), and its new monosulfide derivative, $(Ph_2P)N\{P(S)Ph_2\}(CH_2)_3SMe$ (*P*,P=*S*; **1·S**). Complexes of the latter ligand display an unprecedented equilibrium between a mononuclear form, $[NiCl_2((Ph_2P)N\{P(S)Ph_2\}(CH_2)_3SMe\text{-}P,S)]$ ($[NiCl_2(P,P{=}S)]$, **3**), and a dinuclear ion pair $[Ni((Ph_2P)N\{P(S)Ph_2\}(CH_2)_3SMe\text{-}P,S)_2]NiCl_4$ ($[Ni(P,P{=}S)_2]NiCl_4$, **3′**), which implies the transfer of a chelating ligand from one metal center to another under mild conditions. These two formula isomers were fully characterized, including by multinuclear NMR, UV/Vis, and FTIR spectroscopy, and their solid-state structures were determined by X-ray crystallography. Both compounds **3** and **3′** can be selectively produced (>90%) through tuning of the experimental conditions. These unusual experimental observations were rationalized by quantum chemical calculations.

Results and Discussion

The synthesis of complexes of type $[NiX_2(LL')]$ (e.g., LL′ = P,N or P,O; X = Cl, Br) by treatment of the ligand with a $[NiX_2L_2]$ (L_2 = labile ligand(s)) precursor is well-established.[13] This strategy was readily applied to ligand **1** and afforded the Ni^{II} complex $[NiCl_2\{(Ph_2P)_2N(CH_2)_3SMe\text{-}P,P\}]$, ($[NiCl_2(\mathbf{1})]$, **2**, Scheme 3c). The new ligand, **1·S**, could not

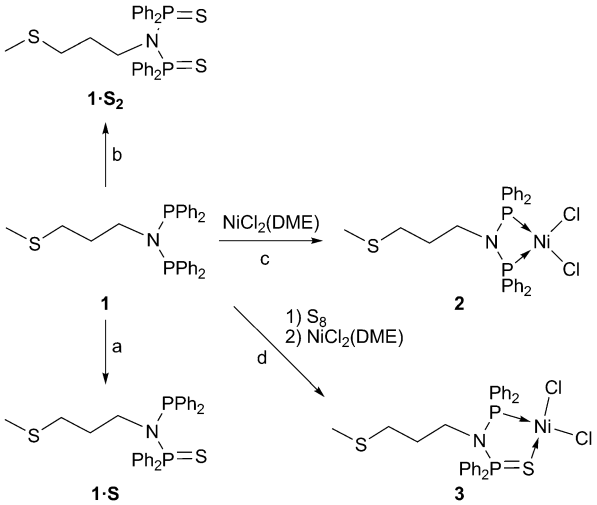

Scheme 3. Synthesis of (*P*,P=*S*) and (P=*S*,P=*S*) ligands **1·S** and **1·S$_2$** and Ni complexes **2** and **3**: a) S_8 (1.5 equiv), CH_2Cl_2, RT, 30 min; b) S_8 (2.2 equiv), toluene, 115 °C, 3 h; c) $[NiCl_2(DME)]$ (1 equiv), CH_2Cl_2, RT, 2 h; d) S_8 (1.5 equiv), CH_2Cl_2, RT, 30 min, then $[NiCl_2(DME)]$ (0.55 equiv), CH_2Cl_2, RT, 4 h. DME = 1,2-dimethoxyethane.

be obtained in its pure form (about 70%), owing to the formation of a bis-sulfide byproduct **1·S$_2$** (about 30%, Scheme 3a), but the latter species could be quantitatively produced by using a slight excess of elemental sulfur (Scheme 3b). Therefore, ligand **1·S** was always prepared in situ for the complexation reactions with Ni^{II} centers; the **1·S$_2$** byproduct was removed by successive washing of the product with toluene (Scheme 3d). Species **1·S** and **1·S$_2$** were both fully characterized, including by X-ray crystallography in the latter case (Figure 1). Similarly to PNP ligand **1** and in contrast to its monosulfide derivative, **1·S** (see below), the $^{31}P\{^1H\}$ NMR spectrum of **1·S$_2$** exhibits a unique singlet for the two equivalent phosphorous atoms at δ = 69.8 ppm. Its coordination properties will not be discussed in this paper. The structural parameters of ligand **1·S$_2$** are

© 2013 Wiley-VCH Verlag GmbH & Co. KGaA, Weinheim

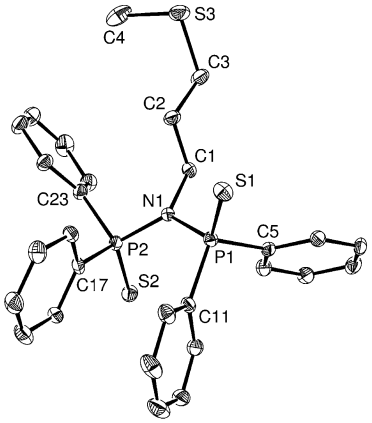

Figure 1. Solid-state molecular structure of compound **1·S$_2$**; only one of the two independent molecules is represented. Thermal ellipsoids are set at 30% probability. Hydrogen atoms are omitted for clarity. Selected bond lengths [Å] and angles [°]: P1–N1 1.713(3), P2–N1 1.697(3), P1–S1 1.944 (1), P2–S2 1.944(1); P1-N1-P2 127.2 (2), N1-P1-S1 113.1(1), N1-P2-S2 115.4(1).

closely related to those of a bis-oxidized (P=O, P=O), *N*-alkyl-substituted DPPA derivative[1e] and a bis-selenide (P=Se, P=Se), *N*-methoxyaryl-substituted DPPA derivative,[1f] in particular, the *anti*-orientation of the two P=E bonds and the PNP angles. The P=S bond lengths in **1·S$_2$** are intermediate between those of the corresponding P=O and P=Se bonds, which reflects their differences in atomic radii.

The reactions of ligands **1**[6k] and **1·S** with [$NiCl_2$(DME)] (DME = 1,2-dimethoxyethane) in a 1:1 ratio led to intensely colored powders of complexes [$NiCl_2${(Ph_2P)$_2$N(CH_2)$_3$SMe-*P,P*}] (**2**, red) and [$NiCl_2$((Ph_2P)N{P(S)Ph_2}(CH_2)$_3$SMe-*P,S*)] (**3**, purple), respectively, in good yields. Both of them were expected to be of the general type [$NiCl_2$(LL′)] (LL′ = *P,P* and *P*,P=*S*, respectively; Scheme 3). These complexes retained their color in solution and they were characterized by ^{31}P{^{1}H} NMR spectroscopy. Although we anticipated similar signals to those of the free ligands, that is, a singlet for the complex that was derived from ligand **1** (δ = 63.5 ppm) and two doublets for the complex that resulted from the reaction with **1·S** (δ = 54.7 and 72.6 ppm; ^2J(P,P) = 88.1 Hz), several unexpected features were observed.

The diamagnetic character of complex **2** allowed its characterization by multinuclear NMR spectroscopy. As expected, the two equivalent phosphorus atoms of the coordinated ligand (**1**) gave rise to a singlet in the ^{31}P{^{1}H} NMR spectrum at δ = 42.9 ppm, which was within the typical range for square-planar [$NiCl_2$(*P*,N,*P*)] complexes.[5a,14] In the ^{1}H NMR spectrum of complex **2**, all of the protons of the N-substituent were assigned, whilst the aromatic protons gave rise to three multiplets. The chemical shifts that corresponded to the CH_2SCH_3 moiety were very close to those of the free ligand (δ = 2.06 and 1.84 ppm (**2**) versus δ = 2.13 and 1.86 ppm (**1**)), thus indicating that no coordination of the thioether function occurred in solution. The expected molecular structure of complex **2** was confirmed by single-crystal X-ray crystallography (Figure 2). The tetra-coordinated

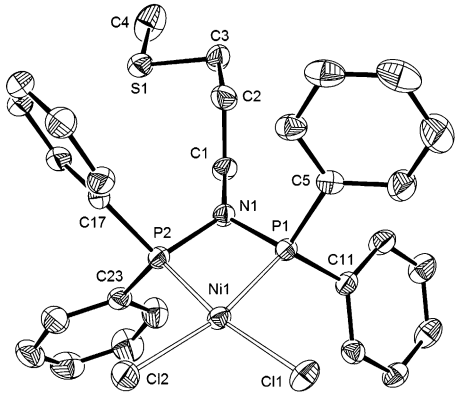

Figure 2. Solid-state molecular structure of complex **2**. Thermal ellipsoids are set at 30% probability. Hydrogen atoms are omitted for clarity. Selected bond lengths and angles are listed in Table 1.

nickel center is in a distorted square-planar environment and the diphosphine ligand (**1**) acts as a chelate, thereby forming a four-membered metallocycle. The coordination sphere of the metal is completed by two chlorine ligands. Selected bond lengths and angles are summarized in Table 1 and they are within the observed range in the only five other [$NiCl_2$(*P*,N,*P*)] structures reported so far.[6j,15] In particular, the P1-N1-P2 bite angle is 73.69(3)°. Deformation away from the ideal square-planar geometry induces the opening of the Cl-Ni-Cl angle to 99.77(3)°. The UV/Vis spectrum of the deep-red solution of complex **2** in CH_2Cl_2

Table 1. Selected bond lengths [Å] and angles [°] in complexes **2**, **3**, **3′**·CH_2Cl_2, **4**·CH_2Cl_2·H_2O, and **5**·4 $CHCl_3$.

	2	**3**		**3′**·CH_2Cl_2	**4**·CH_2Cl_2·H_2O	**5**·4 $CHCl_3$
P1–Ni1	2.1278(8)	2.1393(15)	P2-Ni1	2.2205(9)	2.1873(8)	2.2046(11) (P1)
P2(or S1)–Ni1	2.1164(8)	2.1535(18)	P4–Ni1	2.2045(9)		
P2–S1		2.0119(18)	S1–Ni1	2.1978(9)	2.1904(7)	2.1779(12)
			S3–N1	2.1712(9)		
N1–P1	1.696(2)	1.719(4)		1.671(3))	1.663(3)	1.678(4)
N1–P2	1.687(2)	1.665(5)		1.707(2)	1.706(3)	1.638(4
Ni1–Cl1	2.1901(8)	2.1687(16)	P1–S1	2.0128(12)	2.0170(11)	2.0281(15) (P2)
Ni1–Cl2	2.1990(8)	2.2219(15)	P3–S3	2.0218(11)		
			Ni2–Cl (average)	2.2623(13)		
			N1–Cl1			2.993(4)
P1-Ni1-P2(or S1)	73.69(3)	94.12(6)	P2-Ni1-S1	91.46(3)	90.18(3)	91.96(4) (P1)
			P4-Ni1-S3	91.83(3)		
Cl1-Ni1-Cl2	99.77(3)	95.24(6)	Cl-Ni1-Cl	109.48(5)		
P1-N1-P2	97.59(11)	118.5(2)	P1-N1-P2	114.50(14)	117.32(14)	121.0(2)
			P3-N1-P4	116.68(15)		

© 2013 Wiley-VCH Verlag GmbH & Co. KGaA, Weinheim

was recorded within the range 200–800 nm. In addition to strong absorptions at higher energy (below 300 nm), which can be assigned to π–π* transitions of the phenyl rings on the ligand, an intense band is observed at 468 nm for complex **2** (see the Supporting Information, Figure S1), which originates from metal-to-ligand charge transfer (MLCT). Both the $^{31}P\{^{1}H\}$ NMR spectra and the electronic spectra of complex **2** show no change upon decreasing the temperature.

In contrast to *P,P* complex **2**, the $^{31}P\{^{1}H\}$ NMR spectrum of *P*,P=*S* complex **3**, which resulted from the reaction of ligand **1·S** with $[NiCl_2(DME)]$ (Scheme 3 d), did not show the expected pattern; rather, instead of two doublets for the two non-equivalent P^{III} and P^{V} donors, as observed for the free ligand, a broad singlet centered at $\delta = 86.6$ ppm was observed (Figure 3, bottom). The paramagnetic nature of the sample prevented the recording of well-resolved ^{1}H or ^{13}C NMR spectra. At this stage, we could not establish the exact structure of complex **3**. The occurrence of a dynamic process for complex **3** in solution, which involved a paramagnetic species, could also be suggested in view of the unsymmetrical nature of **1·S**. The dynamic behavior of coordinated phosphorus- and sulfur-based mixed ligands in solution has previously been described for *P,N*-nickel[9,10] and *S,*C_{NHC}-palladium complexes[16] and, more generally, with hybrid ligands, thus leading to hemilabile systems.[12,17]

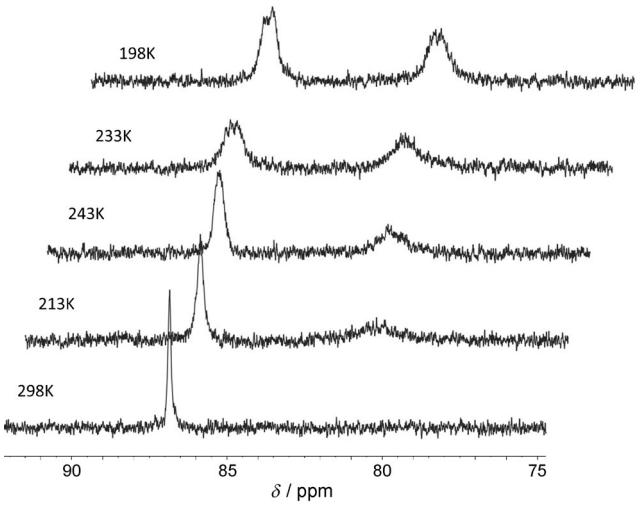

Figure 3. Variable-temperature $^{31}P\{^{1}H\}$ NMR spectra of a solution of complex **3** in CD_2Cl_2, which shows the splitting of the broad singlet at $\delta = 86.6$ ppm into two very broad signals centered at $\delta = 86.3$ and 80.6 ppm and the concomitant increase in the paramagnetic character of the solution.

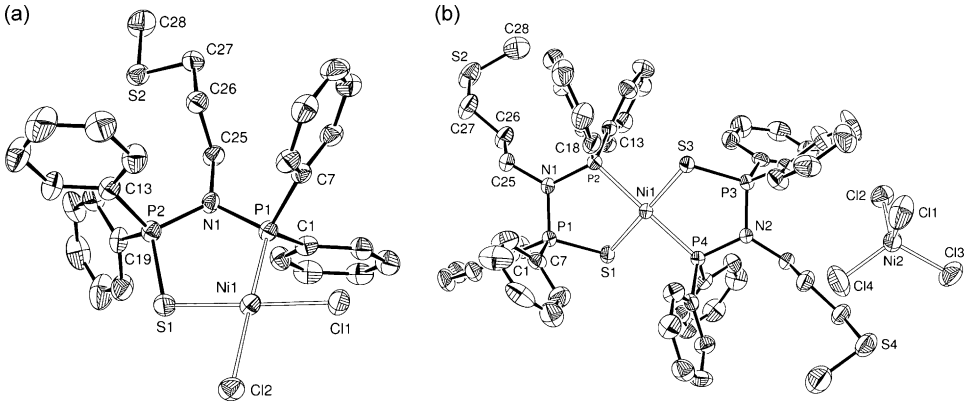

Figure 4. Solid-state molecular structures of formula isomers **3** (a) and **3′** (b). Thermal ellipsoids are set at 30% probability. Hydrogen atoms are omitted for clarity. Selected bond lengths and angles are listed in Table 1.

Interestingly, X-ray diffraction studies on purple crystals that were obtained by the slow diffusion of pentane into a saturated solution of complex **3** revealed the structure shown in Figure 4 a, in which the $[NiCl_2(LL')]$ core was similar to that of complex **2**, with ligand **1·S** replacing **1** as a chelate (Table 1). Notably, no N–C bond cleavage was observed in this reaction, in contrast to observations made when $NiCl_2{\cdot}6H_2O$ was reacted with an *N*-((*S*)-CHMePh)-substituted mono-selenide DPPA-type ligand.[1c] The Ni^{II} center is again tetra-coordinated, in a slightly distorted square-planar geometry, with ligand **1·S** forming a five-membered metallocycle and two chlorine atoms completing the metal coordination sphere. The key structural difference between complexes **2** and **3** is the bite angle of the chelating ligand: 73.69(3)° for the *P,P* ligand in complex **2** versus 94.12(6)° for the *P*,P=*S* analogue in complex **3**. To the best of our knowledge, complex **3** is the first structurally characterized example of a complex of general formula $[NiCl_2(P)(P{=}S)]$. Among all of the structures reported herein, it is in complex **3** that the difference between the N1–P^{III} and N1–P^{V} distances is most pronounced (1.719(4) and 1.665(5) Å, respectively). This result may be related to the electronegativity of the S atom, which strengthens the P–N bond adjacent to it. Similar effects have been observed in related complexes with P=O, P=S, or P=Se groups.[1c–f] The longer Ni1–Cl2 bond (2.2219(15) Å) with respect to the Ni–Cl1 bond (2.1687(16) Å) in complex **3** is due to the stronger *trans* influence of the P donor compared to the S donor. A similar trend was observed for $PdCl_2$ and $PtCl_2$ complexes with the chelating *N*-((*S*)-α-methylbenzyl)-substituted mono-sulfide and mono-selenide ligands, $[PdCl_2(P,S)]$, $[PtCl_2(P,S)]$, $[PdCl_2(P,Se)]$, and $[PtCl_2(P,Se)]$ and a $PtCl_2$ complex that was chelated by an *N*-methoxyaryl-functionalized mono-sulfide DPPA derivative.[1d–f] Although the solid-state structure of complex **3** was as expected (Scheme 3), it did not explain the paramagnetic character that was observed in solution by NMR spectroscopy.

Cooling a solution of complex **3** in CD_2Cl_2 from 298 K to 193 K and recording the $^{31}P\{^{1}H\}$ NMR spectra at regular in-

© 2013 Wiley-VCH Verlag GmbH & Co. KGaA, Weinheim

tervals led to the splitting of the broad singlet ($\delta =$ 86.6 ppm) that was observed at room temperature into two very broad signals centered at $\delta = 86.3$ and 80.6 ppm, with a concomitant increase in the paramagnetic character of the solution (Figure 3 and the Supporting Information, Figure S3). Although these changes could be due to, for example, a modification of the coordination geometry around the metal center from square planar to tetrahedral or to a (reversible) change in the nuclearity of the complex,[9] we will show below that they correspond to the occurrence of a new species (**3′**), which contains the tetrahedral complex $[NiCl_4]^{2-}$. The influence of temperature on the nature of complex **3** is also evidenced by the changes in the electronic spectra recorded in CH_2Cl_2 within the range 193–298 K (Figure 5). The UV/Vis spectrum of complex **3** at room temperature (red line) is significantly different from that of complex **2** in two main aspects: Firstly, whilst complex **2** shows an intense absorption at 468 nm, complex **3** exhibits a shoulder at 345 nm, which can be assigned to a MLCT transition, and a weak absorption at 538 nm, owing to the spin-allowed d–d transition for a square-planar nickel(II) complex. Secondly, the temperature decrease is accompanied by a decrease in the intensity of the d–d transition band of complex **3** at 538 nm, whereas, as stated above, no change was observed for complex **2**. Interestingly, two very weak bands were observed at about 650 and 700 nm in the low-temperature spectra (i.e., 213 and 193 K); these absorptions are characteristic of the tetrahedral $[NiCl_4]^{2-}$ complex.[18]

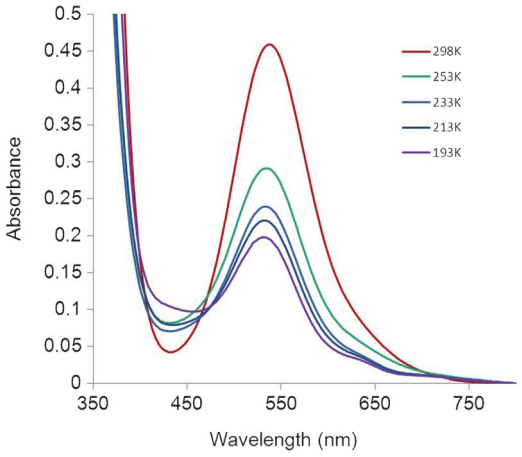

Figure 5. Variable-temperature UV/Vis spectra of a $\times 10^{-2}$ M solution of complex **3** in CH_2Cl_2.

Among the purple crystals that were grown by slow diffusion of pentane into a saturated solution of complex **3** in CH_2Cl_2, very few green crystals were found and X-ray diffraction analysis revealed the exact nature of this green complex as having the formula $[Ni((Ph_2P)N\{P(S)Ph_2\}(CH_2)_3SMe\text{-}P,S)_2]NiCl_4$ (**3′**), as shown in Figure 4b. Complex **3′** is a formula isomer of complex **3**, which consists of an ion pair that is composed of two tetra-coordinated Ni species. The dication fragment of complex **3′** contains a slightly distorted square-planar Ni center that is surrounded by two *P*,P=*S*-chelating **1·S** ligands in a *trans* arrangement (P *trans* to P and S *trans* to S) and the charges are balanced by a tetrahedral $NiCl_4$ dianion. To the best of our knowledge, complex **3′** is the first example of a structurally characterized compound of the general formula $[Ni(P)_2(P{=}S)_2]$, along with complexes **4** and **5** (see below). The isolation and structural characterization of ion-pair **3′** suggested that it could be the species in equilibrium with complex **3** (Scheme 4) and the

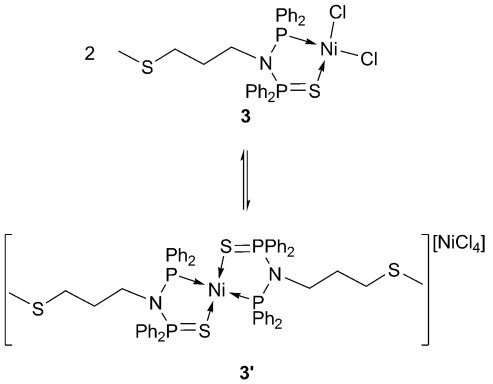

Scheme 4. Equilibrium between structures **3** and **3′** in CH_2Cl_2.

observed paramagnetism would be due to the presence of the $[NiCl_4]^{2-}$ complex. This hypothesis is supported by the low-temperature UV/Vis spectra of complex **3** in CH_2Cl_2, which exhibit characteristic bands for the tetrahedral $[NiCl_4]^{2-}$ dianion (see above). Furthermore, density functional calculations that were performed for ion pair **3′** show that the paramagnetism of the latter complex is caused by the $S = 1$ $[NiCl_4]^{2-}$ fragment, with two unpaired electrons at the Ni^{II} center of approximately D_{2d} symmetry.[19] The dication fragment of complex **3′** has the $S = 0$ ground state and, thus, is diamagnetic (see the Supporting Information, Figures S4 and S5).

Ion pairs that involve a bis-chelated Ni^{II} cationic complex and the $[NiCl_4]^{2-}$ counterion have been investigated since the early report of Schaefer and Uhlig in 1974.[20] However, to the best of our knowledge, the existence of an equilibrium between these ion pairs and the parent mononuclear complex of the type $[NiCl_2LL']$ was only first reported in 2009.[10] Until this work, a pair that was constituted of monochelated $[NiCl_2LL']$ and bis-chelated dinuclear $[Ni(LL')_2]NiCl_4$ formula isomers had never been isolated and fully characterized, including by single-crystal X-ray diffraction.

To gain deeper insight into this system, the complex $[Ni((Ph_2P)N\{P(S)Ph_2\}(CH_2)_3SMe\text{-}P,S)_2](BF_4)_2$ (**4**), a diamagnetic analog of complex **3′**, was synthesized by the reaction of $[Ni(NCMe)_6](BF_4)_2$ with ligand **1·S** in a 1:2 ratio (Scheme 5) and isolated as a red crystalline solid. Its solution in CH_2Cl_2 or in a CH_2Cl_2/MeOH mixture (it is insoluble in pure MeOH) retained its red color. The slightly distorted square-

© 2013 Wiley-VCH Verlag GmbH & Co. KGaA, Weinheim

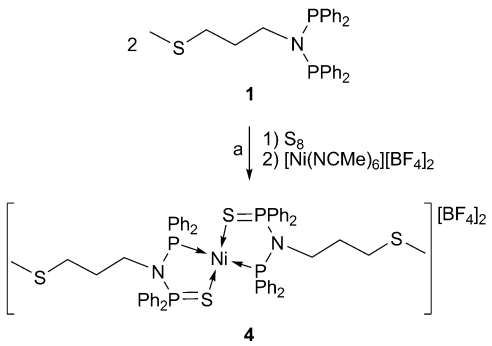

Scheme 5. Synthesis of complex **4**, a diamagnetic analogue of **3′**: a) S_8 (1.5 equiv), CH_2Cl_2, RT, 30 min, then $[Ni(NCMe)_6](BF_4)_2$ (0.25 equiv), CH_2Cl_2, RT, 4 h.

planar coordination geometry around the Ni^{II} center, as well as the *trans*-arrangement of the two **1·S** ligands, were confirmed by single-crystal X-ray diffraction studies (Figure 6). All of the structural parameters (i.e., bond lengths and

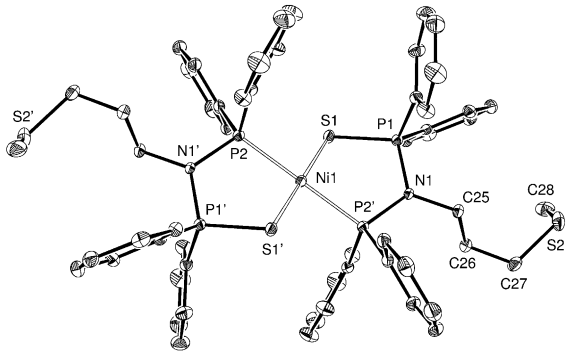

Figure 6. Solid-state molecular structure of complex **4**·CH_2Cl_2·H_2O. Thermal ellipsoids are set at 30% probability. Hydrogen atoms, solvent molecules, and two BF_4 anions are omitted for clarity. Selected bond lengths and angles are listed in Table 1.

angles) that involved the Ni^{II} center were in agreement with those observed for the dicationic fragment of complex **3′** (Table 1). As expected for a square-planar diamagnetic complex, the $^{31}P\{^1H\}$ NMR (CD_2Cl_2, RT) spectrum of complex **4** exhibited two sharp signals, which appeared as "triplets" at $\delta = 95.5$ and 86.3 ppm with a $^2J(P,P)$ coupling constant of 68.3 Hz (see the Experimental Section) for non-equivalent *P*=S and *P* nuclei, respectively (Figure 7, bottom). The UV/Vis spectrum of complex **4** in CH_2Cl_2 ($c = \times 10^{-3}$ M) shows a typical intense absorption between 324–358 nm and, at higher concentrations, a shoulder at 430 nm, but no absorption at 538 nm, at odds with complexes **3/3′** (Figure 11, orange line).

Complex **4** could be easily converted into complexes **3/3′** by the addition of NEt_3·HCl as a chloride source (Scheme 6). The $^{31}P\{^1H\}$ NMR spectra of solutions of complex **4** in CD_2Cl_2 on treatment with one or two equivalents of NEt_3·HCl are shown in Figure 7. This transformation is also apparent from a color change of the solution, from red

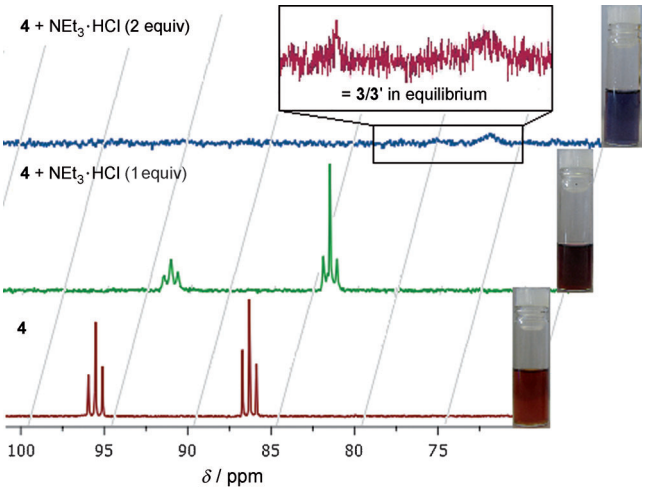

Figure 7. $^{31}P\{^1H\}$ NMR (CD_2Cl_2, 298 K) spectra, which show the re-establishment of the **3/3′** equilibrium, starting from compound **4** upon the addition of NEt_3·HCl (left) and the corresponding colors of the solutions (right). Bottom: red solution for complex **4**; Middle: brown solution after the addition of NEt_3·HCl (1 equiv); Top: purple solution after the addition of NEt_3·HCl (2 equiv), similar to that of **3/3′** in equilibrium.

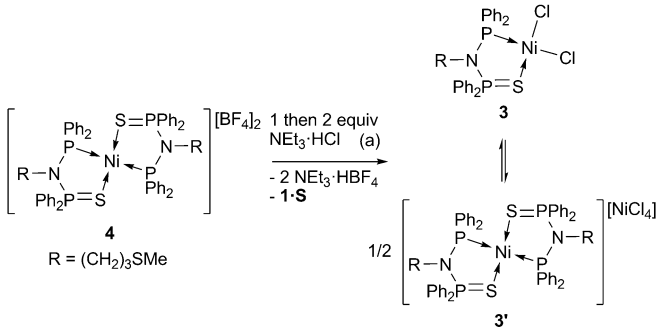

Scheme 6. Re-establishment of the **3/3′** equilibrium, starting from compound **4** upon the addition of NEt_3·HCl (2 equiv): a) CH_2Cl_2, RT, 30 min reaction time after each addition.

(**4**) to purple (**3/3′**) through a brown intermediate (Figure 7, right).

This color change prompted us to follow this transformation by UV/Vis spectroscopy (Figure 8). The shoulder at 430 nm, characteristic of complex **4**, progressively disappeared upon the addition of one and then two equivalents of NEt_3·HCl. At the same time, the absorption band at 538 nm (d–d transition), characteristic of complex **3**, increased until the spectrum recorded could be superimposed over that of complex **3** (Figure 8, light blue versus dark blue). Notably, the two characteristic absorption bands at 650 and 705 nm, which correspond to $[NiCl_4]^{2-}$, clearly appeared after two equivalents of chloride were added to a solution of complex **4** in CH_2Cl_2.

In view of the solid-state structures of complexes **2**, **3**, **3′**, and **4**, in particular that of ion-pair $[Ni(\mathbf{1{\cdot}S})_2]NiCl_4$ (**3′**), we

© 2013 Wiley-VCH Verlag GmbH & Co. KGaA, Weinheim

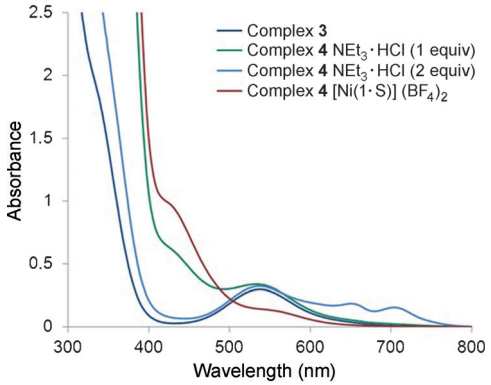

Figure 8. Changes in the UV/Vis spectrum of complex **4** ($c = \times 10^{-2}$ M) in the presence of NEt_3·HCl (1 equiv and 2 equiv) in CH_2Cl_2. The spectrum of complex **3** ($c = \times 10^{-2}$ M, 298 K) is shown for comparison. In this experiment, 1 equiv of free ligand **1·S** was produced after the addition of 2 equiv NEt_3·HCl.

anticipate that the formation of one or the other isomer in the equilibrium between complexes **3** and **3′** in solution is dependent on the polarity of the reaction medium (Scheme 7). This hypothesis was confirmed by COSMO-

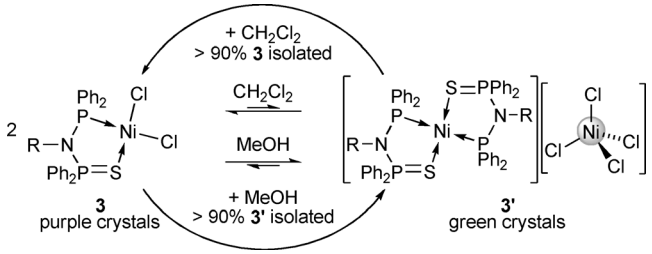

Scheme 7. "Control" of the equilibrium and the selective formation of diamagnetic complex **3** or its paramagnetic formula isomer **3′** as a function of the experimental conditions (the gray dot denotes the paramagnetic center in structure **3′**).

DFT calculations, which showed that the energy costs associated with the equilibrium between the diamagnetic **3** and the paramagnetic ion pair **3′** are strongly influenced by the dielectric constants (ε) of the solvents. The larger the ε value, the more the ion pair is thermodynamically favored and the charges are separated. In MeOH ($\varepsilon = 32.6$), complex **3′** is favored by 54.3 kJ mol^{-1} compared to complex **3**, whereas, in *n*-hexane ($\varepsilon = 1.88$), the difference is only 2 kJ mol^{-1} at the DFT level used (Figure 9, the Supporting Information, Tables S2 and S3, and the discussion on computational methods).

Monitoring of the gradual addition of MeOH to a solution of complexes **3**/**3′** in CD_2Cl_2 by $^{31}P\{^1H\}$ NMR spectroscopy showed the splitting of the broad singlet at $\delta = 86.6$ ppm into two well-defined "triplets" ($\delta = 94.6$ and 86.2 ppm, $^{2+3}J(P,P) = 68.9$ Hz; Figure 10). Considering that complex **4** displays two $^{31}P\{^1H\}$ NMR "triplets" at $\delta = 95.5$ and 86.3 ppm ($^{2+3}J(P,P) = 68.3$ Hz) and that the color of the solution changes from purple to pale yellow, we conclude that the

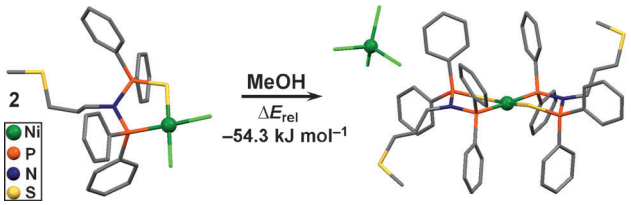

Figure 9. DFT-optimized structures of mononuclear diamagnetic complex **3** (left) and dinuclear complex **3′** (right), which consisted of the paramagnetic $[NiCl_4]^{2-}$ moiety and the diamagnetic $[Ni(\mathbf{1{\cdot}S})_2]^{2+}$ fragment. The relative stability of these structures in MeOH is shown.

addition of MeOH to a solution of complexes **3**/**3′** in CH_2Cl_2 completely shifts the equilibrium towards the formation of the ion-pair complex. This conclusion is further supported by monitoring the changes in the UV/Vis spectra of a solution of complex **3** (red line) as a function of the MeOH/CH_2Cl_2 ratio at constant complex concentration (Figure 11).

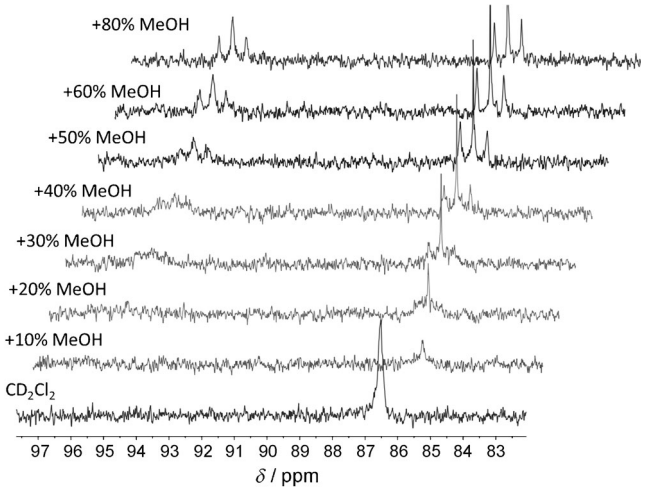

Figure 10. $^{31}P\{^1H\}$ NMR spectra, which show the exclusive formation of **3′** starting from the **3**/**3′** equilibrium in CD_2Cl_2 upon the progressive addition of MeOH.

In the presence of MeOH, the spectrum changes radically: The shoulder at 345 nm becomes a plateau from 320 to 360 nm, the band at 538 nm fully disappears, and the spectrum becomes superimposable over that of complex **4** (Figure 11, orange line). The absorption bands at 650 and 705 nm, characteristic for $[NiCl_4]^{2-}$, were not observed, owing to its solvation to give $[NiCl_4(MeOH)_2]^{2-}$.[21] Furthermore, magnetic susceptibility studies in CD_3OD by using the Evans method (^1H NMR spectroscopy)[22] afforded a value of $\mu = 3.02$ B.M., consistent with an octahedral (rather than a tetrahedral) Ni^{II} complex in solution.[9,23] The magnetic susceptibility of complex **3′** in CD_2Cl_2 could not be determined because the proportion of the latter complex in the **3**/**3′** mixture is unknown. All of these experiments clearly indicate that the **3**/**3′** equilibrium is displaced in MeOH in favor of ion-pair $[Ni(\mathbf{1{\cdot}S})_2][NiCl_4(MeOH)_2]$, owing to the

© 2013 Wiley-VCH Verlag GmbH & Co. KGaA, Weinheim

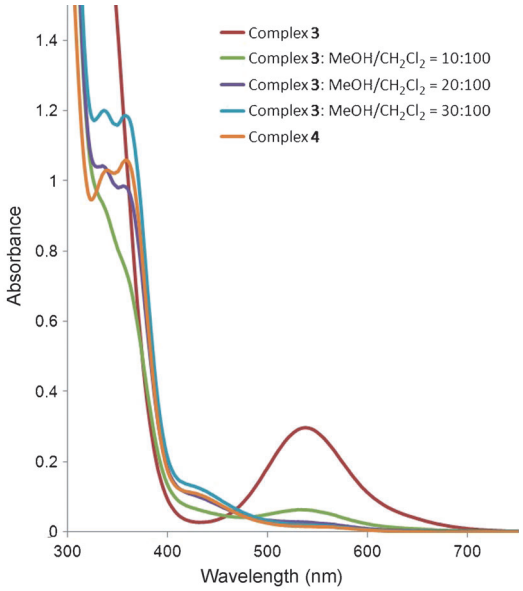

Figure 11. UV/Vis spectra, which show the exclusive formation of structure **3′** starting from the **3**/**3′** equilibrium in CH_2Cl_2 at RT (red line) and upon a progressive increase in the MeOH/CH_2Cl_2 ratio of the solution (10, 20, and 30%; green, purple, and blue lines, respectively; $c = 10^{-3}$ M, RT). The spectrum of complex **4** ($c = \times 10^{-3}$ M) is shown for comparison (orange line). Expansions of the 300–400 and 400–700 nm regions are provided in the Supporting Information, Figures S5 and S6.

larger dielectric constant of this solvent compared to CH_2Cl_2 and its donor properties.

On the basis of the obtained results, the possibility of producing one or the other formula isomer from the equilibrium mixture of complexes **3**/**3′** emerged. Indeed, the precipitation of a purple solution of a mixture of complexes **3**/**3′** in CH_2Cl_2 by the addition of pentane gave rise to the almost-quantitative formation of purple crystalline complex **3**. Dissolution of these purple crystals in MeOH afforded a light-yellow solution of $[Ni(\mathbf{1{\cdot}S})_2][NiCl_4(MeOH)_2]$ (see above), which yielded green crystals of dinuclear complex **3′** after slow evaporation of the solvent. Complex **3′** can be re-solubilized in CH_2Cl_2, thus leading to the purple solution mentioned above, and complex **3** can be recovered as a purple solid (Scheme 7).

For comparison, we performed the reaction between $[NiCl_2(DME)]$ and DPPA·S[24] in a 1:1 metal/ligand ratio in CH_2Cl_2, which led to the bis-chelated complex $[Ni((Ph_2P)NH\{P(S)Ph_2\}\text{-}P,S)_2]Cl_2$ (**5**), while 1 equivalent of the Ni^{II} precursor remained unreacted (Scheme 8). The $^{31}P\{^1H\}$ NMR spectrum of complex **5** exhibited a similar pattern to those of complexes **4** and **3′** ($\delta = 82.8$ and 79.2 ppm, $^{2+3}J(P,P) = 64.1$ Hz). Its molecular structure established the presence of the [Ni(*P*,P=*S*)] arrangement and revealed hydrogen-bonding interactions between the chloride counterions and the acidic DPPA N–H hydrogen atoms (Figure 12). The resulting N1···Cl1 distance (2.993(4) Å) is similar to

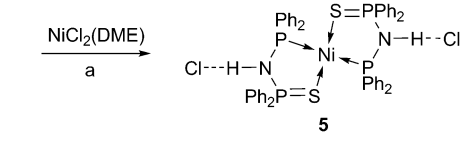

Scheme 8. Synthesis of complex **5**: a) DPPA·S (1.2 equiv), CH_2Cl_2, RT, 4 h.

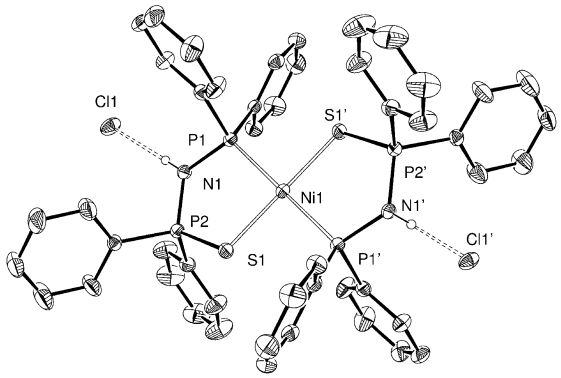

Figure 12. Solid-state molecular structure of structure **5** in **5**·4$CHCl_3$. Thermal ellipsoids are set at 30% probability. Hydrogen atoms are omitted for clarity. Selected bond lengths and angles are listed in Table 1.

those found in related selenium derivatives $[Ni((Ph_2P)NH\{P(Se)Ph_2\}\text{-}P,Se)((Ph_2P)N\{P(Se)Ph_2\}\text{-}P,Se)]Cl$ and *trans*-$Pt[(Ph_2P)NH\{P(Se)Ph_2\text{-}P,Se\}]_2Cl_2$ (2.93 and 2.97 Å, respectively).[1c,j] This experiment clearly illustrates the tendency of such (*P*,P=*S*) ligands to form bis-chelated dicationic complexes in preference to $[NiCl_2(LL')]$-type complexes.

Conclusions

Herein, we reported the unusual behavior of a (*P*,P=*S*) nickel(II) complex compared to its (*P*,*P*) analogue. Experimental investigations, supported by DFT calculations, allowed us to identify the factors that control the equilibrium between the neutral complex, $[NiCl_2LL']$, and the ion pair, $[Ni(LL')_2][NiCl_4]$, and to isolate, characterize, and selectively produce one or the other of these formula isomers. Because the complex $[NiCl_2(DPPA{\cdot}S)]$ does not seem to have been previously reported in the literature and because we could only obtain bis-chelated, dicationic complex **5** upon the reaction of DPPA·S with $[NiCl_2(DME)]$, it is clear that the presence of a N substituent on a DPPA·S-type ligand allows access to a new class of (*P*,P=*S*) nickel(II) complexes that can display an original behavior, such as the equilibrium mentioned above. Because we observed similar behavior in solution for complexes that contained a butyl substituent on the nitrogen atom to those that contained a thioether group of similar length, no specific role of the S atom could be identified. This function could subsequently be used for the deposition and anchoring of such complexes onto, for example, Au surfaces. Our work shows that the transfer of a chelating ligand from one metal center onto another may not require much energy and can be very solvent dependent. These results are

© 2013 Wiley-VCH Verlag GmbH & Co. KGaA, Weinheim

of fundamental interest and are also of particular relevance for those working in the field of homogeneous catalysis by nickel complexes, including the oligo- and polymerization of ethylene, in view of the importance of the nature of the metal-coordination sphere and of the neutral/cationic nature of the pre-catalyst.[6] These results open up the possibility of accessing "on–off" switchable catalytic systems for ethylene oligomerization, because the ion pair **3′** is inactive, in contrast to structure **3**.[25]

Experimental Section

General Procedures

All of the operations were performed by using standard Schlenk techniques under an inert atmosphere. Solvents were purified and dried under a nitrogen atmosphere by using conventional methods. CD_2Cl_2 and $CDCl_3$ were dried over 4 Å molecular sieves, degassed by performing freeze–pump–thaw cycles, and stored under an argon atmosphere. ^1H and ^{13}C NMR spectra were recorded at RT, unless specified, on Bruker AVANCE 300, 400, 500, or 600 spectrometers and referenced to the residual solvent resonance. Assignments are based on ^1H, ^1H COSY, and ^{13}C NMR experiments. Chemical shifts (δ) are given in ppm and coupling constants are in Hz. IR spectra were recorded within the region 4000–100 cm^{-1} on a Nicolet 6700 FTIR spectrometer (ATR mode, SMART ORBIT accessory, Diamond crystal). Elemental analysis was performed at the "Service de Microanalyses", Université de Strasbourg, or at the "Service Central d′Analyse", USR-59/CNRS, Solaize. Electrospray mass spectroscopy was performed on a microTOF (Bruker Daltonics, Bremen, Germany) instrument by using a flow of nitrogen gas as a drying agent and nebulizing gas. Ligands **1**[6k] and DPPA·S[24] and complexes $[NiCl_2(DME)]$[26] and $[Ni(NCMe)_6](BF_4)_2$[27] were prepared according to literature procedures. All other reagents were used as received from commercial suppliers. All iteration-fitting calculations and simulations of the $^{31}P\{^1H\}$ NMR spectra were performed by using the Bruker WIN-DAISY program.[28]

Synthesis of ***1·S₂***

To a solution of bis(diphenylphosphino)(*N*-(methylthio)propyl)amine (**1**, 0.500 g, 1.05 mmol) in toluene (15 mL) was added elemental sulfur (0.074 g, 2.31 mmol). The solution was heated to 115 °C for 3 h. After cooling to RT, pentane was added and a microcrystalline white powder of **1·S₂** precipitated. Colorless crystals suitable for single-crystal X-ray diffraction were grown from a mixture of toluene/pentane. Yield: 0.552 g (98 %); ^1H NMR (CD_2Cl_2, 300 MHz): δ = 7.99–7.92 (m, 8H; aromatic), 7.43–7.28 (m, 12H; aromatic), 3.65–3.50 (m, 2H; NCH_2), 1.83 (t, ^3J(H,H) = 7.0 Hz; CH_2S), 1.72 (s, 3H; SCH_3), 1.70–1.64 ppm (m, 2H; $CH_2CH_2CH_2$); $^{13}C\{^1H\}$ NMR (CD_2Cl_2, 75.5 MHz): δ = 133.27 (m, separation between the external lines = 12.8 Hz; C_{ortho}), 132.89 (d, ^1J(C,P) = 101.46 Hz; C_{ipso}), 131.73 (s; C_{para}), 128.00 (m, separation between the external lines = 13.6 Hz; C_{meta}), 49.01 (s; NCH_2), 31.20 (s; CH_2S) 29.45 (s; $CH_2CH_2CH_2$), 15.20 ppm (s; SCH_3); $^{31}P\{^1H\}$ NMR (CD_2Cl_2, 121.5 MHz): δ = 69.76 ppm (s). FTIR (solid): $\tilde{\nu}_{max}$ = 3053 (vw), 2975 (w), 2918 (vw), 1477 (w), 1435 (s), 1314 (w), 1201 (m), 1098 (s), 1056 (w), 997 (m), 956 (w), 886 (s), 788 (m), 742 (w), 716 (s), 686 (m), 643 (s), 613 cm^{-1} (m); elemental analysis calcd (%) for: $C_{28}H_{29}NP_2S_3$ (537.68): C 62.55, H 5.44, N 2.61; found: C 62.72, H 5.56, N 2.52.

Synthesis of ligand ***1·S***

To a solution of bis(diphenylphosphino)(*N*-(methylthio)propyl)amine (**1**, 1.076 g, 2.27 mmol) in CH_2Cl_2 (15 mL) was added S_8 (0.109 g, 3.41 mmol). The solution was stirred at RT for 30 min. Evaporation of the volatile compounds led to the formation of a pale-yellow oil that was dissolved in toluene (10 mL). The addition of pentane to this solution led to the precipitation of a white crystalline powder of **1·S₂**. After filtration and evaporation of the volatile compounds, a colorless oil was obtained. Examination of this oil by $^{31}P\{^1H\}$ NMR spectroscopy revealed the presence of **1·S** (about 70 %) and **1·S₂** (about 30 %). We could not isolate pure **1·S** and, thus, for the subsequent complexation reactions, **1·S** was prepared in situ. Purification of complexes of **1·S** was readily achieved (see below). ^1H NMR (CD_2Cl_2, 300 MHz): δ = 8.00–7.88 (m, 8H; aromatic), 7.55–7.31 (m, 12H; aromatic), 3.71–3.47 (m, 2H; NCH_2), 1.87 (t, ^3J(H,H) = 7.0 Hz; CH_2S), 1.67 (s, 3H; SCH_3), 1.08–0.98 ppm (m, 2H; $CH_2CH_2CH_2$); $^{31}P\{^1H\}$ NMR (CD_2Cl_2, 121.5 MHz): δ = 72.6 (d, ^{2+3}J(P,P) = 86.1 Hz), 53.91 ppm (d, ^{2+3}J(P,P) = 86.1 Hz).

Synthesis of the Complex $[NiCl_2(\mathbf{1})]$ ***(2)***

To a suspension of $[NiCl_2(DME)]$ (0.130 g, 0.59 mmol) in CH_2Cl_2 (10 mL) was added a solution of ligand **1** (0.200 g, 0.42 mmol) in CH_2Cl_2 (20 mL). The color of the solution quickly turned orange/red and stirring at RT was maintained for 12 h. The solvent was removed under reduced pressure and the red/orange solid was washed with Et_2O and pentane, thus yielding 0.220 g (86 %) of complex **2**. Red crystals suitable for single-crystal X-ray diffraction were grown from a mixture of CH_2Cl_2/pentane. ^1H NMR (CD_2Cl_2, 300 MHz): δ = 8.02–7.95 (m, 8H; aromatic), 7.75–7.70 (m, 4H; aromatic), 7.63–7.58 (m, 8H; aromatic), 2.90 (m, 2H; NCH_2), 2.06 (m, 2H; CH_2S), 1.84 (s, 3H; SCH_3), 1.28–1.19 ppm (m, 2H; $CH_2CH_2CH_2$); $^{13}C\{^1H\}$ NMR (CD_2Cl_2, 75.5 MHz): δ = 133.77 (app t, ^{2+4}J(C,P) = 11.1 Hz; C_{ortho}), 133.47 (s; C_{para}), 129.7 (app t, ^{3+5}J(C,P) = 11.7 Hz; C_{meta}), 127.67 (app t, ^{1+3}J(C,P) = 52.0 Hz; C_{ipso}), 47.73 (s; NCH_2), 30.65 (s; CH_2S) 29.67 (s; $CH_2CH_2CH_2$), 14.58 ppm (s; SCH_3); $^{31}P\{^1H\}$ NMR (CD_2Cl_2, 121.5 MHz): δ = 42.9 ppm (s); FTIR (solid): $\tilde{\nu}_{max}$ = 1478 (w), 1433 (m), 1307 (w), 1223 (w), 1182 (w), 1145 (m), 1098 (s), 1067 (s), 996 (w), 853 (m), 817 (w), 748 (m), 693 cm^{-1} (vs); MS (ESI): *m*/*z* 566.1 $[M-Cl]^+$; elemental analysis calcd (%) for: $C_{28}H_{29}Cl_2NNiP_2S$ (603.15): C 55.76, H 4.85, N 2.32; found: C 55.54, H 4.75, N 2.39.

Synthesis of the Complex $[NiCl_2(\mathbf{1{\cdot}S})]$ ***(3)***

To a solution of bis(diphenylphosphino)(*N*-(methylthio)propyl)amine (**1**, 1.07 g, 2.27 mmol) in CH_2Cl_2 (20 mL) was added elemental sulfur (0.108 g, 3.37 mmol). The solution was stirred at RT for 30 min and then added to a suspension of $[NiCl_2(DME)]$ (0.274 g, 1.25 mmol) in CH_2Cl_2 (20 mL). The mixture quickly turned bright purple and was stirred at RT for 4 h. After filtration, the solvent was removed under reduced pressure and the bright-purple solid was washed with toluene. Purple crystals suitable for single-crystal X-ray diffraction were grown by slow evaporation of a mixture of CH_2Cl_2/pentane. Yield (based on **1·S**, which was formed in situ): 0.581 g (81 %); $^{31}P\{^1H\}$ NMR ($CDCl_3$, 121.5 MHz): δ = 86.60 ppm (s); for variable-temperature data, see text; FTIR (solid): $\tilde{\nu}_{max}$ = 3497 (bw), 3392 (bw), 3054 (vw), 2912 (vw), 1585 (w), 1479 (w), 1461 (vw), 1435 (s), 1311 (m), 1276 (vw), 1221 (m), 1165 (w), 1098 (s), 1044 (s), 1021 (w), 996 (w), 965 (w), 899 (s), 839 (m), 751 (s), 725 (w), 693 cm^{-1} (s); MS (ESI): *m*/*z* 598.02 $[M-Cl]^+$; elemental analysis calcd (%) for: $C_{28}H_{29}Cl_2NNiP_2S_2{\cdot}H_2O$ (653.15): C 51.48, H 4.78, N 2.14; found: C 51.14, H 5.02, N 2.13.

Synthesis of the Complex $[Ni(\mathbf{1{\cdot}S})_2]NiCl_4$ ***(3′)***

Complex $[NiCl_2(\mathbf{1{\cdot}S})]$ was dissolved in MeOH (10 mL). The color of the solution quickly changed from purple to yellow/orange, that is, the color of $[Ni(\mathbf{1{\cdot}S})_2][NiCl_4(MeOH)_2]$. Only a few green crystals of structure **3′** suitable for single-crystal X-ray diffraction were obtained by the slow evaporation of this solution. $^{31}P\{^1H\}$ NMR (CD_3OD, 121.5 MHz): two triplets in a AA′BB′ spin system (Scheme 9): δ_A = 94.39 ppm, δ_B = 86.26 ppm; spectroscopic simulations with WIN-DAISY afforded the following coupling constants (Table 2): $^{2+3}J(P_A,P_B) = {}^{2+3}J(P_{A'},P_{B'}) = 67.24$ Hz, $^{3+4}J(P_A,P_{B'}) = 7.39$ Hz, $^4J(P_A,P_{A'}) = 66.51$ Hz, $^2J(P_B,P_{B'}) = 68.38$ Hz; FTIR: $\tilde{\nu}_{max}$(solid) = 3422 (bw), 3166 (bw), 3052 (vw), 2921 (vw), 2162 (w), 1979 (w), 1584 (w), 1478 (w), 1458 (vw), 1435 (s), 1310 (w), 1217 (vw), 1187 (w), 1161 (vw), 1101 (m), 1067 (m), 1051 (m), 1024 (w), 995 (w), 957

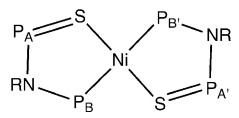

Scheme 9. Spin system used for the assignment of the $^{31}P\{^1H\}$ NMR resonances of complexes **3′**, **4**, and **5**.

 © 2013 Wiley-VCH Verlag GmbH & Co. KGaA, Weinheim

Table 2. Chemical shifts [ppm] and coupling constants [Hz] from the $^{31}P\{^1H\}$ NMR spectroscopic simulations for complexes **3′**, **4**, and **5**.

Complex	δP_A	δP_B	$^{2+3}J(P_A,P_B)=^{2+3}J(P_{A'},P_{B'})$	$^{3+4}J(P_A,P_{B'})$	$^{4}J(P_A,P_{A'})$	$^{2}J(P_B,P_{B'})$
3′	94.39	86.26	67.24	7.39	66.51	68.38
4	95.56	86.28	67.46	5.71	66.08	68.08
5	82.76	79.20	68.94	7.78	66.91	56.60

(vw), 875 (m), 808 (w), 747 (m), 727 (w), 687 cm^{-1} (s); MS (ESI): *m/z* 1233.02 $[M-Cl]^+$.

*Synthesis of the Complex [Ni(**1**·**S**)$_2$](BF$_4$)$_2$ (**4**)*

To a solution of bis(diphenylphosphino)(*N*-(methylthio)propyl)amine (**1**, 0.377 g, 0.83 mmol) in CH_2Cl_2 (20 mL) was added elemental sulfur (0.039 g, 1.24 mmol). The solution was stirred at RT for 30 min and then added to a suspension of $[Ni(NCMe)_6](BF_4)_2$ (0.082 g, 0.20 mmol) in CH_2Cl_2 (20 mL). The mixture quickly turned orange and was stirred at RT for 4 h. After filtration, the solvent was removed under reduced pressure and the orange solid was washed with toluene. Red crystals suitable for single-crystal X-ray diffraction were grown from a mixture of CH_2Cl_2/pentane. Yield (based on **1**·**S**, which was formed in situ): 0.226 g (91%); ^1H NMR (CD_2Cl_2, 400 MHz): $\delta=7.85$ (t, $^3J(H,H)=7.3$ Hz, 4H; aromatic), 7.81–7.77 (m, 4H; aromatic), 7.65–7.58 (m, 24H; aromatic), 7.55–7.50 (m, 8H; aromatic), 3.08–2.98 (m, 4H; NCH_2), 1.85 (t, $^3J(H,H)=6.3$ Hz, 4H; CH_2S), 1.57 (s, 6H; SCH_3), 1.10–1.02 ppm (m, 4H; $CH_2CH_2CH_2$); $^{13}C\{^1H\}$ NMR (CD_2Cl_2, 75.5 MHz): $\delta=136.05$ (s; C_{para}), 134.42 (s; C_{para}) 133.1 (app t, $^{2+4+5}J(C,P)=11.1$ Hz; C_{ortho} of PhP^{III}), 132.53 (d, $^2J(C,P)=12.4$ Hz; C_{ortho} of PhP^V), 130.53 (d, $^2J(C,P)=14.2$ Hz; C_{meta} of PhP^V), 130.34 (app t, $^{3+5+6}J(C,P)=11.3$ Hz; C_{meta} of PhP^{III}), 124.09 (app t, $^{1+3+4}J(C,P)=54.8$ Hz; C_{ipso} at P^{III}), 123.56 (d, $^1J(C,P)=95.5$ Hz; C_{ipso} at P^V), 48.65 (s; NCH_2), 30.51 (s; CH_2S) 28.66 (s; $CH_2CH_2CH_2$), 15.03 ppm (s; SCH_3); $^{31}P\{^1H\}$ NMR (CD_2Cl_2, 121.5 MHz): two triplets in an AA′BB′ spin system (Scheme 9): $\delta_A=95.56$ ppm, $\delta_B=86.28$ ppm; spectroscopic simulations with WIN-DAISY afforded the following coupling constants: $^{2+3}J(P_A,P_B)=^{2+3}J(P_{A'},P_{B'})=67.46$ Hz, $^{3+4}J(P_A,P_{B'})=5.71$ Hz, $^4J(P_A,P_{A'})=66.08$ Hz, $^2J(P_B,P_{B'})=68.08$ Hz; FTIR (solid): $\tilde{\nu}_{max}=3058$ (vw), 2938 (vw), 2161 (w), 2035 (bvw), 1979 (w), 1635 (vw), 1585 (w), 1480 (w), 1457 (w), 1436 (s), 1312 (w), 1282 (w), 1224 (m), 1188 (w), 1050 (vs), 1034 (vs), 995 (w), 904 (s), 814 (m), 760 (m), 746 (m), 727 (w), 695 (s sh), 686 (vs), 616 cm^{-1} (w); MS (ESI): *m/z* 534.09 $[M\text{-}2BF_4]^{2+}$; elemental analysis calcd (%) for: $C_{56}H_{58}N_2NiP_4S_4B_2F_8{\cdot}H_2O$ (1364.49): C 53.32, H 4.79, N 2.22; found: C 52.89, H 4.74, N 2.18.

*Synthesis of the Complex [Ni(DPPA·S)$_2$]Cl$_2$ (**5**)*

Solid $[NiCl_2(DME)]$ (0.134 g, 0.61 mmol) was added to a solution of DPPA·S (0.306 g, 0.73 mmol) in CH_2Cl_2 (20 mL). The mixture quickly turned brown and was stirred at RT for 4 h. After filtration, the addition of pentane led the formation compound **5** as a red solid. Red crystals suitable for single-crystal X-ray diffraction were grown from a mixture of CH_2Cl_2/pentane. Yield: 0.521 g (81%); ^1H NMR (CD_2Cl_2, 300 MHz): $\delta=$ 7.87 (br s, 8H; aromatic), 7.75–7.71 (m, 8H; aromatic), 7.63–7.58 (m, 8H; aromatic), 7.46 ppm (br m, 16H; aromatic); $^{13}C\{^1H\}$ NMR (CD_2Cl_2, 75.5 MHz): $\delta=133.84$ (s; aromatic), 133.21 (s; aromatic), 132.38 (s; aromatic), 132.21 (d, $^2J(C,P)=12.1$ Hz; C_{ortho} of PhP^V), 131.25 (t, $^{1+3+4}J(C,P)=57.4$ Hz; C_{ipso} at P^{III}), 129.01 (d, $^2J(C,P)=14.4$ Hz; C_{meta} of PhP^V), 128.83 (s; aromatic), 128.04 ppm (part of a doublet that was masked by the signal at $\delta=128.83$ ppm, estimated $^1J(P,C)=95$ Hz; C_{ipso} attached to P^V); $^{31}P\{^1H\}$ NMR (CD_2Cl_2, 121.5 MHz): two triplets in an AA′BB′ spin system (Scheme 9): $\delta_A=82.76$ ppm, $\delta_B=79.20$ ppm; spectroscopic simulations with WIN-DAISY afforded the following coupling constants: $^{2+3}J(P_A,P_B)=^{2+3}J(P_{A'},P_{B'})=68.94$ Hz, $^{3+4}J(P_A,P_{B'})=7.78$ Hz, $^4J(P_A,P_{A'})=66.91$ Hz, $^2J(P_B,P_{B'})=56.50$ Hz; FTIR (solid): $\tilde{\nu}_{max}=3050$ (vw), 2961 (vw), 2688 (bw), 1585 (vw), 1480 (w), 1434 (s), 1307 (mw), 1260 (m), 1184 (w), 1158 (vw), 1099 (vs), 1025 (w), 997 (vw), 949 (m), 799 (s), 741 (s), 685 cm^{-1} (vs); MS (ESI): *m/z* 891.10 $[M-Cl-HCl]^+$; elemental analysis calcd (%) for: $C_{48}H_{42}N_2NiP_4S_2{\cdot}CH_2Cl_2{\cdot}H_2O$ (1067.41): C 54.62, H 4.58, N 2.55; found: C 54.48, H 4.33, N 2.55.

Acknowledgements

We are grateful to the CNRS, the Ministère de la Recherche (Paris), the DFH/UFA (International Research Training Group 532-GRK532, PhD grants to C.F. and A.G.), and the *Fundação para a Ciência e Tecnologia* (FCT) (fellowships SFRH/BPD/73253/2010 to C.F. and SFRH/BPD/44262/2008 to V.R.) for funding. We thank the Service de Radiocristallographie, Institut de Chimie (UMR 7177 CNRS-UdS) for performing the X-ray diffraction studies, the UdS High-Performance Computing Center and the Laboratoire de Chimie Quantique (UdS) for the provision of computational facilities, and Mélanie Boucher for providing technical assistance.

[1] For selected reviews, see: a) T. Appleby, J. D. Woolins, *Coord. Chem. Rev.* **2002**, *235*, 121 and references therein; b) P. Bhattacharyya, J. D. Woollins, *Polyhedron* **1995**, *14*, 3367 and references therein. For structurally characterized examples of neutral and anionic P(E)NP ligands and their complexes with Group 10 metals, see: c) N. Levesanos, I. Stamatopoulos, C. P. Raptopoulou, V. Psycharis, P. Kyritsis, *Polyhedron* **2009**, *28*, 3305; d) J. W. Faller, J. Lloret-Fillol, J. Parr, *New J. Chem.* **2002**, *26*, 883; e) A. M. Z. Slawin, J. D. Woolins, Q. Zhang, *J. Chem. Soc. Dalton Trans.* **2001**, 621; f) K. G. Gaw, M. B. Smith, A. M. Z. Slawin, *New J. Chem.* **2000**, *24*, 429; g) M. B. Smith, A. M. Z. Slawin, *Inorg. Chim. Acta* **2000**, *299*, 172; h) P. Bhattacharyya, A. M. Z. Slawin, M. B. Smith, J. D. Woollins, *Inorg. Chem.* **1996**, *35*, 3675; i) M. B. Smith, A. M. Z. Slawin, J. D. Woolins, *Polyhedron* **1996**, *15*, 1579; j) P. Bhattacharyya, A. M. Z. Slawin, D. J. Williams, J. D. Woollins, *J. Chem. Soc. Dalton Trans.* **1995**, 3189; k) M. S. Balakrishna, R. Klein, S. Uhlenbrock, A. A. Pinkerton, R. G. Cavell, *Inorg. Chem.* **1993**, *32*, 5676.

[2] a) V. Rosa, C. Fliedel, A. Ghisolfi, R. Pattacini, T. Avilés, P. Braunstein, *Dalton Trans.* **2013**, DOI: 10.1039/c3dt50555c; b) C. Fliedel, R. Pattacini, P. Braunstein, *J. Cluster Sci.* **2010**, *21*, 397; c) M. Rodriguez-Zubiri, V. Gallo, J. Rosé, R. Welter, P. Braunstein, *Chem. Commun.* **2008**, 64; d) V. Gallo, P. Mastrorilli, C. F. Nobile, P. Braunstein, U. Englert, *Dalton Trans.* **2006**, 2342.

[3] a) T. Posset, F. Rominger, J. Blümel, *Chem. Mater.* **2005**, *17*, 586; b) F. Schweyer-Tihay, P. Braunstein, C. Estournès, J. L. Guille, B. Lebeau, J.-L. Paillaud, M. Richard-Plouet, J. Rosé, *Chem. Mater.* **2003**, *15*, 57; c) P. Braunstein, H.-P. Kormann, W. Meyer-Zaika, R. Pugin, G. Schmid, *Chem. Eur. J.* **2000**, *6*, 4637.

[4] C. Fliedel, V. Faramarzi, V. Rosa, B. Doudin, P. Braunstein, unpublished results.

[5] For recent examples, see: a) O. Akba, F. Durap, M. Aydemir, A. Baysal, B. Gümgüm, S. Özkar, *J. Organomet. Chem.* **2009**, *694*, 731; b) B. Gümgüm, N. Biricik, F. Durap, I. Özdemir, N. Gürbüz, W. H. Ang, P. J. Dyson, *Appl. Organomet. Chem.* **2007**, *21*, 711.

[6] For examples of Ni-based catalysts, see: a) M. Schultz, F. Eisenträger, C. Regius, F. Rominger, P. Hanno-Igels, P. Jakob, I. Gruber, P. Hofmann, *Organometallics* **2012**, *31*, 207; b) F. Speiser, L. Saussine, P. Braunstein, *Acc. Chem. Res.* **2005**, *38*, 784; c) J. N. L. Dennett, A. L. Gillon, K. Heslop, D. J. Hyett, J. S. Fleming, C. E. Lloyd-Jones, A. G. Orpen, P. G. Pringle, D. F. Wass, J. N. Scutt, R. H. Weatherhead, *Organometallics* **2004**, *23*, 6077; d) N. A. Cooley, S. M. Green, D. F. Wass, K. Heslop, A. G. Orpen, P. G. Pringle, *Organometallics* **2001**, *20*, 4769; e) D. F. Wass (BP Chemicals Ltd), WO01/10876; f) P. Hofmann, L. A. Perez-Moya, O. Steigelmann, J. Riede, *Organometallics* **1992**, *11*, 1167; g) P. Hofmann, L. A. Perez-Moya, M. E. Krause, O. Kumberger, G. Müller, *Z. Naturforsch.* **1990**, *45b*, 897. For Cr-based catalysts see e.g.: h) D. S. McGuinness, *Chem. Rev.* **2011**, *111*, 2321 and references therein; i) T. Agapie, *Coord. Chem. Rev.* **2011**, *255*, 861 and references therein; j) B. Reddy Aluri, N. Peulecke, S. Peitz, A. Spannenberg, B. H. Müller, S. Schulz, H.-J. Drexler, D. Heller, M. H. Al-Hazmi, F. M. Mosa, A. Wöhl, W. Müller, U. Rosenthal, *Dalton Trans.* **2010**, *39*, 7911 (Cr and Ni com-

 © 2013 Wiley-VCH Verlag GmbH & Co. KGaA, Weinheim

plexes); k) Z. Weng, T. Shihui, T. S. A. Hor, *Dalton Trans.* **2007**, 3493.
[7] a) S. Dagorne, C. Fliedel, *Top. Organomet. Chem.* **2013**, *41*, 125 and references therein; b) J. D. Azoulay, Z. A. Koretz, G. Wu, G. C. Bazan, *Angew. Chem.* **2010**, *122*, 8062; *Angew. Chem. Int. Ed.* **2010**, *49*, 7890; c) Z. Weng, S. Teo, L. L. Koh, T. S. A. Hor, *Chem. Commun.* **2006**, 1319.
[8] P. Chavez, I. G. Rios, A. Kermagoret, R. Pattacini, A. Meli, C. Bianchini, G. Giambastiani, P. Braunstein, *Organometallics* **2009**, *28*, 1776.
[9] A. Kermagoret, R. Pattacini, P. Chavez Vasquez, G. Rogez, R. Welter, P. Braunstein, *Angew. Chem.* **2007**, *119*, 6558; *Angew. Chem. Int. Ed.* **2007**, *46*, 6438.
[10] M. O′Reilly, R. Pattacini, P. Braunstein, *Dalton Trans.* **2009**, 6092.
[11] H. J. Yoon, J. Kuwabara, J.-H. Kim, C. A. Mirkin, *Science* **2010**, *330*, 66.
[12] For example, see: a) P. Braunstein, J. Zhang, R. Welter, *Dalton Trans.* **2003**, 507; b) P. Braunstein, F. Naud, A. Pfaltz, S. J. Rettig, *Organometallics* **2000**, *19*, 2676.
[13] For example, see: A. Kermagoret, P. Braunstein, *Organometallics* **2008**, *27*, 88.
[14] C. S. Browning, R. A. Burrow, D. H. Farrar, H. A. Mirza, *Inorg. Chim. Acta* **1998**, *271*, 112.
[15] a) B.-S. Yin, T.-B. Li, M.-S. Yang, *Acta Crystallogr. Sect. E* **2011**, *67*, m1571; b) B.-S. Yin, T.-B. Li, M.-S. Yang, *Acta Crystallogr. Sect. E* **2011**, *67*, m1572; c) G. C. Vougioukalakis, I. Stamatopoulos, N. Petzetakis, C. P. Raptopoulou, V. Psycharis, A. Terzis, P. Kyritsis, M. Pitsikalis, N. Hadjichristidis, *J. Polym. Sci. Part A* **2009**, *47*, 5241; d) Z. Sun, F. Zhu, Q. Wu, S. Lin, *Appl. Organomet. Chem.* **2006**, *20*, 175.
[16] a) C. Fliedel, A. Sabbatini, P. Braunstein, *Dalton Trans.* **2010**, *39*, 8820; b) C. Fliedel, P. Braunstein, *Organometallics* **2010**, *29*, 5614; c) C. Fliedel, G. Schnee, P. Braunstein, *Dalton Trans.* **2009**, 2474.
[17] a) P. Braunstein, *J. Organomet. Chem.* **2004**, *689*, 3953; b) P. Braunstein, F. Naud, *Angew. Chem.* **2001**, *113*, 702; *Angew. Chem. Int. Ed.* **2001**, *40*, 680.
[18] a) H. Suzuki, S.-I. Ishiguro, *Bull. Chem. Soc. Jpn.* **1993**, *66*, 83; b) A. P. B. Lever in *Inorganic Electronic Spectroscopy*, *2nd ed.*, Elsevier, Amsterdam, **1984**; c) C. P. Nash, M. S. Jenkins, *J. Phys. Chem.* **1964**, *68*, 356.
[19] a) B. Zheng, M. O. Miranda, A. G. DiPasquale, J. A. Golen, A. L. Rheingold, L. H. Doerrer, *Inorg. Chem.* **2009**, *48*, 4274; b) M. Atanasov, C. Rauzy, P. Baettig, C. Daul, *Int. J. Quantum Chem.* **2005**, *102*, 119.
[20] a) M. E. Cucciolito, V. De Felice, I. Orabona, A. Panunzi, F. Ruffo, *Inorg. Chim. Acta* **2003**, *343*, 209; b) G. Exarchos, S. D. Robinson, J. W. Steed, *Polyhedron* **2001**, *20*, 2951; c) J. T. Mague, S. W. Hawbaker, *J. Chem. Crystallogr.* **1997**, *27*, 603; d) T. Suzuki, A. Morikawa, K. Kashiwabara, *Bull. Chem. Soc. Jpn.* **1996**, *69*, 2539; e) J. G. H. Du Preez, B. J. A. M. Van Brecht, I. Warden, *Inorg. Chim. Acta* **1987**, *131*, 259; f) M. Schäfer, E. Uhlig, *Z. Anorg. Allg. Chem.* **1974**, *407*, 23.
[21] N. S. Gill, R. S. Nyholm, *J. Chem. Soc. A* **1959**, 3997.
[22] a) D. F. Evans, *J. Chem. Soc. A* **1959**, 2003; b) S. K. Sur, *J. Magn. Reson.* **1989**, *82*, 169; c) E. M. Schubert, *J. Chem. Educ.* **1992**, *69*, 62.
[23] a) S. Mukhopadhyay, D. Mandal, D. Ghosh, I. Goldberg, M. Chaudhury, *Inorg. Chem.* **2003**, *42*, 8439; b) J. B. Willis, D. P. Mellor, *J. Am. Chem. Soc.* **1947**, *69*, 1237.
[24] J. D. Woollins, *J. Chem. Soc. Dalton Trans.* **1996**, 2893.
[25] A. Ghisolfi, C. Fliedel, V. Rosa, R. Pattacini, K. Yu. Monakhov, P. Braunstein, unpublished results.
[26] R. J. Errington, *Advanced Practical Inorganic and Metalorganic Chemistry*, CRC Press, Boca Raton, FL, **1997**, pp. 246.
[27] D. Coucouvanis, *Useful Reagents and Ligands, in Inorganic Syntheses*, *Vol. 33*, Wiley, New York, **2002**, Chapter 2, pp. 78.
[28] G. Hägele WIN-DAISY 3.0. Heinrich-Heine-University Düsseldorf, **1993**–**1995**.

Received: May 20, 2013
Published online: June 21, 2013

 © 2013 Wiley-VCH Verlag GmbH & Co. KGaA, Weinheim

CHAPITRE 4

Ce chapitre est présenté sous forme d'une publication à paraître dans *Organometallics*.

Les contributions respectives des auteurs sont:

A.Ghisolfi, C. Fliedel, V. Rosa, P. Braunstein – *développement du projet*

A. Ghisolfi – *Synthèse et caractérisation des ligands et des complexes*, *simulation des spectres RMN*

K. Yu. Monakhov – *calculs théoriques*

Combined Experimental and Theoretical Study of Bis(diphenylphosphino)(*N*-thioether)amine-type Ligands in Nickel(II) Complexes for Catalytic Ethylene Oligomerization

Alessio Ghisolfi,[a] Christophe Fliedel,*[a,b] Vitor Rosa,[b] Kirill Yu. Monakhov,[c] and Pierre Braunstein*[a]

[a] Laboratoire de Chimie de Coordination Institut de Chimi (UMR7177 CNRS), Université de Strasbourg, 4 rue Blaise Pascal, CS 90032, 67081 Strasbourg (France).
[b]Laboratoire de Chimie Biomimétique des Métaux de Transition, Institut de Chimie (UMR 7177 CNRS), Université de Strasbourg, 4 rue Blaise Pascal, CS 90032, 67081 Strasbourg (France).
[c]REQUIMTE, Departamento de Quimica Faculdade de Ciéncias e Tecnologia Universidade Nova de Lisboa, Caparica, 2829-516 (Portugal).
[d]Institut fir Anorganische Chemie RWTH-Aachen University, Landoltweg 1, 52074 Aachen (Germany)

Des informations complémentaires sont disponibles sur internet:

http://pubs.acs.org/doi/suppl/10.1021/om500141k/suppl_file/om500141k_si_001.pdf

Resumé du Chapitre 4

Nous avons poursuivi dans ce travail la chimie présentée dans le chapitre précédent et nous décrivons la synthèse de deux nouveaux complexes de nickel(II) : [$NiCl_2${$(Ph_2P)_2N(p$-$C_6H_4)$SMe-*P*,*P*}] et [$NiCl_2${$(Ph_2P)N${$P(S)Ph_2$}$(p$-$C_6H_4)$SMe-*P*,*S*}] qui ont été caractérisés à partir, respectivement, du ligand fonctionnel phosphoré $(Ph_2P)_2N(p$-$C_6H_4)$SMe et de son dérivé monosulfuré $(Ph_2P)N${$P(S)Ph_2$}$(p$-$C_6H_4)_3$SMe. Ce système constitue l'analogue *para*-thiomethyl-aromatique de celui qui a été présenté dans le chapitre précédent et contenait une fonctionnalisation $(CH_2)_3$SMe. Une nouvelle famille de complexes de type [$NiCl_2${PN(R)P}] et [$NiCl_2${PN(R)P=S}] (R = $(CH_2)_3$S, PhSMe) devient ainsi disponible. Un étude comparative de l'activité de ces complexes en oligomerization catalytique de l'éthylène, en phase homogène, a aussi été réalisée et les résultats obtenus sont discutés à la fois du point structural et théorique.

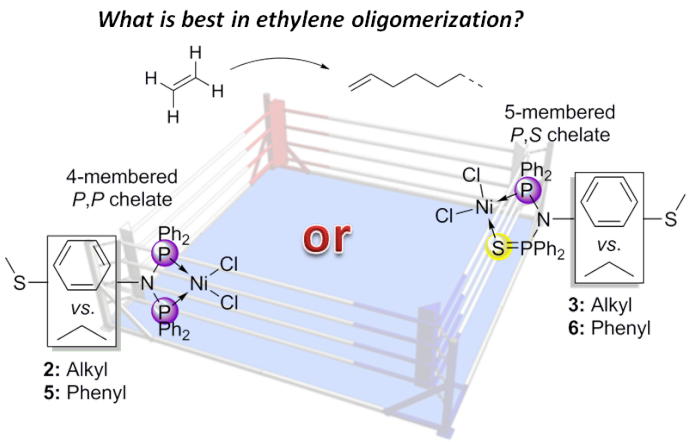

ORGANOMETALLICS

Article

pubs.acs.org/Organometallics

Combined Experimental and Theoretical Study of Bis(diphenylphosphino)(*N*-thioether)amine-Type Ligands in Nickel(II) Complexes for Catalytic Ethylene Oligomerization

Alessio Ghisolfi, Christophe Fliedel,*[,†] Vitor Rosa,[†] Kirill Yu. Monakhov,[‡] and Pierre Braunstein*

Laboratoire de Chimie de Coordination, Institut de Chimie (UMR 7177 CNRS), Université de Strasbourg, 4 rue Blaise Pascal, 67081 Strasbourg Cedex, France

Supporting Information

ABSTRACT: Starting from the new ligands bis(diphenylphosphino)(*N*-4-(methylthio)phenyl)amine (**4**, N(PPh$_2$)$_2$(*p*-C$_6$H$_4$)SMe) and its monosulfide derivative (Ph$_2$P)N{P(S)Ph$_2$}(*p*-C$_6$H$_4$)SMe (**4·S**), we have prepared and characterized, including by X-ray crystallographic studies, their Ni(II) complexes [NiCl$_2${(Ph$_2$P)$_2$N(*p*-C$_6$H$_4$)SMe-*P*,*P*}] (**5**) and [NiCl$_2${(Ph$_2$P)N{P(S)Ph$_2$}(*p*-C$_6$H$_4$)SMe-*P*,*S*}] (**6**), respectively. The bis-sulfide compound N{P(S)Ph$_2$}$_2$(*p*-C$_6$H$_4$)SMe (**4·S$_2$**) was also prepared and structurally characterized. Computational studies showed that the combined influence of stronger P donors and a four-membered-ring *P*,*P* chelate leads to complex **5** being thermodynamically more stable than **6**, which contains one weaker P═S donor group but a five-membered *P*,P═*S* chelate ring. For comparison, the bis-chelate complex [Ni{(Ph$_2$P)N{P(S)Ph$_2$}(*p*-C$_6$H$_4$)SMe-*P*,*S*}$_2$](BF$_4$)$_2$ (**7**), the monochelate complexes [NiBr$_2${(Ph$_2$P)N{P(S)Ph$_2$}(*p*-C$_6$H$_4$)SMe-*P*,*S*}] (**8**) and the Pd(II) analogue of **6**, [PdCl$_2${(Ph$_2$P)N{P(S)Ph$_2$}(*p*-C$_6$H$_4$)SMe-*P*,*S*}] (**9**), were synthesized and structurally characterized and their solution behavior was investigated. The catalytic activity and selectivity in ethylene oligomerization of the Ni(II) complexes **5** and **6** and their known *N*-(methylthio)propyl analogues [NiCl$_2${(Ph$_2$P)$_2$N(CH$_2$)$_3$SMe-*P*,*P*}] (**2**) and [NiCl$_2${(Ph$_2$P)N{P(S)Ph$_2$}(CH$_2$)$_3$SMe-*P*,*S*}] (**3**), which were obtained from the bis(diphenylphosphino)(*N*-(methylthio)propyl)amine ligand N(PPh$_2$)$_2$(CH$_2$)$_3$SMe (**1**) and its monosulfide derivative (Ph$_2$P)N{P(S)Ph$_2$}(CH$_2$)$_3$SMe (**1·S**), respectively, revealed a significant influence of the nature of the *N*-substituent (aryl vs alkyl thioether) and of the chelate ring size (*P*,P vs *P*,P═*S*). DFT calculations showed that the trend in ΔE_{rel}, [NiCl$_2$(*P*,*P*)] > [NiCl$_2$(*P*,P═*S*)] > [NiCl$_2$(P═*S*,P═*S*)], results from the stronger covalent character of the Ni−P vs Ni−S bond. Using AlEtCl$_2$ as cocatalyst, mostly ethylene dimers were produced, with significant amounts of trimers (selectivity in the range 11−36%). Productivities up to 40400 and 48200 g of C$_2$H$_4$/((g of Ni) h), with corresponding TOF values of 84800 and 101100 mol of C$_2$H$_4$/ ((mol of Ni) h), were obtained with precatalysts **2** and **3**, respectively.

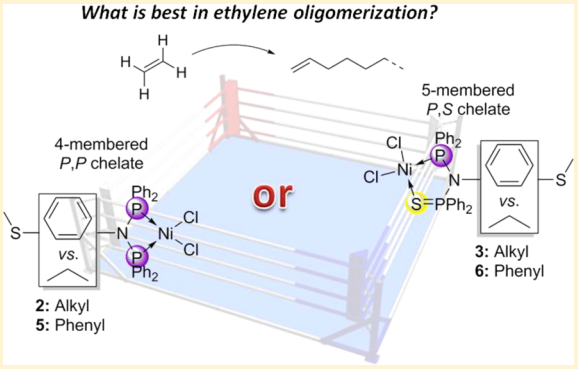

INTRODUCTION

Short-bite ligands, such as bis(diphenylphosphino)methane-type (DPPM) and bis(diphenylphosphino)amine-type (DPPA) ligands, offer a diversity of coordination modes (monodentate, bidentate chelating, or bridging), which is reflected in their rich coordination chemistry. While their neutral forms, Ph$_2$PCH$_2$PPh$_2$ and Ph$_2$PNHPPh$_2$, respectively, act as four-electron donors on coordination to a metal center through both phosphines, an additional X-type donor function is available in their deprotonated forms (Ph$_2$PCHPPh$_2$)$^-$ and (Ph$_2$PNPPh$_2$)$^-$, respectively.[1] Furthermore, various *N*-substituents can be readily introduced in DPPA-type ligands, which may facilitate the formation of polymetallic complexes[2] or the anchoring of coordination compounds into mesoporous materials[3] or on metallic surfaces.[4] Metal complexes of such short-bite ligands are involved in various catalytic reactions,[5] and chromium derivatives in particular have been intensely studied for the selective catalytic tri- and tetramerization of ethylene.[6] Four-membered-ring nickel(II) complexes with chelating short-bite ligands have also been successfully used as precatalysts in ethylene oligo- or polymerization, although they do not display the selectivity of the analogous Cr complexes.[7] The presence of a cocatalyst, such as an organoaluminum compound, is generally required and the characterization of the active species formed remains challenging.[8] To date, no Ni(PNP)/Al system could be isolated, and only one bimetallic Cr(II)/Al complex supported by a DPPA-type ligand, resulting from the reaction of [CrCl$_3${(Ph$_2$P)$_2$N(Cy)-*P*,*P*}] with AlMe$_3$ as activator, could be structurally characterized.[9]

Five- and six-membered-ring Ni(II) complexes have been successfully applied to ethylene oligomerization, and typical examples are shown in Chart 1.[10−12]

Received: February 7, 2014

 © XXXX American Chemical Society dx.doi.org/10.1021/om500141k | *Organometallics* XXXX, XXX, XXX−XXX

Chart 1. Examples of "Post-Metallocene" Nickel Catalysts for Olefin Oligo-/Polymerization[10−12]

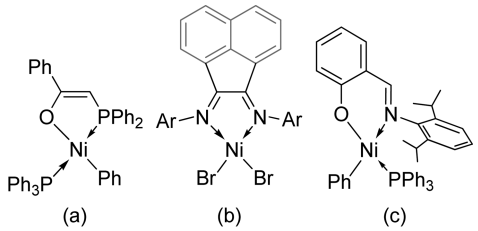

Ar = Phenyl, 2,6-di(*i*-Pr)phenyl

Scheme 1. Bis(diphenylphosphino)(*N*-(methylthio)propyl)amine Ligand 1 and Its Chelate Complex $[NiCl_2(P,P)]$ (2) (Top) and Equilibrium between the Neutral Diamagnetic Complex $[NiCl_2(P,P{=}S)]$ (3) and the Paramagnetic Ion Pair $[Ni(P,P{=}S)_2][NiCl_4]$ (3′) Containing the Monosulfide Derivative Ligand 1·S (Bottom)

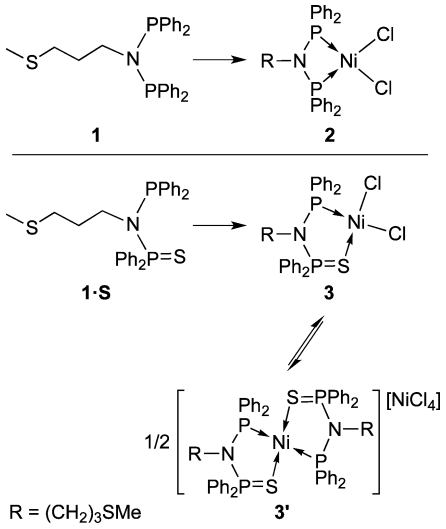

Our interest in catalytic ethylene oligomerization has led us inter alia to prepare various Ni complexes with mixed *P,L* ligands (*L* = N, O) (Chart 2).[13] The association within a functional ligand of donor sets of different hard−soft properties leads to so-called hybrid ligands,[14] which have been of longstanding interest to us.[14a,b] Hybrid ligands bring about stereoelectronic differentiation within the metal coordination sphere, in particular in the positions *trans* to these donor atoms. Their metal complexes can exhibit in solution a hemilabile behavior resulting from the reversible coordination−decoordination of the weaker donor. This feature allows stabilization of potentially coordinatively unsaturated species and facilitates substrate coordination for improved catalytic performance.[14]

Starting from short-bite ligands, one can readily obtain a hybrid ligand by selective mono-oxidation of one P-donor group into a phosphorus oxide or sulfide, which can potentially form a five-membered-ring chelate upon metal coordination. Oxidation of both P(III) centers would of course restore a symmetrical bidentate ligand, suitable for the formation of six-membered-ring metal complexes. Starting from bis(diphenylphosphino)(*N*-(methylthio)propyl)amine (**1**, N-$(PPh_2)_2(CH_2)_3SMe$), we recently prepared its monosulfide $(Ph_2P)N\{P(S)Ph_2\}(CH_2)_3SMe$ (**1·S**) and obtained their corresponding Ni(II) complexes $[NiCl_2\{(Ph_2P)_2N(CH_2)_3SMe\text{-}P,P\}]$ (**2**) and $[NiCl_2\{(Ph_2P)N\{P(S)Ph_2\}(CH_2)_3SMe\text{-}P,S\}]$ (**3**), which contain a *P,P* (**2**) or a *P,*P═*S* (**3**) chelate, respectively. These complexes exhibit very different reactivities in solution.[15] In contrast to the symmetrical chelate complex $[NiCl_2(P,P)]$ (**2**), which is stable in solution at various temperatures and in the presence of MeOH, a solvent-dependent reversible ligand exchange was found to be remarkably easy in the unsymmetrical chelate complex $[NiCl_2(P,P{=}S)]$ (**3**) (Scheme 1).

An equilibrium was established in CH_2Cl_2 at room temperature between the neutral diamagnetic complex $[NiCl_2(P,P{=}S)]$ (**3**) and the paramagnetic ion pair $[Ni(P,P{=}S)_2][NiCl_4]$ (**3′**), which involves the reversible transfer of the chelating ligand **1·S**, accompanied by chloride migration. This equilibrium was studied by multinuclear NMR, UV−visible, and FTIR spectroscopic methods and density functional theory (DFT) calculations.[15] After identifying the factors responsible for the equilibrium, we have isolated, characterized, and produced selectively one isomer or the other.

The coordination chemistry of the Ni(II) ion with other hybrid ligands, of the *P,N* type, was recently shown to lead to high versatility and facile structural modifications.[16] These included (i) the pressure-induced fragmentation of a tetranuclear complex with 20-electron Ni centers into mononuclear complexes $[NiCl_2(P,N)]$ with 16-electron Ni centers,[17] (ii) the formation of mono- or dinuclear isomers as a function of the crystallization temperature,[13a,18] and (iii) the equilibrium in solution between the two formula isomers $[Ni(P,N)_2][NiCl_4]$ and $[NiCl_2(P,N)]$.[19]

Starting from short-bite ligands, we were interested in studying how small changes in the metal catalyst design may modify their catalytic properties. We examined first the influence of the *N*-substituent in DPPA-type ligands (type **1** vs type **4** ligands with a flexible or more rigid tail, respectively) and then that of the size of the chelate ring in the complex,

Chart 2. Examples of Ni(II) Precatalysts with Phosphorus-Based *P,L* Chelates for Ethylene Oligomerization from Our Laboratory[13]

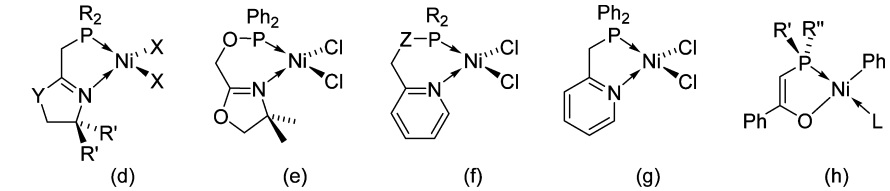

X = Br, Cl
Y = O; R = Ph; R' = H, Me
Y = S; R = Ph, *t*-Bu; R' = H

Z = O, CH_2
R = Ph, *t*-Bu

L = PPh_3, Py
R' = Ph; R" = *t*-Bu
R' = Ph; R" = *n*-Bu
R' = R" = *n*-Bu

dx.doi.org/10.1021/om500141k | *Organometallics* XXXX, XXX, XXX−XXX

although we realize that this is accompanied by a change in the nature of one of the donor groups (four-membered ring in *P,P* chelates vs five-membered ring in the corresponding *P,*P═*S* chelates). One objective was to provide unambiguous characterization, preferably both in the solid state and in solution, of precatalysts to be used in ethylene oligomerization.

We report here the synthesis, characterization, and DFT calculations of the Ni(II) complexes [$NiCl_2${$(Ph_2P)_2N$(*p*-C_6H_4SMe)-*P,P*}] (**5**) and [$NiCl_2${$(Ph_2P)N${P(S)Ph_2}(*p*-C_6H_4SMe)-*P,S*}] (**6**), prepared from the ligand bis(diphenylphosphino)(*N*-4-(methylthio)phenyl)amine (**4**) and its monosulfide derivative **4·S**, respectively. These complexes are *N*-aryl thioether analogues of complexes **2** and **3** obtained with *N*-alkyl thioether DPPA-type ligands. We also discuss the catalytic activities of the corresponding $NiCl_2$ complexes (**2**, **3** and **5**, **6**) in ethylene oligomerization, with ethylaluminum dichloride as cocatalyst, as a function of the influence of the *N*-substituent (aryl vs alkyl function) in the chelating diphosphine ligand and of the size of the chelate ring formed upon coordination to the Ni(II) center.

RESULTS AND DISCUSSION

Synthesis and Spectroscopic Characterization of the *N*-Arylthioether DPPA-Type Ligands. The preparation of bis(diphenylphosphino)(*N*-4-(methylthio)phenyl)amine (**4**) was readily achieved by reaction of the corresponding amines with 2 equiv of PPh_2Cl in the presence of excess NEt_3 as HCl scavenger (Scheme 2, reaction *a*).[20]

Scheme 2. Synthesis of (*P,P*), (*P,*P═*S*), and (P═*S,*P═*S*) Ligands 4, 4·S, and 4·S_2[a]

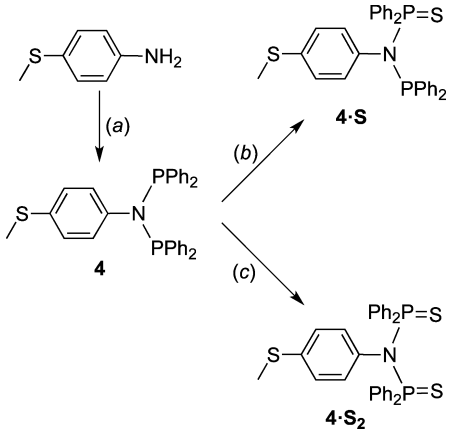

[a]Legend; (*a*) PPh_2Cl (2 equiv), NEt_3 (2.5 equiv), THF, room temperature, 3 h; (*b*) S_8 (1.5 equiv), CH_2Cl_2, room temperature, 30 min; (*c*) S_8 (2.2 equiv), toluene, 115 °C, 3 h.

The ligand **4** was obtained in good yield (71%) as an air- and moisture-sensitive white powder. Its $^{31}P\{^1H\}$ NMR spectrum contains a singlet resonance at 69.4 ppm for the two equivalent phosphorus atoms (Table 1). This chemical shift is in agreement with the values observed for *N*-aryl-substituted DPPA-type ligands (62.2−71.1 ppm), higher values being found for compounds with aryl groups substituted at the *para* position (66.1−71.1 ppm).[21] The monosulfide derivative **4·S** could not be obtained in pure form, owing to the concomitant formation of the bis-sulfide byproduct **4·S_2** in a ca. 70:30 ratio (Scheme 2, reactions *b* and *c*)). A similar situation was observed in the case of ligand **1·S**, which like **4·S** was prepared and used in situ for the synthesis of the desired Ni(II) complexes. The undesired compound **4·S_2** can easily be removed by successive washings of its Ni(II) complexes with toluene (see below). However, the bis-sulfide derivative **4·S_2** can be quantitatively obtained, as an air-stable white powder, using a slight excess of elemental sulfur, but its coordination properties will not be discussed here (Scheme 2, reaction *c*). Both **4·S** and **4·S_2** were fully characterized, and their $^{31}P\{^1H\}$ NMR spectra exhibit the expected patterns: i.e., two doublets (55.3 (P^{III}) and 72.4 (P^V) ppm; $^2J_{P,P}$ = 104.5 Hz) for the mixed *P,*P═*S* ligand **4·S** and a singlet (69.0 ppm) for the two equivalent phosphorus atoms of **4·S_2** (Table 1). These chemical shifts are comparable to those reported for other mono- and bis-sulfide DPPA-type ligands, which were found in the respective ranges: 51.5−54.5 (P^{III}) and 67.5−73.5 (P^V)[21g,h,22] (monosulfide derivatives) and 67.5−73.6 ppm (bis-sulfide derivatives).[21a−d,g,23] The experimental $^{31}P\{^1H\}$ NMR chemical shifts of the *N*-thioether-functionalized P,P═S and P═S,P═S ligands (**1·S**, **1·S_2**, **4·S**, and **4·S_2**) measured in $CDCl_3$ and CD_2Cl_2 solutions were well reproduced by NMR calculations on the BP86/TZ2P minimum-energy gas-phase structures of **1·S^{DFT}**, **1·S_2^{DFT}**, **4·S^{DFT}**, and **4·S_2^{DFT}** (Supporting Information, Tables S4−S8).

The molecular structures of ligands **4** and **4·S_2** were determined by single-crystal X-ray diffraction studies and are depicted in Figures 1 and 2, respectively. To the best of our knowledge, only four other bis(diarylphosphino)(*N*-4-(R)-phenyl)amine ligands have been structurally characterized (**A**−**D**),[3a,21a,24,25] and interesting structural differences with ligand **4** were observed (Scheme 3 and Figure S-1 (Supporting Information)).

While in the reported compounds **A**,[3a] **B**,[24] and **C**,[21a] as well as in ligand **1**,[20] the P lone pairs display a *syn* conformation (pointing in the same direction, a typical chelating coordination orientation), those of ligand **4** and the P-benzyl derivative **D**[25] present an *anti* orientation (pointing in opposite directions; Scheme 3, bottom). The structure of **4** also exhibited a stronger tilt of the angle (α) between the aryl ring and the PNP plane (α = 62.1°) in comparison to **A** (α = 82.4°), **B** (α = 80.5°), **C** (α = 81.7°), and **D** (α = 78.3°) (Scheme 3, top). In view of the structures of ligands **A^{DFT}** (α = 84.4°), **B^{DFT}** (α = 83.5°), and **4^{DFT}** (α = 61.7°) calculated in the gas phase, one can say that the conformational difference associated with the α angle is rather "intrinsic" to **4** instead of being caused by packing effects (Supporting Information, Table S9). The other possible

Table 1. $^{31}P\{^1H\}$ NMR Data of Ligands 4, 4·S_2, and 4·S and Complexes 5−9

	4[a]	**4·S_2**[a]	**4·S**[a]	**5**[b]	**6**[a]	**7**[b]	**8**[a,d]	**9**[a,d]
δ (ppm)	69.4	69.0	55.3; 72.4	45.4	83.8	84.6; 105.8	83.7	80.1; 106.7
mult	s	s	d; d	s	br s	t; t	br s	d; d
J (Hz)			$^2J_{P,P}$ = 104.5			$^{2,2+3,3,4}J_{P,P}$[c]		$^{2+3}J_{P,P}$ = 59.9

[a]NMR solvent $CDCl_3$. [b]NMR solvent CD_2Cl_2. [c]Detailed in the Experimental Section. [d]See the Supporting Information.

dx.doi.org/10.1021/om500141k | *Organometallics* XXXX, XXX, XXX−XXX

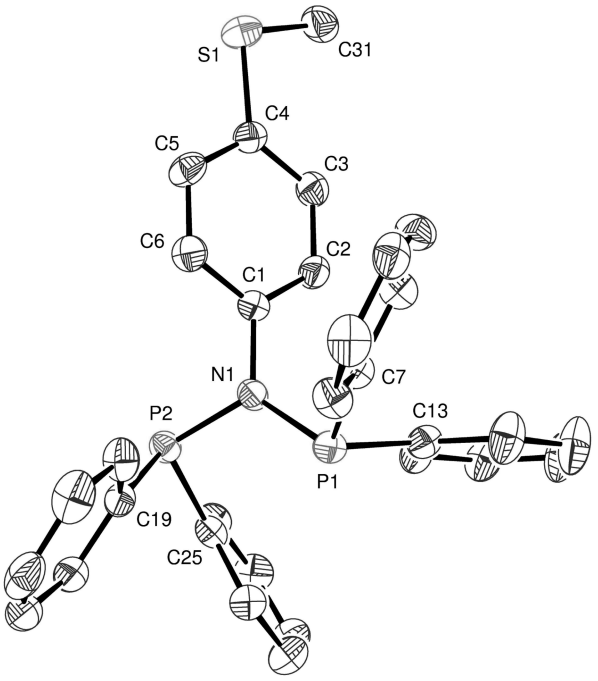

Figure 1. ORTEP drawing of the molecular structure of $N(PPh_2)_2(p\text{-}C_6H_4)SMe$ (**4**). Thermal ellipsoids are set at the 50% probability level. Hydrogen atoms are omitted for clarity. Selected bond distances (Å) and angles (deg): P1−N1 1.732(2), P2−N1 1.728(2), C1−N1 1.452(3); P1−N1−P2 120.8(1).

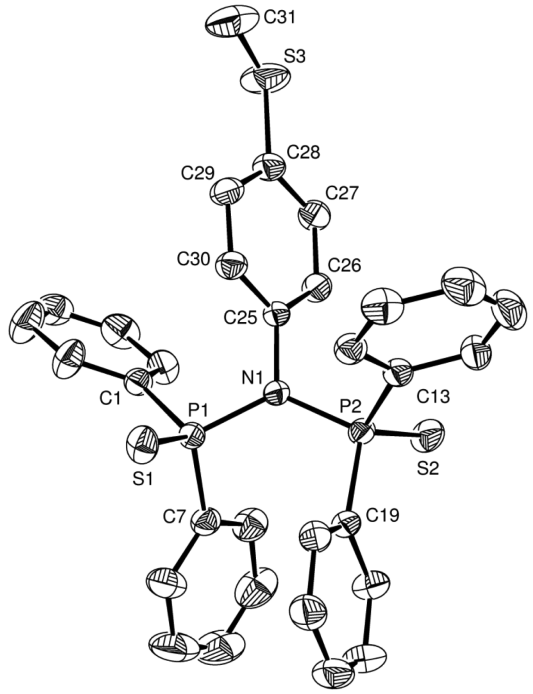

Figure 2. ORTEP drawing of the molecular structure of $N\{P(S)Ph_2\}_2(p\text{-}C_6H_4)SMe$ (**4·S$_2$**). Thermal ellipsoids are set at the 50% probability level. Hydrogen atoms are omitted for clarity. Selected bond distances (Å) and angles (deg): P1−N1 1.708(1), P2−N1 1.717(1), P1−S1 1.9452(6), P2−S2 1.9350(6), N1−C25 1.457(2); P1−N1−P2 127.11(7), S1−P1−N1 115.16(5), S2−P2−N1 114.82(5).

relationships between the orientation of P lone pairs and the α angle were not explored further.

Scheme 3. Main Structural Differences between Ligand 4 and the known Ligands A−D

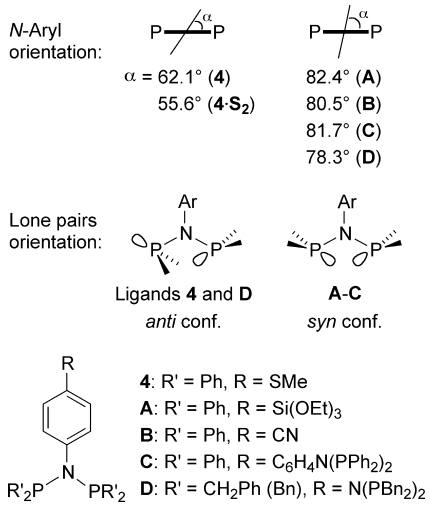

The solid-state structure of **4·S$_2$** revealed characteristic P═S, P−N, and C−N bond lengths and a P−N−P angle in the usual range.[21c,22d,23a,26] All attempts to obtain suitable crystals of ligand **4·S** for X-ray diffraction were unsuccessful, which may explain the relatively small number of structures of mono-sulfide-DPPA derivatives reported.[22d,e] Interestingly, the oxidation of the P centers and the formation of the bis-sulfide ligand **4·S$_2$** result in only slight structural differences in comparison to **4**. The P−N and C−N bond lengths are almost similar (average 1.73 Å (**4**) vs 1.71 Å (**4·S$_2$**)), while the most affected parameters are the PNP angle (120.8(1)° (**4**) vs 127.1(7)° (**4·S$_2$**)) and the angle between the PNP moiety[27] and the phenyl ring (α = 62.1° (**4**) vs. 55.6° (**4·S$_2$**)) (Scheme 3). The BP86/TZ2P calculations provide values for the angles α comparable to those determined experimentally. Thus, the α angle between the planes of the PNP moiety and the *N*-aryl ring was calculated to be 61.7° for **4**^{DFT}, 57.6° for **4·S$_2$**^{DFT}, and 79.3° for the hypothetical structure **4·S**^{DFT}. The calculated PNP angles in **4**^{DFT}, **4·S$_2$**^{DFT}, and **4·S**^{DFT} are 120.8, 129.0, and 117.2°, respectively. As a result, a correlation between the α and PNP angles was observed: the greater the α angle (**4·S$_2$**^{DFT} < **4**^{DFT} < **4·S**^{DFT}), the smaller the PNP angle (**4·S$_2$**^{DFT} > **4**^{DFT} > **4·S**^{DFT}).

Synthesis of the Ni(II) Complexes. With the objective of developing new (pre)catalysts for ethylene oligomerization and evaluating the influence of the ligand properties (*P,P* vs *P,*P═*S*, chelate ring size, nature of the *N*-substituent), we prepared nickel(II) complexes with ligands **4** and **4·S** by analogy with complexes of the type $[NiX_2(LL')]$ (e.g. LL′ = P,N, P,O, or P,P ligand and X = Cl, Br).[13a,b,28] Reaction of **4** with $[NiCl_2(DME)]$ (DME = 1,2-dimethoxyethane) in a 1:1 ratio in dichloromethane at room temperature afforded $[NiCl_2\{(Ph_2P)_2N(p\text{-}C_6H_4SMe)\text{-}P,P\}]$ (**5**) in high yield (83%) as a red crystalline powder (Scheme 4, reaction *a*). This color is consistent with the square-planar structure and diamagnetic nature of Ni(II) complex **5**, which could therefore be fully characterized by multinuclear NMR spectroscopic methods. Its $^{31}P\{^1H\}$ NMR spectrum exhibits a singlet at 45.4 ppm, shifted upfield with respect to the free ligand **4** (s, 69.4 ppm, Table 1). This value compares well with those found for the other $[NiX_2(P,P)]$ (X = Cl, Br, I and *P,P* = *N*-functionalized DPPA-type ligand) complexes reported (38.6−58.3 ppm).[7b,c,e,15,23c,29]

dx.doi.org/10.1021/om500141k | *Organometallics* XXXX, XXX, XXX−XXX

Scheme 4. Synthesis of the Ni Complexes 5−7[a]

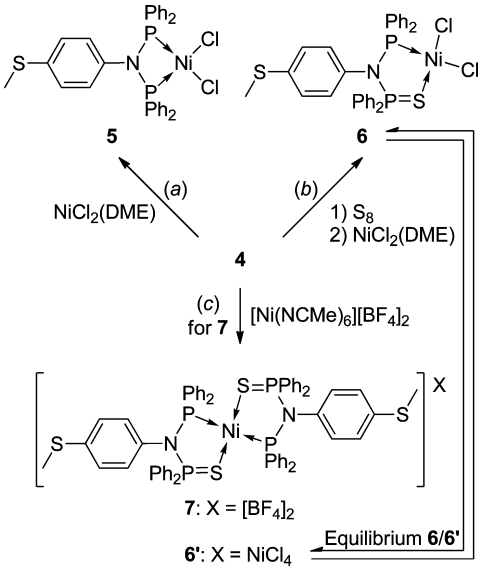

[a]Legend: (*a*) 1 equiv of [$NiCl_2$(DME)], CH_2Cl_2, room temperature, 4 h; (*b*) 1.5 equiv of S_8, CH_2Cl_2, room temperature, 30 min and 0.55 equiv of [$NiCl_2$(DME)], CH_2Cl_2, room temperature, 4 h; (*c*) 1.5 equiv. of S_8, CH_2Cl_2, room temperature, 30 min followed by 0.25 equiv of [Ni(NCMe)$_6$][BF_4]$_2$, CH_2Cl_2, room temperature, 4 h. Note: complexes **6** and **6'** are in equilibrium in solution. DME = 1,2-dimethoxyethane.

Since **4·S** could not be isolated in pure form, it was prepared in situ (see above), and subsequent addition of 0.5 equiv of [$NiCl_2$(DME)] led to the formation of [$NiCl_2${(Ph_2P)N{P(S)Ph_2}(*p*-C_6H_4SMe)-*P*,*S*}] (**6**) in good yield (82%) as a crystalline solid, after removal of the undesired **4·S$_2$** by successive washings with toluene (Scheme 4, reaction *b*). Its purple color, both in the solid state and in solution, contrasts with that of the diamagnetic complex **5** (red). The $^{31}P\{^1H\}$ NMR spectrum of a solution of **6** exhibited a broad singlet centered at 83.8 ppm (Table 1) instead of the expected pattern of two doublets for the nonequivalent P^{III} and P^{V} donors, as observed for the free ligand. A similar $^{31}P\{^1H\}$ NMR spectrum was obtained for the complex [$NiBr_2$(**4·S**)] (**8**), which suggests no significant influence of the halide nature on the solution behavior of such *P*,P═*S*-chelate Ni(II) complexes (see Table 1 and the Supporting Information). The paramagnetic character of the solution prevented the recording of well-resolved ^1H and ^{13}C NMR spectra. We recently showed in the case of complex **3** (Scheme 1), which is the analogue of **6** with the *N*-alkyl thioether ligand **1·S**, that this broad signal observed in the NMR is due to a fast equilibrium in solution between the neutral diamagnetic [$NiCl_2$(**1·S**)] (**3**) species and its paramagnetic ion pair formula isomer [Ni(**1·S**)$_2$][$NiCl_4$] (**3′**).[15] This equilibrium was found to be dependent on the temperature and the solvent polarity and could be unambiguously characterized by ^{31}P VT-NMR and UV−vis (variable temperature and polarity gradient) spectroscopic techniques and rationalized by computational studies. On the basis of this previous work, we reasonably assume that a similar equilibrium between the anticipated [$NiCl_2$(**4·S**)] structure and the ion pair formula isomer [Ni(**4·S**)$_2$][$NiCl_4$] (**6′**) (Scheme 4), as well as for its $NiBr_2$ analogue **8**, can be envisaged. Furthermore, the ESI-MS spectrum of a CH_2Cl_2 purple solution of complex **6** confirmed this hypothesis by revealing peaks at *m*/*z* 632.01 and 1298.99, which can be attributed to {[$NiCl_2$(**4·S**)] − Cl}$^+$ and {[Ni(**4·S**)$_2$][$NiCl_4$] − Cl}$^+$, respectively. Unfortunately, direct comparison of NMR data with literature values was not possible since, as far as we know, no other $NiCl_2$ complex of monosulfide *N*-functionalized DPPA-type ligands has been reported. Only $PdCl_2$ and $PtCl_2$ complexes have been described, which of course exhibit well-resolved signals, such as [$PdCl_2$(**4·S**)] (**9**) (see Table 1 and the Supporting Information).[21g,h,22b,c,e] It is worth noting that no change in the $^{31}P\{^1H\}$ NMR spectrum of **9** was observed, even by modification of the solvent polarity or recording temperature, in contrast to its Ni(II) analogues **6** and **8**, reflecting the higher kinetic stability in solution of Pd derivatives. While isomer **6** could be isolated in pure form, all attempts to isolate the hypothetical isomer **6′** by increasing the solvent polarity upon addition of MeOH (as for **3′**)[15] led to a metal-induced dismutation-type reaction of the phosphorus atoms, resulting in the formation of the non-P═S-containing complex **5** and the bis-sulfide ligand **4·S$_2$** in a 1:1 ratio (NMR evidence). This transformation, from **6** to **5** and **4·S$_2$**, was also observed when pure **6** was dissolved d_6-DMSO, an aprotic but polar solvent. The latter characteristic thus appears decisive for the occurrence of this ligand transformation.

Since the paramagnetic component of **6′** is $[NiCl_4]^{2-}$, we prepared the diamagnetic bis-chelated complex [Ni{(Ph_2P)N{P(S)Ph_2}(*p*-C_6H_4)SMe-*P*,*S*}$_2$][BF_4]$_2$ (**7**), containing the same dication as the hypothetical complex **6′**, using [Ni(NCMe)$_6$][BF_4]$_2$ as precursor instead of [$NiCl_2$(DME)] (Scheme 4, reaction *c*). Complex **7** was obtained in good yield (85%) as a crystalline solid, its red color (yellow in diluted solution) being characteristic of a square-planar arrangement of the ligands around the metal center. Its diamagnetic nature therefore allowed its full characterization by multinuclear NMR experiments, and its $^{31}P\{^1H\}$ NMR spectrum exhibited two tripletlike resonances (AA′BB′ spin system) at 105.8 (P^{V}) and 84.6 (P^{III}) ppm (Table 1).

An NMR experiment consisting of the addition of Cl^- anions (from $HNEt_3Cl$) to a solution of **7** showed an evolution of the NMR spectrum, from two well-resolved "triplets" to one broad singlet centered at 83.8 ppm, similar to that of **6**, and the liberation of uncoordinated ligand **4·S** (see the Experimental Section and Figure S2 (Supporting Information)). This reaction is accompanied by a significant color change from yellow (**7**) to the familiar purple of complex **6**. These observations are reminiscent of the behavior of analogous complexes containing the *N*-alkyl thioether ligand **1·S** (Scheme 1).[15] From the unambiguously characterized equilibrium between **3** and **3′**, we conclude the existence of a similar process between **6** and **6′**.

The chemical shifts observed for the methyl protons in complexes **5** and **7** (2.32 and 2.26 ppm, respectively) remain very close to that for the free diphosphines **4** and **4·S** (2.35 and 2.23 ppm, respectively), indicating no S···Ni interaction in solution.

Solid-State Structure of the Ni(II) Complexes. Single crystals of complexes **5**−**7** suitable for X-ray diffraction studies were obtained as described in the Experimental Section. Their solid-state structures are depicted in Figures 3−5, and selected bond lengths and angles are reported in Table 2. In all three complexes, the Ni center displays a distorted-square-planar coordination geometry, with the *P*,*P* (**4**) and *P*,P═*S* (**4·S**) ligands acting as chelates, forming four- (**5**) and five-membered (**6**, **7**) metallacycles. The metal coordination sphere in

dx.doi.org/10.1021/om500141k | *Organometallics* XXXX, XXX, XXX−XXX

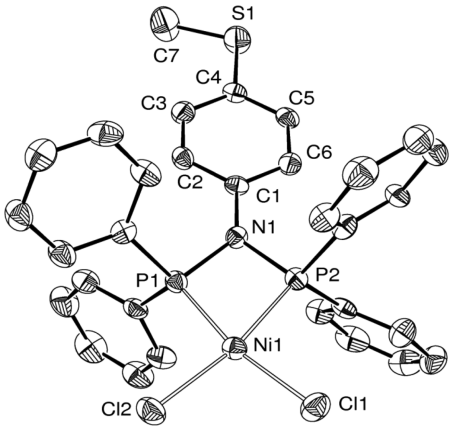

Figure 3. ORTEP drawing of the molecular structure of $[NiCl_2\{(Ph_2P)_2N(p\text{-}C_6H_4)SMe\text{-}P,P\}]$ (**5**) in **5**·$2CH_2Cl_2$. Thermal ellipsoids are set at the 50% probability level. Hydrogen atoms and solvent molecules are omitted for clarity.

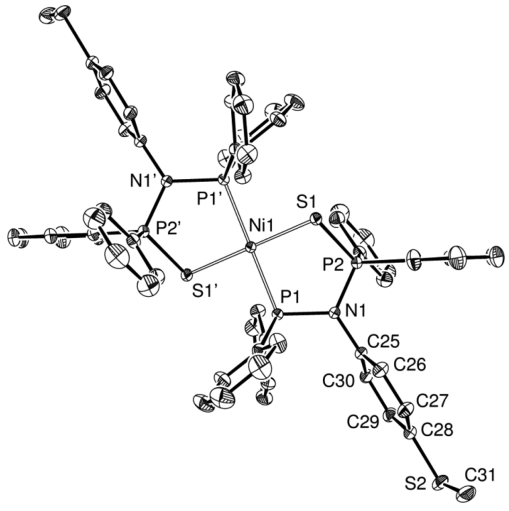

Figure 5. ORTEP drawing of the molecular structure of $[Ni\{(Ph_2P)\text{-}N\{P(S)Ph_2\}(p\text{-}C_6H_4)SMe\text{-}P,S\}_2](BF_4)_2$ (**7**) in **7**·$4CH_2Cl_2$. Thermal ellipsoids are set at the 50% probability level. Hydrogen atoms, BF_4 anions, and solvent molecules are omitted for clarity.

complexes **5** and **6** is completed by two chlorine ligands, while in the centrosymmetric structure of **7**, a second *P*,P═*S* ligand is found in an *anti* arrangement.

The characteristic bond lengths and angles in **5** are similar to those found in related $[NiCl_2(P,P)]$ (*P*,*P* = *N*-functionalized DPPA-type ligand) complexes.[6c,29b,e,30] With the exception of complex **3**, which was recently described,[15] no other example of a $[NiCl_2(P,P{=}S)]$ complex is available for comparison, to the best of our knowledge.

Interestingly, while the two N−P bond lengths are similar in the (*P*,*P*)-Ni(II) complex **5**, the difference between the N1−$P1^{III}$ and the N1−$P2^{V}$ distances in the (*P*,P═*S*)-Ni(II) complexes **6** and **7** is more pronounced (1.731(3) and 1.678(3) Å (**6**) and 1.716(1) and 1.680(1) Å (**7**), respectively). This could be related to the electronegativity of the sulfur atom, which strengthens the P−N bond, as observed in related complexes with P═S, P═O, and P═Se groups.[15,21g,22,22e,31] The P−N−P angle of the ligand is strongly affected by the presence of the sulfur donor (96.7° (**5**) vs 118.0 (**6**) and 114.7° (**7**)). In the $[NiCl_2(P,P)]$ complex **5**, the rectangular distortion of the coordination geometry around the metal is due to the four-membered chelate ring, which imposes a P−Ni−P angle of 74.2°, while in the $[Ni(P,P{=}S)]$-type complexes, the P−Ni−S angle is closer to the preferred 90° (94.3° (**6**), 93.2° (**7**)).

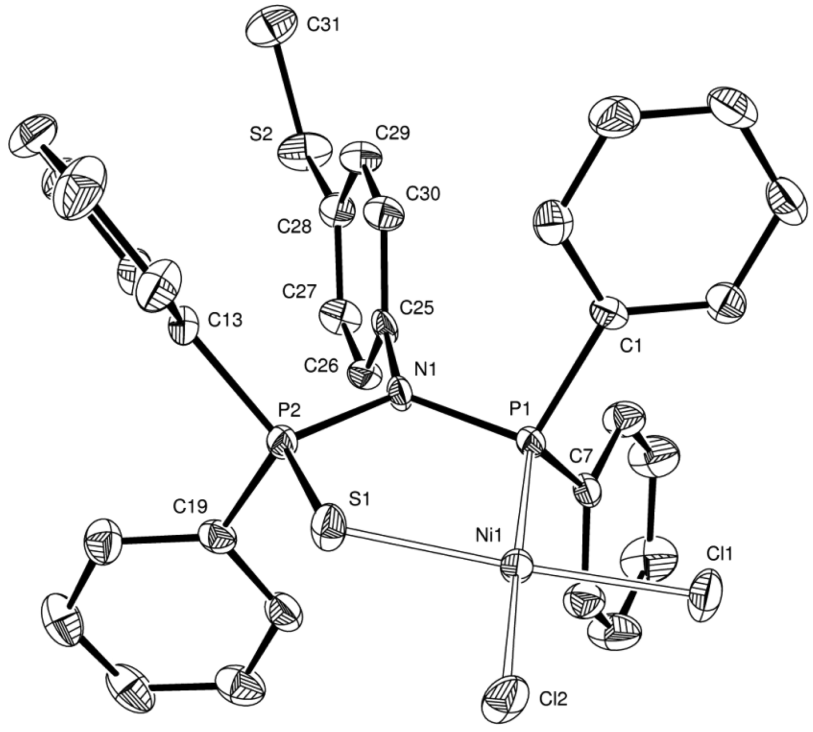

Figure 4. ORTEP drawing of the molecular structure of $[NiCl_2\{(Ph_2P)N\{P(S)Ph_2\}(p\text{-}C_6H_4)SMe\text{-}P,S\}]$ (**6**) in **6**·C_3H_6O. Thermal ellipsoids are set at the 50% probability level. Hydrogen atoms and solvent molecules are omitted for clarity.

dx.doi.org/10.1021/om500141k | *Organometallics* XXXX, XXX, XXX−XXX

Table 2. Selected Bond Lengths (Å) and Angles (deg) in the Solid-State Structures of 5·2CH_2Cl_2, 6·C_3H_6O, and 7·4CH_2Cl_2

	5	6	7
N1−P1	1.706(5)	1.731(3)	1.716(1)
N1−P2	1.716(5)	1.678(3)	1.680(1)
P2−S1		2.004(1)	2.020(4)
P1−Ni1	2.110(2)	2.138(1)	2.198(3)
P2(S1)−Ni1	2.128(2)	2.163(1)	2.180(3)
Ni1−Cl1	2.183(2)	2.173(1)	
Ni1−Cl2	2.202(2)	2.211(1)	
Cl1−Ni1−Cl2	99.26(6)	94.91(4)	
P1−Ni1−P2(S1)	74.20(6)	94.26(4)	93.16(1)
P1−N1−P2	96.70(2)	118.0 (2)	114. 7(6)

However, the Cl−Ni−Cl angle is only slightly affected (99.3° (**5**) vs. 94.9° (**6**)).

As expected, the two P−Ni bond lengths in complex **5** are nearly equivalent (average 2.12 Å) and similar to the P1−Ni bond (2.14 Å) in complex **6**. The slightly stronger *trans* influence of the P donor compared to S in the mixed (*P*,P═*S*) nickel complex **6**, results in a longer Ni−Cl2 bond compared to Ni−Cl1, as also observed in related $PdCl_2$ and $PtCl_2$ complexes with (*P*,P═*S*) or (*P*,P═*Se*) DPPA-type ligands.[21g,22c,e] In the bis-chelated dicationic complex of **7**, both L−Ni bonds (L = P, S) were found to be 0.2−0.6 Å longer than in complex **6**. The solid-state molecular structures of [$NiBr_2$(**4·S**)] (**8**·CH_2Cl_2) and [$PdCl_2$(**4·S**)] (**9**) are very similar to that of complex **6** (see the Supporting Information, Figure S3 and Table S3).

The DFT relative energies (ΔE_{rel}) calculated for the reaction processes associated with the formation of the Ni(II) complexes of the *N*-alkyl thioether functionalized DPPA-type ligands **1**^{DFT}, **1·S**^{DFT}, and **1·S$_2$**^{DFT} (type A) and those of their *N*-aryl thioether counter parts **4**^{DFT}, **4·S**^{DFT}, and **4·S$_2$**^{DFT} (type B) show that the presence of sulfur atoms at P significantly influences the energetics of the nickel−ligand bonding, thus resulting in decreased thermodynamic stability of the optimized Ni(II) complexes with the (*P*,P═*S*) and (P═*S*,P═*S*) ligands (Figure 6). The trend in ΔE_{rel} is thus as follows: [$NiCl_2$(*P*,*P*)] > [$NiCl_2$(*P*,P═*S*)] > [$NiCl_2$(P═*S*,P═*S*)]. From these data, we may expect that the overall stability of the compounds, which in the case of [$NiCl_2$(*P*,P═*S*)] is the combined result of a modification in the chelate ring size (five-membered chelates are usually more stable than four-membered chelates) and the associated change in the nature of the donor groups (a P═S moiety is a poorer donor for Ni(II) than P) may influence the catalytic properties of the Ni(II) complexes in ethylene oligomerization.

Catalytic Ethylene Oligomerization. The nickel(II) complexes with *N*-(methylthio)propyl (**2**, **3**) or *N*-4-(methylthio)phenyl (**5**, **6**) functionalized PNP or P(S)NP-type ligands, containing a four- (**2**, **5**) or five-membered chelate (**3**, **6**), were evaluated as precatalysts in the oligomerization of ethylene with $AlEtCl_2$ as cocatalyst. Various amounts of cocatalyst and different concentrations of precatalysts were tested, and the catalytic results are presented in Table 3. To allow comparisons with previous studies, we kept the reaction time constant at 35 min and the ethylene consumption during catalysis progressively decreased but was retained up to at least 60 min (entries 2 and 9, Table 3). The reaction products did not follow a Schulz−Flory distribution of their chain length, since mostly dimers and significant amounts of trimers (selectivity in the range 11−36%) were obtained. The percentages of C8 and C10 measured are in the ranges 0−3.4% and 0−2.7%, respectively, and no longer chains were observed.

Comparison between [$NiCl_2$(P,P)]- and [$NiCl_2$(P,P═S)]-Type Complexes. Such a comparison, made with a constant *N*-substituent, allows us to examine the combined effect of a change in the chelate ring size and of the resulting difference in the nature of the donor atoms on the catalytic activity and/or the selectivity. In the *N*-(methylthio)propyl series, the activity of the *P*,P═*S* complex **3** was found to be higher than that of its *P*,*P* counterpart **2** at high Al/Ni ratios (10 and 40, entries 1−3 and 6, 7, respectively), with turnover frequencies (TOFs) of 47400 and 101100 mol of C_2H_4/((mol of Ni) h) for **3** and 35800 and 84800 mol of C_2H_4/((mol of Ni) h) for **2**,

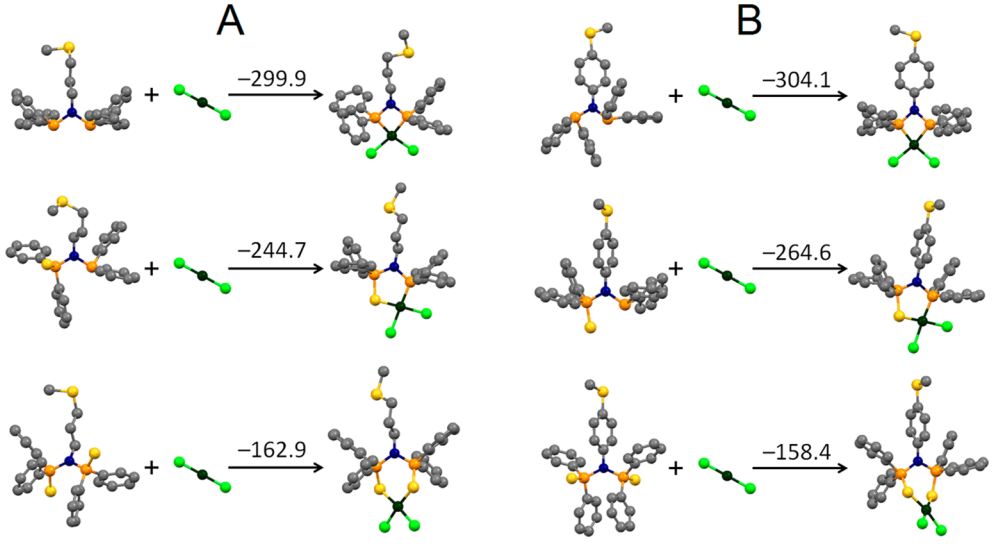

Figure 6. BP86/TZ2P relative energies (ΔE_{rel} in kJ mol^{-1}, including zero-point energy corrections) calculated for the gas-phase reaction processes involving minimum energy structures of the ligands analyzed herein and their Ni(II) complexes of types A and B. Color code: C, gray; N, blue; P, orange; S, yellow; Cl, light green; Ni, dark green. For more details on the computational methodology, see the Supporting Information.

dx.doi.org/10.1021/om500141k | *Organometallics* XXXX, XXX, XXX−XXX

Table 3. Pairwise Comparison of the Catalytic Data for Complexes 2, 3, 5, and 6 in the Oligomerization of Ethylene with $AlEtCl_2$ as Cocatalyst[a]

				selectivity (%)						
entry no.	complex	$n_{complex}$ (10^{-5} mol)	$AlEtCl_2$ (equiv)	C4	C6	C8	>C8	productivity[b,d]	TOF[c,d]	1-butene[e] (%)
1	**2**	4	10	77	20	2	1	17100	35800	17
2[f]	**2**	2	10	64	31	4	1	23000	48300	8.4
3	**3**	4	10	71	26	2	<1	22600	47400	7
4	**2**	4	3	77	21	2	0	3100	6600	16
5	**3**	4	3	70	21	7	2	2300	4800	35
6	**2**	1	40	70	26	3	1	40400	84800	16
7	**3**	1	40	66	26	5	2	48200	101100	25
8	**5**	4	10	69	27	3	<1	23100	48400	4
9[f]	**5**	2	10	68	26	3	2	32800	68800	9
10	**6**	4	10	82	16	1	<1	12700	26700	9
11	**5**	4	3	58	36	5	1	12900	27100	9
12	**6**	4	3	87	11	1	<1	3900	8200	15
13	**5**	1	40	79	20	1	0	20000	41900	26
14	**6**	1	40	73	23	3	1	32200	67400	13

[a]Conditions: T = 28−30 °C, 10 bar of C_2H_4, time 35 min, solvent 10 mL chlorobenzene and 5 mL of the cocatalyst solution (8×10^{-5} M) for 10 and 40 equiv of $AlEtCl_2$ or 13.5 mL of chlorobenzene and 1.5 mL of the cocatalyst solution (8×10^{-5} M) for 3 equiv of $AlEtCl_2$. [b]In g of C_2H_4/((g of Ni) h)). [c]In mol of C_2H_4/((mol of Ni) h). [d]Values rounded off to the lower hundred. [e]Within the C_4 fraction. [f]Reaction time 60 min.

respectively. The chain-length selectivity was only slightly affected on going from **2** and **3** (entries 1−7), but a higher selectivity for C_4 oligomers was observed for the *P*,*P* derivative **2** at all precatalyst concentrations and Al/Ni ratios examined. Although modest, the best selectivity for 1-butene within the C_4 cut was achieved with complex **3**, using 3 equiv of $AlEtCl_2$ and 4×10^{-5} mol catalyst loading and reached 35% (entry 5).

In the *N*-4-(methylthio)phenyl series, complex **6** exhibited TOF values between 8200 and 26700 mol of C_2H_4/((mol of Ni) h), while for **5**, values between 27100 and 48400 mol of C_2H_4/((mol of Ni) h) (entries 12 and 10 (**6**) and entries 11 and 8 (**5**), respectively) were obtained. At higher Al/Ni ratios, the trend was reversed, since with 40 equiv of $AlEtCl_2$ and 1×10^{-5} mol catalyst loading, complex **6** exhibited a higher TOF (67400 vs 41900 mol of C_2H_4/((mol of Ni) h)) than **5**. The selectivity in C_4 oligomers was generally improved, with 3 or 10 equiv of $AlEtCl_2$, by the introduction of the S donor and the associated increase in the chelating ligand ring size, since it reached 58 and 69% (entries 11 and 8) for complex **5** and 87 and 82% (entries 12 and 10), for complex **6**, respectively. The lower activity of **6** in comparison to that of **5** was associated with an higher selectivity in C_4 oligomers (73 vs 79%) (entries 14 and 13).

Influence of the N-Substituent. Let us now compare the results obtained as a function of the *N*-substituent of the ligand, keeping the chelate ring size constant: i.e., comparing **2**/**5** and **3**/**6**. While complex **2** (*P*,*P*; *N*-alkyl thioether) showed similar C4 selectivities when different amounts of Ni and Al cocatalyst were used (70−77%, entries 1, 4, and 6), the C4 selectivity observed for complex **5** (*P*,*P*; *N*-aryl thioether) varied much more (58−79%, entries 8, 11, 13) and remained generally lower than for **2**. A greater difference in selectivity was observed for the *P*,P=*S*-containing Ni(II) complexes **3** and **6**, and the latter always exhibited a higher selectivity, up to 87% for C_4 oligomers (entry 12), than its *N*-alkyl thioether counterparts **3** (70% under the same conditions, entry 5).

Within the *P*,*P* derivatives, we found better activities for the *N*-aryl complex **5** than for the *N*-alkyl complex **2** at lower Al/Ni ratios, with TOFs of 27100 (3 equiv of $AlEtCl_2$) and 48400 (10 equiv of $AlEtCl_2$) mol of C_2H_4/((mol of Ni) h) (entries 11 and 8, respectively) and 6600 (3 equiv of $AlEtCl_2$) and 35800 (10 equiv of $AlEtCl_2$) mol of C_2H_4/((mol of Ni) h) (entries 4 and 1), respectively. However, at higher Al/Ni ratios, using 40 equiv of $AlEtCl_2$, complex **2** led to TOF values more than twice those of **5** (84800 vs 41900 mol of C_2H_4/((mol of Ni) h), entries 6 and 13, respectively). For the *P*,P=*S* systems, however, the *N*-alkyl complex **3** was found to be more active than its *N*-aryl analogue **6** at high Al/Ni ratios (10 and 40 equiv of $AlEtCl_2$, entries 3 and 7 vs entries 10 and 14), and a lower TOF was observed for **3** (4800 mol of C_2H_4/((mol of Ni) h), entry 4) in comparison to **6** (8200 mol of C_2H_4/((mol of Ni) h), entry 12) when only 3 equiv of $AlEtCl_2$ was used.

Under the different conditions studied, the selectivity for α-olefins remained modest (4−35%) due to the typical fast isomerization process in Ni(II)-catalyzed oligomerization of ethylene.[11c,32] No saturated hydrocarbons were produced during the catalytic process. The C6 and C8 oligomers produced contained a small percentage of linear chains in a larger distribution of branched olefins, which is indicative of the occurrence of both stepwise chain growth and of codimerization reactions (C4 + ethylene).

CONCLUSION

The selective oligomerization of ethylene remains an active field of research, and the present work highlights, via a combination of experimental and computational studies, how subtle changes in the ligand design of the well-known (PNP)-$NiCl_2$ (pre)catalyst strongly influence their catalytic activity and selectivity. Our synthesis and characterization of the new bis(diphenylphosphino)(*N*-4-(methylthio)phenyl)amine ligand **4**, its monosulfide derivative **4·S**, and their Ni(II) complexes **5** and **6** follow our recent report on similar $NiCl_2$ derivatives (**2** and **3**) of the bis(diphenylphosphino)(*N*-(methylthio)propyl)-amine ligand **1** and its monosulfide derivative **1·S**.[15] The DFT geometry optimizations and relative binding energy calculations indicated that the [$NiCl_2$(*P*,*P*)] complexes have enhanced thermodynamic stability in comparison to the [$NiCl_2$(*P*,P=*S*)] and [$NiCl_2$(P=*S*,P=*S*)] complexes, and this is due to the stronger covalent character of the Ni−P vs the Ni−S bond. The series of $NiCl_2$ complexes (**2**, **3** and **5**, **6**) of *N*-thioether-

dx.doi.org/10.1021/om500141k | Organometallics XXXX, XXX, XXX−XXX

functionalized DPPA-type ligands (**1**, **1·S** and **4**, **4·S**) was applied to the catalytic oligomerization of ethylene. Using $AlEtCl_2$ as cocatalyst, mostly ethylene dimers were produced, with significant amounts of trimers (selectivity in the range 11−36%). Productivities up to 40400 and 48200 g of C_2H_4/((g of Ni) h), with corresponding TOF values of 84800 and 101100 mol of C_2H_4/((mol of Ni) h), were obtained with precatalysts **2** and **3**, respectively. It was clearly shown that both factors, (i) the chelate ring size formed upon coordination of the *P*,*P* and the *P*,P=*S* ligands to the Ni(II) center and (ii) the nature of the *N*-substituent, by comparison of the *N*-alkyl thioether and *N*-aryl thioether species, are important molecular characteristics, at constant cocatalyst, that should be considered in the development of active and selective (pre)catalysts for ethylene oligomerization. However, there is currently no clear explanation for the different catalytic performances as a function of the P,P or P,S donors and associated change in chelate ring size, of the *N*-substituent, and of the excess of cocatalyst used. It would be interesting in future work to examine to what extent interactions between the S atom of the *N*-substituent and the cocatalyst has an impact on its properties and also, perhaps, by bringing it closer to the nickel center.

EXPERIMENTAL SECTION

General Procedures. All operations were carried out using standard Schlenk techniques under an inert atmosphere. Solvents were purified and dried under nitrogen by conventional methods. CD_2Cl_2 and $CDCl_3$ were dried over 4 Å molecular sieves, degassed by freeze−pump−thaw cycles, and stored under argon. NMR spectra were recorded at room temperature on a Bruker AVANCE 300 spectrometer (^1H, 300 MHz; ^{13}C, 75.47 MHz; ^{31}P, 121.49 MHz) and referenced using the residual proton solvent (^1H) or solvent (^{13}C) resonance. Chemical shifts (δ) are given in ppm. IR spectra were recorded in the region 4000−100 cm^{-1} on a Nicolet 6700 FT-IR spectrometer (ATR mode, SMART ORBIT accessory, Diamond crystal). Elemental analyses were performed by the "Service de microanalyses", Université de Strasbourg. Electrospray mass spectra (ESI-MS) were recorded on a microTOF (Bruker Daltonics, Bremen, Germany) instrument using nitrogen as drying agent and nebulizing gas. Gas chromatographic analyses were performed on a Thermoquest GC8000 Top series gas chromatograph using a HP Pona column (50 m, 0.2 mm diameter, 0.5 μm film thickness). The complexes $[NiCl_2(DME)]$,[33] $[Ni(NCMe)_6](BF_4)_2$,[34] $[PdCl_2(COD)]$,[35] **2**,[15] and **3**[15] were prepared according to literature methods. All other reagents were used as received from commercial suppliers. All iteration-fitting calculations and simulations of the $^{31}P\{^1H\}$ NMR spectra were performed by using the Bruker WIN-DAISY program.[36]

Synthesis of the Ligands. *Ligand* ***4***. An excess of chlorodiphenylphosphine (6.342 g, 28.73 mmol) was added dropwise to a solution of 4-(methylthio)aniline (2.000 g, 14.37 mmol) and triethylamine (3.631 g, 35.91 mmol) in 150 mL of THF under an inert atmosphere. The reaction mixture was stirred for 3 h. After filtration, the volatiles were removed under reduced pressure and the residue was washed twice with pentane to give **4** as a colorless solid. Yield: 5.178 g, 71%. Anal. Calcd for $C_{31}H_{27}NP_2S$ (507.57): C, 73.36; H, 5.36; N, 2.76. Found: C, 72.98; H, 5.48; N, 2.51. FTIR: ν_{max}(solid)/cm^{-1} 3050 w, 3022 vw, 2983 vw, 2922 vw, 1489 m, 1477 m, 1432 s, 1398 w, 1327 vw, 1308 w, 1266 vw, 1217 m, 1174 m, 1110 w, 1093 ms, 1070 w, 1024 w, 1012 w, 996 w, 974 w, 954 w, 941 w, 916 w, 886 vs, 807 m, 741 vs, 707 vw, 691 vs. ^1H NMR (CD_2Cl_2, 300 MHz): δ 7.40−7.27 (m, 20H, Ar), 6.84 (AA′ part of a AA′BB′ spin system, d, 2H, $^3J_{H,H}$ = 8.6 Hz, $N(C_6H_4)S$, $H_{meta/N}$), 6.56 (BB′ part of a AA′BB′ spin system d, 2H, $^3J_{H,H}$ = 8.6 Hz, $N(C_6H_4)S$, $H_{ortho/N}$), 2.35 (s, 3H, SCH_3) ppm. $^{13}C\{^1H\}$ NMR (CD_2Cl_2, 75.5 MHz): δ 145.00 (t, $^2J_{C,P}$ = 2.1 Hz, $N(C_6H_4)S$, $C_{ipso/N}$), 139.54 (virtual t, $^{1+3}J_{C,P}$ = 13.6 Hz, Ar, C_{ipso}), 135.50 (t, $^5J_{C,P}$ = 0.9 Hz, $N(C_6H_4)S$, $C_{ipso/S}$), 133.65 (virtual t, $^{2+4}J_{C,P}$ = 23.1 Hz, Ar, C_{ortho}), 129.94 (t, $^3J_{C,P}$ = 3.0 Hz, $N(C_6H_4)S$, $C_{ortho/N}$), 129.52 (s, Ar, C_{para}), 128.46 (virtual t, $^{3+5}J_{C,P}$ = 6.5 Hz, Ar, C_{meta}), 126.77 (s, $N(C_6H_4)S$, $C_{meta/N}$), 16.34 (s, SCH_3) ppm. $^{31}P\{^1H\}$ NMR ($CDCl_3$, 121.5 MHz): δ 69.36 (s) ppm.

Ligand ***4·S₂***. To a solution of **4** (0.300 g, 0.59 mmol) in 15 mL of toluene was added elemental sulfur (0.038 g, 1.18 mmol). The solution was heated to 115 °C for 3 h. After the mixture was cooled to room temperature, pentane was added to the solution and a microcrystalline white powder of **4·S₂** precipitated. Colorless crystals suitable for single-crystal X-ray diffraction were grown from a toluene/pentane mixture. Yield: 0.300 g, 89%. Anal. Calcd for $C_{31}H_{27}NP_2S_3$ (571.70): C, 65.13; H, 4.76; N, 2.45. Found: C, 65.18; H, 4.90; N, 2.36. FTIR: ν_{max}(solid)/cm^{-1} 3053 w, 2923 vw, 2858 vw, 2827 vw, 2682 vw, 2581 vw, 2364 w, 2344 w, 2324 w, 1586 w, 1560 w, 1491 m, 1480 m, 1437 s, 1405 w, 1308 mw, 1197 m, 1178 m, 1094 s, 1018 w, 999 w, 968 w, 953 s, 916 s, 880 s, 816 m, 746 w, 732 w, 715 vs, 697 vs, 686 vs, 645 vs, 631 w, 613 m. ^1H NMR ($CDCl_3$, 300 MHz): δ 8.07−8.03 (m, 8H, Ar), 7.54 (AA′ part of a AA′BB′ spin system, 2H, $^3J_{H,H}$ = 8.4 Hz, $N(C_6H_4)S$, $H_{meta/N}$), 7.28−7.25 (m, 4H, Ar), 7.20−7.17 (m, 8H, Ar), 6.71 (BB′ part of a AA′BB′ spin system, 2H, $^3J_{H,H}$ = 8.4 Hz, $N(C_6H_4)S$, $H_{ortho/N}$), 2.23 (s, 3H, SCH_3) ppm. $^{13}C\{^1H\}$ NMR ($CDCl_3$, 75.5 MHz): δ 137.59 (t, $^2J_{C,P}$ = 2.0 Hz, $N(C_6H_4)S$, $C_{ipso/N}$), 135.83 (s, $N(C_6H_4)S$, $C_{ipso/S}$), 133.61−133.48 (five-line multiplet of a simulated AXX′ spin system, $^{2+4}J_{C,P}$ = 11.1 Hz ($^4J_{AX'} \approx 0$ Hz), Ar, C_{ortho}), 132.73 (t, $^3J_{C,P}$ = 3.0 Hz, $N(C_6H_4)S$, $C_{ortho/N}$), 131.61 (d, $^1J_{C,P}$ = 101.5 Hz, Ar, C_{ipso}), 131.46 (virtual t, $^{4+6}J_{C,P}$ = 1.2 Hz, Ar, C_{para}), 127.69−127.53 (five line multiplet of a simulated AXX′ spin system, $^{3+5}J_{C,P}$ = 13.9 Hz ($^5J_{AX'} \approx 0$ Hz), Ar, C_{meta}), 125.59 (t, $^4J_{C,P}$ = 1.5 Hz, $N(C_6H_4)S$, $C_{meta/N}$), 15.54 (s, SCH_3) ppm. $^{31}P\{^1H\}$ NMR ($CDCl_3$, 121.5 MHz): δ 69.03 (s) ppm.

Ligand ***4·S***. To a solution of **4** (0.220 g, 0.43 mmol) in 15 mL of CH_2Cl_2 was added elemental sulfur (0.021 g, 0.65 mmol). The solution was stirred at room temperature for 30 min. Evaporation of the volatiles led to the formation of a pale yellow oil that was dissolved in 10 mL of toluene. Addition of pentane to this solution led to the precipitation of a white crystalline powder of **4·S₂**. After filtration and evaporation of the volatiles, a colorless oil was obtained. Its examination by $^{31}P\{^1H\}$ NMR spectroscopy revealed the presence of **4·S** (ca. 70%) and **4·S₂** (ca. 30%). We could not isolate pure **4·S**, and in the subsequent complexation reactions, **4·S** was thus prepared in situ. Purification of the complexes with **4·S** and **4·S₂** was readily achieved (see below). ^1H NMR (CD_2Cl_2, 300 MHz): δ 8.11−8.05 (m, 4H, Ar), 8.02−7.05 (m, 4H, Ar), 7.43−7.31 (m, 12H, Ar), 6.68 (AA′ part of a AA′BB′ spin system, d, 2H, $^3J_{H,H}$ = 8.6 Hz, $N(C_6H_4)S$, $H_{meta/N}$), 6.59 (BB′ part of a AA′BB′ spin system, d, 2H, $^3J_{H,H}$ = 8.6 Hz, $N(C_6H_4)S$, $H_{ortho/N}$), 2.27 (s, 3H, S-CH_3) ppm. $^{31}P\{^1H\}$ NMR ($CDCl_3$, 121.5 MHz): δ 72.38 (d, $^2J_{P,P}$ = 104.5 Hz, P^V), 55.34 (d, $^2J_{P,P}$ = 104.5 Hz, P^{III}) ppm.

Synthesis of the Ni(II) Complexes. *Complex* ***5***. To a suspension of $[NiCl_2(DME)]$ (0.130 g, 0.59 mmol) in CH_2Cl_2 (10 mL) was added a solution of **4** (0.300 g, 0.59 mmol) in CH_2Cl_2 (20 mL). The solution quickly turned orange-red and was stirred at room temperature for 4 h. The solvent was removed under reduced pressure, and the red solid obtained was washed with pentane. Red crystals suitable for single-crystal X-ray diffraction were grown from a CH_2Cl_2/pentane mixture. Yield: 0.312 g, 83%. Anal. Calcd for $C_{31}H_{27}Cl_2NNiP_2S$ (637.16): C, 58.44; H, 4.27; N, 2.20. Found: C, 58.48; H, 4.19; N, 2.31. FTIR: ν_{max}(solid)/cm^{-1} 3053 w, 2919 w, 1589 m, 1492 ms, 1480 m, 1433s, 1332 vw, 1309 w, 1255 vs, 1182 w, 1162 vw, 1105 vs, 1096 vs, 1023 vw, 1007 vw, 997 w, 951 s, 907 vs, 852 vw, 824 m, 749 w, 736 s, 720 w, 694 vw, 686 vs, 562 w, 548 s, 508 m, 495 m, 483 vs, 448 vw, 439 vw, 415 w, 343 w, 326 vs, 269 w, 236 w, 214 w, 172 vw, 157 vw, 142 w. ^1H NMR (CD_2Cl_2, 300 MHz): δ 8.01 (q, 8H, $^3J_{H,H}$ = 7.0 Hz, H_{meta} of Ar), 7.71 (t, 4H, $^3J_{H,H}$ = 7.0 Hz, H_{para} of Ar), 7.57 (t, 8H, $^3J_{H,H}$ = 7.0 Hz, H_{ortho} of Ar), 6.84 (AA′ part of a AA′BB′ spin system, 2H, $^3J_{H,H}$ = 8.4 Hz, $N(C_6H_4)S$, $H_{meta/N}$), 6.38 (BB′ part of a AA′BB′ spin system, 2H, $^3J_{H,H}$ = 8.4 Hz, $N(C_6H_4)S$, $H_{ortho/N}$), 2.32 (s, 3H, SCH_3) ppm. $^{13}C\{^1H\}$ NMR (CD_2Cl_2, 75.5 MHz): δ 137.59 (s, $N(C_6H_4)S$, $C_{ipso/S}$), 136.17 (t, $^2J_{C,P}$ = 5.6 Hz $N(C_6H_4)S$, $C_{ipso/N}$), 133.66 (virtual t, $^{2+4}J_{C,P}$ = 11.2 Hz, C_{ortho}, Ar), 133.24 (virtual t, $^{4+6}J_{C,P}$ = 1.5 Hz, C_{para}, Ar), 129.28 (virtual t, $^{3+5}J_{C,P}$ = 11.9 Hz, C_{meta}, Ar),

dx.doi.org/10.1021/om500141k | *Organometallics* XXXX, XXX, XXX−XXX

126.80 (virtual t, $^{1+3}J_{C,P}$ = 50.8 Hz, C_{ipso}, Ar), 126.63 (s, $N(C_6H_4)S$, $C_{meta/N}$), 124.55 (t, $^{3}J_{C,P}$ = 3.4 Hz, $N(C_6H_4)S$, $C_{ortho/N}$), 15.15 (s, SCH_3) ppm. $^{31}P\{^{1}H\}$ NMR (CD_2Cl_2, 121.5 MHz): δ 45.38 (s) ppm. MS (ESI): m/z 600.00 $[M - Cl]^+$.

Complex **6**. To a solution of **4** (0.300 g, 0.59 mmol) in CH_2Cl_2 (20 mL) was added elemental sulfur (0.028 g, 0.88 mmol). The solution was stirred at room temperature for 30 min and then added to a suspension of $[NiCl_2(DME)]$ (0.065 g, 0.29 mmol) in CH_2Cl_2 (20 mL). The mixture quickly turned bright purple and was stirred at room temperature for 4 h. After filtration, the solvent was removed under reduced pressure and the bright purple solid was washed with toluene. Purple single crystals suitable for X-ray diffraction were grown by slow evaporation of an acetone/pentane mixture. Yield (based on **4·S** formed in situ and estimated by ^{31}P NMR): 0.132 g, 82%. Anal. Calcd for $C_{28}H_{29}Cl_2NNiP_2S_2$·(acetone) (727.31): C, 55.31; H, 4.65; N, 1.95. Found: C, 54.96; H, 4.54; N, 1.88. FTIR: ν_{max}(solid)/cm^{-1} 3057 w, 2921 w, 2682 w, 2584 w, 1706 s, 1583 w, 1560 w, 1483 s, 1432 vs, 1400 vw, 1359 m, 1309 w, 1222 w, 1201 s, 1179 m, 1161 w, 1098 vs, 1010 w, 998 w, 973 s, 937 m, 918 w, 897 vs, 745 m, 731 w, 709 w, 688 vs, 646 m, 557w , 524 s, 513 vs, 489 w, 480 w, 455 vw, 440 w, 415 vw, 393 vw, 382 m, 339 s, 315 w, 309 m, 291 m, 271 w, 233 w, 210 vw, 179 m, 150 s, 139 vw, 134 vw, 121 vw, 108 w. $^{31}P\{^{1}H\}$ NMR ($CDCl_3$, 121.5 MHz): δ 83.81 (br s, see text). MS (ESI): m/z 632.01 $[M - Cl]^+$, 1298.99 $[Ni(\mathbf{4{\cdot}S})_2][NiCl_3]^+$.

Complex **7**. To a solution of **4** (0.200 g, 0.40 mmol) in CH_2Cl_2 (20 mL) was added elemental sulfur (0.019 g, 0.60 mmol). The solution was stirred at room temperature for 30 min and then added to a suspension of $[Ni(NCMe)_6](BF_4)_2$ (0.039 g, 0.10 mmol) in CH_2Cl_2 (20 mL). The mixture quickly turned yellow-orange, and stirring at room temperature was maintained for 4 h. After filtration, the solvent was removed under reduced pressure and the orange solid was washed with toluene. Red crystals suitable for single-crystal X-ray diffraction were grown from a CH_2Cl_2/pentane mixture. Yield (based on **4·S** formed in situ and estimated by ^{31}P NMR): 0.105 g, 85%. Anal. Calcd for $C_{62}H_{54}N_2NiP_4S_4BF_4$ (1131.56): C, 56.78; H, 4.15; N, 2.13. Found: C, 56.64; H, 4.24; N, 2.00. FTIR: ν_{max}(solid)/cm^{-1} 3048 vw, 2920 vw, 2679 vw, 1583 w, 1480 m, 1437 s, 1400 vw, 1318 w, 1286 vw, 1202 m, 1095 m, 1048 vs, 1037 w, 1024 vw, 996 w, 960 w, 933 w, 925 w, 890 m, 812 vw, 756 w, 744 w, 733 m, 705 w, 689 s, 634 w, 620 m, 598 s, 558 w, 521 s, 509 s, 493 s, 458 m, 432 w, 395 w, 382 m, 364 m, 353 vw, 320 w, 255 w, 235 w, 221 w, 194 m, 179 m, 140 vw, 125 w, 117 vw, 106 vs. ^{1}H NMR ($CDCl_3$, 300 MHz): δ 7.72−7.56 (m, 40H, Ar), 6.64 (AA′ part of a AA′BB′ spin system, 4H, $^{3}J_{H,H}$ = 8.6 Hz, $N(C_6H_4)S$, $H_{meta/N}$), 6.06 (BB′ part of a AA′BB′ spin system, 4H, $^{3}J_{H,H}$ = 8.6 Hz, $N(C_6H_4)S$, $H_{ortho/N}$), 2.26 (s, 6H, SCH_3) ppm. $^{13}C\{^{1}H\}$ NMR ($CDCl_3$, 75.5 MHz): δ 142.10 (s, $N(C_6H_4)S$, $C_{ipso/S}$), 135.64 (d, $^{4}J_{C,P}$ = 2.6 Hz, C_{para}, Ar−P^{V}), 134.29 (s, C_{para}, Ar−P^{III}), 134.00 (virtual t, $^{2+4+5}J_{C,P}$ = 13.0 Hz, C_{ortho} of Ar−P^{III}), 133.03 (d, $^{2}J_{C,P}$ = 11.6 Hz, C_{ortho}, Ar−P^{V}), 131.53 (s, $N(C_6H_4)S$, $C_{ortho/N}$), 130.31−130.20 (m, C_{meta}, Ar−P^{III} + Ar−P^{V}), 129.96 (t, $^{2}J_{C,P}$ = 2.1 Hz, $C_{ipso/N}$), 125.86 (s, $N(C_6H_4)S$, $C_{meta/N}$), 124.53 (virtual t, $^{1+3+4}J_{C,P}$ = 56.7 Hz, C_{ipso}, Ar−P^{III}), 125.35 (d, $^{1}J_{C,P}$ = 96.3 Hz, C_{ipso}, Ar−P^{V}), 14.73 (s, SCH_3) ppm. $^{31}P\{^{1}H\}$ NMR (CD_2Cl_2, 121.5 MHz): δ two triplets of a AA′BB′ spin system (Scheme 5): δ_A 105.80 ppm, δ_B 84.61 ppm; spectroscopic simulations afforded the coupling constants $^{2+3}J(P_AP_B)$ = $^{2+3}J(P_{A'}P_{B'})$ = 77.30 Hz, $^{3}J(P_AP_{B'})$ = 66.34 Hz, $^{4}J(P_AP_{A'})$ = 76.44 Hz, $^{2}J(P_BP_{B'})$ = 76.39 Hz. MS (ESI): m/z 568.07 $[M]^{2+}$.

General Procedure for the Catalytic Ethylene Oligomerization Reaction. All catalytic reactions were carried out in a magnetically stirred (900 rpm) 145 mL stainless steel autoclave. A 125 mL glass container was used to protect the inner walls of the autoclave from corrosion. All catalytic tests were started at 30 °C, and no cooling of the reactor was done during the reaction. After injection of the catalytic solution and of the cocatalyst under a constant low flow of ethylene, the reactor was pressurized to 10 bar. A temperature increase was observed which resulted solely from the exothermicity of the reaction. The 10 bar working pressure was maintained during the experiments through a continuous feed of ethylene from a reserve bottle placed on a balance to allow continuous monitoring of the ethylene uptake. The oligomerization products and remaining ethylene were only collected from the reactor at the end of the catalytic experiment. At the end of each test (35 min) a dry ice bath, and in the more exothermic cases also liquid N_2, was used to rapidly cool the reactor, thus stopping the reaction. When the inner temperature reached 0 °C, the ice bath was removed, allowing the temperature to slowly rise to 10 °C. The gaseous phase was then transferred into a 10 L polyethylene tank filled with water. An aliquot of this gaseous phase was transferred into a Schlenk flask, previously evacuated, for GC analysis. The products in the reactor were hydrolyzed in situ by the addition of ethanol (1 mL), transferred into a Schlenk flask, and separated from the metal complexes by trap-to-trap evaporation (20 °C, 0.3 mmHg) into a second Schlenk flask previously immersed in liquid nitrogen in order to avoid any loss of product. For GC analyses, 1-heptene was used as an internal reference. $AlEtCl_2$ was used as a cocatalyst and, depending on the amount used (3, 10, or 40 equiv), the required quantity of Ni(II) complex was dissolved in 13.5 (3 equiv of EADC) or 10 mL (10 and 40 equiv of EADC) of chlorobenzene, and this solution was injected into the reactor. The cocatalyst solution, 1.5 or 5 mL corresponding to 3 or 10 and 40 equiv, respectively, was then added. Therefore, the total volume of the solution inside the reactor was 15 mL.

Scheme 5. Spin System Used for the Assignment of the $^{31}P\{^{1}H\}$ NMR Resonances of Complex 7

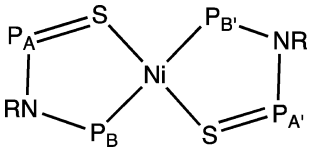

■ ASSOCIATED CONTENT

Supporting Information

Tables giving X-ray data collection, structure solution, and structure refinement details for compounds **4**, **4**·S_2, **5**·$2CH_2Cl_2$, and **6**·C_3H_6O (Table S1) and for compounds **7**·$4CH_2Cl_2$, **8**·CH_2Cl_2 and **9** (Table S2) and CIF files giving crystallographic data for all seven compounds, and text, tables, and figures giving structural comparisons between ligand **4** and three *p*-phenyl-functionalized DPPA-type ligands, the $^{31}P\{^{1}H\}$ NMR spectra of complex **7** and their evolution after addition of NEt_3·HCl (1 and 2 equiv), and computational details. This material is available free of charge via the Internet at http://pubs.acs.org. CIF files of these compounds have also been deposited with the CCDC, 12 Union Road, Cambridge CB2 1EZ, U.K., and can be obtained on request free of charge, by quoting the publication citation and deposition numbers 873232 and 985336−985341.

■ AUTHOR INFORMATION

Corresponding Authors

*C.F.: e-mail, christophe.fliedel@fct.unl.pt; fax, +351 212 948 550.

*P.B.: e-mail, braunstein@unistra.fr; fax, +33 368 851 322.

Present Addresses

†REQUIMTE, Departamento de Quimica, Faculdade de Ciências e Tecnologia, Universidade Nova de Lisboa, Caparica 2829-516, Portugal.

‡Institut für Anorganische Chemie, RWTH Aachen University, Landoltweg 1, 52074 Aachen, Germany

Notes

The authors declare no competing financial interest.

■ ACKNOWLEDGMENTS

We are grateful to the CNRS, the Ministère de la Recherche (Paris), the DFH/UFA (International Research Training Group 532-GRK532, Ph.D. grants to C.F. and A.G.), and the *Fundação para a Ciência e Tecnologia* (FCT) (fellowships SFRH/BPD/73253/2010 to C.F. and SFRH/BPD/44262/2008 to V.R.) for funding. We thank Drs. Roberto Pattacini and Pierre de Frémont and the Service de Radiocrystallographie, Institut de Chimie (UMR 7177 CNRS-UdS), for performing the X-ray diffraction studies, the UdS High-Performance Computing Center and the Laboratoire de Chimie Quantique (UdS) for the provision of computational facilities, and Marc Mermillon-Fournier and Mélanie Boucher for providing technical assistance.

■ REFERENCES

(1) For selected reviews see e.g.: (a) Hierso, J.-C.; Amardeil, R.; Bentabet, E.; Broussier, R.; Gautheron, B.; Meunier, P.; Kalck, P. *Coord. Chem. Rev.* **2003**, *236*, 143. (b) Appleby, T.; Woollins, J. D. *Coord. Chem. Rev.* **2002**, *235*, 121 and references therein. (c) Bhattacharyya, P.; Woollins, J. D. *Polyhedron* **1995**, *14*, 3367 and references therein. Other specific examples are cited in the manuscript.

(2) (a) Rosa, V.; Fliedel, C.; Ghisolfi, A.; Pattacini, R.; Avilés, T.; Braunstein, P. *Dalton Trans.* **2013**, *42*, 12109. (b) Fliedel, C.; Pattacini, R.; Braunstein, P. *J. Cluster Sci.* **2010**, *21*, 397. (c) Ganesamoorthy, C.; Balakrishna, M. S.; Mague, J. T. *Inorg. Chem.* **2009**, *48*, 3768. (d) Rodriguez-Zubiri, M.; Gallo, V.; Rosé, J.; Welter, R.; Braunstein, P. *Chem. Commun.* **2008**, 64. (e) Gallo, V.; Mastrorilli, P.; Nobile, C. F.; Braunstein, P.; Englert, U. *Dalton Trans.* **2006**, 2342.

(3) (a) Posset, T.; Rominger, F.; Blümel, J. *Chem. Mater.* **2005**, *17*, 586. (b) Schweyer-Tihay, F.; Braunstein, P.; Estournès, C.; Guille, J. L.; Lebeau, B.; Paillaud, J.-L.; Richard-Plouet, M.; Rosé, J. *Chem. Mater.* **2003**, *15*, 57. (c) Braunstein, P.; Kormann, H.-P.; Meyer-Zaika, W.; Pugin, R.; Schmid, G. *Chem. Eur. J.* **2000**, *6*, 4637.

(4) Fliedel, C.; Faramarzi, V.; Rosa, V.; Doudin, B.; Braunstein, P. *Chem. Eur. J.* **2014**, *20*, 1263.

(5) For recent examples see e.g.: (a) Aydemir, M.; Baysal, A.; Sahin, E.; Gümgüm, B.; Özkar, S. *Inorg. Chim. Acta* **2011**, *378*, 10. (b) Ganesamoorthy, C.; Balakrishna, M. S.; Mague, J. T. *J. Organomet. Chem.* **2009**, *694*, 3390. (c) Ganesamoorthy, C.; Balakrishna, M. S.; Mague, J. T.; Tuononen, H. M. *Inorg. Chem.* **2008**, *47*, 7035. (d) Paolillo, R.; Gallo, V.; Mastrorilli, P.; Nobile, C. F.; Rosé, J.; Braunstein, P. *Organometallics* **2008**, *27*, 741. (e) Gümgüm, B.; Biricik, N.; Durap, F.; Özdemir, I.; Gürbüz, N.; Ang, W. H.; Dyson, P. J. *Appl. Organomet. Chem.* **2007**, *21*, 711. (f) Mandal, S. K.; Gowda, G. A. N.; Krishnamurthy, S. S.; Zheng, C.; Li, S.; Hosmane, N. S. *J. Organomet. Chem.* **2003**, *676*, 22. More examples are available in refs 21a−d and 23b−e.

(6) See e.g.: (a) McGuinness, D. S. *Chem. Rev.* **2011**, *111*, 2321 and references therein. (b) Agapie, T. *Coord. Chem. Rev.* **2011**, *255*, 861 and references therein. (c) Reddy Aluri, B.; Peulecke, N.; Peitz, S.; Spannenberg, A.; Müller, B. H.; Schulz, S.; Drexler, H.-J.; Heller, D.; Al-Hazmi, M. H.; Mosa, F. M.; Wöhl, A.; Müller, W.; Rosenthal, U. *Dalton Trans.* **2010**, *39*, 7911 (Cr and Ni complexes). (d) Dixon, J. T.; Green, M. J.; Hess, F. M.; Morgan, D. H. *J. Organomet. Chem.* **2004**, *689*, 3641 and references therein.

(7) See e.g.: (a) Schultz, M.; Eisenträger, F.; Regius, C.; Rominger, F.; Hanno-Igels, P.; Jakob, P.; Gruber, I.; Hofmann, P. *Organometallics* **2012**, *31*, 207. (b) Song, K.; Gao, H.; Liu, F.; Pan, J.; Guo, L.; Zai, S.; Wu, Q. *Eur. J. Inorg. Chem.* **2009**, 3016. (c) Lavanant, L.; Rodrigues, A.-S.; Kirillov, E.; Carpentier, J.-F.; Jordan, R. F. *Organometallics* **2008**, *27*, 2107. (d) Dennett, J. N. L.; Gillon, A. L.; Heslop, K.; Hyett, D. J.; Fleming, J. S.; Lloyd-Jones, C. E.; Orpen, A. G.; Pringle, P. G.; Wass, D. F.; Scutt, J. N.; Weatherhead, R. H. *Organometallics* **2004**, *23*, 6077. (e) Cooley, N. A.; Green, S. M.; Wass, D. F.; Heslop, K.; Orpen, A. G.; Pringle, P. G. *Organometallics* **2001**, *20*, 4769. (f) Wass, D. F. (BP Chemicals Ltd) WO01/10876, 2001. (g) Hofmann, P.; Perez-Moya, L. A.; Krause, M. E.; Kumberger, O.; Müller, G. *Z. Naturforsch., B* **1990**, *45b*, 897.

(8) (a) Dagorne, S.; Fliedel, C. *Top. Organomet. Chem.* **2013**, *41*, 125 and references therein. Specific examples of Ni/Al bimetallic complexes: (b) Azoulay, J. D.; Koretz, Z. A.; Wu, G.; Bazan, G. C. *Angew. Chem.* **2010**, *122*, 8062; *Angew. Chem., Int. Ed.* **2010**, *49*, 7890. (c) Weng, Z.; Teo, S.; Koh, L. L.; Hor, T. S. A. *Chem. Commun.* **2006**, 1319.

(9) Jabri, A.; Crewdson, P.; Gambarotta, S.; Korobkov, I.; Duchateau, R. *Organometallics* **2006**, *25*, 715.

(10) (a) Keim, W. *Angew. Chem., Int. Ed.* **1990**, *29*, 235 and references therein.. (b) Keim, W.; Behr, A.; Gruber, B.; Hoffmann, B.; Kowaldt, F. H.; Kürschner, U.; Limbäcker, B.; Sistig, F. P. *Organometallics* **1986**, *5*, 2356.

(11) (a) Svejda, S. A.; Brookhart, M. *Organometallics* **1999**, *18*, 65. (b) Killian, C. M.; Johnson, L. K.; Brookhart, M. *Organometallics* **1997**, *16*, 2005. (c) Johnson, L. K.; Killian, C. M.; Brookhart, M. *J. Am. Chem. Soc.* **1995**, *117*, 6414.

(12) Wang, C.; Friedrich, S.; Younkin, T. R.; Li, R. T.; Grubbs, R. H.; Bansleben, D. A.; Day, M. W. *Organometallics* **1998**, *17*, 3149.

(13) (a) Chavez, P.; Guerrero Rios, I.; Kermagoret, A.; Pattacini, R.; Meli, A.; Bianchini, C.; Giambastiani, G.; Braunstein, P. *Organometallics* **2009**, *28*, 1776. (b) Kermagoret, A.; Braunstein, P. *Organometallics* **2008**, *27*, 88. (c) Kermagoret, A.; Braunstein, P. *Dalton Trans.* **2008**, 822. (d) Braunstein, P.; Chauvin, Y.; Mercier, S.; Saussine, L. *C. R. Chim.* **2005**, *8*, 31. (e) Speiser, F.; Braunstein, P.; Saussine, L. *Acc. Chem. Res.* **2005**, *38*, 784 and references therein.

(14) (a) Braunstein, P. *J. Organomet. Chem.* **2004**, *689*, 3953. (b) Braunstein, P.; Naud, F. *Angew. Chem., Int. Ed.* **2001**, *40*, 680. (c) Slone, C. S.; Weinberger, D. A.; Mirkin, C. A. *Prog. Inorg. Chem.* **1999**, *48*, 233. (d) Zhang, W.-H.; Chien, S. W.; Hor, T. S. A. *Coord. Chem. Rev.* **2011**, *255*, 1991.

(15) Ghisolfi, A.; Fliedel, C.; Rosa, V.; Pattacini, R.; Thibon, A.; Monakhov, K. Yu.; Braunstein, P. *Chem Asian J.* **2013**, *8*, 1795.

(16) Zhang, S.; Pattacini, R.; Braunstein, P. In *Advances in Organometallic Chemistry and Catalyis: The Silver/Gold Jubilee International Conference on Organometallic Chemistry Celebratory Book*; Pombeiro, A. J. L., Ed.; Wiley: Hoboken, NJ, 2014.

(17) Kermagoret, A.; Pattacini, R.; Chavez Vasquez, P.; Rogez, G.; Welter, R.; Braunstein, P. *Angew. Chem.* **2007**, *119*, 6558; *Angew. Chem., Int. Ed.* **2007**, *46*, 6438.

(18) Flapper, J.; Kooijman, H.; Lutz, M.; Spek, A. L.; van Leeuwen, P. W. N. M.; Elsevier, C. J.; Kamer, P. C. J. *Organometallics* **2009**, *28*, 3272.

(19) O'Reilly, M.; Pattacini, R.; Braunstein, P. *Dalton Trans.* **2009**, 6092.

(20) See e.g. the synthesis of ligand **1**: Weng, Z.; Teo, S.; Hor, T. S. A. *Dalton Trans.* **2007**, 3493.

(21) (a) Kayan, C.; Biricik, N.; Aydemir, M.; Scopelliti, R. *Inorg. Chim. Acta* **2012**, *385*, 164. (b) Kayan, C.; Biricik, N.; Aydemir, M. *Transition Met. Chem.* **2011**, *36*, 513. (c) Biricik, N.; Kayan, C.; Gümgüm, B.; Fei, Z.; Scopelliti, R.; Dyson, P. J.; Gürbüz, N.; Özdemir, İ. *Inorg. Chim. Acta* **2010**, *363*, 1039. (d) Durap, F.; Baysal, A.; Akba, O.; Gümgüm, B.; Özkar, S.; Yıldırım, L. T. *Polyhedron* **2009**, *28*, 2313. (e) Biricik, N.; Durap, F.; Kayan, C.; Gümgüm, B. *Heteroat. Chem.* **2007**, *6*, 613. (f) Biricik, N.; Fei, Z.; Scopelliti, R.; Dyson, P. J. *Helv. Chim. Acta* **2003**, *86*, 3281. (g) Gaw, K. G.; Smith, M. B.; Slawin, A. M. Z. *New J. Chem.* **2000**, *24*, 429. (h) Balakrishna, M. S.; Klein, R.; Uhlenbrock, S.; Pinkerton, A. A.; Cavell, R. G. *Inorg. Chem.* **1993**, *32*, 5676. (i) Seidel, W.; Alexiev, M. *Z. Anorg. Allg. Chem.* **1978**, *438*, 68.

(22) (a) Venkatakrishnan, T. S.; Krishnamurthy, S. S.; Nethaji, M. *J. Organomet. Chem.* **2005**, *690*, 4001. (b) Raghuraman, K.; Krishnamurthy, S. S.; Nethaji, M. *J. Organomet. Chem.* **2003**, *669*, 79. (c) Faller, J. W.; Lloret-Fillol, J.; Parr, J. *New J. Chem.* **2002**, *26*, 883. (d) Simón-Manso, E.; Valderrama, M.; Gantzel, P.; Kubiak, P. K. *J. Organomet. Chem.* **2002**, *651*, 90. (e) Slawin, A. M. Z.; Woollins, J. D.; Zhang, Q. *Dalton Trans.* **2001**, 621. (f) Balakrishna, M. S.; Panda, R.; Smith, D. C., Jr.; Klaman, A.; Nolan, S. P. *J. Organomet. Chem.*

2000, *599*, 159. (g) Babu, R. P. K.; Aparna, Z.; Krishnamurthy, S. S.; Nethaji, M. *Phosphorus, Sulfur Silicon Relat. Elem.* **1995**, *103*, 39.
(23) (a) Al-Masri, H. T. *Synth. React. Inorg., Met.-Org., Nano-Met. Chem.* **2013**, *43*, 102. (b) Aydemir, M.; Baysal, A.; Özkar, S.; Yıldırım, L. T. *Polyhedron* **2011**, *30*, 796. (c) Akba, O.; Durap, F.; Aydemir, M.; Baysal, A.; Gümgüm, B.; Özkar, S. *J. Organomet. Chem.* **2009**, *694*, 731. (d) Biricik, N.; Durap, F.; Kayan, C.; Gümgüm, B.; Gürbüz, N.; Özdemir, İ.; Ang, W. H.; Fei, Z.; Scopelliti, R. *J. Organomet. Chem.* **2008**, *693*, 2693. (e) Aydemir, M.; Baysal, A.; Gümgüm, B. *J. Organomet. Chem.* **2008**, *693*, 3810. (f) Durap, F.; Biricik, N.; Gümgüm, B.; Özkar, S.; Ang, W. H.; Fei, Z.; Scopelliti, R. *Polyhedron* **2008**, *27*, 196. (g) Biricik, N.; Durap, F.; Gümgüm, B.; Fei, Z.; Scopelliti, R. *Transition Met. Chem.* **2007**, *32*, 877.
(24) Fei, Z.; Scopelliti, R.; Dyson, P. J. *Dalton Trans.* **2003**, 2772.
(25) Naik, S.; Mague, J. T.; Balakrishna, M. S. *Inorg. Chim. Acta* **2013**, *407*, 139.
(26) Ajibade, P. A.; Onwudiwe, D. C.; Omondi, B. *Acta Crystallogr.* **2012**, *E68*, o3491.
(27) For a discussion about the effective Tolman-based *N*-substituent steric parameter ($\theta_{N\text{-}sub}$) for the PNP ligands, see: Cloete, N.; Visser, H. G.; Engelbrecht, I.; Overett, M. J.; Gabrielli, W. F.; Roodt, A. *Inorg. Chem.* **2013**, *52*, 2268.
(28) See e.g.: (a) Li, C.; Pattacini, R.; Braunstein, P. *Inorg. Chim. Acta* **2010**, *363*, 4337. (b) Hamada, A.; Braunstein, P. *Inorg. Chem.* **2009**, *48*, 1624.
(29) (a) Stamatopoulos, I.; Placek, M.; Psycharis, V.; Terzis, A.; Svoboda, J.; Kyritsis, P.; Vohlidal, J. *Inorg. Chim. Acta* **2012**, *387*, 390. (b) Vougioukalakis, G. C.; Stamatopoulos, I.; Petzetakis, N.; Raptopoulou, C. P.; Psycharis, V.; Terzis, A.; Kyritsis, P.; Pitsikalis, M.; Hadjichristidis, N. *J. Polym. Sci., Part A: Polym. Chem.* **2009**, *47*, 5241. (c) Sun, Z.; Zhu, F.; Wu, Q.; Lin, S.-a. *Appl. Organomet. Chem.* **2006**, *20*, 175. (d) Sushev, V. V.; Kornev, A. N.; Kurskii, Y. A.; Kuznetsova, O. V.; Fukin, G. K.; Budnikova, Y. H.; Abakumov, G. A. *J. Organomet. Chem.* **2005**, *690*, 1814. (e) Browning, C. S.; Burrow, R. A.; Farrar, D. H.; Mirza, H. A. *Inorg. Chim. Acta* **1998**, *271*, 112.
(30) (a) Yin, B.-S.; Li, T.-B.; Yang, M.-S. *Acta Crystallogr., Sect. E* **2011**, *67*, m1571. (b) Yin, B.-S.; Li, T.-B.; Yang, M.-S. *Acta Crystallogr., Sect. E* **2011**, *67*, m1572.
(31) Levesanos, N.; Stamatopoulos, I.; Raptopoulou, C. P.; Psycharis, V.; Kyritsis, P. *Polyhedron* **2009**, *28*, 3305.
(32) (a) Yang, Q.-Z.; Kermagoret, A.; Agostinho, M.; Siri, O.; Braunstein, P. *Organometallics* **2006**, *25*, 5518. (b) Heinicke, J.; Köhler, M.; Peulecke, N.; Kindermann, M. K.; Keim, W.; Köckerling, M. *Organometallics* **2005**, *24*, 344. (c) Rieger, B.; Baugh, L. S.; Kacker, S.; Striegler, S. *Late Transition Metal Polymerization Catalysis*; Wiley-VCH: Weinheim, Germany, 2003; p 331.
(33) Errington, R. J. *Advanced Practical Inorganic and Metalorganic Chemistry*; CRC Press: Boca Raton, FL, 1997; p 246.
(34) Coucouvanis, D. Useful Reagents and Ligands. In *Inorganic Syntheses*; Wiley: New York, 2002; Vol. 33, Chapter 2, p 78.
(35) Drew, D.; Doyle, J. R. *Inorg. Synth.* **1972**, *13*, 47.
(36) Hägele, G. *WIN-DAISY 3.0*; Heinrich-Heine-University Düsseldorf, Dusseldorf, Germany, 1993−1995.

CHAPITRE 5

Ce chapitre est présenté sous forme d'une publication à paraître dans *Inorg. Chem*.

Les contributions respectives des auteurs sont:

A. Ghisolfi, L. Routaboul, P. Braunstein – *développement du projet*

A. Ghisolfi, A. Waldvogel – *Synthèse et caractérisation du ligand et des complexes*

Reversible Switching of the Coordination Modes of a Pyridine-Functionalized Quinonoid Zwitterion ; Its Di- and Tetranuclear Palladium Complexes

Alessio Ghisolfi,[a] Audrey Waldvogel,[a] Lucie Routaboul,[a] Pierre Braunstein[a]*

[a]Laboratoire de Chimie de Coordination, Institut de Chimie (UMR 7177 CNRS), Université de Strasbourg, 4 rue Blaise Pascal, 67081 Strasbourg Cedex, France

Des informations complémentaires sont disponibles sur internet:

http://pubs.acs.org/doi/suppl/10.1021/ic500194y/suppl_file/ic500194y_si_001.pdf

Resumé du Chapitre 5

Nous avons étudié dans ce travail la chimie de coordination d'un nouveau ligand quinonoïde zwitterionique polyfonctionnel, potentiellement hexadentate N_2, O_2, N_{Py}, N_{Py}, ~~bis(2-(pyridin-2-yl)ethyl) N-substitué~~ donner le nom complet (**H_2L**). Cette étude nous a permis d'isoler plusieurs complexes de Pd dans lesquels le ligand agit comme bidentate, tetradentate ou hexadentate. En particulier, nous avons montré comment les interactions entre ce ligand multidentate et le Pd(II) pouvaient être finement réglées en changent les condition expérimentales pour conduire, de manière inattendue, à la migration réversible du centre métallique accompagnée d'un échange de sites donneurs du ligand. En raison de la facilité avec laquelle la sphère de coordination des centres métalliques peut être modifiée, ces observations peuvent être pertinentes pour l'étude de transformations se produisant *in situ* pendant des réactions de couplage catalysées par le Pd ainsi que pour la fonctionnalisation de surfaces.

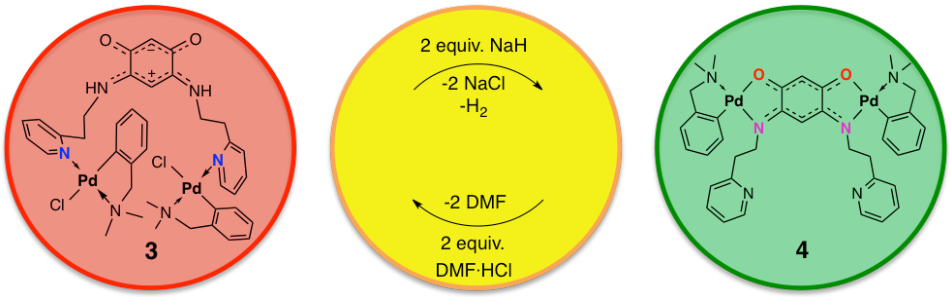

Inorganic Chemistry

Article

pubs.acs.org/IC

Reversible Switching of the Coordination Modes of a Pyridine-Functionalized Quinonoid Zwitterion; Its Di- and Tetranuclear Palladium Complexes†

Alessio Ghisolfi, Audrey Waldvogel, Lucie Routaboul, and Pierre Braunstein*

Laboratoire de Chimie de Coordination, Institut de Chimie (UMR 7177 CNRS), Université de Strasbourg, 4 rue Blaise Pascal, F-67081 Strasbourg Cedex, France

Supporting Information

ABSTRACT: The coordination chemistry of a new functional quinonoid zwitterion (*E*)-3-oxo-4-((2-(pyridin-2-yl)ethyl)-amino)-6-((2-(pyridin-2-yl)ethyl)iminio)cyclohexa-1,4-dienolate (**2**, H_2L), in which a CH_2CH_2 spacer connects the N substituents of the quinonoid core with a pyridine group, was explored in Pd(II) chemistry. Different coordination modes have been observed, depending on the experimental conditions and the reagents. The reaction of H_2L with $[Pd(\mu\text{-}Cl)(dmba)]_2$ (dmba = *o*-$C_6H_4CH_2NMe_2$-*C*,*N*) afforded the dinuclear complex $[\{PdCl(dmba)\}_2(H_2L)]$ (**3**) in which H_2L acts as a N_{Py},N_{Py} bidentate ligand. Deprotonation of this complex with NaH resulted in the formation of the dinuclear complex $[\{Pd(dmba)\}_2(\mu\text{-}L)]$ (**4**) in which a shift of the Pd(II) centers from the N_{Py} sites to the N,O donor sites of the zwitterion core has occurred, resulting in a N_2O_2 tetradentate behavior of ligand L. Reaction of **4** with HCl regenerates **3** quantitatively. Chloride abstraction from **3** with AgOTf (OTf = trifluoromethanesulfonate) resulted in loss of one of the two dmba ligands and formation of an unusual tetranuclear Pd(II) complex, $[\{Pd(dmba)\}(\mu\text{-}L)Pd]_2(OTf)_2$ (**5**), in which two dinuclear entities have dimerized, one pyridine donor group from each dimer forming a bridge with the other dinuclear entity. This results in a N_2, O_2, N_{Py}, N_{Py} hexadentate behavior for the ligand L. Complexes **3** and **4** constitute an unprecedented reversible, switchable system where deprotonation or protonation promotes the reversible migration of the $[Pd(dmba)]^+$ moieties, from the N_{Py} sites in **3**, to the N,O donor sites of the quinonoid core in **4**, respectively. This switch modifies the extent of π-delocalization involving the potentially antiaromatic quinonoid moiety and is accompanied by a significant color change, from red in **3** to green in **4**. The presence of uncoordinated pyridine donor groups in **4** allowed the use of this complex for the preparation of the neutral tetranuclear complex $[\{Pd(dmba)\}_2(\mu\text{-}L)\{PdCl(dmba)\}_2]$ (**6**) in which **4** acts as a N_{Py},N_{Py}-bidentate metalloligand toward two PdCl(dmba) moieties. Halide abstraction from **6** afforded the monocationic, tetranuclear complex $[\{Pd(dmba)\}_2(\mu\text{-}L)\{Pd(dmba)\}_2(\mu\text{-}Cl)]PF_6$ (**7**) in which the two Pd(dmba) moieties are connected by ligand L and a bridging chloride. By Cl/PF_6 anion metathesis, it was possible to switch quantitatively from complex **6** to **7** and *vice versa*. All new compounds were unambiguously characterized by IR, NMR, and mass spectroscopy. Single-crystal X-ray diffraction is also available for molecules **2**−**5** and **7**.

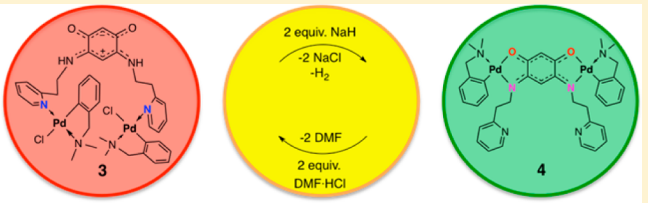

INTRODUCTION

Quinonoid molecules have long been of special interest in coordination chemistry as O-donor and/or π-donor ligands.[1] Additional functionalities can be incorporated into these molecules, which enhance and diversify their coordination properties. This has become particularly notable with quinonoid molecules possessing N-donor groups of the enamino- or imino-type in *ortho*-position to the O-donor atoms. During the last 10 years, our group has investigated the properties of a versatile family of potentially antiaromatic[2] zwitterionic benzoquinonemonoimines derived from the "parent" zwitterion 4-(amino)-6-(iminio)-3-oxocyclohexa-1,4-dien-1-olate (**1**) (Scheme 1).[3] These molecules contain two electronically delocalized but not mutually conjugated six-π-electron systems, chemically connected by two C−C single bonds.[2] They readily form one-dimensional (1D) supramolecular associations in the solid state by virtue of NH···O intermolecular interactions.[4] Because of their ability as donor ligands to easily involve their delocalized electronic π systems with metal centers, significant synergistic effects may be anticipated in their metal complexes. Thus, such zwitterions have been used for the synthesis of functional, mixed-valence[5] and redox-active multinuclear complexes,[6] of homogeneous

Scheme 1. Transamination Reactions from the "Parent" Zwitterion 1

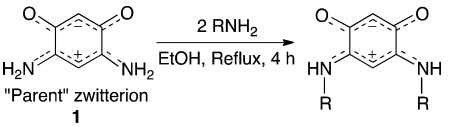

Received: January 25, 2014

 © XXXX American Chemical Society dx.doi.org/10.1021/ic500194y | *Inorg. Chem.* XXXX, XXX, XXX−XXX

precatalysts for the oligomerization of ethylene,[6b,7] and of complexes with potential applications in optical recording.[8] These organic zwitterions can also be deposited on various metal or semiconductor surfaces and on graphene, giving rise to the occurrence of interesting physical properties.[9] Although unprecedented in quinonoid chemistry, a simple transamination reaction allows the functionalization of **1** without affecting the quinonoid core and thus allows the fine-tuning or amplification of its chemical properties (Scheme 1).[4a,10] Here we describe our first results on the coordination chemistry of the new polyfunctional zwitterionic quinonoid, potentially hexadentate N_2, O_2, N_{Py}, N_{Py} ligand, bis(2-(pyridin-2-yl)ethyl) N-substituted zwitterion **2** (H_2L) (Scheme 2). We will show

Scheme 2. Bis(2-(pyridin-2-yl)ethyl) N-substituted Zwitterion (2, H_2L)

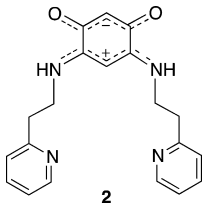

2

how the interactions between this multidentate ligand and Pd(II) centers can be fine-tuned, by changing the experimental conditions, to result in an unexpected reversible switching of the donor sites. Coordination switching can be triggered, for example, by redox processes,[11] deprotonation and/or halide abstraction,[12] reaction with the solvent,[13] and thermal[14] or photochemical[15] activation. Because of the ease with which the coordination environment of the Pd(II) center can be modified, our observations may have relevance to *in situ* transformations occurring, for example, during Pd-catalyzed cross-coupling reactions[16] and surface functionalization.[17]

RESULTS AND DISCUSSION

The new functional zwitterion **2** was obtained as a brown solid, in good yield (78%), from the reaction of the "parent" zwitterion **1** with 2 equiv of 2-(pyridin-2-yl)ethanamine in refluxing ethanol, following an established transamination procedure.[4a,10] Like its precursor, this zwitterion presents a planar, potentially antiaromatic core,[2] constituted by a 12-π-electron system divided into two delocalized 6-π-electron subunits, mutually connected by two C−C single bonds.[2] Each nitrogen group is functionalized by a dangling *ortho*-pyridine, and the CH_2CH_2 spacer between them offers a much better flexibility and solubility when compared to the derivative with a single CH_2 spacer.[18] The latter was indeed found to be only poorly soluble in polar solvents (e.g., MeOH, DMSO, water) and afforded insoluble complexes not suitable for our purpose. The molecular structure of **2**·CH_2Cl_2 was determined by X-ray crystallography (Figure 1).

Compound **2** crystallizes in the orthorhombic space group $Pna2_1$, and the molecule presents a symmetry axis passing through the carbon atoms C1 and C4. Selected bond lengths are listed in Table 1 (for crystal data and selected bond angles, see Supporting Information, Tables S1 and S2, respectively). The structure of **2** confirms its zwitterionic character, with a fully delocalized π system within the O1−C3−C4−C5−O2 and N1−C2−C1−C6−N3 moieties: the C═O, C═N, and C═C bond lengths are very similar, and the C2−C3 and C5−C6 distances

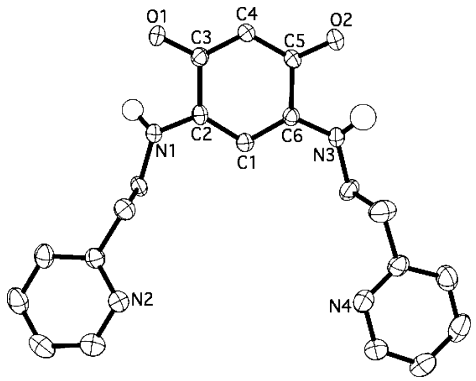

Figure 1. Crystalmaker view of **2** (H_2L) in **2**·CH_2Cl_2. Thermal ellipsoids are drawn at the 50% probability level. Only the NH protons are shown.

of 1.530(5) Å correspond to typical single bonds. In the solid state, the N1H−O2 and N3H−O1 moieties are involved in intermolecular hydrogen bonding interactions (N1···O2 = 2.862(4) Å, N3···O1 = 2.923(4) Å), resulting in a head-to-tail, zigzaglike 1D supramolecular network (Figure 2) in which a stabilizing $\pi-\pi$ stacking between the quinonoid rings of two different chains occurs, with a C1···C4 separation of 3.437(5) Å. If ligand **2** reacted with metal centers solely as a bis-pyridine-type N_{Py},N_{Py} ligand, the zwitterionic core would not be affected and would retain its strong dipolar nature. This could have a beneficial effect in subsequent reactivity studies since it has been shown recently that the addition of an ionic liquid-type zwitterion to a palladium complex improved its catalytic performance in ethylene methoxycarbonylation.[19]

When **2** was treated in CH_2Cl_2 with 1 equiv of [Pd(μ-Cl)(dmba)]$_2$ (dmba = *o*-$C_6H_4CH_2NMe_2$-*C*,*N*), the neutral dinuclear complex [{PdCl(dmba)}$_2$(H_2L)] (**3**) was obtained quantitatively (yield: 92%) (Scheme 3). The pyridine donors induce the cleavage of the chloride bridges in the dinuclear metal precursor and coordinate the two PdCl(dmba) moieties in a slightly distorted, square-planar fashion. Only the pyridine moieties are involved in metal coordination, and they adopt a *cis* arrangement and a perpendicular orientation with respect to the dmba aryl ring, as shown by an X-ray diffraction study of single crystals of **3** (Figure 3). Selected bond lengths are listed in Table 1 (for crystal data and selected bond angles see Supporting Information, Tables S1 and S2, respectively). The coordination of the Pd centers by the pyridines leads to Pd1−N2 and Pd2−N4 distances of 2.036(7) and 2.038(7) Å, respectively. As anticipated, the bonding parameters within the quinonoid core, in particular the C−O, C−C, and C−N distances, remain unaffected in comparison with **2** (Table 1). Complex **3** presents, in the solid state, the same head-to-tail, zigzag, supramolecular arrangement already displayed in the free zwitterion, owing to the formation of hydrogen bonding intermolecular interactions between the N1H−O2 and the N3H−O1 moieties (see Figure 4). Their distances of 2.783(9) Å for N1H···O2 and 2.830(9) Å for N3H···O1 are slightly shorter than they are in **2**. The resulting linear array is decorated with dangling PdCl(dmba) moieties coordinated by the pyridines, which prevent the formation of the $\pi-\pi$ stacking interaction observed in **2**. Fourier transform-far-infrared (FT-far-IR) analysis of **3** showed a typical ν(Pd−Cl) stretching vibration at 296 cm^{-1}.[20]

Solution NMR analyses of **3** revealed a temperature-dependent dynamic behavior. In particular, room-temperature

dx.doi.org/10.1021/ic500194y | *Inorg. Chem.* XXXX, XXX, XXX−XXX

Table 1. Selected Bond Distances (Å) in 2−5 and 7

	2·CH_2Cl_2	3	4	5	7·CH_2Cl_2
O1−C3	1.250(4)	1.230(1)	1.273(5)	1.268(8)	1.268(8)
C3−C4	1.391(4)	1.390(1)	1.384(5)	1.414(9)	1.360(1)
C4−C5	1.395(4)	1.390(1)	1.382(5)	1.363(9)	1.390(1)
C2−O5	1.248(4)	1.260(1)	1.273(4)	1.307(8)	1.278(9)
C2−C3	1.530(5)	1.560(1)	1.509(6)	1.498(9)	1.520(1)
C5−C6	1.530(5)	1.510(1)	1.502(6)	1.497(9)	1.540(1)
N1−C2	1.309(4)	1.270(1)	1.322(5)	1.325(8)	1.341(9)
C1−C2	1.394(4)	1.410(1)	1.400(5)	1.417(9)	1.400(1)
C1−C6	1.400(4)	1.390(1)	1.393(5)	1.405(9)	1.390(1)
N3−C6	1.315(4)	1.310(1)	1.332(5)	1.320(8)	1.314(9)
Pd1−N4		2.038(7)		2.038(6)	
Pd1−Cl1		2.431(3)			
Pd1−N5		2.078(7)	2.067(3)		2.081(6)
Pd1−C21		1.870(1)	1.979(4)		1.981(7)
Pd1−N3			2.027(3)	1.969(6)	2.033(6)
Pd1−O2			2.103(3)	1.998(5)	2.115(4)
Pd1−N2				2.033(5)	
Pd2−N2		2.036(7)			
Pd2−Cl2		2.412(3)			
Pd2−C30		1.970(1)	1.995(4)	1.972(9)	1.991(9)
Pd2−N6		2.068(7)	2.067(3)	2.074(6)	2.083(6)
N1−Pd2			2.049(3)	2.026(6)	2.031(6)
O1−Pd2			2.101(3)	2.142(5)	2.147(6)
Pd3−N4					2.033(1)
Pd3−C39					1.964(1)
Pd3−N7					2.064(1)
Pd3−Cl1					2.380(2)
N2−Pd4					2.030(1)
Pd4−C48					1.978(9)
Pd4−N8					2.068(1)
Pd4−Cl1					2.435(2)

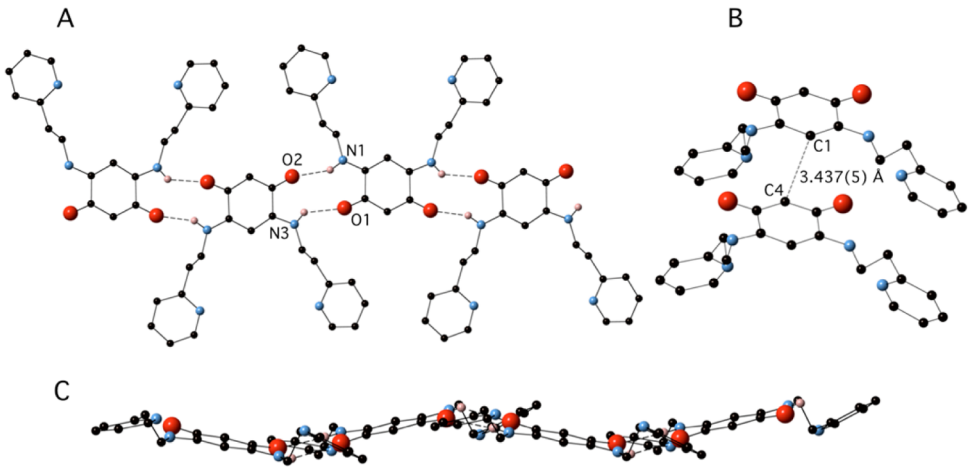

Figure 2. Crystalmaker views of the supramolecular array generated by **2** in 2·CH_2Cl_2, in the solid state. (A) Top view. (B) Interchain $\pi-\pi$ stacking view. (C) Side view. Color coding: nitrogen, blue; oxygen, red; hydrogen, pink.

rotating frame nuclear Overhauser effect spectroscopy (ROESY) (see Supporting Information, Figure S8) indicated a chemical exchange between two conformers involving the hydrogen atoms on each CH_2 group of the CH_2CH_2 spacers linking the quinonoid nitrogen atoms and the pyridyl rings. This interconversion was slowed down by lowering the temperature and suppressed at 263 K (see Supporting Information, Figure S9), where integration of the ^{1}H NMR signals at this temperature indicated a 1:1 ratio between the two conformers. Therefore, ^{13}C, ^{1}H/^{13}C heteronuclear single quantum correlation (HSQC), and ^{1}H correlation spectroscopy (COSY) spectra were also recorded at this temperature and allowed the complete discrimination of the signals belonging to each conformer (named **3a** and **3b** in the Experimental Section) (see Supporting Information, Figures S1−S7). Both conformers show the typical chemical shifts of the zwitterionic quinonoid core[7b] and a signal for the *ortho* H7 hydrogen of the dmba phenyl (see Experimental Section, Scheme 9) at 5.61

dx.doi.org/10.1021/ic500194y | *Inorg. Chem.* XXXX, XXX, XXX−XXX

Scheme 3. Synthesis of the Dipalladium Complex 3

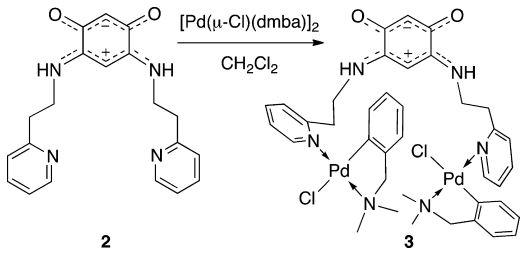

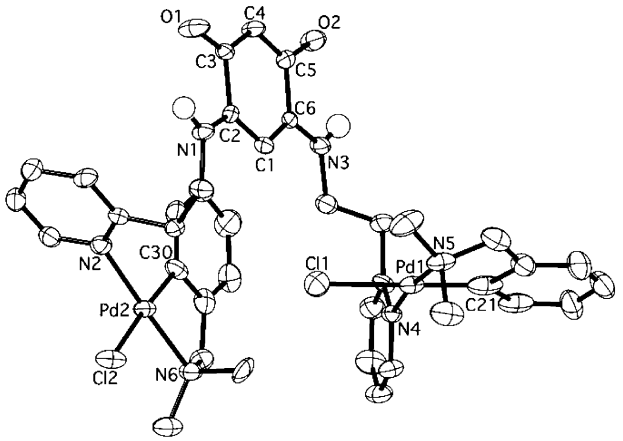

Figure 3. Crystalmaker view of **3**. Thermal ellipsoids are drawn at the 50% probability level. Only the NH protons are shown.

ppm. Such a low value is typical for a dmba phenyl ring *cis* and orthogonal to a pyridine ring.[21] An equilibrium between possible conformers **3a** and **3b** is shown in Scheme 4, where nonequivalent orientations of the metal centers are made possible by the high flexibility of the CH_2CH_2 spacers, resulting from easy rotation about their C−N and C−C bonds.

Addition of 2 equiv of NaH to a solution of complex **3** in CH_2Cl_2 led to deprotonation and loss of the chloride ligands, with formation of the neutral complex $[\{Pd(dmba)\}_2(\mu\text{-L})]$ (**4**) (Scheme 5). We shall see below that this transformation is fully reversible.

The green complex **4** was isolated in good yield (72%), and crystals suitable for X-ray diffraction were obtained by stratification of a toluene solution of the complex with *n*-pentane. Selected bond lengths are listed in Table 1 (for crystal data and selected bond angles see Supporting Information, Tables S1 and S2, respectively). Complex **4** crystallizes in the *Pbca* orthorhombic space group, and the molecule possesses a C_2 symmetry axis passing through C1 and C4. The structure of **4** depicted in Figure 5 shows that the deprotonation of **3** has formally resulted in the migration of the two cationic $[Pd(dmba)]^+$ moieties from the pyridine to the quinonoid site, which now acts as a bis(N,O)-chelating, bridging ligand connected to two free dangling pyridines. As will be shown below, these latter can act as donors for additional metal centers.

Both metal centers in **4** display a distorted square planar coordination geometry. The values of the bond distances within the O1−C3−C4−C5−O2 and N1−C2−C1−C6−N3 moieties indicate notable bond equalization, which is a clear indication that the electronic delocalization within these π systems results in bond orders intermediate between one and two. The C2−C3 and C5−C6 distances of 1.509(6) and 1.502(6) Å, respectively, confirm the lack of electronic conjugation between the two π systems. The pattern of the ^1H and ^{13}C NMR signals of **4** is consistent with the high molecular symmetry found in the solid

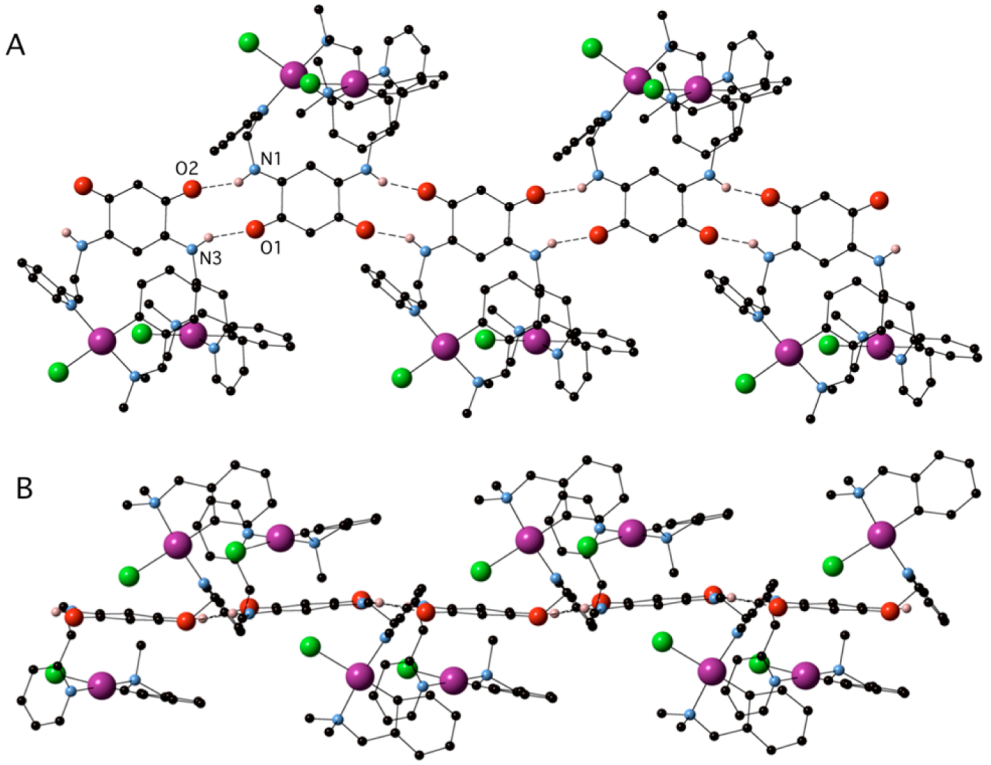

Figure 4. Crystalmaker view of the supramolecular array generated by **3** in the solid state. (A) Top view. (B) Side view. Color coding: nitrogen, blue; oxygen, red; hydrogen, pink; palladium, magenta; chlorine, green.

dx.doi.org/10.1021/ic500194y | *Inorg. Chem.* XXXX, XXX, XXX−XXX

Scheme 4. Two Possible Conformers, 3a and 3b, Present in Solution[a]

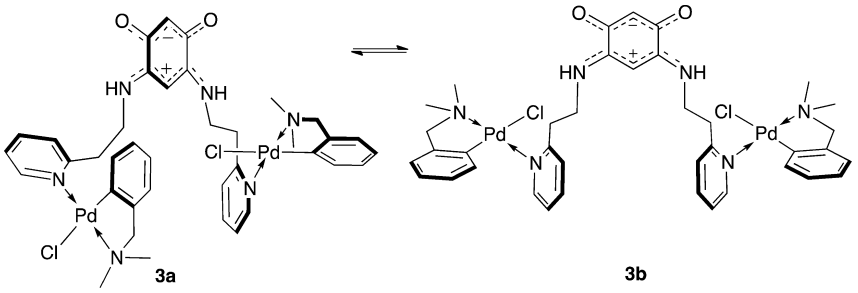

[a]Conformer **3a** is taken arbitrarily as corresponding to the structure of the complex in the solid state.

Scheme 5. Deprotonation−Reprotonation-Triggered Transformations Involving 3 and 4 Leading to a Reversible, Switchable System

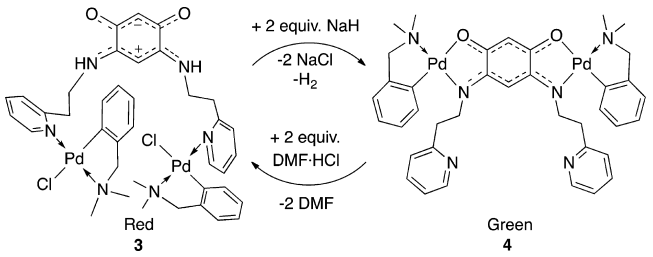

state. The chemical shifts of the N=C and O=C carbon nuclei at 188.30 and 164.87 ppm, respectively, support the presence of the delocalized π systems.[7b] All the data are consistent with the fact that deprotonation of **3** has led to a new neutral dinuclear complex **4** in which a direct interaction occurs between the Pd centers and the quinonoid core. This results in an extension of the two delocalized π systems that now involve the quinonoid moiety and the metal centers. The associated modification in the electronic structure is accompanied by a color change from red, for **3**, to green, for **4**.[7b] The ultraviolet−visible (UV−vis) spectra of complexes **3** and **4** are shown in Figure 6. Compound **3** displays a broad absorption band at 518 nm, which is assigned to intraquinone transitions of the zwitterionic part.[5c] The spectrum of complex **4** exhibits an absorption band and a shoulder at 430 and 454 nm, respectively, consistent with a ligand-to-metal charge transfer transition (LMCT), and a broad absorption band at 628 nm, assigned to intraquinone transitions.[5c] The pronounced red shift of the intraquinone transition absorptions between **3** (518 nm) and **4** (628 nm) is consistent with an increase of the delocalization of the conjugated π system.[22]

Interestingly, the deprotonation-induced conversion of **3** in **4** is reversible, and reaction of the latter complex with 2 equiv of DMF·HCl[23] allowed quantitative recovery of complex **3** (Scheme 5). Complexes **3** and **4** thus define an unprecedented switchable system, in which deprotonation or protonation of the complex allows a reversible change of the donor atoms and of the position of the metal centers on the functional ligand (Scheme 5). Accordingly, the spatial extension of the π delocalization involving the quinonoid ring is modified. Preliminary cyclic voltammetric measurements were carried out in CH_2Cl_2 on complex **4**, but unfortunately most processes were irreversible, and the sample underwent decomposition during analysis (see Supporting Information, Figures S10−S14), even upon increasing the scan rate.

The discovery of this tunable metal migration prompted us to investigate the reactivity of **3** toward simple halide abstraction (without deprotonation). We thus reacted complex **3** with 2 equiv of AgOTf in MeOH. Rapid precipitation of AgCl occurred with formation of a red intermediate that was not isolated and is likely to be a solvento species where MeOH coordinates the metal in place of Cl. The color of the solution progressively changed from red to green, and the dicationic complex $[\{Pd(dmba)\}(\mu\text{-L})Pd]_2(OTf)_2$ (**5**) was isolated as a green solid in 68% yield (Scheme 6).

Green crystals of **5** suitable for X-ray diffraction analysis were obtained by stratification of an acetone solution of the complex with *n*-pentane. The structure of **5** is shown in Figure 7, and selected bond lengths are listed in Table 1 (for crystal data and selected bond angles see Supporting Information, Tables S1 and S2, respectively). Both metal centers present a distorted square-planar coordination geometry. The structural parameters within the quinonoid core are still consistent with the presence of two, nonconjugated, delocalized π systems, and the two Pd centers are involved in the electronic delocalization. This is also confirmed by ^1H and ^{13}C NMR spectroscopy, in

Scheme 6. Synthesis of the Tetranuclear Pd(II) Complex 5

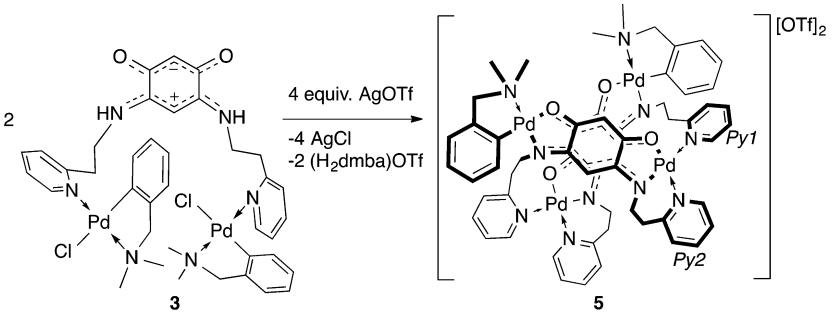

dx.doi.org/10.1021/ic500194y | Inorg. Chem. XXXX, XXX, XXX−XXX

Scheme 7. Synthesis of the Tetranuclear Pd(II) Complexes 6 and 7

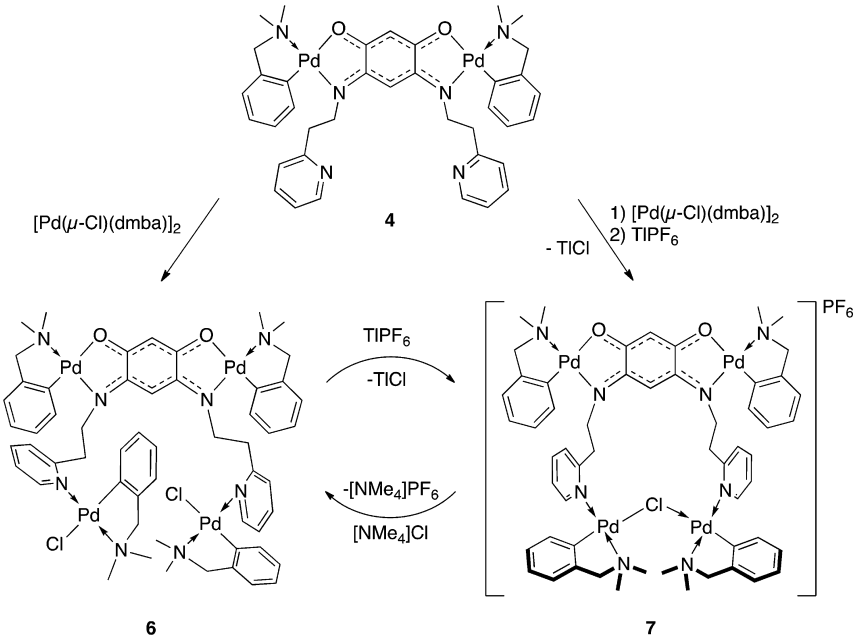

Scheme 8. Overview of the Synthetic Transformations Involving Ligand 2

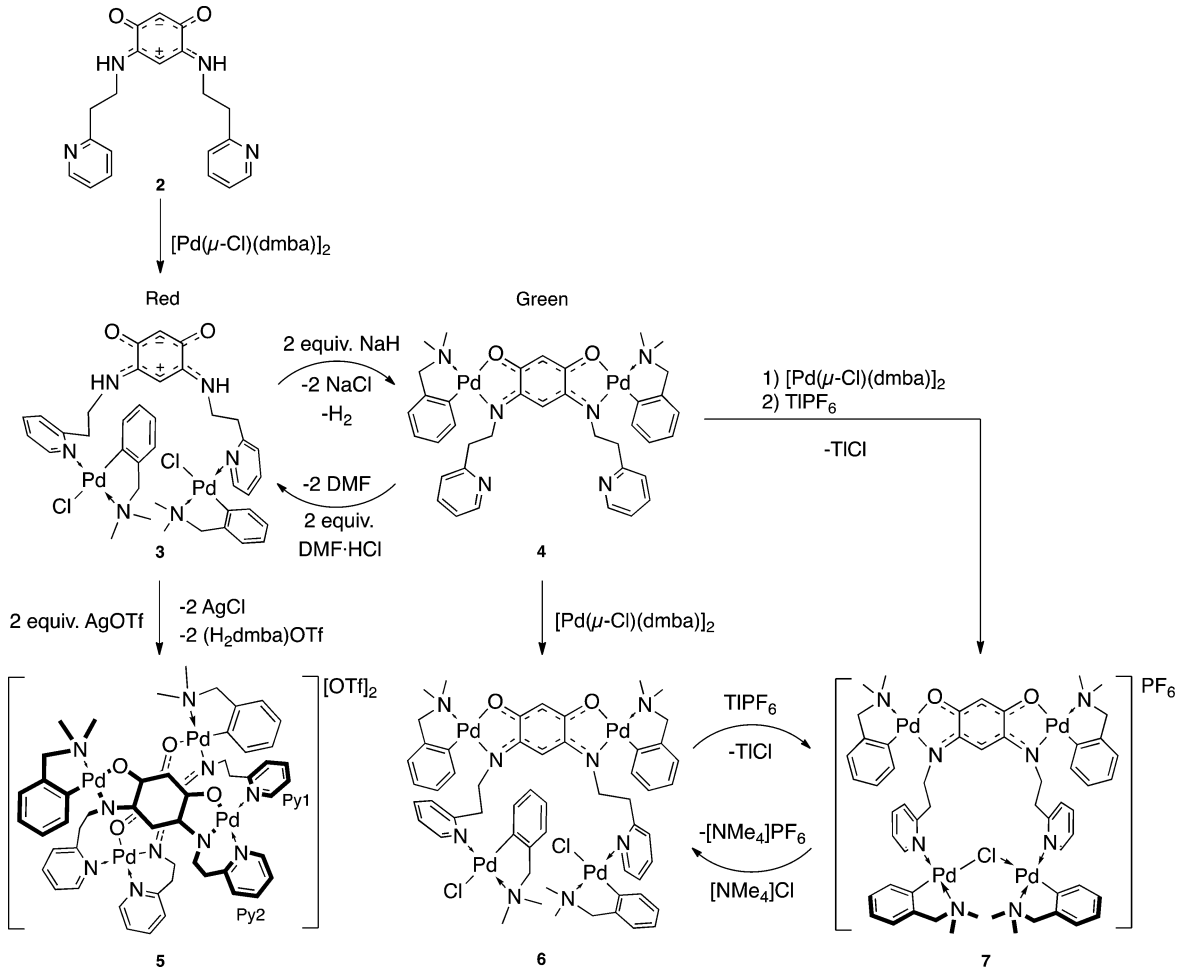

particular by the ^{13}C chemical shifts of the O2=*C*5 and O1=*C*3 carbons at 189.63 and 189.86 ppm, respectively, and by the signals of the *C*6=N2 and *C*2=N1 carbons at 165.94 and 165.04 ppm, respectively.[7b] The green color of the complex is very similar to that of **4** and appears typical for the electronic delocalization involving two metal centers and the quinonoid

dx.doi.org/10.1021/ic500194y | *Inorg. Chem.* XXXX, XXX, XXX−XXX

Scheme 9. Atom Numbering Scheme Used for NMR Description[a]

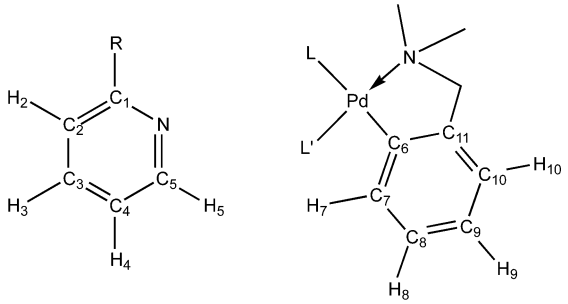

[a]In case of complex **5**, the two non-equivalent pyridines (Py1 and Py2) are named as in Scheme 6.

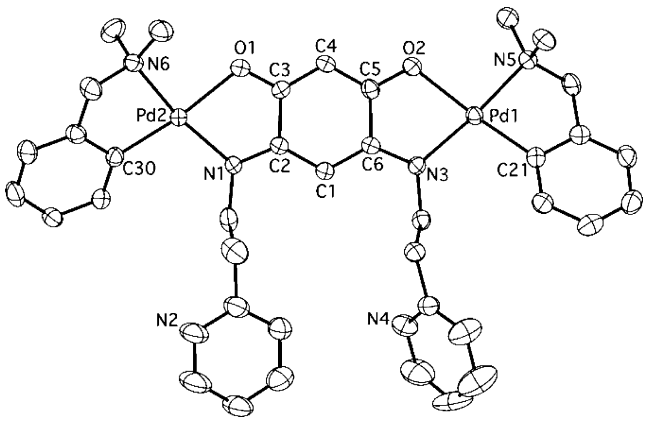

Figure 5. Crystalmaker view of **4** (H atoms not shown). Thermal ellipsoids are drawn at the 50% probability level.

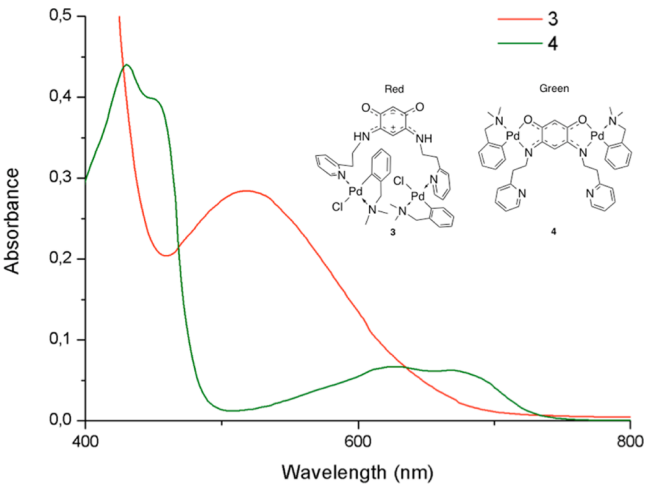

Figure 6. UV−vis absorption spectra of compounds **3** ($c = 1.1 \times 10^{-3}$ M) and **4** ($c = 1.1 \times 10^{-5}$ M) in CH_2Cl_2 at room temperature.

core, as observed previously with Ni(II), Pd(II), and Pt(II) dinuclear complexes.[5a,7b,24]

This new complex results from an interesting transformation of **3** upon chloride abstraction: despite the lack of an external base, spontaneous deprotonation occurred by elimination of one equivalent of (H_2dmba)OTf, which resulted in the formation of a dicationic, tetranuclear dimeric complex, formed by two dipalladium moieties mutually connected by two pyridine arms. Within each dinuclear moiety, the quinonoid core acts again as a bis(N,O)-chelating, bridging ligand for two Pd centers, which then complete their coordination spheres in two different ways. While Pd2 retains its chelating dmba ligand and displays a coordination environment similar to that in complex **4**, Pd1 has lost its dmba chelate and completes its coordination sphere with two inequivalent pyridines: one originates from the ligand itself (intramolecular Py2), while the other is shared by the other half of the dimer (intermolecular Py1) and becomes part of a bridge between the two dinuclear moieties. The resulting double positive charge is balanced by two triflate anions.

Because of its two uncoordinated pyridines, complex **4** could still react with metal centers and act as a pyridinic N_{Py},N_{Py}-bidentate metalloligand.[25] Thus, the reaction of **4** with [Pd(μ-Cl)(dmba)]$_2$ in a L/Pd ratio of 1:2 afforded the neutral tetranuclear complex [{Pd(dmba)}$_2$(μ-L){PdCl(dmba)}$_2$] (**6**) (Scheme 7) in 71% yield. NMR data of **6** in solution suggested that this reaction did not affect the quinonoid part with respect to the precursor metalloligand **4**, while the two pyridines coordinate the Pd centers in a similar way to what is observed in complex **3**. In particular, **6** displayed only one conformer constituted by two inequivalent pyridinic arms, each bearing a PdCl(dmba) moiety. The chemical shift of the *ortho*-H of the dmba phenyl (H7, see Experimental Section and Scheme 9) at 5.73 ppm confirmed the *cis* and orthogonal orientation of the pyridine rings with respect to the dmba phenyls (see above). Furthermore, in the far-IR spectrum, the ν(Pd−Cl) stretching vibration of 299 cm^{-1} is consistent with the value found in complex **3** (295 cm^{-1}).

The reaction of **6** with 1 equiv of $TlPF_6$ resulted in the abstraction of one chloride ligand and the formation of the monocationic tetranuclear complex [{Pd(dmba)}$_2$(μ-L){Pd(dmba)}$_2$(μ-Cl)]PF_6 (**7**) (Scheme 7) in 83% yield.

As established by an X-ray diffraction on single crystals obtained by layering a CH_2Cl_2 solution of the complex with pentane, the assembling ligand L in **7** acts as a N_2, O_2, N_{Py}, N_{Py} hexadentate donor where the dinuclear quinonoid moiety of the precursor complex **4** remains unaffected, while the two pyridines are involved in coordination to two additional metal centers from the cationic [(dmba)Pd(μ-Cl)Pd(dmba)]$^+$ moiety (Figure 8). The resulting positive charge is balanced by one PF_6^- anion. All the metal centers present a distorted square planar coordination geometry. Selected bond lengths for **7** are listed in Table 1 (for crystal data and selected bond angles see Supporting Information, Tables S1 and S2, respectively). As confirmed by the X-ray diffraction analysis, the two pyridine rings are orthogonal and *cis* to the dmba aryls, as found for complex **3** (see above). This is consistent with the NMR data in solution (δ of H7 (*ortho* H of the dmba phenyl) = 5.35 ppm, see Experimental Section and Scheme 9). The average Pd−(μ-Cl) distance of 2.407 Å is similar to values found in the literature for a related complex (average 2.443 Å).[26] The presence of a bridging μ-Cl ligand between the Pd centers results in a shift of the ν(Pd−Cl) stretching vibration, from 299 cm^{-1} for complex **6** to 246 cm^{-1} for **7**. The latter value is typical for a ν[Pd(μ-Cl)] vibration involving a chloride ligand in *trans* position to a σ-bonded carbon, and this absorption disappears upon LiBr metathesis.[27] Furthermore, as depicted in Scheme 7, it was possible via Cl/PF_6 anion exchange to switch quantitatively from complex **6** to **7** and *vice versa*. Complex **7** could also be obtained (in lower yield: 57%) by the one-pot reaction of **4** with [Pd(μ-Cl)(dmba)]$_2$ and $TlPF_6$ in 1:1:1 ratio. By analogy with the formation of **7**, we reacted complex **3** with

dx.doi.org/10.1021/ic500194y | Inorg. Chem. XXXX, XXX, XXX−XXX

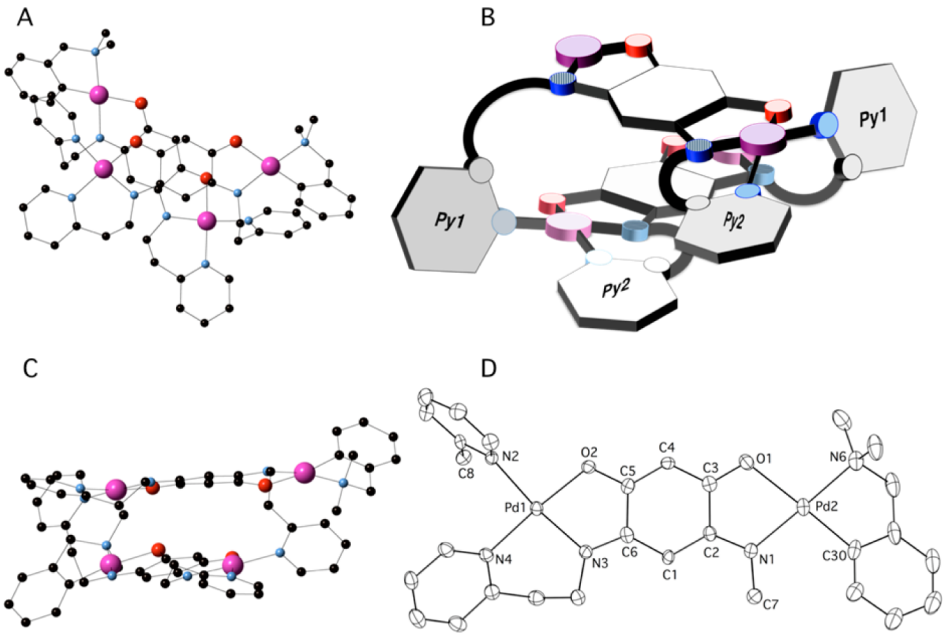

Figure 7. Views of the crystal structure of **5**. The OTf^- anions were omitted for clarity. (A) and (C) Perspective views. (B) Simplified perspective model, dmba ligands omitted for clarity. (D) Dinuclear fragment constitutive of **5**, thermal ellipsoids are drawn at the 50% probability level. Color coding: nitrogen, blue; oxygen, red; palladium, magenta.

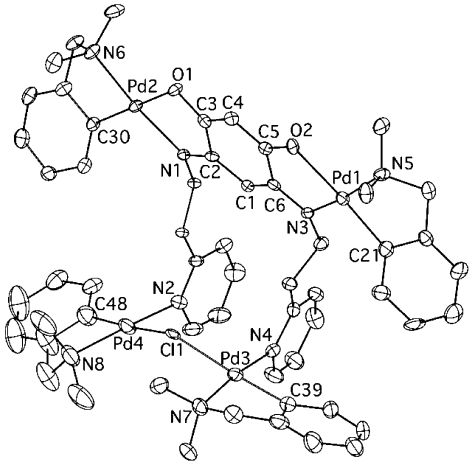

Figure 8. Crystalmaker view of **7** in **7**·CH_2Cl_2. The PF_6^- anion is omitted for clarity. Thermal ellipsoids are drawn at the 50% probability level.

only 1 equiv AgOTf in CH_2Cl_2 or MeOH. Although a reaction took place (^1H and IR monitoring), we could not characterize the species formed, and far-IR data indicated the presence of terminal chloride(s).

CONCLUSIONS

The synthesis and coordination chemistry of the new zwitterionic, multidentate ligand **2** (H_2L) have further demonstrated the tunability of this class of quinonoid-type ligands. Its reactivity with various Pd(II) complexes has led to di- and tetranuclear complexes, and the corresponding transformations are summarized in Scheme 8. Modulation of the ligand denticity and the chemoselectivity of its coordination led to various situations in which **2** acts as a N_{Py}, N_{Py} bidentate ligand, as in complex **3**, and L acts as a N_2O_2 tetradentate (complex **4**) or N_2, O_2, N_{Py}, N_{Py} hexadentate (complexes **5**, **6**, and **7**) ligand, respectively.

Complexes **3** and **4** constitute a novel reversible switchable system, triggered by protonation or deprotonation, which allows the selection of the chemoselective binding of the cationic moiety $[Pd(dmba)]^+$ on the ligand and, consequently, the modification of the extent of π delocalization in the quinonoid π system. Simple dehalogenation of **3** led to a spontaneous deprotonation of the complex by elimination of 1 equiv of (H_2dmba)OTf and formation of the dicationic, dimeric, tetranuclear quinonoid complex **5**, where the ligand acts as N_2, O_2, N_{Py}, N_{Py} hexadentate. The presence of uncoordinated pyridine donor groups in **4** opens the possibility of using this complex as a metalloligand, and this was demonstrated by the isolation of the neutral tetranuclear complex **6** and the monocationic, tetranuclear complex **7**, in which complex **4** act as a N_{Py}, N_{Py} pyridinic bidentate metalloligand and, respectively, coordinates two PdCl(dmba) fragments (**6**) and chelates the $[(dmba)Pd(\mu\text{-}Cl)Pd(dmba)]^+$ moiety (**7**). Furthermore, complexes **3** and **4** represent potential candidates for deposition and anchoring on surfaces, and this will be examined in future work.

EXPERIMENTAL SECTION

General Procedure. All operations were carried out by using standard Schlenk techniques under an inert atmosphere. Solvents were purified and dried under a nitrogen atmosphere by using conventional methods. CD_2Cl_2 and $CDCl_3$ were dried over 4 Å molecular sieves, degassed by performing freeze−pump−thaw cycles, and stored under an argon atmosphere. ^1H and ^{13}C NMR spectra were recorded at room temperature, unless specified, on Bruker AVANCE 400, 500, or 600 spectrometers and referenced to the residual solvent resonance. Assignments are based on ^1H, ^1H COSY, $^1H/^{13}C$ HSQC, ROESY, and ^{13}C NMR experiments. Chemical shifts (δ) are given in ppm, coupling constants are in Hz, and the atom numbering used is shown in Scheme 9. IR spectra were recorded within the region of 4000−100 cm^{-1} on a Nicolet 6700 FTIR spectrometer (ATR mode, SMART ORBIT accessory, Diamond crystal). Elemental analysis was performed by the

dx.doi.org/10.1021/ic500194y | Inorg. Chem. XXXX, XXX, XXX−XXX

"Service de Microanalyses," Université de Strasbourg, or by the "Service Central d'Analyse," USR-59/CNRS, Solaize. Electrospray mass spectroscopy was performed on a microTOF (Bruker Daltonics, Bremen, Germany) instrument by using a flow of nitrogen gas as a drying agent and nebulizing gas. Matrix-assisted laser desorption-ionization time-of-flight mass spectrometry (MALDI-TOF-MS) spectra were acquired on a TOF mass spectrometer (MALDI-TOF-TOF Autoflex II TOF-TOF, Bruker Daltonics, Bremen, Germany) equipped with a nitrogen laser (λ = 337 nm). An external multipoint calibration was carried out before each measurement. Scan accumulation and data processing were performed with FlexAnalysis 3.0 software. Matrix solutions were freshly prepared: α-cyano-4-hydroxycinnamic acid (CHCA) was dissolved to saturation in a H_2O/CH_3CN/HCOOH (50/50, 1%) solution, and Dithranol was dissolved in tetrahydrofuran (THF) to obtain a 20 mg/mL solution. Typically, 0.5 μL of a mixture containing the sample solution and the matrix (1/1) was deposited on the stainless steel plate. The UV−vis spectra were recorded on an Analytic Jena Specord 205 spectrophotometer, using optically transparent glass cells. The complex $[Pd(\mu\text{-Cl})(dmba)]_2$ was synthesized according to the literature.[28] Other chemicals were commercially available and were used as received.

Synthesis of Zwitterion **2**. To a dispersion of **1** (0.607 g, 4.40 mmol) in 10 mL of EtOH was added 2-(pyridin-2-yl)ethanamine (0.950 g, 7.91 mmol). The reaction mixture was heated to reflux for 4 h and then cooled to room temperature. Volatiles were removed under vacuum, the dark purple solid obtained was dissolved in CH_2Cl_2, and the solution was filtered through Celite. Addition of *n*-pentane to the filtrate led to the precipitation of a brown powder of **2**. Red crystals suitable for X-ray diffraction were grown by slow diffusion of *n*-pentane into a solution of **2** in CH_2Cl_2. Yield: 1.204 g, 3.45 mmol (78%). Anal. Calcd for $C_{20}H_{20}N_4O_2$ (348.40): C, 68.95; H, 5.79; N, 16.08. Found: C, 68.60; H, 5.80; N, 15.74%. FTIR: ν_{max}(solid)/cm^{-1}: 3184 ms, 3047vw, 3015vw, 1644w, 1535vs, 1477s, 1461w, 1432s, 1387w, 1356m, 1311w, 1285m, 1261w, 1205w, 1186w, 1148mw, 1103w, 1050w, 998m, 887vw, 848w, 821vw, 767vs, 746vs, 724vs, 684vw, 631mw. ^{1}H NMR (CD_2Cl_2, 400 MHz) δ: 8.90 (br, 2H, NH), 8.69 (br-d, 2H, $^3J_{H,H}$ = 4.6 Hz, H^{5}Py), 7.77 (dt, 2H, $^3J_{H,H}$ = 7.6, $^4J_{H,H}$ = 1.9 Hz, H_3Py), 7.34−7.31 (m, 4H, H^{2,4}Py), 5.39 (s, 1H, N=C−CH), 5.32 (s, 1H, O=C−CH), 3.94 (t, 4H, $^3J_{H,H}$ = 6.7 Hz, HNCH_2CH$_2$Py), 3.29 (t, 4H, $^3J_{H,H}$ = 6.7 Hz, HNCH$_2$CH_2Py) ppm.^{13}C{^{1}H} NMR (CD_2Cl_2, 75.5 MHz) δ: 172.51 (s, C=O), 158.12 (s, C^{1}Py), 157.01 (s, C=N), 149.94 (s, C^{5}Py), 137.15 (s, C^{3}Py), 123.88 (s, C^{2}Py), 122.41 (s, C^{4}Py), 98.01 (s, O=C−C), 81.37 (s, HN=C−C), 42.79 (s, HNCH$_2$CH$_2$Py), 36.29 (s, HNCH$_2$CH$_2$Py) ppm.

Synthesis of Complex **3**. To a solution of **2** (0.098 g, 0.28 mmol) in 10 mL of CH_2Cl_2 was added $[Pd(\mu\text{-Cl})(dmba)]_2$ (0.155 g, 0.28 mmol). The reaction mixture was stirred for 4 h. Addition of *n*-pentane to this solution led to the precipitation of a red solid of **3** that was filtered and washed with THF. Red crystals suitable for X-ray diffraction were grown by slow diffusion of *n*-pentane into a solution of **3** in CH_2Cl_2. Yield: 0.232 g, 0.26 mmol (92%). Anal. Calcd for $C_{38}H_{44}Cl_2N_6O_2Pd_2$ (900.49): C: 50.68; H: 4.92; N: 9.33. Found: C, 50.75; H, 5.20; N, 8.84%. FTIR: ν_{max}(solid)/cm^{-1}: 3168w, 3050w, 2975w, 2910vw, 2886vw, 1534vs, 1476m, 1449w, 1437m, 1352w, 1313vw, 1289w, 1260vw, 1207vw, 1178vw, 1107w, 1065vw, 1046vw, 1018mw, 983w, 968mw, 930vw, 901vw, 866mw, 850mw, 798vw, 769vw, 738vs, 658vw, 518m, 479vw, 445w, 423mw, 398m, 362s, 334vw, 296s (ν(Pd−Cl)), 226vs, 151vw, 126s, 108vw. An equilibrium is present in solution between two conformers **3a** and **3b** in ca. 1:1 ratio (see text), which can be discriminated by low temperature combined ^{1}H, ^{13}C, ^{1}H COSY, and HSQC NMR analysis. ^{1}H NMR ($CDCl_3$, 500 MHz, 263 K) δ: 9.01 (d, 2H, $^3J_{H,H}$ = 5.7 Hz, H^{5}Py of **3a**), 8.97 (d, 2H, $^3J_{H,H}$ = 5.7 Hz, H^{5}Py, **3b**), 8.53 (t, 2H, $^3J_{H,H}$ = 6.8 Hz, NH, **3a**), 8.43 (t, 2H, $^3J_{H,H}$ = 6.8 Hz, NH, **3b**), 7.80−7.75 (m, 4H, $^3J_{H,H}$ = 7.8 Hz, $^4J_{H,H}$ = 1.5 Hz, H_3Py, **3a**+**3b**), 7.56−7.52 (m, 4H, H^{2}Py, **3a**+**3b**), 7.33−7.30 (m, 2H, H^{4}Py, **3b**), 7.27−7.25 (m, 2H, H^{4}Py, **3a**), 6.99−6.95 (m, 8H, H^{8,10}Ph, **3a**+**3b**), 6.70−6.67 (m, 4H, H^{9}Ph, **3a**+**3b**), 5.87 (s, 1H, N=C−CH, **3a**), 5.64 (s, 1H, N=C−CH, **3b**), 5.61 (d, 4H, $^3J_{H,H}$ = 7.6 Hz, H^{7}Ph, **3a**+**3b**), 5.38 (s, 1H, O=C−CH, **3a**), 5.37 (s, 1H, O=C−CH, **3b**), 4.37−4.08 and 3.60−3.52 (m, 12H + 4H, NCH_2CH_2Py, **3a**+**3b**), 4.08−3.96 (m, 8H, NCH$_2$Ph, **3a**+**3b**), 2.97, 2.95, and 2.93 (s, 12H, 6H, 6H, NCH$_3$, **3a**+**3b**) ppm. ^{13}C{^{1}H} NMR ($CDCl_3$, 150.9 MHz, 263 K) δ: 172.79 (s, C=O, **3a**), 172.75 (s, C=O, **3b**), 158.51 (s, C^{1}Py, **3a**), 158.49 (s, C^{1}Py, **3b**), 156.76 (s, N=C, **3a**), 156.72 (s, N=C, **3b**), 153.29 (s, C^{5}Py, **3a**), 153.25 (s, C^{5}Py, **3b**), 147.63 (s, C^{6}Ph, **3a**), 147.61 (s, C^{6}Ph, **3b**), 146.64 (s, C^{11}Ph, **3a**+**3b**), 138.40 (s, C^{3}Py, **3a**), 138.38 (s, C^{3}Py, **3b**), 131.27 (s, C^{7}Ph, **3a**), 131.23 (s, C^{7}Ph, **3b**), 127.01 (s, C^{2}Py, **3a**), 126.95 (s, C^{2}Py, **3b**), 125.63 (s, C^{9}Ph, **3a**+**3b**), 124.97 (s, C^{8}Ph, **3a**+**3b**), 123.75 (s, C^{4}Py, **3a**), 123.73 (s, C^{4}Py, **3b**), 122.07 (s, C^{10}Ph, **3a**+**3b**), 99.14 (s, O=C=*C*, **3a**), 99.03 (s, O=C=*C*, **3b**), 82.68 (s, N=C=*C*, **3a**), 82.64 (s, N=C=*C*, **3b**), 73.93 (s, NCH$_2$Ph, **3a**), 73.92 (s, NCH$_2$Ph, **3b**), 52.93 and 52.79 (s, N(CH$_3$)$_2$, **3a**), 52.91 and 52.76 (s, N(CH$_3$)$_2$, **3a**), 42.20 (s, NCH$_2$CH$_2$Py, **3a**), 42.10 (s, NCH$_2$CH$_2$Py, **3b**), 40.75 (s, NCH$_2$CH$_2$Py, **3a**), 40.69 (s, NCH$_2$CH$_2$Py, **3b**) ppm. MS (ESI): *m*/*z* = 865.13 $[M - Cl]^+$.

Synthesis of Complex **4**. Solid NaH (0.012 g, 0.51 mmol) was added to a solution of **3** (0.230 g, 0.25 mmol) in 15 mL of CH_2Cl_2. The reaction mixture was stirred for 2 h, during which it changed color from red to bright green. After filtration, the volatiles were removed under vacuum, and the green solid obtained was redissolved in toluene. Addition of *n*-pentane to this solution led to the precipitation of a dark green solid of **4**, which was filtered and washed with *n*-pentane. Green crystals suitable for X-ray diffraction were grown by stratification of a solution of **4** in toluene with *n*-pentane. Yield: 0.151 g, 0.18 mmol (72%). Anal. Calcd for $C_{38}H_{42}N_6O_2Pd_2{\cdot}H_2O$ (845.63): C, 53.97; H, 5.24; N, 9.93. Found: C, 54.03; H, 5.29; N, 9.53%. FTIR: selected ν_{max}(solid)/cm^{-1}: 3043vw, 2970vw, 2915w, 2801vw, 1589m, 1570w, 1493vs, 1439w, 1402w, 1361w, 1292s, 1266vw, 1203w, 1180w, 1148w, 1104vw, 1075w, 1043w, 1021w, 990w, 969vw, 926w, 905w, 863mw, 848mw, 827mw, 773m, 742s, 697vw, 659w, 635w, 615m, 567w, 534m, 520s, 505vw, 494vw, 479vw, 466vw, 457w, 442w, 427w, 402m, 365s, 340vw, 311vw, 277vw, 246vw, 222vw, 172vs, 141vw, 128vw, 121w, 106w. ^{1}H NMR (CD_2Cl_2, 400 MHz) δ: 8.40 (br-d, 2H, $^3J_{H,H}$ = 4.5 Hz, H^{5}Py), 7.50 (dt, 2H, $^3J_{H,H}$ = 7.6, $^4J_{H,H}$ = 1.8 Hz, H^{3}Py), 7.35−7.34 (m, 2H, H^{8}Ph), 7.19 (d, 2H, $^3J_{H,H}$ = 7.6 Hz, H^{2}Py), 7.05−7.03 (m, 2H, H^{4}Py), 6.98 (m, 4H, H^{9,7}Ph), 6.95 (m, 2H, H^{10}Ph), 5.50 (s, 1H, N=C−CH), 5.41 (s, 1H, O=C−CH), 3.90 (m, 6H, NCH_2Ph + NCH_2CH$_2$Py), 3.14 (m, 4H, NCH$_2$CH_2Py), 2.78 (s, 12H, NCH$_3$) ppm. ^{13}C{^{1}H} NMR (CD_2Cl_2, 75.5 MHz) δ: 188.30 (s, O=C), 164.87 (s, N=C), 159.88 (s, C^{1}Py), 149.35 (s, C^{5}Py), 148.06 (s, C^{11}Ph), 147.37 (s, C^{6}Ph), 135.92 (s, C^{3}Py), 133.34 (s, C^{8}Ph), 125.37 (s, C^{7}Ph), 124.02 (s, C^{9}Ph), 123.31 (s, C^{2}Py), 121.65 (s, C^{4}Py), 121.01 (C^{10}Ph), 102.23 (s, O=C−C), 85.41 (s, N=C−C), 72.62 (s, NCH$_2$Ph), 51.29 (s, NCH$_3$), 50.79 (s, NCH$_2$CH$_2$Py), 37.4 (s, NCH$_2$CH$_2$Py) ppm. MS (ESI): *m*/*z* = 829.15 $[M + H]^+$.

Synthesis of Complex **5**. To a dispersion of **3** (0.230 g, 0.25 mmol) in 15 mL of MeOH was added solid AgOTf (0.131 g, 0.51 mmol). Precipitation of AgCl started rapidly. The reaction mixture was stirred for 2 h and then filtered; the filtrate was allowed to stand overnight at room temperature. During this time, the color of the solution changed from red to bright green, and a green crystalline solid of **5** precipitated. The product was isolated by filtration, dissolved in the minimum amount of CH_2Cl_2, precipitated by addition of *n*-pentane, and collected by filtration. Green crystals suitable for X-ray diffraction were grown by stratification of a solution of **5** in acetone with *n*-pentane. Yield: 0.282 g, 0.17 mmol (68%). Anal. Calcd for $C_{60}H_{60}F_6N_{10}O_{10}Pd_4S_2{\cdot}CH_2Cl_2$ (1769.93): C, 41.39; H, 3.53; N, 7.91. Found: C, 41.25; H, 3.58; N, 8.04%. FTIR: selected ν_{max}(solid)/cm^{-1}: 3361w, 2972vw, 2941vw, 2901vw, 1610w, 1581vw, 1548m, 1497vw, 1484mw, 1440mw, 1413w, 1371w, 1340w, 1261vs, 1225w, 1159m, 1140m, 1113w, 1073w, 1029s, 967w, 908vw, 890vw, 873vw, 823mw, 804w, 788w, 769m, 756w, 720vw, 660vw, 636s, 584s, 572s, 559s, 532w, 512vs, 488w, 458mw, 437 ms, 390m, 350m, 334w, 324w, 315w, 280w, 265m, 255w, 247vw, 227w, 208 ms, 172m, 158vw, 151w, 140vw, 132vw, 125vw, 121vw, 105ms. ^{1}H NMR (CD_2Cl_2, 500 MHz) δ: 8.88 (br d, 1H, $^3J_{H,H}$ = 5.6 Hz, H$_5$Py1), 7.91 (dt, 1H, $^3J_{H,H}$ = 7.6, $^4J_{H,H}$ = 1.4 Hz, H^{4}Py2), 7.72 (d, 1H, $^3J_{H,H}$ = 7.6 Hz, H^{2}Py2), 7.55−7.52 (m, 1H, H^{4}Py1), 7.45 (dt, 1H, $^3J_{H,H}$ = 7.8, $^4J_{H,H}$ = 1.4 Hz, H^{3}Py1), 7.20 (br-d, 1H, $^3J_{H,H}$ = 7.6 Hz, H^{5}Py2), 7.16−7.14 (m, 1H, H^{8}Ph), 7.10−7.08 (m,

3H, H^3Py2 + $H^{7,8}$Ph), 6.99−6.97 (m, 1H, H^{10}Ph), 6.93 (d, 1H, $^3J_{H,H}$ = 7.8 Hz, H^2Py1), 5.72 (s, 1H, N=C=CH), 5.16 (s, 1H, O=C=CH), 4.96 (dt, 1H, $^2J_{H,H}$ = 14.2 $^3J_{H,H}$ = 4.5 Hz, $NCH_2CHHPy1$), 4.47 (dt, 1H, $^2J_{H,H}$ = 12.8 and 3.6 Hz, $NCH_2CHHPy2$), 4.24 (br-d, 1H, $^2J_{H,H}$ = 12.8 Hz,, $NCH_2CHHPy2$), 3.95 (d, 1H, A part of an AB system, $^2J_{H,H}$ = 13.5 Hz, NCHPh), 3.71−3.63 (m, 2H, $NCHHCH_2Py1-2$), 3.36 (d, 1H, $^2J_{H,H}$ = 12.8 Hz, $NCHHCH_2Py1$), 3.31 (d, 1H, B part of an AB system, $^2J_{H,H}$ = 13.5 Hz, NCHPh), 3.17 (d, 1H, $^2J_{H,H}$ = 12.5 Hz, $NCHHCH_2Py2$), 2.96 (br-d, 1H, $^2J_{H,H}$ = 14.2 Hz, $NCH_2CHHPy1$), 2.68 (s, 3H, $N(CH_3)CH_3$), 2.43 (s, 3H, $N(CH_3)CH_3$) ppm. $^{13}C\{^1H\}$ NMR (CD_2Cl_2, 125.7 MHz) δ: 189.63 (s, (dmba)PdO=C), 189.86 (s, $(Py)_2PdO=C$), 165.94 (s, (dmba)PdN=C), 165.04 (s, $(Py)_2PdN=C$), 161.26 (s, C^1Py2), 159.22 (s, C^1Py1), 150.48 (s, C^5Py2 + C^6Ph), 150.23 (s, C^5Py1), 147.91 (s, C^{11}Ph), 141.08 (s, C^3Py2), 139.17 (s, C^3Py1), 133.33 (s, C^8Ph), 128.32 (s, C^2Py1), 128.00 (s, C^2Py2), 126.41 (s, C^4Py2), 124.66 (s, C^4Py1), 125.10 (s, C^7Ph), 124.66 (s, C^9Ph), 122.56 (s, C^{10}Ph), 105.08 (s, O=C=C), 85.84 (s, N=C=C), 72.81 (s, NCH_2Ph), 52.00 and 50.52 (s, $N(CH_3)_2$), 48.42 (s, NCH_2CH_2Py2), 45.34 (s, NCH_2CH_2Py2), 41.85 (s, NCH_2CH_2Py1), 37.79 (s, NCH_2CH_2Py1) ppm. MS (ESI): m/z = 693.53 $[M]^{2+}$.

Synthesis of Complex **6**. To a solution of **4** (0.190 g, 0.21 mmol) in 10 mL of CH_2Cl_2 was added $[Pd(\mu\text{-}Cl)(dmba)]_2$ (0.116 g, 0.21 mmol). The reaction mixture was stirred for 4 h. Addition of *n*-pentane to this solution led to the precipitation of a green solid of **6** that was filtered and washed with *n*-pentane. Yield 0.206 g, 0.15 mmol (71%). Anal. Calcd for: $C_{56}H_{66}Cl_2N_8O_2Pd_4{\cdot}CH_2Cl_2$ (1464.71): C, 46.74; H, 4.68; N, 7.30. Found: C, 46.76; H, 5.11; N, 7.65%. FTIR: selected ν_{max}(solid)/cm^{-1}: 3044vw, 2969vw, 2909vw, 2886vw, 2856vw, 1502vs, 1441w, 1400w, 1295s, 1201w, 1179vw, 1156vw, 1106w, 1045w, 1022m, 987mw, 969w, 891vw, 863mw, 847m, 832vw, 771w, 738vs, 520vs, 477vw, 443w, 425s, 365vs, 299s (Pd−Cl), 270vw, 260vw, 226vs, 219vs, 192m, 185vw, 175vs, 157w, 142vw, 128vs, 122vw, 106s. ^{1}H NMR (CD_2Cl_2, 500 MHz) δ: 8.81 and 8.77 (br-d, 1H +1H, $^3J_{H,H}$ = 5.4 Hz, H^5Py), 7.68 (t, 2H, $^3J_{H,H}$ = 7.9 H^3Py), 7.33 and 7.30 (d, 1H+1H, $^3J_{H,H}$ = 7.9 Hz, H^2Py), 7.19−7.13 (overlapping multiplet, 4H, H^4Py + H^7PhPd(O,N)), 7.01−6.91 (m, 10H, H^{8-10}PhPd(O,N) + H^{9-10}PhPd(Cl)), 6.50 and 6.44 (t, 1H + 1H, $^3J_{H,H}$ = 7.5 Hz, H^8PhPd(Cl)), 5.73 (d, 2H, $^3J_{H,H}$ = 7.5 Hz, H_7PhPd(Cl)), 5.66 (s, 1H, N=C=CH), 5.21 (s, 1H, O=C=CH), 3.99−3.84 and 3.80−3−66 (overlapping multiplets, 8H + 8H, NCH_2CH_2Py + $NCH_2PhPd(O,N)$ + $NCH_2PhPd(Cl)$), 2.84, 2.77, 2.73, 2.71, and 2.69 (s, 6H + 3H + 3H + 6H + 6H, $N(CH_3)_2Pd(Cl)$ + $N(CH_3)_2Pd(N,O)$) ppm. $^{13}C\{^1H\}$ NMR (CD_2Cl_2, 125.7 MHz) δ: 188.23 (s, O=C), 164.64 (s, N=C), 161.19 (s, C^1Py), 152.19 (s, C^5Py), 152.53 and 152.48 (s, C^5Py), 148.63 (s, C^{11}PhPd(O,N)), 147.93 (s, C^6PhPd(O,N)), 147.80 (s, C^6PhPd(Cl)), 137.31 and 137.20 (s, C^3Py), 133.27 and 133.18 (s, C^7PhPd(O,N)), 132.01 and 131.82 (s, C^7PhPd(Cl)), 125.66 and 125.55 (s, C^8PhPd(Cl)), 125.10 (s, C^2Py), 121.84 (C^4Py), 125.20, 125.16, 124.21, 124.07, 124.03, 123.99, 122.54, 122.24, 121.26, and 121.18 (s, C^{8-10}PhPd(O,N) + C^{9-10}PhPd(Cl)), 101.78 (s, O=C=C), 87.12 (s, N=C=C), 73.79 (s, $NCH_2Pd(Cl)$), 72.30 (s, $NCH_2Pd(O,N)$), 52.54, 52.45, 52.18, and 52.09 (s, $N(CH_3)_2Pd(Cl)$), 50.93 (br s, $N(CH_3)_2Pd(O,N)$), 48.01 and 47.89 (s, NCH_2CH_2Py), 42.21 and 42.14 (s, NCH_2CH_2Py) ppm. MS (ESI): m/z = 865.12 $[M + H - (Pd(dmba)) - PdCl(dmba)]^+$, 588.01 $[M + H - (Pd(dmba)) - (PdCl(dmba))_2]^+$, 516.19 $[(dmba)Pd(\mu\text{-}Cl)Pd(dmba)]^+$.

Synthesis of Complex **7**. To a solution of **6** (0.290 g, 0.21 mmol) in 10 mL of CH_2Cl_2, was added $TlPF_6$ (0.073 g, 0.21 mmol). The reaction mixture was stirred for 4 h at room temperature. After filtration, addition of *n*-pentane led to the precipitation of a green solid of **7**, which was filtered and washed with *n*-pentane. Green crystals suitable for X-ray diffraction were grown by stratification of a solution of **7** in CH_2Cl_2 with *n*-pentane. Yield: 0.259 g, 0.17 mmol (83%). Anal. Calcd for: $C_{56}H_{66}ClN_8O_2Pd_4F_6P$ (1489.29): C, 45.16; H, 4.67; N, 7.52. Found: C, 45.32; H, 4.64; N, 7.59%. FTIR: selected ν_{max}(solid)/cm^{-1}: 3049vw, 2974vw, 2914brw, 1604w, 1580vw, 1509s, 1485vw, 1468vw, 1450mw, 1403mw, 1288m, 1206vw, 1181vw, 1161vw, 1110vw, 1064vw, 1044mw, 1023mw, 987mw, 969w, 834vs, 776w, 734s, 659w, 579vw, 555vs, 518m, 469mw, 455vw, 438vw, 420m, 398w, 359m, 342vw, 327vw, 314w, 302w, 289vw, 280mw, 266w, 246s (ν(Pd−μ-Cl)), 225vs, 209vw, 202w, 177m, 158w, 151s, 140w, 133w, 121m, 104m. ^{1}H NMR (CD_2Cl_2, 500 MHz) δ: 8.62 (dd, 2H, $^3J_{H,H}$ = 4.7 Hz, $^4J_{H,H}$ = 1.5 Hz, H^5Py), 7.79 (dt, 2H, $^3J_{H,H}$ = 7.7, $^4J_{H,H}$ = 1.5 Hz, H^3Py), 7.47 (d, 2H, $^3J_{H,H}$ = 7.7 Hz, H^2Py), 7.28 (overlapping ddd, 2H, $^3J_{H,H}$ = 7.7, 4.7 Hz, $^4J_{H,H}$ = 1.5 Hz, H^4Py), 7.15 (d, 2H, $^3J_{H,H}$ = 7.6 Hz, H^7PhPd(O,N)), 7.03−6.99 and 6.96−6.93 (m, 4H + 6H, $H^{9,10}$PhPd-(μ-Cl) + $H^{8,9,10}$PhPd(O,N)), 6.58−6.54 (m, 2H, H^8PhPd(μ-Cl)), 5.35 (d, 2H, $^3J_{H,H}$ = 7.8 Hz, H^7PhPd(μ-Cl)), 5.28 (s, 1H, O=C=CH), 4.64 (s, 1H, N=C=CH), 4.10 and 3.88 (4H, AB system, $^2J_{H,H}$ = 14.2 Hz, NCHPhPd(μ-Cl)), 3.99 and 3.93 (4H, AB system, $^2J_{H,H}$ = 13.0 Hz, NCHPhPd(O,N)), the signals for the NCH_2CH_2Py protons overlap with the signals in the 4.12−3.81 range, 2.94 and 2.90 (s, 6H + 6H, $N(CH_3)_2Pd(\mu\text{-}Cl)$), 2.75 (s, 12H, $N(CH_3)_2Pd(O,N)$) ppm. $^{13}C\{^1H\}$ NMR (CD_2Cl_2, 125.7 MHz) δ: 187.92 (s, O=C), 165.19 (s, N=C), 161.43 (s, C^1Py), 152.19 (s, C^5Py), 148.89 (s, C^{11}PhPd(O,N)), 147.08 (s, C^6PhPd(O, N)), 146.67 (s, C^{11}PhPd(μ-Cl)), 143.63 (s, C^6PhPd(μ-Cl)), 138.38 (s, C^3Py), 132.39 (s, C_7PhPd(O,N)), 131.02 (s, C^7PhPd(μ-Cl)), 127.93 (s, C^2Py), 125.70, 125.18, 124.42, 123.22, and 122.28 (s, $C^{8,9,10}$PhPd(O,N)+$C_{9,10}$PhPd(μ-Cl)), 125.39 (s, C_8PhPd(μ-Cl)), 101.58 (s, O=C=C), 86.00 (s, N=C=C), 73.00 (s, $NCH_2Pd(\mu\text{-}Cl)$), 72.56 (s, $NCH_2Pd(O,N)$), 52.86 and 52.57 (s, $N(CH_3)_2Pd(\mu\text{-}Cl)$), 51.15 and 51.08 (s, $N(CH_3)_2Pd(O,N)$), 49.38 (s, NCH_2CH_2Py), 42.40 (s, NCH_2CH_2Py) ppm. MS (ESI): m/z = 829.15 $[4 + H]^+$, 516.97 $[(dmba)Pd(\mu\text{-}Cl)Pd(dmba)]^+$. MALDI-TOF-MS: m/z = 1068.14 $[4{\cdot}Pd(dmba)]^+$, 829.12 $[4 + H]^+$.

X-ray Data Collection, Structure Solution, and Refinement for All Compounds. Suitable crystals for the X-ray diffraction analysis of all compounds were obtained as described above. The intensity data for **2** and **3** were collected on a Nonius Kappa CCD diffractometer (graphite monochromated Mo Kα radiation, λ = 0.710 73 Å) at 173(2) K.[22] Data for **4**−**7** were collected on a Bruker APEX-II Kappa CCD (triumph monochromated Mo Kα radiation, λ = 0.710 73 Å). Crystallographic and experimental details for the structures are summarized in Supporting Information, Table S1. The structures were solved by direct methods (SHELXS-97) and refined by full-matrix least-squares procedures (based on F^2, SHELXL-97)[23] with anisotropic thermal parameters for all the non-hydrogen atoms. The hydrogen atoms were introduced into the geometrically calculated positions (SHELXL-97 procedures) and refined riding on the corresponding parent atoms. Except for complex **2** where the NH protons were located from Fourier difference maps and refined isotropically, for **3**, **4**, **5**, and **7** semiempirical absorption correction was applied using the MULTISCAN-ABS in PLATON[24] or SAD-ABS in APEX-II.[25] For complex **3** a SQUEEZE procedure[24] was applied, and the residual electron density was assigned to five molecules of disordered pentane. In **5**, there is half a molecule in the asymmetric unit, and a SQUEEZE procedure was also applied; the residual electron density was assigned to one molecule of acetone. In **7** a SQUEEZE procedure was also applied, and the residual electron density was assigned to one molecule of CH_2Cl_2. The thermal ellipsoid of Cl1 is flattened, but the nature of this atom was confirmed by other analytical methods.

■ ASSOCIATED CONTENT

Supporting Information

Crystallographic data, including selected bond angles and CIF files, NMR characterization of conformers **3a** and **3b**, and cyclic voltammetry for complex **4**. This material is available free of charge via the Internet at http://pubs.acs.org. Crystallographic information files (CIF) of the compounds **2**·CH_2Cl_2, **3**−**5**, and **7**·CH_2Cl_2 were deposited with the CCDC, 12 Union Road, Cambridge, CB2 1EZ, U.K., and can be obtained on request free of charge, by quoting the publication citation and deposition numbers 982040−982044.

dx.doi.org/10.1021/ic500194y | Inorg. Chem. XXXX, XXX, XXX−XXX

AUTHOR INFORMATION

Corresponding Author

*E-mail: braunstein@unistra.fr. Fax: +33 368 851 322.

Author Contributions

The manuscript was written through contributions of all authors. All authors have given approval to the final version of the manuscript.

Notes

The authors declare no competing financial interest.

ACKNOWLEDGMENTS

We are grateful to the CNRS, the Ministère de la Recherche (Paris), and the DFH/UFA (International Research Training Group 532-GRK532, Ph.D. grant to A.G.) for funding. We thank Drs. L. Karmazin-Brelot and C. Bailly, Service de Radiocrystallographie, Institut de Chimie (UMR 7177 CNRS-UdS), for the X-ray diffraction studies and the UdS NMR service for helpful suggestions. We are grateful to Prof. B. Sarkar (F.U. Berlin) for the electrochemical experiments.

DEDICATION

[†]Dedicated to Prof. Barry Lever, Distinguished Research Professor Emeritus at York University in Toronto, for his numerous and outstanding contributions to inorganic chemistry.

REFERENCES

(1) (a) Vigalok, A.; Milstein, D. *Acc. Chem. Res.* **2001**, *34*, 798. (b) Reingold, J. A.; Uk Son, S.; Bok Kim, S.; Dullaghan, C. A.; Oh, M.; Frake, P. C.; Carpenter, G. B.; Sweigart, D. A. *Dalton Trans.* **2006**, 2385. (c) Dei, A.; Gatteschi, D.; Sangregorio, C.; Sorace, L. *Acc. Chem. Res.* **2004**, *37*, 827. (d) Agarwala, H.; Das, D.; Mobin, S. M.; Mondal, T. K.; Lahiri, G. K. *Inorg. Chim. Acta* **2011**, *374*, 216. (e) Das, D.; Agarwala, H.; Chowdhury, A. D.; Patra, T.; Mobin, S. M.; Sarkar, B.; Kaim, W.; Lahiri, G. K. *Chem.—Eur. J.* **2013**, *19*, 7384. (f) Kim, S. *J. Inorg. Organomet. Polym. Mater.* **2013**, 1. (g) Schweinfurth, D.; Khusniyarov, M. M.; Bubrin, D.; Hohloch, S.; Su, C.-Y.; Sarkar, B. *Inorg. Chem.* **2013**, *52*, 10332. (h) Damas, A. l.; Ventura, B.; Axet, M. R.; Esposti, A. D.; Chamoreau, L.-M.; Barbieri, A.; Amouri, H. *Inorg. Chem.* **2010**, *49*, 10762. (i) Al-Jibori, S. *Transition Met. Chem.* **1995**, *20*, 120. (j) Das, D.; Mondal, T. K.; Chowdhury, A. D.; Weisser, F.; Schweinfurth, D.; Sarkar, B.; Mobin, S. M.; Urbanos, F. a.; Jiménez-Aparicio, R.; Lahiri, G. K. *Dalton Trans.* **2011**, *40*, 8377. (k) T. Moriuchi, T. W.; Ikeda, I.; Ogawa, A.; Hirao, T. *Eur. J. Inorg. Chem.* **2001**, 277.

(2) Braunstein, P.; Siri, O.; Taquet, J.-P.; Rohmer, M.-M.; Bénard, M.; Welter, R. *J. Am. Chem. Soc.* **2003**, *125*, 12246.

(3) Siri, O.; Braunstein, P. *Chem. Commun.* **2002**, *379*, 208.

(4) (a) Yang, Q.-Z.; Siri, O.; Braunstein, P. *Chem.—Eur. J.* **2005**, *11*, 7237. (b) Oh, M.; Carpenter, G. B.; Sweigart, D. A. *Acc. Chem. Res.* **2003**, *37*, 1. (c) Moussa, J.; Amouri, H. *Angew. Chem., Int. Ed.* **2008**, *47*, 1372.

(5) (a) Siri, O.; Taquet, J.-P.; Collin, J.-P.; Rohmer, M.-M.; Bénard, M.; Braunstein, P. *Chem.—Eur. J.* **2005**, *11*, 7247. (b) Cotton, F. A.; Jin, J.-Y.; Li, Z.; Murillo, C. A.; Reibenspies, J. H. *Chem. Commun.* **2008**, 211. (c) Schweinfurth, D.; Rechkemmer, Y.; Hohloch, S.; Deibel, N.; Peremykin, I.; Fiedler, J.; Marx, R.; Neugebauer, P.; Slageren, J. V.; Sarkar, B. *Chem.—Eur. J.* **2014**, *20*, 3475.

(6) (a) Siri, O.; Braunstein, P.; Taquet, J.-P.; Collin, J.-P.; Welter, R. *Dalton Trans.* **2007**, 1481. (b) Hohloch, S.; Braunstein, P.; Sarkar, B. *Eur. J. Inorg. Chem.* **2012**, *2012*, 546. (c) Das, H. S.; Das, A. K.; Pattacini, R.; Hübner, R.; Sarkar, B.; Braunstein, P. *Chem. Commun.* **2009**, *70*, 4387. (d) Das, D.; Mondal, T. K.; Mobin, S. M.; Lahiri, G. K. *Inorg. Chem.* **2009**, *48*, 9800. (e) Deibel, N.; Schweinfurth, D.; Huebner, R.; Braunstein, P.; Sarkar, B. *Dalton Trans.* **2011**, *40*, 431. (f) Braunstein, P.; Bubrin, D.; Sarkar, B. *Inorg. Chem.* **2009**, *48*, 2534. (g) Deibel, N.; Hohloch, S.; Sommer, M. G.; Schweinfurth, D.; Ehret, F.; Braunstein, P.; Sarkar, B. *Organometallics* **2013**, *32*, 7366.

(7) (a) Yang, Q.-Z.; Kermagoret, A.; Agostinho, M.; Siri, O.; Braunstein, P. *Organometallics* **2006**, *25*, 5518. (b) Taquet, J.-P.; Siri, O.; Braunstein, P.; Welter, R. *Inorg. Chem.* **2004**, *43*, 6944.

(8) Braunstein, P.; Siri, O.; Steffanut, P.; Winter, M.; Yang, Q. *C. R. Chim.* **2006**, *9*, 1493.

(9) (a) Simpson, S.; Kunkel, D. A.; Hooper, J.; Nitz, J.; Dowben, P. A.; Routaboul, L.; Braunstein, P.; Doudin, B.; Enders, A.; Zurek, E. *J. Phys. Chem. C* **2013**, *117*, 16406. (b) Dowben, P. A.; Kunkel, D. A.; Enders, A.; Rosa, L. G.; Routaboul, L.; Doudin, B.; Braunstein, P. *Top. Catal.* **2013**, *56*, 1096. (c) Routaboul, L.; Braunstein, P.; Xiao, J.; Zhang, Z.; Dowben, P. A.; Dalmas, G.; Da Costa, V.; Félix, O.; Decher, G.; Rosa, L. G.; Doudin, B. *J. Am. Chem. Soc.* **2012**, *134*, 8494. (d) Rosa, L. G.; Velev, J.; Zhang, Z.; Alvira, J.; Vega, O.; Diaz, G.; Routaboul, L.; Braunstein, P.; Doudin, B.; Losovyj, Y. B.; Dowben, P. A. *Phys. Status Solidi B* **2012**, *249*, 1571. (e) Kong, L.; Perez Medina, G. J.; Colón Santana, J. A.; Wong, F.; Bonilla, M.; Colón Amill, D. A.; Rosa, L. G.; Routaboul, L.; Braunstein, P.; Doudin, B.; Lee, C.-M.; Choi, J.; Xiao, J.; Dowben, P. A. *Carbon* **2012**, *50*, 1981. (f) Xiao, J.; Zhang, Z.; Wu, D.; Routaboul, L.; Braunstein, P.; Doudin, B.; Losovyj, Y. B.; Kizilkaya, O.; Rosa, L. G.; Borca, C. N.; Gruverman, A.; Dowben, P. A. *Phys. Chem. Chem. Phys.* **2010**, *12*, 10329. (g) Kong, L.; Routaboul, L.; Braunstein, P.; Park, H.-G.; Choi, J.; Cordova, J. P. C.; Vega, E.; Rosa, L. G.; Doudin, B.; Dowben, P. A. *RSC Adv.* **2013**, *3*, 10956. (h) Fang, Y.; Nguyen, P.; Ivasenko, O.; Aviles, M. P.; Kebede, E.; Askari, M. S.; Ottenwaelder, X.; Ziener, U.; Siri, O.; Cuccia, L. A. *Chem. Commun.* **2011**, *47*, 11255.

(10) (a) Yang, Q.-Z.; Siri, O.; Braunstein, P. *Chem. Commun.* **2005**, *5*, 2660. (b) Tamboura, F. B.; Cazin, C. S. J.; Pattacini, R.; Braunstein, P. *Eur. J. Org. Chem.* **2009**, *2009*, 3340.

(11) (a) McNitt, K. A.; Parimal, K.; Share, A. I.; Fahrenbach, A. C.; Witlicki, E. H.; Pink, M.; Bediako, D. K.; Plaisier, C. L.; Le, N.; Heeringa, L. P.; Griend, D. A. V.; Flood, A. H. *J. Am. Chem. Soc.* **2009**, *131*, 1305. (b) Kalny, D.; Elhabiri, M.; Moav, T.; Vaskevich, A.; Rubinstein, I.; Shanzer, A.; Albrecht-Gary, A.-M. *Chem. Commun.* **2002**, 1426. (c) Bofinger, R.; Ducrot, A.; Jonusauskaite, L.; McClenaghan, N. D.; Pozzo, J.-L.; Sevez, G.; Vives, G. *Aust. J. Chem.* **2011**, *64*, 1301. (d) Kuwamura, N.; Kitano, K. i.; Hirotsu, M.; Nishioka, T.; Teki, Y.; Santo, R.; Ichimura, A.; Hashimoto, H.; Wright, L. J.; Kinoshita, I. *Chem.—Eur. J.* **2011**, *17*, 10708. (e) Murahashi, T.; Shirato, K.; Fukushima, A.; Takase, K.; Suenobu, T.; Fukuzumi, S.; Ogoshi, S.; Kurosawa, H. *Nat. Chem.* **2012**, *4*, 52. (f) Zelikovich, L.; Libman, J.; Shanzer, A. *Nature* **1995**, *374*, 790.

(12) (a) Schuster, E. M.; Botoshansky, M.; Gandelman, M. *Organometallics* **2009**, *28*, 7001. (b) Chao, S. T.; Lara, N. C.; Lin, S.; Day, M. W.; Agapie, T. *Angew. Chem., Int. Ed.* **2011**, *50*, 7529.

(13) Knight, J. C.; Amoroso, A. J.; Edwards, P. G.; Prabaharan, R.; Singh, N. *Dalton Trans.* **2010**, *39*, 8925.

(14) Beves, J. E.; Blanco, V.; Blight, B. A.; Carrillo, R.; D'Souza, D. M.; Howgego, D.; Leigh, D. A.; Slawin, A. M. Z.; Symes, M. D. *J. Am. Chem. Soc.* **2014**, *136*, 2094.

(15) Kojima, T.; Sakamoto, T.; Matsuda, Y. *Inorg. Chem.* **2004**, *43*, 2243.

(16) Chen, X.; Engle, K. M.; Wang, D.-H.; Yu, J.-Q. *Angew. Chem., Int. Ed.* **2009**, *48*, 5094.

(17) (a) Croizat, P.; Müller, F.; Mantz, H.; Englisch, A.; Welter, R.; Hüfner, S.; Braunstein, P. *C. R. Chim.* **2009**, *12*, 1228. (b) Soriaga, M. P.; Binamira-Soriaga, E.; Hubbard, A. T.; Benziger, J. B.; Pang, K. W. P. *Inorg. Chem.* **1985**, *24*, 65.

(18) Yang, Q.-Z.; Siri, O.; Brisset, H.; Braunstein, P. *Tetrahedron Lett.* **2006**, *47*, 5727.

(19) Khokarale, S. G.; García-Suárez, E. J.; Xiong, J.; Mentzel, U. V.; Fehrmann, R.; Riisager, A. *Catal. Commun.* **2014**, *44*, 73.

(20) Clark, R. J. H.; Natile, G.; Belluco, U.; Cattalini, L.; Filippin, C. *J. Chem. Soc. A* **1970**, 659.

(21) Deeming, A. J.; Rothwell, I. P.; Hursthouse, M. B.; New, L. *Dalton Trans.* **1978**, *7*, 1490.

(22) Siri, O.; Braunstein, P.; Rohmer, M.-M.; Bénard, M.; Welter, R. *J. Am. Chem. Soc.* **2003**, *125*, 13793.
(23) Roberts, D. A.; Steinmetz, G. R.; Breen, M. J.; Shulman, P. M.; Morrison, E. D.; Duttera, M. R.; Debrosse, C. W.; Whittle, R. R.; Geoffroy, G. L. *Organometallics* **1983**, *2*, 846.
(24) Siri, O.; Braunstein, P. *Chem. Commun.* **2000**, 2223.
(25) Das, M. C.; Xiang, S.; Zhang, Z.; Chen, B. *Angew. Chem., Int. Ed.* **2011**, *50*, 10510.
(26) Dai, L.-X.; Zhou, Z.-H.; Zhang, Y.-Z.; Ni, C.-Z.; Zhang, Z.-M.; Zhou, Y.-F. *Chemm. Commun.* **1987**, 1760.
(27) (a) Braunstein, P.; Dehand, J.; Pfeffer, M. *Inorg. Nucl. Chem. Lett.* **1974**, *10*, 521. (b) Crociani, B.; Boschi, T.; Pietropaolo, R.; Belluco, U. *J. Chem. Soc. A* **1970**, 531.
(28) Cope, A. C.; Friedrich, E. C. *J. Am. Chem. Soc.* **1968**, *90*, 909.

dx.doi.org/10.1021/ic500194y | *Inorg. Chem.* XXXX, XXX, XXX−XXX

CHAPITRE 6

Ce chapitre est présenté sous forme d'une publication parue dans *Dalton Trans.*, **2014**, 43, 7847.

Les contributions respectives des auteurs sont :

A. Ghisolfi, K.Yu. Monakhov, P. Braunstein – *développement du projet*

A. Ghisolfi – *Synthèse et caractérisation du ligand et des complexes*

K. Yu. Monakhov, X. López, C. de Graaf – *Calculs DFT*

M. Speldrich, J. van Leusen, H. Schilder, P. Kögerler, K. Yu. Monakhov – *études des propriétés magnétiques*

R. Pattacini – *étude structurale par diffraction des rayons X*

A comparative synthetic, magnetic and theoretical study of functional M_4Cl_4 cubane-type Co(II) and Ni(II) complexes

Alessio Ghisolfi,[a] Kirill Yu. Monakhov,*[b] Roberto Pattacini,[a] Pierre Braunstein,*[a] Xavier López,[c] Coen de Graaf,[c,d] Manfred Speldrich,[b] Jan van Leusen,[b] Helmut Schilder[b] and Paul Kögerler*[b,e]

[a]Laboratoire de Chimie de Coordination, Institut de Chimie (UMR 7177 CNRS), Université de Strasbourg, 4 rue Blaise Pascal, 67081 Strasbourg, France.

[b]Institut für Anorganische Chemie, RWTH Aachen University, Landoltweg 1, 52074 Aachen, Germany.

[c]Departament de Química Física i Inorgànica, Universitat Rovira i Virgili, c/Marcel·lí Domingo s/n, 43007 Tarragona, Spain

[d]Institució Catalana de Recerca y Estudis Avançats (ICREA), Passeig Lluís Companys 23, 08010 Barcelona, Spain

[e]Peter Grünberg Institute (PGI-6), Forschungszentrum Jülich, 52425 Jülich, Germany

Des informations complémentaires sont disponibles sur internet:

http://www.rsc.org/suppdata/dt/c4/c4dt00306c/c4dt00306c1.pdf

Résumé du Chapitre 6

Deux nouveaux complexes possédant une structure de type cubane [M(μ3-Cl)Cl(**HL(S)**)]4 (M = Co, Ni) ont été préparés par réaction de $CoCl_2$ et de $NiCl_2$ avec le nouveau ligand pyridyl-alcool **HL(S)** qui possède une fonction thio-éther cyclique sur le substituant en ortho de la pyridine, bien adapté pour interagir avec des surfaces métalliques. Ces complexes ont été caractérisés par analyses élémentaires, spectrométrie infrarouge, analyses thermogravimétriques et par diffraction des rayons X. Leurs propriétés magnétiques ont été étudiées et analysées à l'aide de calculs DFT. Bien que les structures des complexes du Co(II) et du Ni(II) soient quasi identiques, ces deux complexes présentent des propriétés physiques très différentes. Le cubane de Co(II) est moins stable (DFT) que celui du Ni(II), et même si les deux complexes sont paramagnétiques, le complexe du Ni a un comportement de SMM (Single Molecule Magnet) alors que celui du Co(II) est le siège de couplages antiferromagnétiques. Cette particularité, associée à la présence d'un groupement thio-éther, font de ce composé de Ni un très bon candidat pour la fonctionnalisation d'une surface d'Au(111).

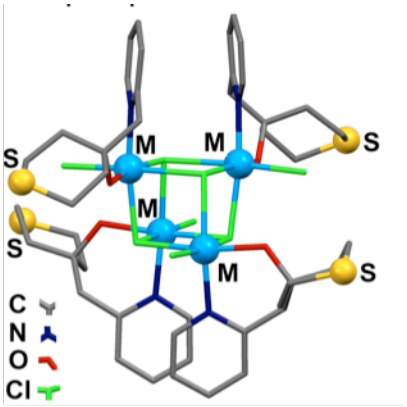

M = Ni, Co

Published on 10 March 2014. Downloaded by Université de Strasbourg, Service Commun de la Documentation on 09/04/2014 10:04:09.

Dalton Transactions

PAPER

View Article Online
View Journal

A comparative synthetic, magnetic and theoretical study of functional M_4Cl_4 cubane-type Co(II) and Ni(II) complexes†

Cite this: DOI: 10.1039/c4dt00306c

Alessio Ghisolfi,[a] Kirill Yu. Monakhov,*[b] Roberto Pattacini,[a] Pierre Braunstein,*[a] Xavier López,[c] Coen de Graaf,[c,d] Manfred Speldrich,[b] Jan van Leusen,[b] Helmut Schilder[b] and Paul Kögerler*[b,e]

We describe the synthesis, structures, and magnetochemistry of new M_4Cl_4 cubane-type cobalt(II) and nickel(II) complexes with the formula $[M(\mu_3\text{-}Cl)Cl(\mathbf{HL{\cdot}S})]_4$ (**1**: M = Co; **2**: M = Ni), where **HL·S** represents a pyridyl-alcohol-type ligand with a thioether functional group, introduced to allow subsequent binding to Au surfaces. Dc and ac magnetic susceptibility data of **1** and **2** were modeled with a full spin Hamiltonian implemented in the computational framework CONDON 2.0. Although both coordination clusters **1** and **2** are isostructural, with each of their transition metal ions in a pseudo-octahedral coordination environment of four Cl atoms and N,O-donor atoms of one chelating **HL·S** ligand, the substantially different ligand field effects of Co(II) and Ni(II) results in stark differences in their magnetism. In contrast to compound **1** which exhibits a dominant antiferromagnetic intramolecular coupling (J = −0.14 cm^{-1}), **2** is characterised by a ferromagnetic coupling (J = +10.6 cm^{-1}) and is considered to be a single-molecule magnet (SMM), a feature of special interest for future surface deposition studies. An analysis based on density functional theory (DFT) was performed to explore possible magnetostructural correlations in these compounds. Using a two-J model Hamiltonian, it revealed that compound **1** has four positive and two (small) negative $J_{Co\cdots Co}$ isotropic interactions leading to a S_{HS} = 6 ground state. Taking into account the magnetic anisotropy, one would recover a M_S = 0 ground state since D > 0 from computations. In **2**, all the J constants are positive and, in this framework, the zero-field splitting energy characterising the axial anisotropy was estimated to be negative (D = −0.44 cm^{-1}). The computational results are consistent with compound **2** being an SMM.

Received 28th January 2014,
Accepted 9th March 2014

DOI: 10.1039/c4dt00306c

www.rsc.org/dalton

Introduction

In the course of studies originally devoted to the development of new homogeneous Ni(II) pre-catalysts for ethylene oligomerisation,[1] we have reported in recent years on the synthesis, structures and magnetic behaviour of cubane-, pseudo-cubane-, and wheel-shaped complexes formed in the reactions between chelating pyridyl-alcohol/-ate ligands and Ni(II) precursors.[2] For comparison, extensions to the assembly of Co(II) ions using the same N,O ligands were performed.[3] In view of the interesting magnetic properties[4] displayed by some of the resulting structures, including slow relaxation of the magnetisation, we considered the possibility of functionalising such structurally well-defined coordination clusters by electron donating groups in order to assist their subsequent adsorption on a metal surface (substrate). Surface-grafted molecules[5] with magnetic responses are indeed of high current interest in the area of spin transport electronics that interfaces synthetic chemistry with molecular magnetism[6] and condensed matter physics.

Although thiol (−SH) groups exhibit a high affinity for gold, thus allowing the covalent binding of molecules to a substrate or offering a well-defined tunnelling interface in a single-molecule junction between two Au electrodes,[7] their sensitivity

[a]Laboratoire de Chimie de Coordination, Institut de Chimie (UMR 7177 CNRS), Université de Strasbourg, 4 rue Blaise Pascal, 67081 Strasbourg, France. E-mail: braunstein@unistra.fr
[b]Institut für Anorganische Chemie, RWTH Aachen University, Landoltweg 1, 52074 Aachen, Germany. E-mail: kirill.monakhov@ac.rwth-aachen.de, paul.koegerler@ac.rwth-aachen.de
[c]Departament de Química Física i Inorgànica, Universitat Rovira i Virgili, c/Marcel·lí Domingo s/n, 43007 Tarragona, Spain
[d]Institució Catalana de Recerca i Estudis Avançats (ICREA), Passeig Lluís Companys 23, 08010 Barcelona, Spain
[e]Peter Grünberg Institute (PGI-6), Forschungszentrum Jülich, 52425 Jülich, Germany

†Electronic supplementary information (ESI) available: Crystallographic data of **1** and **2** and details of DFT calculations. CCDC 964328 and 964329. For ESI and crystallographic data in CIF or other electronic format see DOI: 10.1039/c4dt00306c

Published on 10 March 2014. Downloaded by Université de Strasbourg, Service Commun de la Documentation on 09/04/2014 10:04:09.

towards oxidation limits the application of thiol-containing metal complexes. In contrast, thioether functions are air-stable and also allow molecular anchoring to surfaces.[8] We thus aimed at the synthesis of a new polytopic multidentate ligand containing a pendant thioether group along with N,O-donor groups, which were shown previously to provide effective chelation of metal ions in coordination clusters. As a result, we describe here the synthesis and structural chemistry of open-shell cubane-type cobalt(II) (**1**) and nickel(II) (**2**) complexes resulting from the coordination of a new tridentate pyridyl-alcohol-type ligand to Co(II) and Ni(II) centres. Decorated at their periphery with thioether functions,[9] the isostructural nature of the complexes $[M(\mu_3\text{-}Cl)Cl(\mathbf{HL{\cdot}S})]_4$ (**1**: M = Co; **2**: M = Ni) provides an ideal basis for a detailed comparative experimental and computational analysis of their molecular magnetic characteristics. These comparisons have led to a clear-cut identification and understanding of the similarities and differences between **1** and **2**. Herein, we discuss the dc and ac magnetic susceptibility, the magnetochemical modelling with our computational framework CONDON 2.0 for molecular spin structures,[10] and the results of *broken-symmetry* DFT[11] calculations. We note that although cubane-shaped coordination clusters are numerous in transition metal chemistry, a direct comparison between the magnetic properties of two isostructural compounds is rather rare,[12] despite its great fundamental interest since the spin exchange interactions and the single-ion effects in such metal complexes are frequently difficult to deconvolute.

Results and discussion

Synthesis of the complexes and description of their crystal structures

To increase the coordination versatility of the pyridyl-alcohol ligands used in previous studies on polynuclear open-shell transition metal compounds,[2,3] we designed a tridentate ligand comprising N, O, and S donor atoms. The new ligand 4-(pyridin-2-ylmethyl)tetrahydro-2*H*-thiopyran-4-ol (=**HL·S**) with amino-alcohol and dialkyl sulphide (or thioether) functional groups was synthesised in good yield (73%) by reaction of lithiated 2-picoline with tetrahydro-4*H*-thiopyran-4-one in THF (Scheme 1).

The reaction of one equivalent of the **HL·S** ligand with one equivalent of $CoCl_2$ or $[NiCl_2(dme)]$ (dme = dimethoxyethane) in THF at room temperature afforded tetranuclear cubanes: the blue Co(II) complex $[Co(\mu_3\text{-}Cl)Cl(\mathbf{HL{\cdot}S})]_4$ (**1**) and the yellow Ni(II) complex $[Ni(\mu_3\text{-}Cl)Cl(\mathbf{HL{\cdot}S})]_4$ (**2**), in *ca.* 63% and 74% yield, respectively (Scheme 2). According to thermogravimetric analyses (TGA), **2** exhibits higher thermal stability against degradation under N_2 than **1**. The crystallinity of **1** and **2** was retained upon heating to *ca.* 210 °C and 250 °C, respectively. Broad signals in the ^1H and ^{13}C NMR spectra of **1** and **2** pointed to the magnetic nature of these complexes.

The solid-state molecular structures of **1** and **2** were established by single-crystal X-ray diffraction analyses.[13] Both **1** and **2** crystallise in the tetragonal space group $I4_1/a$ (Table S1, ESI†), have crystallographically imposed S_4 symmetry and display cubane-like $\{M_4(\mu_3\text{-}Cl)_4\}$ core structures composed of four mononuclear $[MCl_2(\mathbf{HL{\cdot}S})]$ formula isomers (Fig. 1).

Each metal centre in the isostructural complexes **1** and **2** is coordinated by one terminal Cl atom, three triply-bridging μ_3-Cl atoms, and one **HL·S** ligand chelated through the N,O-donor atoms. Alternatively, these structures can be viewed as formed by two interpenetrating M_4 and Cl_4 tetrahedra. The S atoms in the tail of the **HL·S** chelate are not involved in any coordination bond (Fig. 1); no specific structural influence of the thioether functions was thus identified at this stage. The divalent metal centres in the representative structures are in local pseudo-octahedral environments, with the metal–ligand bonds in the $\{CoCl_4NO\}$ fragments being slightly longer than those in the $\{NiCl_4NO\}$ ones (Fig. 2).

There are four shorter (**1**: $d_{Co\cdots Co}$ = 3.6804(5) Å; **2**: $d_{Ni\cdots Ni}$ = 3.6029(6) Å) and two longer (**1**: $d_{Co\cdots Co}$ = 3.8559(5) Å; **2**: $d_{Ni\cdots Ni}$ = 3.7378(6) Å) sets of non-bonding metal···metal separations in **1** and **2**. As a result, the central $\{Ni_4(\mu_3\text{-}Cl)_4\}$ cubane core of **2** is somewhat contracted with respect to the $\{Co_4(\mu_3\text{-}Cl)_4\}$ core of **1**, in line with the differences between the crystal radii ($\sum r_{cryst}$) and the effective ionic radii ($\sum r_{ion}$) of the hexa-coordinate Co and Ni dications ($\sum r_{cryst}$: 0.89 Å for high-spin Co^{2+} and 0.83 Å for Ni^{2+}; $\sum r_{ion}$: 0.75 Å for high-spin Co^{2+} and 0.69 Å for Ni^{2+}) or the covalent radii ($\sum r_{cov}$) of the Co and Ni atoms ($\sum r_{cov}$: 1.50 Å for high-spin Co and 1.24 Å for Ni).[14] The magnetic relevant M–(μ_3-Cl)–M bond angles fall in the ranges 93.48(2)–98.38(2)° for **1** (M = Co) and 93.88(3)–97.43(3)° for **2** (M = Ni).

Note that cubane-like structures with cobalt[15] and nickel[2,16] ions are not scarce but generally feature $\{M_4(\mu_3\text{-}O)_4\}$ cubane

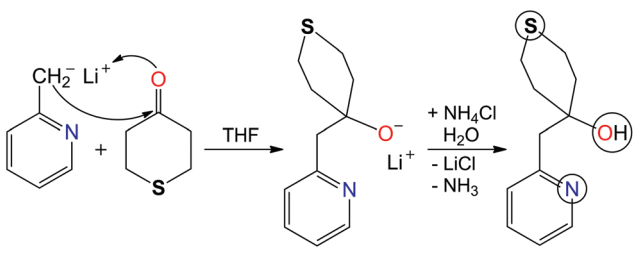

Scheme 1 Synthesis of the tridentate **HL·S** ligand (right) from lithiated 2-picoline and tetrahydro-4*H*-thiopyran-4-one (left).

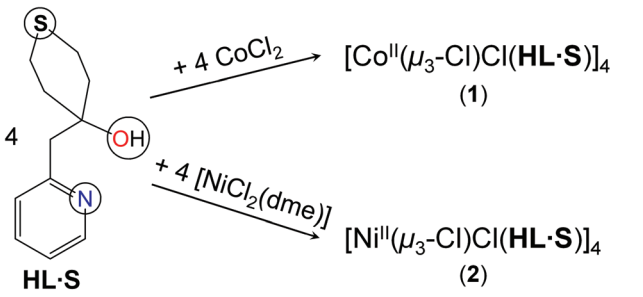

Scheme 2 Synthesis of the tetranuclear Co(II) and Ni(II) complexes with the general formula $[M(\mu_3\text{-}Cl)Cl(\mathbf{HL{\cdot}S})]_4$ (**1**: M = Co; **2**: M = Ni).

 This journal is © The Royal Society of Chemistry 2014

Published on 10 March 2014. Downloaded by Université de Strasbourg, Service Commun de la Documentation on 09/04/2014 10:04:09.

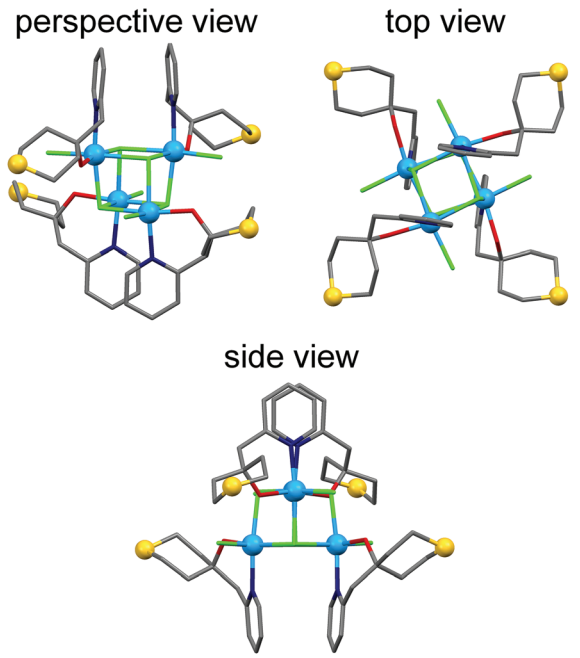

Fig. 1 Different views of the molecular structures of **1** and **2**. Hydrogen atoms are omitted for clarity. Colour code: C, dark grey; N, dark blue; O, red; S, yellow; Cl, light green; M, light blue (**1**: M = Co; **2**: M = Ni). The metal and sulphur atoms are represented as ball-and-stick models.

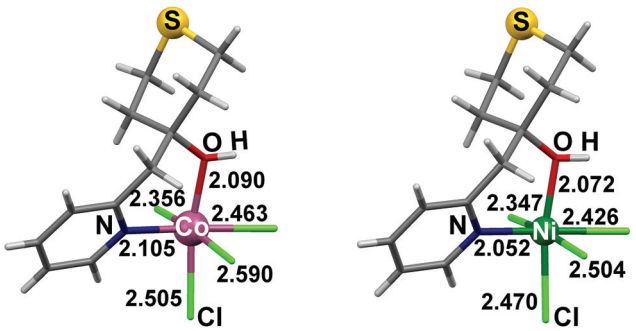

Fig. 2 Pseudo-octahedral coordination geometries of the Co(II) and Ni(II) centres constitutive of **1** and **2**, respectively. Relevant bond lengths (Å) are shown and more details are provided in the caption of Fig. 3.

cores. The first cubane-shaped Co(II) SMM, $[Co(hmp)(MeOH)Cl]_4$ (hmp^- = 2-hydroxymethylpyridine), was reported in 2002[17] and the first cubane-shaped Ni(II) SMMs, $[Ni(hmp)(ROH)Cl]_4$ (R=Me, CH_2Me, $CH_2CH_2CMe_3$), in 2003.[18] Despite the various ligand systems that have been used to form cubane-type Co(II) and Ni(II) complexes, **1** and **2** belong to the rare family of compounds with the general formula $[MX_2Z_2]_4$ where M is a divalent transition metal, X a halogen, and Z a two-electron donor ligand.[2c,19] Thus, **1** represents the first cubane complex having the core vertices occupied by four Co(II) centres and four μ_3-capping halides (X = Cl) and **2** is a rare representative of the family of compounds displaying a $\{Ni_4(\mu_3\text{-}X)_4\}$ cubane core (X = F, Cl).[2c,16h,y] Their magnetochemistry is not yet fully understood.

Another interesting feature shared by complexes **1** and **2** is the intramolecular O–H···Cl non-classical hydrogen bonding[2c,16j,l] illustrated in Fig. 3. Each of the four terminal Cl atoms in **1** and **2** is involved in such a bonding to the H atom from the closest OH functional group of the **HL·S** ligand. The four resulting O–H···Cl interactions, fully identical in each cluster ($d_{O\cdots Cl}$ = 3.233(2) Å in **1** and 3.206(3) Å in **2**), are likely to substantially contribute to the stability of these cubane-like structures. An additional source of stabilisation associated with the self-aggregation of the mononuclear $[MCl_2(\mathbf{HL{\cdot}S})]$ units leading to the formation of **1** or **2** may be the intramolecular π–π stacking interactions between crystallographically pairwise parallel pyridyl (Py) fragments of the **HL·S** ligands (Fig. 1). The intramolecular distances between the geometrical centres of these Py rings are $d(\pi_{Py}\cdots\pi_{Py})$ = 3.770(2) Å in **1** and 3.757(2) Å in **2**.

Magnetism and magnetochemical modelling

The molecular magnetism of complexes **1** and **2** was studied by measuring the dc and ac magnetic susceptibility, and the results obtained were analysed using the CONDON 2.0 computational framework.[10] The magnetochemical analysis of Co(II) complexes is commonly complicated by a multitude of factors,[3] notably the fact that the Co^{2+} free-ion ^4F ground term is separated from the first excited term ^4P by more than 10^4 cm^{-1}.[20] In a weak ligand field with octahedral symmetry, the ^4F term splits into the $^4T_1(F)$, $^4T_2$, and $^4A_2$ states, whereas the ^4P term transforms into a $^4T_1(P)$ state. The magnetic properties of high-spin octahedral Co(II) ($3d^7$) complexes are characterised by a significant temperature dependence of the magnetic moment μ_{eff} caused by orbital momentum contributions due to the $^4T_1(F)$ ground state. On the other hand, high-spin octahedral Ni(II) ($3d^8$) complexes with an orbital singlet ground state $^3A_2(F)$ represent near-ideal pure spin systems.[21]

Due to the two types of ligands (Cl *vs.* N, O of **HL·S**) present in **1** and **2**, a proper description of the ligand field around the

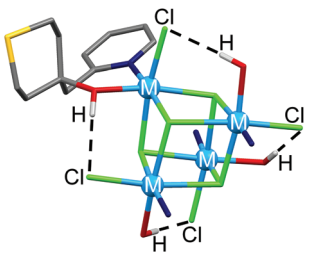

Fig. 3 Weak intramolecular O–H···Cl interactions in the $[M(\mu_3\text{-}Cl)Cl(\mathbf{HL{\cdot}S})]_4$ complexes (**1**: M = Co; **2**: M = Ni). For clarity, only one **HL·S** ligand is explicitly depicted. Hydrogen atoms, except those from the OH functional groups, are omitted for clarity. Selected bond lengths (Å) for **1**: Co–μ_3-Cl 2.4629(6), 2.5046(7), 2.5896(7); Co–Cl 2.3558(7); Co–N 2.105(2); Co–O 2.090(2). Selected bond lengths (Å) for **2**: Ni–μ_3-Cl 2.4264(9), 2.4700(9), 2.5042(9); Ni–Cl 2.347(1); Ni–N 2.052(3); Ni–O 2.072(3). Colour code: H, off-white; C, dark grey; N, dark blue; O, red; S, yellow; Cl, light green; M, light blue. ORTEPs of the structures are reported in the ESI† with the complete labeling scheme of the heteroatoms (Fig. S1 and S2†).

Published on 10 March 2014. Downloaded by Université de Strasbourg, Service Commun de la Documentation on 09/04/2014 10:04:09.

magnetic centres needs to include C_{2v} instead of octahedral symmetry. This, combined with spin–orbit coupling, leads to further splitting of the states into Kramer's doublets (**1**) or B_1 singlets (**2**).

Results for [Co(μ$_3$-Cl)Cl(HL·S)]$_4$ (1). The temperature dependence of the effective magnetic moment μ_{eff} and of the reciprocal molar susceptibility χ_m^{-1} (dc measurements) for various applied magnetic fields is shown in Fig. 4. The μ_{eff} of **1** at 300 K is 9.71 and lies within the range 8.6–10.4 expected as a result of spin and first-order orbital contributions for high-spin Co(II) complexes with negligible exchange interaction contributions.[22] Since μ_{eff} shows almost pure single-ion effects and no maximum at low temperatures, only weak antiferromagnetic (AFM) net exchange interactions are anticipated.

For simulations of the dc susceptibility data, CONDON 2.0[10] allows us to reproduce both intramolecular exchange coupling and single-ions effects: interelectronic repulsion ($\hat{H}_{ee}$), spin–orbit coupling ($\hat{H}_{so}$), the ligand-field effect ($\hat{H}_{lf}$), and the Zeeman effect of an applied field ($\hat{H}_{mag}$). In particular, the Landé factor can be treated as the physical constant g = 2.00232 for all elements and not a fitting parameter. Intramolecular exchange between magnetic centres was modeled using the Heisenberg approach:

$$\hat{H}_{ex} = -J_1(\hat{S}_1 \cdot \hat{S}_2 + \hat{S}_3 \cdot \hat{S}_4) - J_2(\hat{S}_1 \cdot \hat{S}_3 + \hat{S}_2 \cdot \hat{S}_4 + \hat{S}_1 \cdot \hat{S}_4 + \hat{S}_2 \cdot \hat{S}_3).$$

The following standard Racah and spin–orbit constants were employed for Co(II):[20c] B = 1115 cm^{-1}, C = 4366 cm^{-1}, and ζ = 533 cm^{-1}. The ligand-field effects, spin–orbit coupling and exchange coupling have all been taken into account. To limit the number of free parameters, we restricted the modelling procedure to a uniform ligand field environment for all four Co(II) sites. Due to the otherwise enormous demand for main memory, the basis sets for each Co(II) (full basis: 120 microstates per ion, *i.e.* 120^4 microstates for the whole complex) had to be reduced. An elegant solution is the implementation of the combined model[23] that applies the full Hamiltonian to the ground state (and optionally following excited states) and models the exchange interactions of a definite number of higher excited states in the molecular-field approximation. Thus, this approach includes possible anisotropic exchange interactions and simultaneously reduces the number of fit parameters. Based on an analysis of the splitting of the energy states in a C_{2v}-symmetric ligand-field, it is sufficient to take four microstates (related to $^4B_1$) for the full Hamiltonian and an additional 12 (= 8 + 4) for the molecular-field approximation, *i.e.* 16 microstates for each Co(II) in **1**.

The fit procedure yielded the ligand-field parameters given in Table 1 (Wybourne notation) and a uniform interaction parameter $J_1 = J_2 = -0.14$ cm^{-1}. This best fit describes the structure of **1** with very weakly interacting Co(II) centres, *i.e.* quasi-isolated centres. The energy gap between the ground and the first excited doublet of a single Co(II) is 45 cm^{-1}, leading to a corresponding gap of 0.04 cm^{-1} for the cubane-like structure.

The ac susceptibility measurements revealed no significant out-of-phase components for **1**, thus confirming the dc measurement and indicating no SMM behaviour for this compound. It is interesting to note that the cubane-type complexes featuring a {Co$_4$(μ$_3$-O)$_4$} core are usually SMMs.[15,17]

Results for [Ni(μ$_3$-Cl)Cl(HL·S)]$_4$ (2). The temperature-dependence of the effective magnetic moment μ_{eff} and of the reciprocal molar susceptibility χ_m^{-1} (dc measurements) for various applied magnetic fields is shown in Fig. 5. The μ_{eff} of **2** of 6.58 at 300 K is close to the upper limit of the range 5.6–7.0 expected for spin contributions of four non-interacting high-spin Ni(II) centres.[22] Since μ_{eff} shows a clear deviation from pure single-ion effects in terms of a maximum at low temperatures, ferromagnetic (FM) net exchange interactions are anticipated.

The fitting procedure used for **2** was similar to that for **1** but using the following standard Racah and spin–orbit constants for Ni(II):[20c] B = 1084 cm^{-1}, C = 4831 cm^{-1}, and ζ = 649 cm^{-1}. The full basis set for Ni(II) of 45 microstates per ion was reduced based on the analysis of the splitting of the energy states. It is sufficient to take three microstates (related to $^3B_1$) for the full Hamiltonian and an additional 9 (= 6 + 3) for the molecular-field approximation, *i.e.* 12 microstates for each Ni(II) in **2**.

The fit yielded the ligand-field parameters given in Table 1 (Wybourne notation) and a uniform interaction parameter J_1 =

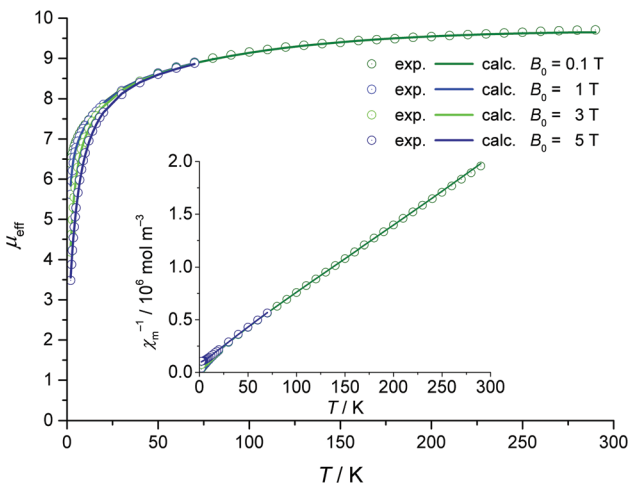

Fig. 4 Temperature dependence of μ_{eff} and χ_m^{-1} (inset) for **1**.

Table 1 Ligand-field (Wybourne notation) and exchange coupling parameters of **1** (M = Co) and **2** (M = Ni)

	1	**2**
B^2_0/cm^{-1}	−13 800	−8650
B^2_2/cm^{-1}	32 200	22 080
B^4_0/cm^{-1}	−17 780	7850
B^4_2/cm^{-1}	13 700	−16 920
B^4_4/cm^{-1}	16 600	15 700
$J_1 = J_2$/cm^{-1}	−0.14	+10.6
SQX[a]/%	1.4	1.0

[a] SQX = $(FQ/n)^{1/2}$, FQ = $\sum_i (\chi_{m,\,obs}(i) - \chi_{m,\,calc}(i))^2/(\chi_{m,\,obs}(i))^2$.

 This journal is © The Royal Society of Chemistry 2014

Published on 10 March 2014. Downloaded by Université de Strasbourg, Service Commun de la Documentation on 09/04/2014 10:04:09.

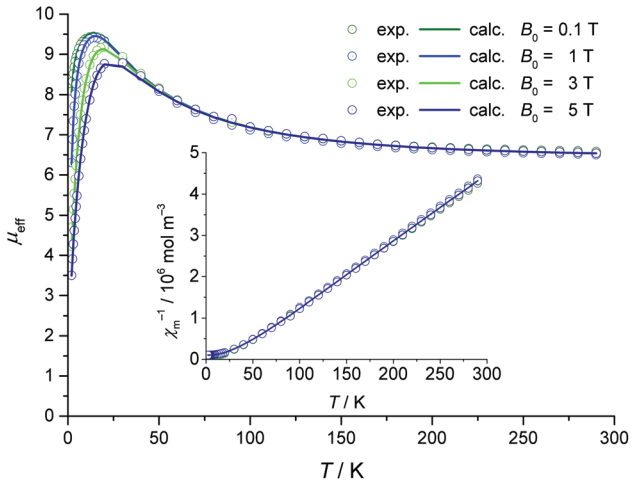

Fig. 5 Temperature-dependence of μ_{eff} and χ_m^{-1} (inset) for **2**.

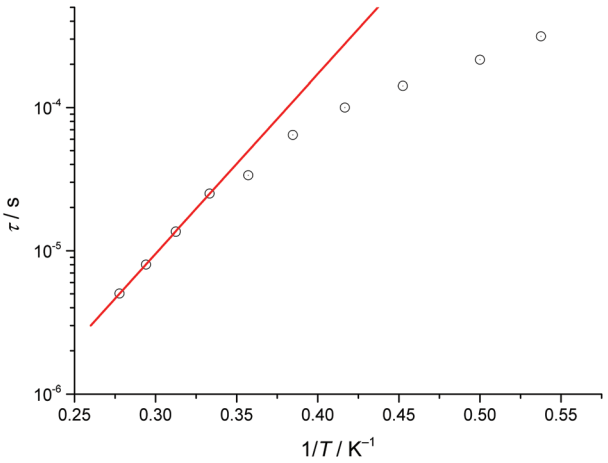

Fig. 7 Arrhenius plot to determine the relaxation constant τ_0 and the effective relaxation energy barrier ΔE of **2**.

J_2 = +10.6 cm^{-1}. This best fit describes the structure of **2** with the Ni(II) centres exhibiting ferromagnetic exchange interactions. The energy gap between the ground state and the first excited singlet of a single Ni(II) is 14 cm^{-1}, leading to a corresponding gap of 2.3 cm^{-1} for the cubane-like structure.

The ac susceptibility measurements of **2** were performed to determine whether an effective slowing-down of the relaxation of the magnetisation can be observed after changing the external field. This behaviour is a fundamental feature of an SMM.[24,25]

The variation of the in-phase and out-of-phase ac molar susceptibilities (χ'_m and χ''_m, respectively) as a function of temperature is depicted in Fig. 6. The susceptibility components were measured with an ac amplitude of 3 Gauss and no dc bias, and revealed slow relaxation behaviour up to 3.8 K.

For each temperature, the data were fitted to a Cole–Cole equation.[26] To determine the relaxation constant τ_0 and the effective relaxation energy barrier ΔE on the basis of an Arrhenius expression $\tau = \tau_0 \exp(\Delta E/(k_B T))$, the corresponding parameters of the Cole–Cole fitting procedure above the quantum regime ($T > 3$ K) were considered (Fig. 7).

The resulting parameters are ΔE = 20.1 ± 0.1 cm^{-1} and τ_0 = (1.64 ± 0.06) × 10^{-9} s. In the generalised Debye model, the parameter α quantifies the distribution width τ. The value of α = 0.060 ± 0.041 averaged over all isotherms shows that several relaxation mechanisms seem to coexist. Despite the results of the ac susceptibility analysis, no hysteresis of the dc magnetisation was observed down to 1.9 K.

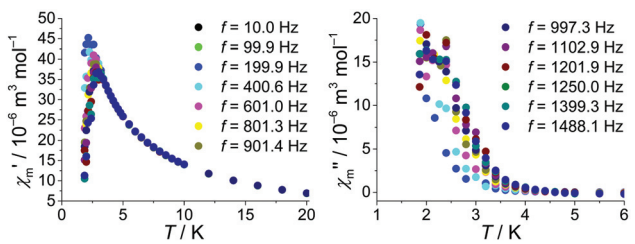

Fig. 6 In-phase (left) and out-of-phase (right) ac susceptibility for **2**.

Density functional theory calculations

We conducted DFT calculations on complexes **1** and **2**. The optimised structures, abbreviated respectively as $\mathbf{1}_{DFT}$ and $\mathbf{2}_{DFT}$, were obtained under the constraints of the C_2 point group at the UBP86-D3[27] level in the high-spin states[28] (see Computational details). The structural deficiencies associated with the BP86 level of theory were partly compensated by the inclusion of Grimme's dispersion correction of D3-generation, especially for the π–π stacking interactions. The optimised structures are, thus, in good agreement with the experimental ones (Table 2).

We estimated the relative energies of tetramerisation (ΔE_{tetra}) of discrete [MCl_2(**HL·S**)] units ($\mathbf{1'}_{DFT}$: M = Co; $\mathbf{2'}_{DFT}$: M = Ni) involved in the formation of the high-spin cubanes, [M(μ$_3$-Cl)Cl(**HL·S**)]$_4$. The tetrahedral and square-planar coordination geometries were postulated for the metal ions in the minimum energy structures of $\mathbf{1'}_{DFT}$ and $\mathbf{2'}_{DFT}$, respectively. Indeed, the ground states of the [MCl_2(**HL·S**)] complexes vary between $\mathbf{1'}_{DFT}$ with S' = 3/2 and $\mathbf{2'}_{DFT}$ with S' = 0. As seen in Fig. 8, $\mathbf{2}_{DFT}$ has an enhanced thermodynamic stability (by *ca.* 100 kJ mol^{-1}) in solution when compared to $\mathbf{1}_{DFT}$ at the DFT level used. In fact, this is compatible with the higher thermal stability of **2** than **1**, according to TGA.

We carried out DFT calculations on structures **1** and **2** to help rationalise the experimental information on molecular magnetism. Since the DFT deals with single Slater determinants to describe open-shell electronic configurations instead of spin-adapted states, we applied the *broken-symmetry* approach to compute the energies of the open-shell configurations, namely those with $M_S \leq S_{HS}$. The Ising spin Hamiltonian was applied to get an adequate mapping between the DFT energies and the different spin-polarised states. The M–(μ$_3$-Cl)–M angles in both compounds are close to 95°, a critical value that often separates the FM and AFM regimes.

Published on 10 March 2014. Downloaded by Université de Strasbourg, Service Commun de la Documentation on 09/04/2014 10:04:09.

Table 2 Comparison between the structural parameters of $\mathbf{1}_{DFT}$ and $\mathbf{2}_{DFT}$ optimised at the UBP86-D3 level and **1** and **2** determined by single-crystal X-ray crystallography. Bond distances are given in Å and bond angles in °

	M = Co		M = Ni	
	$\mathbf{1}_{DFT}$	**1**	$\mathbf{2}_{DFT}$	**2**
M···M	3.638–3.769	3.6804(5)–3.8559(5)	3.577–3.644	3.6029(6)–3.7378(6)
M–μ_3-Cl	2.462–2.550	2.4629(6)–2.5896(7)	2.436–2.458	2.4264(9)–2.5042(9)
M–Cl	2.347	2.3558(7)	2.365	2.347(1)
M–N	2.080	2.105(2)	2.027	2.052(3)
M–O	2.068	2.090(2)	2.058	2.072(3)
O···Cl	3.107	3.233(2)	3.086	3.206(3)
$\pi_{Py}\cdots\pi_{Py}$	3.921[a]	3.770(2)	3.870[a]	3.757(2)
M–Cl–M	92.4–97.5	93.48(2)–98.38(2)	93.4–96.3	93.88(3)–97.43(3)

[a] $d(\pi_{Py}\cdots\pi_{Py})$ = 4.725 Å and 4.735 Å for $\mathbf{1}_{DFT}$ and $d(\pi_{Py}\cdots\pi_{Py})$ = 4.568 Å and 4.572 Å for $\mathbf{2}_{DFT}$ at the non-dispersion corrected UBP86 level.

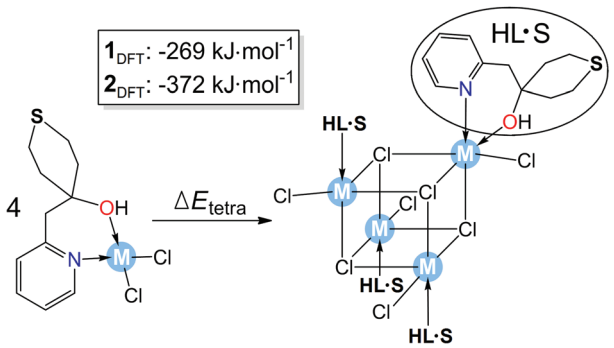

Fig. 8 Relative energies of tetramerisation (ΔE_{tetra}) of discrete [MCl_2(**HL·S**)] units (**1**′$_{DFT}$: M = Co; **2**′$_{DFT}$: M = Ni) in solution towards the formation of the cubane-like [M(μ_3-Cl)Cl(**HL·S**)]$_4$ structures (**1**$_{DFT}$: M = Co; **2**$_{DFT}$: M = Ni).

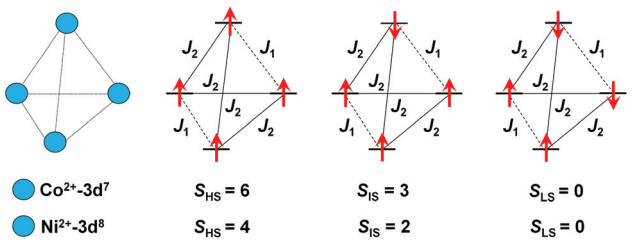

Fig. 9 Three possible orientations of local spin moments (arrows: spin 3/2 for Co, spin 1 for Ni) and total (S, sum of arrows) spin quantum numbers for the cubane-type [M(μ_3-Cl)Cl(**HL·S**)]$_4$ complexes. The coupling constants J_1 and J_2 represent the strength of the interactions between the M ions bridged by μ_3-Cl ligands.

Therefore, it is difficult to anticipate whether the J parameters are positive (FM) or negative (AFM), being close to zero due to the competition between both regimes. By inspection of the structural parameters listed in Table 2, we considered a two-J model based on the presence of two longer (J_1) and four shorter (J_2) M···M distances to determine the sign and magnitude of the magnetic interactions between the local spin moments of M(II) ions. As deduced from the μ_{eff} values at high T shown in Fig. 4 and 5, the Co(II) and Ni(II) ions in **1** and **2** are characterised by the local spins of 3/2 and 1, respectively. Thus, to extract the J_1 and J_2 parameters we computed the three situations depicted in Fig. 9: the high-spin (S_{HS} = ↑↑↑↑), the intermediate-spin (S_{IS} = ↑↑↑↓) and the low-spin (S_{LS} = ↑↑↓↓) configurations, where each arrow represents spin 3/2 for Co and spin 1 for Ni.

The spin Hamiltonian used to characterise the magnetic coupling parameters contains a summation extending over all possible interacting spin pairs:

$$\hat{H} = -J_1 \sum_{i,j} \hat{S}_{z,i}\hat{S}_{z,j} - J_2 \sum_{k,l} \hat{S}_{z,k}\hat{S}_{z,l}$$

From this model, the energy spectrum for M = Ni^{2+} is:

$$E_{HS} = -2J_1 - 4J_2;\ E_{IS} = 0;\ E_{LS} = -2J_1 + 4J_2$$

and for M = Co^{2+}:

$$E_{HS} = -\frac{9}{2}J_1 - 9J_2;\quad E_{IS} = 0;\quad E_{LS} = -\frac{9}{2}J_1 + 9J_2$$

The main results arising from computations performed with the B3LYP and PBE0 density functionals for the BP86-optimised ($\mathbf{1}_{DFT}$ and $\mathbf{2}_{DFT}$) and experimental (**1** and **2**) geometries are listed in Table 3. The agreement between the B3LYP and PBE0 values of J_1 and J_2 is significant and gives robustness to the conclusions derived from computations. An estimate of the molecular zero-field splitting (ZFS) parameter, D, was computed applying the *giant spin approximation*. This model considers that a single total molecular spin (S) prevails by the strong alignment of the local spin moments. For the total spin, the anisotropy can be calculated with H^{GSA} = SDS. The applicability of this model is subject to the fact that the strength of the isotropic coupling of spin moments must be much larger than that of the anisotropic coupling, $J \gg D$, also called the 'strong exchange limit'. In the 'weak exchange limit' characterised by $D \sim J$, the giant spin approximation cannot be properly applied. We will see later that compound **1** is in the 'weak exchange limit' and the extraction of a total D is an inaccurate procedure. The local ZFS parameters for Co^{2+} and Ni^{2+} are also computed and detailed in this section. The following discussion is based on the PBE0 results obtained for the experimental structures only.

 This journal is © The Royal Society of Chemistry 2014

Published on 10 March 2014. Downloaded by Université de Strasbourg, Service Commun de la Documentation on 09/04/2014 10:04:09.

Table 3 Magnetic quantities[a] of the [M(μ_3-Cl)Cl(**HL·S**)]$_4$ complexes computed at the UB3LYP-D3 and UPBE0 levels[b]

	UB3LYP-D3				UPBE0			
	M = Co		M = Ni		M = Co		M = Ni	
	$\mathbf{1}_{DFT}$	**1**	$\mathbf{2}_{DFT}$	**2**	$\mathbf{1}_{DFT}$	**1**	$\mathbf{2}_{DFT}$	**2**
J_1	−1.34	−8.07	+19.56	+18.15	−0.54	−1.25	+16.74	+15.93
J_2	+3.99	+5.91	+17.44	+13.91	+3.50	+2.96	+15.43	+12.40
D^c						0.81		−0.44

[a] Values in cm^{-1}. [b] Using the UBP86-D3 optimised ($\mathbf{1}_{DFT}$ and $\mathbf{2}_{DFT}$) or the X-ray crystal (**1** and **2**) structures. [c] ZFS molecular parameters calculated assuming the giant spin approximation.

For structure **1**, the present DFT calculations and application of the Ising Hamiltonian give a negative $J_1 = -1.25$ cm^{-1} and a positive $J_2 = +2.96$ cm^{-1}, leading to a parallel spin alignment ($S_{HS} = 6$ situation, see Fig. 9). This result is in apparent contradiction with the experimental evidence (Fig. 4), namely a low-spin ground state. However, magnetic anisotropy may bridge both results. The value of 0.81 cm^{-1} calculated for the ZFS parameter D may explain the low-spin ground state since it stabilizes the $M_S = 0$ state by virtue of $E = D{\cdot}M_S^2$ (considering a small rhombic anisotropy, $E \ll D$), the Kramer's doublets $M_S = \pm1, \pm2, \ldots, \pm6$ appearing above the $M_S = 0$ state. The splittings of the various M_S states computed with this D parameter span an energy range (29.2 cm^{-1}) that merges with the energy separation of the $S_{HS} = 6$ and $S_{IS} = 3$ states (computed 21 cm^{-1}). In other words, we are in the 'weak exchange limit' and the giant spin model is inappropriate. To have *an estimate* of the local D parameter in Co^{2+},[29] we studied the single-ion (local) ZFS using a $CoZn_3$ model where the Co^{2+} centre is in its real molecular environment. We obtained $D = 4.0$ cm^{-1} that, compared with $J_1 = -1.25$ cm^{-1} and $J_2 = +2.96$ cm^{-1}, confirms the 'weak exchange limit' scenario in **1**. In principle, a more elaborate description of the iso- and anisotropic coupling is mandatory, although for such a tetranuclear compound the quantum mechanical extraction of accurate parameters is nearly unaffordable. Nevertheless, even the crude DFT calculations presented here could qualitatively explain the absence of a net spin moment in the ground state of [Co(μ_3-Cl)Cl(**HL·S**)]$_4$.

For the Ni(II) compound, the computed isotropic coupling constants, J_1 and J_2, are both positive and similar in magnitude (Table 3). They are also larger than those found in complex **1**, resulting in ferromagnetically coupled local spins and a total high-spin ground state, $S_{HS} = 4$ (Fig. 9). The energy difference between the lowest $S_{HS} = 4$ and the first excited $S_{IS} = 2$ states is $\Delta E = 81.5$ cm^{-1} from DFT calculations. This is a sufficiently large value to accept the 'strong exchange limit', *i.e.* the isotropic exchange is much larger than the ZFS and the giant spin approximation can be applied. The axial anisotropy parameter (D) computed with the PBE0 functional is therefore relevant thanks to the strong ferromagnetism of the system. For **2**, $D = -0.44$ cm^{-1} with a negligible rhombic anisotropy ($E/D = 0.0002$ cm^{-1}). The main implication is that complex **2** has an easy axis of magnetisation with a $M_s \neq 0$ ground state. The same conclusion concerning the ground state can be extracted from the curve in Fig. 5. The computed molecular D parameter produces a ZFS of the $M_S = \pm4, \pm3, \ldots, 0$ states with respectively $E = D{\cdot}M_S^2 = -4.1, -1.0, 1.2, 2.5$ and 2.9 cm^{-1} when considering the $S_{HS} = 4$ manifold before spin–orbit coupling. The single-ion (local) magnetic anisotropy obtained using a $NiZn_3$ model gives $D = -0.79$ cm^{-1}. This is in agreement with a total $M_s \neq 0$ ground state due to the dominant FM coupling deduced from J_1 and J_2. If the local $M_s \neq 0$ states are ferromagnetically aligned, we recover the same solution as that obtained using the giant spin approximation to get the lowest total M_S. The cubane-type Ni(II) complex was thus revealed to be a candidate to join the family of SMMs, and this result is consistent with the magnetochemical data of this compound. To better understand the physical picture of the ground states and magnetic interactions within **2**, we plan to perform mK magnetisation measurements of the latter at high magnetic fields in the near future.

The present computational study has helped in interpreting the magnetic coupling scheme in the Co_4Cl_4 and Ni_4Cl_4 cubane systems by considering a two-J model. Although the magnetic anisotropy issue has been theoretically treated in an approximate fashion, future joint experimental–theoretical work will include accurate calculations on the anisotropy properties of polynuclear complexes.

Conclusions

We demonstrated that two new isostructural coordination clusters [M(μ_3-Cl)Cl(**HL·S**)]$_4$ (**1**: M = Co; **2**: M = Ni) exhibit substantially different spin behaviours caused by factors such as the nature of the transition metal ions, ligand-field effects, and magnetic anisotropy characteristics arising from single-ion effects. In this context, DFT calculations permitted a detailed modelling of the distinct coupling pathways (J_1 and J_2). In complex **1**, there is one positive and one negative exchange coupling constant, yielding a high-spin $S_{HS} = 6$ ground state. This might not be in contradiction with experiments if the ZFS parameter, D, is positive as suggested by the DFT calculations on a single Co^{2+} ion. In this scenario, a $M_S = 0$ ground state is predicted. It must be pointed out that an accurate description of the magnetic properties of **1** is out of reach using DFT. In complex **2**, the two J constants are positive, which leads to a

Published on 10 March 2014. Downloaded by Université de Strasbourg, Service Commun de la Documentation on 09/04/2014 10:04:09.

S_{HS} = 4 ground state. The total D < 0 magnetic anisotropy in **2** suggests an easy axis of magnetization ($M_s \neq 0$ ground state), in agreement with the FM behaviour observed. This complex can thus be envisaged as an SMM. In view of the structures of both complexes, where the structurally exposed thioether functional groups of the pyridyl-alcohol ligands (**HL·S**) can bind to substrates without steric hindrance, studies of these molecules on metal surfaces will represent an important step towards the development of molecular electronics based on single-molecule junctions.[30] Furthermore, the isostructural compounds **1** and **2** generate considerable interest for ultrafast time-resolved spectroscopy and photophysics since a task of high importance is to gain a better understanding of the influence of intramolecular exchange between magnetic centres on the absorption and emission processes in coordination complexes.[31] Finally, the basic explanatory concepts for physics and magnetostructural correlations in transition metal complexes containing $\{M_4(\mu_3\text{-}N_3)_4\}$, $\{M_4(\mu_3\text{-}O)_4\}$ and $\{M_4(\mu_3\text{-}X)_4\}$ (X = F, Cl) cubane cores[32] with a high sensitivity to the ligands and their coordination modes are yet to be established. All these aspects are currently being explored in our laboratories by experimental and computational methods. We believe that such combined approaches are essential for a deeper understanding of molecular-based properties of the type presented in this work.

Experimental and computational

Materials and methods

$[NiCl_2(dme)]$ was prepared following a published procedure.[33] The reactions were performed under dry argon using standard Schlenk techniques. All solvents used were freshly distilled before use. NMR spectra were recorded at room temperature on a Bruker AVANCE 300 spectrometer (^{1}H, 300 MHz; ^{13}C, 75.47 MHz) and referenced using the residual proton solvent (^{1}H) or solvent (^{13}C) resonance. Chemical shifts (δ) are given in ppm. The FTIR spectra were recorded on a Thermo-Nicolet 6700 spectrometer equipped with a diamond crystal SMART ORBIT ATR accessory. The FTIR spectra of single crystals were recorded using a Thermo-Nicolet Centaurus FTIR microspectrometer in diamond window microcompression cells. Unless otherwise stated, all products were commercially available and used as received.

Synthesis of 4-(pyridin-2-ylmethyl)tetrahydro-2*H*-thiopyran-4-ol (HL·S)

A solution of *n*-BuLi (16.2 mL, 26.00 mmol, 1.60 M in hexane) was added dropwise over 15 min to a solution of 2-picoline (2.420 g, 26.00 mmol) in 150 mL of THF at −78 °C. After complete deprotonation, a red solid precipitated and after further stirring for 1 h at −78 °C, a solution of tetrahydro-4*H*-thiopyran-4-one (3.00 g, 26.00 mmol) in 50 mL of THF was added dropwise to the suspension. The resulting pale yellow solution was allowed to reach room temperature overnight. After addition of 100 mL of a saturated solution of NH_4Cl in water, the reaction mixture was extracted with Et_2O (3 × 30 mL). The organic phases were collected and dried with Na_2SO_4, which was then filtered off. Evaporation of the volatiles produced brown crystals of **HL·S**. Yield: 4.00 g (73%). Anal. calcd for $C_{11}H_{15}NOS$ (209.31): C, 63.12; H, 7.22; N, 6.69. Found: C, 62.96; H, 6.87; N, 6.61. FTIR: ν_{max}(solid)/cm^{-1}: 3210s, 3078vw, 3055vw, 3021vw, 2955w, 2917s, 1592s, 1569s, 1480s, 1423vs, 1353vw, 1339w, 1320m, 1302m, 1277s, 1259s, 1242w, 1222mw, 1164vw, 1149w, 1140m, 1101s, 1080m, 1054vs, 1020w, 1002s, 937s, 921vs, 898vw, 882m, 838vw, 819vw, 790m, 772m, 755vs, 721m, 670w, 658m, 637w, 628m, 602w, 479s, 435m, 428m, 406vs, 366vs, 288s, 270vs, 246m, 219s, 161vw, 151vw, 129vs, 119w, 102vs. In the following NMR description, the atom numbering used is shown in Fig. 10. ^{1}H NMR ($CDCl_3$, 300 MHz) δ: 8.61 (brd, 1H, $^3J_{H,H}$ = 4.9 Hz, H_8Py), 7.76 (dt, 1H, $^3J_{H,H}$ = 7.6 and 1.8 Hz, H_6Py), 7.32–7.28 (dd, 1H, $^3J_{H,H}$ = 7.5 Hz and 4.9 Hz, H_7Py), 7.25 (d, 1H, $^3J_{H,H}$ = 7.6 Hz, H_5Py), 6.07 (br, 1H, OH), 3.24–3.14 (m, 2H, CH of C_4 and $C_{4'}$), 3.00 (s, 2H, C_1), 2.54–2.47 (m, 2H, CH of C_4 and $C_{4'}$), 2.00–1.93 (m, 2H, CH of C_3 and $C_{3'}$), 1.85–1.76 (m, 2H, CH of C_3 and $C_{3'}$) ppm. ^{13}C{^{1}H} NMR ($CDCl_3$, 75.5 MHz) δ: 158.98 (s, C_{ipso}Py), 148.45 (s, C_8Py), 137.18 (s, C_6Py), 124.80 (s, C_5, Py), 121.84 (s, C_7, Py), 69.92 (s, C_2), 48.12 (s, C_1), 38.88 (s, C_4, $C_{4'}$), 24.47 (s, C_3, $C_{3'}$) ppm.

Synthesis of $[Co(\mu_3\text{-}Cl)Cl(HL\cdot S)]_4$ (1)

A slurry of anhydrous $CoCl_2$ (0.252 g, 1.94 mmol) in 30 mL of THF was sonicated for 1 h until complete dissolution. A solution of **HL·S** (0.406 g, 1.94 mmol) in 15 mL of THF was then added and the reaction mixture was stirred for 2 h at room temperature. The volatiles were removed under reduced pressure and the blue powder obtained was dissolved in CH_2Cl_2 and filtered. The filtrate was then layered with Et_2O. Octahedral blue crystals of **1**, suitable for X-ray diffraction analysis, were obtained at room temperature after 3 days. Yield: 0.414 g (63%). Anal. calcd for $C_{44}H_{60}Cl_8Co_4N_4O_4S_4\cdot 2CH_2Cl_2$ (1526.47): C, 36.19; H, 4.22; N, 3.67. Found: C, 35.82; H, 4.45; N, 3.62. FTIR: ν_{max}(KBr pellet)/cm^{-1}: 3178mbr, 2932mbr, 2855vw, 1605vs, 1570m, 1560w, 1541w, 1533vw, 1508vw, 1483m, 1443s, 1400sh, 1351w, 1294w, 1269m, 1244w, 1213m, 1158w, 1141vw, 1124vw, 1108w, 1077w, 1036vs, 1020s, 993w, 969vw, 920s, 866m, 834w, 774vw, 760m, 731s, 715w, 699w, 669vw, 658vw, 645w, 608vw, 572w, 513w, 481w, 450vw, 425m, 309w, 296w, 285w, 256s, 230sh, 213vs, 200sh, 143w, 135w, 130w, 122w, 115w, 102w.

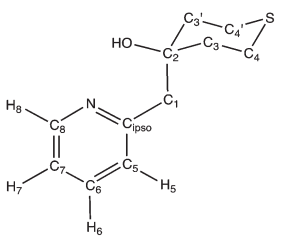

Fig. 10 Atom numbering scheme used for the NMR description of the ligand **HL·S**.

 This journal is © The Royal Society of Chemistry 2014

Published on 10 March 2014. Downloaded by Université de Strasbourg, Service Commun de la Documentation on 09/04/2014 10:04:09.

Synthesis of $[Ni(\mu_3\text{-}Cl)Cl(HL{\cdot}S)]_4$ (2)

To a slurry of $[NiCl_2(dme)]$ (0.315 g, 1.43 mmol) in 15 mL of THF was added a solution of **HL·S** (0.300 g, 1.43 mmol) in 15 mL of THF. The reaction mixture was stirred for 2 h at room temperature whereupon the orange dispersion became a yellow solution. The volatiles were evaporated under reduced pressure and the yellow powder obtained was dissolved in CH_2Cl_2. The solution was filtered and the filtrate was layered with Et_2O. Octahedral yellow crystals of **2**, suitable for X-ray diffraction analysis, were obtained at room temperature after 3 days. Yield: 0.360 g (74%). Anal. calcd for $C_{44}H_{60}Cl_8Ni_4N_4O_4S_4$ (1355.64): C, 38.98; H, 4.46; N, 4.13. Found: C, 39.03; H, 4.67; N, 4.04. FTIR: ν_{max}(KBr pellet)/cm^{-1}: 3178brs, 3113brs, 2957w, 2943vw, 2926w, 2914w, 2857w, 2800vw, 1607s, 1571m, 1486m, 1446vs, 1430shw, 1424vw, 1397w, 1362vw, 1343w, 1318vw, 1295vw, 1284vw, 1259s, 1233m, 1219vw, 1210vw, 1203vw, 1159w, 1145w, 1112s, 1091vw, 1078vw, 1065vw, 1053w, 1039s, 1024w, 1013w, 1000vw, 945vw, 918vs, 865w, 854m, 829m, 784sh, 775s, 756s, 737vw, 715ms, 693w, 651ms, 638w, 628vw, 608vw, 576m, 517m, 488m, 470vw, 453w, 429m, 405vw, 352m, 335w, 302vw, 263s, 225vs, 205sh, 182vw, 150w, 131vw, 121vw, 104vw.

X-ray crystallography

Suitable crystals for the X-ray analyses of **1** and **2** were obtained as described above. The intensity data were recorded on an APEX II DUO Kappa-CCD area detector diffractometer[34] (graphite monochromated Mo-Kα radiation, λ = 0.71073 Å). The structures were solved by direct methods (SHELXS-97) and refined by full-matrix least-squares procedures (based on F^2, SHELXL-97)[35] with anisotropic thermal parameters for all the non-hydrogen atoms. The hydrogen atoms were introduced into the geometrically calculated positions (SHELXL-97 procedures) and refined *riding* on the corresponding parent atoms, except the ones from OH functional groups (see below). A summary of crystal data and structure refinements for **1** and **2** is given in Table S1 of the ESI† and in ref. 13. In both structures, a dichloromethane molecule was found disordered over at least six positions with no atom in common. Any attempt to give a reasonable model of this disorder, severely affecting the model quality, failed. A PLATON SQUEEZE procedure[36] was applied using complete anisotropic models, resulting in an improved model quality. Details are given in the CIF files. The OH hydrogen atom was found in the difference maps and was refined with a restrained O–H distance of 0.9 Å. CCDC 964328 for **1** and 964329 for **2** contain the supplementary crystallographic data.

Magnetic susceptibility measurements

Magnetic susceptibility data of **1** and **2** were recorded using a Quantum Design MPMS-5XL SQUID magnetometer for direct current (dc) as well as alternating current (ac) measurements. The polycrystalline samples were compacted and immobilised into cylindrical PTFE capsules. The dc susceptibility data were acquired as a function of the field (0.1–5.0 T) and temperature (2.0–290 K). The ac susceptibility data were measured in the absence of a static bias field in the frequency range 10–1500 Hz (T = 1.8–50 K, B_{ac} = 3 G). Only compound **2** exhibited out-of-phase components above 1.8 K. All data were corrected for the contribution of the sample holder (PTFE capsule) and the diamagnetic contributions of compounds **1** and **2** calculated from tabulated values (-9.59×10^{-9} m^3 mol^{-1} and -8.51×10^{-9} m^3 mol^{-1}, respectively).

Computational details and theory

Density functional theory (DFT) geometry optimisations were conducted using the Amsterdam Density Functional (ADF) program.[37,38] The numerical integration was performed using the procedure developed by te Velde *et al*.[38g,h] The molecular orbitals were expanded in a large set of uncontracted Slater-type orbitals (STOs) of triple-ζ quality augmented with two sets of polarisation functions for all atoms (TZ2P basis set[38i]), *i.e.* 2p and 3d on H, 3d and 4f on C, N, O, S, and Cl, and 4d and 4f on Co and Ni. The core shells of C, N, and O (1s), S and Cl (up to 2p), and Co and Ni (up to 2p) were treated by the frozen (small) core approximation.[38c] An auxiliary set of s, p, d, f, and g STOs was used to fit the molecular density and to represent the Coulomb and exchange potentials accurately in each self-consistent field cycle.[38j] All the structures were optimised with the BP86 density functional as has been shown to be one of the three best generalised gradient approximation (GGA) DFT functionals (along with PBE and PW91) for geometry optimisations with the ADF program package.[39] The electronic exchange was described by Slater's Xα potential[38l] with self-consistent nonlocal corrections of Becke[38m,n] and the electron correlation was treated in the Vosko–Wilk–Nusair (VWN) parameterisation[38o] with self-consistent nonlocal corrections of Perdew[38p] (BP86).[38q] Grimme's dispersion correction of D3-generation[27,40] to DFT functionals was implemented (referred to as BP86-D3[41]). A spin-restricted and a spin-unrestricted formalism were applied at the GGA level. Scalar relativistic effects were accounted for using the zeroth-order regular approximation (ZORA).[42] All DFT calculations were carried out in homogeneous solvent media (THF, ε = 7.58) as THF was used in the synthetic preparation of **1** and **2**. ZORA-(U)BP86-D3/TZ2P was combined with the COnductor-like Screening MOdel (COSMO) of solvation with the solvent-excluding surface (SES) to define the cavities surrounding the complexes.[43] The atomic radii were issued from the ADF program. The minimum energy structures were verified through vibrational analysis with detailed surface scans to have zero imaginary frequencies.[44] The single-point energy calculations on the UBP86-D3 equilibrium structures $\mathbf{1}_{DFT}$ (M = Co) and $\mathbf{2}_{DFT}$ (M = Ni) and the X-ray crystal structures of **1** and **2** were also performed at COSMO/ZORA-UPBE0/TZ2P and COSMO/ZORA-UB3LYP-D3/TZ2P to obtain the energy differences between the high-spin and *broken-symmetry* states of the specified compounds. At these levels of theory, the non-dispersion corrected, hybrid UPBE0 functional[45] and the dispersion-corrected (D3), hybrid UB3LYP functional[46] were used in conjunction with the all-electron TZ2P basis sets implemented for

Published on 10 March 2014. Downloaded by Université de Strasbourg, Service Commun de la Documentation on 09/04/2014 10:04:09.

all elements. The zero-field splitting (ZFS) parameter, D, was computed using the ORCA program[47] with the perturbative Pederson–Khanna method,[48] taking the experimental geometries of **1** and **2** and performing the single-point energy calculations at the DFT-UPBE0/TZ2P level of theory.

Acknowledgements

We are grateful to the CNRS, the Ministère de la Recherche (Paris), the DFH/UFA (International Research Training Group 'GRK532', Ph.D. grant to A.G.), the International Centre for Frontier Research in Chemistry, Strasbourg (icFRC, http://www.icfrc.fr), the DFG (postdoctoral reintegration fellowship to K.Y.M.), and the Spanish Government (project no. CTQ2011-23140 and the Ramón y Cajal program with grant no. RYC-2008-02493 to X.L.). We also thank the Service de Radiocristallographie, Institut de Chimie (UMR 7177 CNRS-UdS) for the X-ray diffraction studies.

Notes and references

1 (*a*) F. Speiser, L. Saussine and P. Braunstein, *Inorg. Chem.*, 2004, **43**, 4234; (*b*) A. Kermagoret and P. Braunstein, *Dalton Trans.*, 2008, 1564.

2 (*a*) J. Zhang, P. Teo, R. Pattacini, A. Kermagoret, R. Welter, G. Rogez, T. S. A. Hor and P. Braunstein, *Angew. Chem., Int. Ed.*, 2010, **49**, 4443; (*b*) L. Kayser, R. Pattacini, G. Rogez and P. Braunstein, *Chem. Commun.*, 2010, **46**, 6461; (*c*) S. Hameury, L. Kayser, R. Pattacini, G. Rogez, W. Wernsdorfer and P. Braunstein, *Dalton Trans.*, 2013, **42**, 5013.

3 R. Pattacini, P. Teo, J. Zhang, Y. Lan, A. K. Powell, J. Nehrkorn, O. Waldmann, T. S. A. Hor and P. Braunstein, *Dalton Trans.*, 2011, **40**, 10526.

4 K. Yu. Monakhov, X. López, M. Speldrich, J. van Leusen, P. Kögerler, P. Braunstein and J. M. Poblet, *Chem.–Eur. J.*, 2014, **20**, 3769.

5 (*a*) L. Bogani and W. Wernsdorfer, *Nat. Mater.*, 2008, **7**, 179; (*b*) M. Mannini, F. Pineider, P. Sainctavit, C. Danieli, E. Otero, C. Sciancalepore, A. Maria Talarico, M.-A. Arrio, A. Cornia, D. Gatteschi and R. Sessoli, *Nat. Mater.*, 2009, **8**, 194; (*c*) A. Cornia, M. Mannini, P. Sainctavit and R. Sessoli, *Chem. Soc. Rev.*, 2011, **40**, 3076; (*d*) M. J. Rodriguez-Douton, M. Mannini, L. Armelao, A.-L. Barra, E. Tancini, R. Sessoli and A. Cornia, *Chem. Commun.*, 2011, **47**, 1467.

6 (*a*) G. Christou, D. Gatteschi, D. N. Hendrickson and R. Sessoli, *MRS Bull.*, 2000, **25**, 66; (*b*) A. J. Nelson, J. G. Reynolds and G. Christou, *MRS Symp. Proc.*, 2001, **635**, C4.13.1; (*c*) W. Wernsdorfer, N. Aliaga-Alcalde, D. N. Hendrickson and G. Christou, *Nature*, 2002, **416**, 406; (*d*) J. R. Long, in *Chemistry of Nanostructured Materials*, ed. P. Yang, World Scientific Publishing, Hong Kong, 2003, p. 291; (*e*) G. Christou, *Polyhedron*, 2005, **24**, 2065; (*f*) C. J. Milios, A. Vinslava, W. Wernsdorfer, S. Moggach, S. Parsons, S. P. Perlepes, G. Christou and E. K. Brechin, *J. Am. Chem. Soc.*, 2007, **129**, 2754; (*g*) O. Waldmann, *Inorg. Chem.*, 2007, **46**, 10035; (*h*) R. Bagai and G. Christou, *Chem. Soc. Rev.*, 2009, **38**, 1011.

7 (*a*) A. Ulman, *Chem. Rev.*, 1996, **96**, 1533; (*b*) F. Schreiber, *Prog. Surf. Sci.*, 2000, **65**, 151; (*c*) J. C. Love, L. A. Estroff, J. K. Kriebel, R. G. Nuzzo and G. M. Whitesides, *Chem. Rev.*, 2005, **105**, 1103; (*d*) I. S. Kristensen, D. J. Mowbray, K. S. Thygesen and K. W. Jacobsen, *J. Phys.: Condens. Matter*, 2008, **20**, 374101; (*e*) L. Kankate, A. Turchanin and A. Gölzhäuser, *Langmuir*, 2009, **25**, 10435; (*f*) M. del Carmen Gimenez-Lopez, M. T. Räisänen, T. W. Chamberlain, U. Weber, M. Lebedeva, G. A. Rance, G. A. D. Briggs, D. Pettifor, V. Burlakov, M. Buck and A. N. Khlobystov, *Langmuir*, 2011, **27**, 10977; (*g*) H. Rath, G. A. Timco, V. Corradini, A. Ghirri, U. del Pennino, A. Fernandez, R. G. Pritchard, C. A. Muryn, M. Affronte and R. E. P. Winpenny, *Chem. Commun.*, 2013, **49**, 3404.

8 (*a*) M. W. J. Beulen, B.-H. Huisman, P. A. van der Heijden, F. C. J. M. van Veggel, M. G. Simons, E. M. E. F. Biemond, P. J. de Lange and D. N. Reinhoudt, *Langmuir*, 1996, **12**, 6170; (*b*) C.-J. Zhong, R. C. Brush, J. Anderegg and M. D. Porter, *Langmuir*, 1999, **15**, 518; (*c*) J. Noh, T. Murase, K. Nakajima, H. Lee and M. Hara, *J. Phys. Chem. B*, 2000, **104**, 7411; (*d*) P. Croizat, F. Müller, H. Mantz, A. Englisch, R. Welter, S. Hüfner and P. Braunstein, *C. R. Chim.*, 2009, **12**, 1228; (*e*) H. L. Tierney, J. W. Han, A. D. Jewell, E. V. Iski, A. E. Baber, D. S. Sholl and E. C. H. Sykes, *J. Phys. Chem. C*, 2011, **115**, 897; (*f*) P. Angelova, E. Solel, G. Parvari, A. Turchanin, M. Botoshansky, A. Gölzhäuser and E. Keinan, *Langmuir*, 2013, **29**, 2217.

9 For pendant thioether functions in transition-metal complexes see, *e.g.*, recent studies: (*a*) V. Rosa, C. Fliedel, A. Ghisolfi, R. Pattacini, T. Avilés and P. Braunstein, *Dalton Trans.*, 2013, **42**, 12109 and references cited therein; (*b*) A. Ghisolfi, C. Fliedel, V. Rosa, R. Pattacini, A. Thibon, K. Yu. Monakhov and P. Braunstein, *Chem.–Asian J.*, 2013, **8**, 1795.

10 M. Speldrich, H. Schilder, H. Lueken and P. Kögerler, *Isr. J. Chem.*, 2011, **51**, 215.

11 (*a*) L. Noodleman, *J. Chem. Phys.*, 1981, **74**, 5737; (*b*) M. Orio, D. A. Pantazis and F. Neese, *Photosynth. Res.*, 2009, **102**, 443; (*c*) F. Neese, *Coord. Chem. Rev.*, 2009, **253**, 526 and references cited therein.

12 See, *e.g.*: G. Aromí, A. S. Batsanov, P. Christian, M. Helliwell, O. Roubeau, G. A. Timco and R. E. P. Winpenny, *Dalton Trans.*, 2003, 4466.

13 Crystal data for **1**: $C_{44}H_{60}Cl_8Co_4N_4O_4S_4$, M = 1356.52, tetragonal, a = 19.2769(8) Å, b = 19.2769(8) Å, c = 18.5886(8) Å, α = 90.00°, β = 90.00°, γ = 90.00°, V = 6907.5(5) Å^3, T = 173(2) K, space group $I4_1/a$, Z = 4, μ = 1.410 mm^{-1}, 14447 reflections measured, 5026 independent reflections (R_{int} = 0.0268). The final R_1 values were 0.0451 ($I > 2\sigma(I)$). The final w$R(F^2)$ values were 0.1184 ($I > 2\sigma(I)$). The final R_1 values were 0.0613 (all data). The final w$R(F^2)$ values were 0.1284 (all data). The goodness of fit on F^2 was 1.083. Crystal data

 This journal is © The Royal Society of Chemistry 2014

Published on 10 March 2014. Downloaded by Université de Strasbourg, Service Commun de la Documentation on 09/04/2014 10:04:09.

for **2**: $C_{44}H_{60}Cl_8Ni_4N_4O_4S_4$, M = 1355.64, tetragonal, a = 19.091(1) Å, b = 19.091(1) Å, c = 18.729(1) Å, α = 90.00°, β = 90.00°, γ = 90.00°, V = 6826.5(8) Å^3, T = 173(2) K, space group $I4_1/a$, Z = 4, μ = 1.558 mm^{-1}, 39794 reflections measured, 3351 independent reflections (R_{int} = 0.0261). The final R_1 values were 0.0546 ($I > 2\sigma(I)$). The final w$R(F^2)$ values were 0.1257 ($I > 2\sigma(I)$). The final R_1 values were 0.0623 (all data). The final w$R(F^2)$ values were 0.1314 (all data). The goodness of fit on F^2 was 1.167.

14 (*a*) R. D. Shannon, *Acta Crystallogr., Sect. A: Cryst. Phys., Diffr., Theor. Gen. Cryst.*, 1976, **32**, 751; (*b*) B. Cordero, V. Gómez, A. E. Platero-Prats, M. Revés, J. Echeverría, E. Cremades, F. Barragán and S. Alvarez, *Dalton Trans.*, 2008, 2832.

15 For Co_4 cubane-type complexes, see: (*a*) K. Dimitrou, K. Folting, W. E. Streib and G. Christou, *J. Am. Chem. Soc.*, 1993, **115**, 6432; (*b*) K. Dimitrou, K. Folting, W. E. Streib and G. Christou, *J. Chem. Soc., Chem. Commun.*, 1994, 1385; (*c*) A. Tsohos, S. Dionyssopoulou, C. P. Raptopoulou, A. Terzis, E. G. Bakalbassis and S. P. Perlepes, *Angew. Chem., Int. Ed.*, 1999, **38**, 983; (*d*) T. A. Hudson, K. J. Berry, B. Moubaraki, K. S. Murray and R. Robson, *Inorg. Chem.*, 2006, **45**, 3549; (*e*) M.-H. Zeng, M.-X. Yao, H. Liang, W.-X. Zhang and X.-M. Chen, *Angew. Chem., Int. Ed.*, 2007, **46**, 1832; (*f*) K. W. Galloway, A. M. Whyte, W. Wernsdorfer, J. Sanchez-Benitez, K. V. Kamenev, A. Parkin, R. D. Peacock and M. Murrie, *Inorg. Chem.*, 2008, **47**, 7438; (*g*) B. Moubaraki, K. S. Murray, T. A. Hudson and R. Robson, *Eur. J. Inorg. Chem.*, 2008, 4525; (*h*) J. Liu, S. Datta, E. Bolin, J. Lawrence, C. C. Beedle, E.-C. Yang, P. Goy, D. N. Hendrickson and S. Hill, *Polyhedron*, 2009, **28**, 1922; (*i*) A. Scheurer, A. M. Ako, R. W. Saalfrank, F. W. Heinemann, F. Hampel, K. Petukhov, K. Gieb, M. Stocker and P. Müller, *Chem.–Eur. J.*, 2010, **16**, 4784; (*j*) K. W. Galloway, M. Schmidtman, J. Sanchez-Benitez, K. V. Kamenev, W. Wernsdorfer and M. Murrie, *Dalton Trans.*, 2010, **39**, 4727; (*k*) L. R. Falvello, E. Forcén-Vázquez, I. Mayoral, M. Tomás and F. Palacio, *Acta Crystallogr., Sect. C: Cryst. Struct. Commun.*, 2011, **67**, m359; (*l*) K. Zhang, J. Dai, Y.-H. Wang, M.-H. Zeng and M. Kurmoo, *Dalton Trans.*, 2013, **42**, 5439; (*m*) F. J. Klinke, A. Das, S. Demeshko, S. Dechert and F. Meyer, *Inorg. Chem.*, 2014, **53**, 2976.

16 For Ni_4 cubane-type complexes, see: (*a*) M. A. Halcrow, J. C. Huffman and G. Christou, *Angew. Chem., Int. Ed. Engl.*, 1995, **34**, 889; (*b*) M. A. Halcrow, J.-S. Sun, J. C. Huffman and G. Christou, *Inorg. Chem.*, 1995, **34**, 4167; (*c*) A. Escuer, M. Font-Bardía, S. B. Kumar, X. Solans and R. Vicente, *Polyhedron*, 1999, **18**, 909; (*d*) J. M. Clemente-Juan, B. Chansou, B. Donnadieu and J.-P. Tuchagues, *Inorg. Chem.*, 2000, **39**, 5515; (*e*) S. Mukherjee, T. Weyhermüller, E. Bothe, K. Wieghardt and P. Chaudhuri, *Eur. J. Inorg. Chem.*, 2003, 863; (*f*) M. Moragues-Cánovas, M. Helliwell, L. Ricard, É. Rivière, W. Wernsdorfer, E. Brechin and T. Mallah, *Eur. J. Inorg. Chem.*, 2004, 2219; (*g*) T. Shiga and H. Oshio, *Sci. Technol. Adv. Mater.*, 2005, **6**, 565; (*h*) M. Schröter, E. Lork and R. Mews, *Z. Anorg. Allg. Chem.*, 2005, **631**, 1609; (*i*) G. S. Papaefstathiou, A. Escuer, F. A. Mautner, C. Raptopoulou, A. Terzis, S. P. Perlepes and R. Vicente, *Eur. J. Inorg. Chem.*, 2005, 879; (*j*) A. Ferguson, J. Lawrence, A. Parkin, J. Sanchez-Benitez, K. V. Kamenev, E. K. Brechin, W. Wernsdorfer, S. Hill and M. Murrie, *Dalton Trans.*, 2008, 6409; (*k*) Q. Liang, R. Huang, X. Chen, Z. Li, X. Zhang and B. Sun, *Inorg. Chem. Commun.*, 2010, **13**, 1134; (*l*) J.-P. Sun, L.-C. Li and X.-J. Zheng, *Inorg. Chem. Commun.*, 2011, **14**, 877; (*m*) C. G. Efthymiou, C. Papatriantafyllopoulou, G. Aromi, S. J. Teat, G. Christou and S. P. Perlepes, *Polyhedron*, 2011, **30**, 3022; (*n*) S.-H. Zhang, N. Li, C.-M. Ge, C. Feng and L.-F. Ma, *Dalton Trans.*, 2011, **40**, 3000; (*o*) S. Petit, P. Neugebauer, G. Pilet, G. Chastanet, A.-L. Barra, A. B. Antunes, W. Wernsdorfer and D. Luneau, *Inorg. Chem.*, 2012, **51**, 6645; (*p*) S.-Y. Zhang, W.-Q. Chen, B. Hu, Y.-M. Chen, W. Li and Y. Li, *Inorg. Chem. Commun.*, 2012, **16**, 74; (*q*) A. Scheurer, K. Gieb, M. S. Alam, F. W. Heinemann, R. W. Saalfrank, W. Kroener, K. Petukhov, M. Stocker and P. Muller, *Dalton Trans.*, 2012, **41**, 3553; (*r*) S. Liu, S. Wang, F. Cao, H. Fu, D. Li and J. Dou, *RSC Adv.*, 2012, **2**, 1310; (*s*) J.-P. Costes, G. Novitchi, L. Vendier, G. Pilet and D. Luneau, *C. R. Chim.*, 2012, **15**, 849; (*t*) A. N. Ponomaryov, N. Kim, J. Hwang, H. Nojiri, J. van Tol, A. Ozarowski, J. Park, Z. Jang, B. Suh, S. Yoon and K.-Y. Choi, *Chem.–Asian J.*, 2013, **8**, 1152; (*u*) S. T. Meally, S. M. Taylor, E. K. Brechin, S. Piligkos and L. F. Jones, *Dalton Trans.*, 2013, **42**, 10315; (*v*) S. Shit, M. Nandy, G. Rosair, C. J. Gómez-García, J. J. Borras Almenar and S. Mitra, *Polyhedron*, 2013, **61**, 73; (*w*) C. Ding, C. Gao, S. Ng, B. Wang and Y. Xie, *Chem.–Eur. J.*, 2013, **19**, 9961; (*x*) J. Liu and S. Hill, *Polyhedron*, 2013, **66**, 147; (*y*) M. K. Ainooson, I. A. Guzei, L. C. Spencer and J. Darkwa, *Polyhedron*, 2013, **53**, 295; (*z*) A. Das, F. J. Klinke, S. Demeshko, S. Meyer, S. Dechert and F. Meyer, *Inorg. Chem.*, 2012, **51**, 8141.

17 (*a*) E.-C. Yang, D. N. Hendrickson, W. Wernsdorfer, M. Nakano, L. N. Zakharov, R. D. Sommer, A. L. Rheingold, M. Ledezma-Gairaud and G. Christou, *J. Appl. Phys.*, 2002, **91**, 7382; (*b*) T. Baruah and M. R. Pederson, *Chem. Phys. Lett.*, 2002, **360**, 144; (*c*) T. Baruah and M. R. Pederson, *Int. J. Quantum Chem.*, 2003, **93**, 324.

18 (*a*) E.-C. Yang, W. Wernsdorfer, S. Hill, R. S. Edwards, M. Nakano, S. Maccagnano, L. N. Zakharov, A. L. Rheingold, G. Christou and D. N. Hendrickson, *Polyhedron*, 2003, **22**, 1727; (*b*) E. del Barco, A. D. Kent, E.-C. Yang and D. N. Hendrickson, *Polyhedron*, 2005, **24**, 2695; (*c*) D. N. Hendrickson, E.-C. Yang, R. M. Isidro, C. Kirman, J. Lawrence, R. S. Edwards, S. Hill, A. Yamaguchi, H. Ishimoto, W. Wernsdorfer, C. Ramsey, N. Dalal and M. M. Olmstead, *Polyhedron*, 2005, **24**, 2280; (*d*) E.-C. Yang, W. Wernsdorfer, L. N. Zakharov, Y. Karaki, A. Yamaguchi, R. M. Isidro, G.-D. Lu, S. A. Wilson, A. L. Rheingold, H. Ishimoto and D. N. Hendrickson, *Inorg. Chem.*, 2006, **45**, 529; (*e*) J. Lawrence, E.-C. Yang, R. Edwards, M. M. Olmstead, C. Ramsey, N. S. Dalal,

Published on 10 March 2014. Downloaded by Université de Strasbourg, Service Commun de la Documentation on 09/04/2014 10:04:09.

P. K. Gantzel, S. Hill and D. N. Hendrickson, *Inorg. Chem.*, 2008, **47**, 1965.

19 (*a*) M. A. El-Sayed, *Polyhedron*, 1992, **11**, 1261; (*b*) G. Z. Cai, G. Davies, A. El-Toukhy, T. R. Gilbert and M. Henary, *Inorg. Chem.*, 1985, **24**, 1701; (*c*) A. El-Toukhy, G. Z. Cai, G. Davies, T. R. Gilbert, K. D. Onan and M. Veidis, *J. Am. Chem. Soc.*, 1984, **106**, 4596; (*d*) L. L. de Oliveira, R. R. Campedelli, A. L. Bergamo, A. H. D. P. dos Santos and O. L. Casagrande, *J. Braz. Chem. Soc.*, 2010, **21**, 1318.

20 (*a*) B. N. Figgs and M. A. Hitchman, *Ligand-Field Theory and its Applications*, Wiley-VCH, New York, 2000; (*b*) C. J. Ballhausen, *Introduction to Ligand-Field Theory*, McGraw-Hill, New York, 1962; (*c*) J. S. Griffith, *The Theory of Transition-Metal Ions*, Cambridge University Press, Cambridge, 1961.

21 O. Kahn, *Molecular Magnetism*, VCH, Weinheim, 1993.

22 (*a*) E. König and S. Kremer, *Magnetism Diagrams for Transition Metal Ions*, Plenum Press, New York, 1979; (*b*) A. B. P. Lever, *Inorganic Electronic Spectroscopy*, Elsevier, Amsterdam, 1984.

23 (*a*) M. E. Lines, *J. Chem. Phys.*, 1971, **55**, 2977; (*b*) H. Lueken, P. Hannibal, K. Handrick and J. Schmitz, *Z. Kristallogr.*, 1989, **186**, 185.

24 (*a*) G. Aromi, S. M. J. Aubin, M. A. Bolcar, G. Christou, H. J. Eppley, K. Folting, D. N. Hendrickson, J. C. Huffman, R. C. Squire, H. L. Tsai, S. Wang and M. W. Wemple, *Polyhedron*, 1998, **17**, 3005; (*b*) *From the molecular to the nanoscale: Synthesis, structure, and properties*, ed. M. Fujita, A. Powell and C. Creutz, Elsevier Ltd., Oxford, U.K., 2004, vol. 7; (*c*) See also special issues of *J. Mater. Chem.*, 2006, **16**, 2501; *Chem. Soc. Rev.*, 2011, **40**, 3053; *Dalton Trans.*, 2012, **44**, 13555 and the ACS virtual issue on "Quantum Molecular Magnets", ed. K. R. Dunbar, *Inorg. Chem.*, 2012, **51**, 12055.

25 (*a*) R. Sessoli, D. Gatteschi, A. Caneschi and M. A. Novak, *Nature*, 1993, **365**, 141; (*b*) D. Gatteschi and R. Sessoli, *Angew. Chem., Int. Ed.*, 2003, **42**, 268; (*c*) R. E. P. Winpenny, *Adv. Inorg. Chem.*, 2001, **52**, 1; (*d*) G. Aromí and E. K. Brechin, *Struct. Bonding*, 2006, **122**, 1; (*e*) A. M. Ako, I. J. Hewitt, V. Mereacre, R. Clérac, W. Wernsdorfer, C. E. Anson and A. K. Powell, *Angew. Chem., Int. Ed.*, 2006, **45**, 4926; (*f*) T. C. Stamatatos and G. Christou, *Inorg. Chem.*, 2009, **48**, 3308; (*g*) R. Sessoli and A. K. Powell, *Coord. Chem. Rev.*, 2009, **253**, 2328; (*h*) T. Taguchi, W. Wernsdorfer, K. A. Abboud and G. Christou, *Inorg. Chem.*, 2010, **49**, 199; (*i*) C. Lampropoulos, G. Redler, S. Data, K. A. Abboud, S. Hill and G. Christou, *Inorg. Chem.*, 2010, **49**, 1325; (*j*) C. Papatriantafyllopoulou, W. Wernsdorfer, K. A. Abboud and G. Christou, *Inorg. Chem.*, 2011, **50**, 421.

26 K. S. Cole and R. H. Cole, *J. Chem. Phys.*, 1941, **9**, 341.

27 (*a*) S. Grimme, J. Antony, S. Ehrlich and H. Krieg, *J. Chem. Phys.*, 2010, **132**, 154104; (*b*) S. Grimme, *WIREs Comput. Mol. Sci.*, 2011, **1**, 211; (*c*) S. Grimme, *Chem.–Eur. J.*, 2012, **18**, 9955.

28 For a review about high-spin molecules, see: H. Oshio and M. Nakano, *Chem.–Eur. J.*, 2005, **11**, 5178.

29 R. Boča, *Coord. Chem. Rev.*, 2004, **248**, 757.

30 (*a*) L. A. Zotti, E. Leary, M. Soriano, J. C. Cuevas and J. J. Palacios, *J. Am. Chem. Soc.*, 2013, **135**, 2052; (*b*) Y. Kitagawa, T. Matsui, Y. Nakanishi, Y. Shigeta, T. Kawakami, M. Okumura and K. Yamaguchi, *Dalton Trans.*, 2013, **42**, 16200.

31 D. E. Wheeler and J. K. McCusker, *Inorg. Chem.*, 1998, **37**, 2296.

32 See, *e.g.*: J. Tercero, E. Ruiz, S. Alvarez, A. Rodríguez-Fortea and P. Alemany, *J. Mater. Chem.*, 2006, **16**, 2729.

33 R. J. Errington, *Advanced Practical Inorganic and Metal-organic Chemistry*, CRC Press, 1997, p. 246.

34 Bruker-Nonius, *Kappa CCD Reference Manual*, Nonius BV, The Netherlands, 1998.

35 G. M. Sheldrick, *Acta Crystallogr., Sect. A: Fundam. Crystallogr.*, 2008, **64**, 112.

36 A. L. Spek, *J. Appl. Crystallogr.*, 2003, **36**, 7.

37 E. J. Baerends, J. Autschbach, A. Bérces, C. Bo, P. M. Boerrigter, L. Cavallo, D. P. Chong, L. Deng, R. M. Dickson, D. E. Ellis, L. Fan, T. H. Fischer, C. Fonseca Guerra, S. J. A. van Gisbergen, J. A. Groeneveld, O. V. Gritsenko, M. Grüning, F. E. Harris, P. van den Hoek, H. Jacobsen, G. van Kessel, F. Kootstra, E. van Lenthe, D. A. McCormack, V. P. Osinga, S. Patchkovskii, P. H. T. Philipsen, D. Post, C. C. Pye, W. Ravenek, P. Ros, P. R. T. Schipper, G. Schreckenbach, J. G. Snijders, M. Solà, M. Swart, D. Swerhone, G. te Velde, P. Vernooijs, L. Versluis, O. Visser, E. van Wezenbeek, G. Wiesenekker, S. K. Wolff, T. K. Woo and T. Ziegler, *ADF2010.01, SCM, Theoretical Chemistry*, *Vrije Universiteit*, Amsterdam, The Netherlands, http://www.scm.com

38 (*a*) G. te Velde, F. M. Bickelhaupt, E. J. Baerends, C. Fonseca Guerra, S. J. A. van Gisbergen, J. G. Snijders and T. Ziegler, *J. Comput. Chem.*, 2001, **22**, 931; (*b*) C. Fonseca Guerra, O. Visser, J. G. Snijders, G. te Velde and E. J. Baerends, in *Methods and Techniques for Computational Chemistry*, ed. E. Clementi and G. Corongiu, STEF, Cagliari, 1995, p. 305; (*c*) E. J. Baerends, D. E. Ellis and P. Ros, *Chem. Phys.*, 1973, **2**, 41; (*d*) E. J. Baerends and P. Ros, *Chem. Phys.*, 1975, **8**, 412; (*e*) E. J. Baerends and P. Ros, *Int. J. Quantum Chem. Symp.*, 1978, **12**, 169; (*f*) C. Fonseca Guerra, J. G. Snijders, G. te Velde and E. J. Baerends, *Theor. Chem. Acc.*, 1998, **99**, 391; (*g*) P. M. Boerrigter, G. te Velde and E. J. Baerends, *Int. J. Quantum Chem.*, 1988, **33**, 87; (*h*) G. te Velde and E. J. Baerends, *J. Comput. Phys.*, 1992, **99**, 84; (*i*) E. van Lenthe and E. J. Baerends, *J. Comput. Chem.*, 2003, **24**, 1142; (*j*) J. Krijn and E. J. Baerends, *Fit-Functions in the HFS-Method; Internal Report (in Dutch)*, Vrije Universiteit, Amsterdam, 1984; (*k*) L. Versluis and T. Ziegler, *J. Chem. Phys.*, 1988, **88**, 322; (*l*) J. C. Slater, *Quantum Theory of Molecules and Solids*, McGraw-Hill, New York, 1974, vol. 4; (*m*) A. D. Becke, *J. Chem. Phys.*, 1986, **84**, 4524; (*n*) A. D. Becke, *Phys. Rev. A*, 1988, **38**, 3098; (*o*) S. H. Vosko, L. Wilk and M. Nusair, *Can. J. Phys.*, 1980,

 This journal is © The Royal Society of Chemistry 2014

Published on 10 March 2014. Downloaded by Université de Strasbourg, Service Commun de la Documentation on 09/04/2014 10:04:09.

58, 1200; (*p*) J. P. Perdew, *Phys. Rev. B: Condens. Matter*, 1986, **33**, 8822, (Erratum*: Phys. Rev. B: Condens. Matter*, 1986, **34**, 7406); (*q*) L. Fan and T. Ziegler, *J. Chem. Phys.*, 1991, **94**, 6057.

39 M. Swart and J. G. Snijders, *Theor. Chem. Acc.*, 2003, **110**, 34, (Erratum*: Theor. Chem. Acc.*, 2004, **111**, 56).

40 (*a*) S. Grimme, *J. Comput. Chem.*, 2006, **27**, 1787; (*b*) S. Grimme, J. Antony, S. Ehrlich and H. Krieg, *J. Chem. Phys.*, 2010, **132**, 154104; see also: (*c*) S. Grimme, *J. Comput. Chem.*, 2004, **25**, 1463; (*d*) S. Grimme, *J. Comput. Chem.*, 2006, **27**, 1787; (*e*) S. Grimme, J. Antony, T. Schwabe and C. Muck-Lichtenfeld, *Org. Biomol. Chem.*, 2007, **5**, 741; (*f*) S. Grimme, J. Anthony, S. Ehrlich and H. Krieg, *J. Chem. Phys.*, 2010, **132**, 154104; (*g*) S. Grimme, R. Huenerbein and S. Ehrlich, *ChemPhysChem*, 2011, **12**, 1258.

41 For the use of BP86-D3, see *e.g.*: (*a*) J. M. Ruiz, C. Fonseca Guerra and F. M. Bickelhaupt, *J. Phys. Chem. A*, 2011, **115**, 8310; (*b*) A. Banerjee, F. S. Raad, N. Vankova, B. S. Bassil, T. Heine and U. Kortz, *Inorg. Chem.*, 2011, **50**, 11667; (*c*) W. Ames, D. A. Pantazis, V. Krewald, N. Cox, J. Messinger, W. Lubitz and F. Neese, *J. Am. Chem. Soc.*, 2011, **133**, 19743.

42 E. van Lenthe, E. J. Baerends and J. G. Snijders, *J. Chem. Phys.*, 1994, **101**, 9783.

43 (*a*) A. Klamt and G. Schüürmann, *J. Chem. Soc., Perkin Trans. 2*, 1993, 799; (*b*) A. Klamt, *J. Phys. Chem.*, 1995, **99**, 2224; (*c*) A. Klamt and V. Jones, *J. Chem. Phys.*, 1996, **105**, 9972.

44 (*a*) A. Bérces, R. M. Dickson, L. Fan, H. Jacobsen, D. Swerhone and T. Ziegler, *Comput. Phys. Commun.*, 1997, **100**, 247; (*b*) H. Jacobsen, A. Bérces, D. Swerhone and T. Ziegler, *Comput. Phys. Commun.*, 1997, **100**, 263; (*c*) S. K. Wolff, *Int. J. Quantum Chem.*, 2005, **104**, 645.

45 (*a*) M. Ernzerhof and G. E. Scuseria, *J. Chem. Phys.*, 1999, **110**, 5029; (*b*) C. Adamo and V. Barone, *J. Chem. Phys.*, 1999, **110**, 6158.

46 P. J. Stephens, F. J. Devlin, C. F. Chabalowski and M. J. Frisch, *J. Phys. Chem.*, 1994, **98**, 11623.

47 F. Neese, *ORCA – An Ab Initio, Density Functional and Semi-empirical Program Package, Version 2.9.0*, Germany.

48 M. R. Pederson and S. N. Khanna, *Phys. Rev. B: Condens. Matter*, 1999, **60**, 9566.

CONCLUSION GENERALE ET PERSPECTIVES

Bilan

Ce travail a permis d'élaborer et de synthétiser un grand nombre de nouvelles molécules répondant aux objectifs que nous nous étions fixés. La maîtrise des conditions réactionnelles nous a permis d'obtenir les complexes organométalliques cibles. Par ailleurs, des résultats inattendus et des assemblages moléculaires originaux ont pu être obtenus et analysés. Finalement, les complexes de coordination formés ont montré, comme nous l'espérions, des activités catalytiques ou une prédisposition à la formation de nanomatériaux.

Phosphines Fonctionnelles

Dans ce travail, nous avons étudié la chimie de coordination de deux bis(diphenylphosphino)amines fonctionnalisées par un groupement thio-éther, connu pour sa capacité à interagir avec des surfaces métalliques (Au, Ag, Cu). La réactivité de ces molécules vis à vis de centres métalliques est influencée par la nature de l'espaceur entre le groupe donneur diphosphine et la fonction d'ancrage thio-éther. L'importance de la nature de la fonctionnalisation a été mise en évidence dans le chapitre 2 dans lequel nous avons démontré comment, selon la nature du substituant fonctionnel, des conditions réactionnelles et du centre métallique (*e.g.* argent(I)), il a été possible d'observer une réactivité surprenante et inattendue qui nous a permis d'isoler des complexes très variés et intéressants. Dans les chapitres 3 et 4, nous avons exploré la réactivité de ces ligands ainsi que de leurs dérivés monosulfurés vis-à-vis du nickel(II). Tous ces complexes ont montré une bonne activité en tant que catalyseurs pour l'oligomérisation de l'éthylène en phase homogène. En particulier, les dérivés monosulfurés ont aussi montré une réactivité inattendue en solution, qui nous a permis de caractériser deux espèces différentes en équilibre entre-elles : un complexe mono-chélate diamagnétique, plan-carré, et un couple cation-anion caractérisé par un cation bis-chélate diamagnétique et un anion paramagnétique. Cette réactivité, ainsi que

l'activité catalytique de tous les complexes, a été l'objet d'une discussion détaillée basée sur des comparaisons structurelles et des calculs théoriques.

En perspective, pour développer cette thématique de recherche, il serait important, à court terme, de chercher à comprendre le mécanisme qui conduit à la formation du cluster d'argent triangulaire décrit dans le chapitre 2. Sur le plus long terme, il serait intéressant de tester la réactivité des ligands monosulfurés vis-à-vis de précurseurs d'argent dans les mêmes conditions que celles décrites dans le chapitre 2 et d'étudier comment cette chimie peut évoluer en ajoutant un élément d'asymétrie dans le ligand. Concernant la chimie destinée à la préparation de catalyseurs pour l'oligomérisation de l'éthylène, je trouve qu'il serait très intéressant d'étudier la réactivité et l'activité des complexes formés par cette famille de ligands vis-à-vis des autres métaux connus pour leur activité en catalyse comme Cr, Co, Fe ou Pd.

Zwitterions et ligands quinonoïdes

Dans ce travail, nous avons développé la chimie de coordination d'un nouveau ligand zwitterionique quinonoïde, potentiellement hexadentate, vis-à-vis d'un précurseur métallique comme le Pd(II). Selon les conditions expérimentales et la stœchiométrie utilisée, il a été possible de modifier la denticité du ligand et de caractériser différents complexes dans lesquels le ligand se comporte comme bidentate, tétradentate ou hexadentate. Parmi les molécules isolées, certaines sont de bons candidats pour la fonctionnalisation de surfaces ou pour la catalyse de réactions de couplage C-C.

Amino-alcools

Deux nouveaux complexes avec une structure de type cubane [M(μ_3-Cl)(μ_3-Cl)**HL(S)**]$_4$ (M = Co, Ni) ont été préparés par réaction de $CoCl_2$ et de $NiCl_2$ avec un nouveau ligand pyridyl-alcool **HL(S)** qui possède une fonction thio-éther cyclique sur le substituant en ortho de la pyridine, adaptée pour interagir avec des surfaces métalliques. Ces complexes ont été caractérisés par analyse élémentaire, spectrométrie infrarouge, analyse thermogravimétrique et par diffraction des rayons X. Leurs propriétés physiques ont été étudiées par le biais de mesures magnétiques et de calculs DFT. Bien que les structures des complexes du Co(II) et du Ni(II) soient quasi identiques, ces deux complexes présentent des propriétés physiques très différentes. Le cubane de Co(II) est moins stable énergétiquement (DFT) que celui du Ni(II), et même si les deux complexes sont paramagnétiques, le complexe du Ni présente un comportement de SMM (Single Molecule Magnet) alors que celui du Co(II) est le siège des couplages antiferromagnétiques. Cette particularité, associée à la présence d'un groupement thio-éther, font de ce composé du Ni un très bon candidat pour la fonctionnalisation d'une surface d'Au(111). En perspective, nous envisageons de déposer ce cluster sur une surface métallique, d'étudier les propriétés du matériau fonctionnalisé obtenu et d'explorer une éventuelle activité catalytique de ces complexes en oligomérisation de l'éthylène. Il serait également intéressant de continuer à développer la chimie de **HL(S)** en cherchant à assembler de nouveaux complexes polynucléaires avec d'autres espèces paramagnétiques, comme le Cu ou le Fe.

Alessio GHISOLFI

Applications de ligands diphosphines fonctionnelles et de zwitterions quinonoïdes à la chimie de coordination et à la fonctionalisation de surfaces

Résumé

Le but de ce travail de thèse était de développer de nouvelles familles de ligands polyfonctionnels pour étudier, dans un premier temps, leur chimie de coordination vis-à-vis de métaux de transition et, dans un second temps, en fonction des espèces formées, leurs propriétés physiques (magnétiques par exemple) et/ou catalytiques. L'évaluation de leur potentiel pour la formation de nouveaux matériaux ou la fonctionnalisation de supports métalliques faisait également partie intégrante des objectifs de cette thèse. De ce fait, chaque ligand a été fonctionnalisé avec des groupements adaptés à l'ancrage sur surfaces, comme des fonctions zwitterioniques ou des thio-éthers.

Mots clés: Phosphines fonctionnelles, Zwitterions, Ligands quinonoïdes, Amino-alcools, Organométalliques, Oligomérisation catalytique de l'éthylène, Aimants moléculaires.

Résumé en anglais

The aim of this thesis was to develop new families of polyfunctional ligands to study their coordination chemistry towards transition metals and, depending on the products formed, to investigate their physical (e.g. magnetic) and / or catalytic properties. The evaluation of their potential for the formation of new materials as well as for the functionalization of metal surfaces was also part of the objective of this thesis. Therefore, each ligand has been functionalized with groups suitable for the anchoring on metallic surfaces, such as zwitterionic or thioethers moieties.

Keywords: Functional phosphines, Zwitterions, Quinonoid ligands, Amino-alcohols, Organometallic, Catalytic ethylene oligomerization, Single molecule magnets (smm).